

# Perceptually-based Modelling of Human Contrast Vision

Thesis submitted in accordance with the requirements of the  
UNIVERSITY OF LIVERPOOL  
Liverpool, UK

for the degree of  
Doctor of Philosophy

by  
Maliha Ashraf  
MS in Colour Science (EMJMD, Saint-Étienne, France), 2018  
BE in Electronic Engineering (NEDUET, Karachi, Pakistan), 2016



Defended on: 29-05-2024

Supervised by

Professor Jeremy Smith  
Professor Sophie Wuergler

Examined by

Professor Stephen Westland  
Professor Maria Vanrell

© 2024

Maliha Ashraf  
ORCID: 0000-0002-8142-5611

وہ لوگ بہت خوش قسمت تھے  
جو عشق کو کام سمجھتے تھے  
یا کام سے عاشقی کرتے تھے  
ہم حتیٰ جی مصروف رہے  
کچھ عشق کیا کچھ کام کیا  
کام عشق کے آڑے آتا رہا  
اور عشق سے کام الجھتا رہا  
پھر آخر تنگ آ کر ہم نے  
دونوں کو ادھورا چھوڑ دیا

فیضِ احمد فیض

## ACKNOWLEDGEMENTS

I cannot possibly thank every individual who has supported me in this journey but none more so than Sophie whose untimely passing has left many of us heartbroken. Prof. Sophie Wuerger has been an amazing advisor and mentor to me personally, and I am extremely grateful for the time we had together, however brief it may seem now. I will dearly miss our random chats when I would go to her with a question and she would somehow know a dozen references off the top of her head explaining the exact problem I had. Sophie was not just a brilliant scholar but also a person of unparalleled empathy and kindness. I could not thank her enough for all the support she had shown me with my visa and funding debacles. I hope this thesis does justice to everything she had taught me.

I am very thankful to Prof. Jeremy Smith who has been very supportive throughout my PhD journey and helped me navigate all the administrative stuff that comes with it. I owe a great deal to Prof. Rafał Mantiuk who unofficially adopted me as one of his students. He was and still is an amazing mentor and an excellent supervisor and colleague to work with. All the support from Dr. Jasna Martinovic especially with the dark arts of statistics is deeply appreciated. Dr. Minjung Kim, though her tenure with us was brief, left an indelible mark with her enthusiasm for research as well as for keeping the social vibe in the lab alive. I am truly thankful to Dr. Alex Chapiro whose Meta sponsorship could not have come at a better time and who has been a great colleague and collaborator.

The diligence and dedication of Olivia Kingston and Kristof Santa who were a great help in facilitating all the data collection cannot be forgotten. Also thanks to Prof. J D Yan and Dr. Kai Hoettges for their constructive feedback on my annual progress reports. All of my fellow PhDs at the labs in Liverpool and Cambridge; thank you for your friendship and camaraderie.

I am very fortunate to have a loving family back home who have been a constant source of support but also of entertainment with their ridiculous stories. And finally, thanks to my partner Josh who showed me that it's possible to do a PhD without it taking over your whole life. Your terrible jokes and antics instantly cure me of my imposter syndrome and your attempts at pronouncing Urdu words have been a constant source of amusement for me.

## ABSTRACT

Contrast vision, a fundamental aspect of human visual perception, involves discerning brightness and chromatic differences within the visual field. This thesis advances the understanding of contrast vision by presenting new psychophysical data and models that characterise human contrast sensitivity at both threshold and suprathreshold levels. This research is based on collecting and analysing psychophysical data on how well humans can detect differences in light and colour across a range of conditions, such as different spatial frequency patterns, brightness levels, stimulus sizes, and colours.

The thesis first addresses the fundamental aspect of contrast sensitivity functions (CSFs), quantifying the change in sensitivity along different stimulus parameters as well as the age of the human observers. It was found that the contrast sensitivity increased with the mean luminance level but the rate of this increment was much higher in low luminance (scotopic/mesopic) regions compared to high luminance (photopic) regions. The sensitivity also shifted towards higher spatial frequencies with increasing mean luminance levels. The sensitivity of older observers was affected considerably more for high spatial frequency and low luminance stimuli. Building on the findings from threshold data, the characteristics of suprathreshold vision were investigated. It was found that at higher contrast levels, the sensitivity matches across luminance are not independent of threshold sensitivity as assumed from the contrast constancy literature.

A novel contribution of this research is the analysis and computational modelling of CSFs, which includes a consideration of the impact of ageing on contrast vision. This work proposes quantitative models of spatiochromatic contrast sensitivity across high dynamic range (HDR) luminance conditions as well as age-related contrast sensitivity decline across spatial frequencies and under varying light conditions. A model of contrast matching functions, which attempts to explain suprathreshold contrast perception across luminance levels, was also introduced based on novel data. This model extends to investigate the influence of rod photoreceptors on colour difference metrics, proposing a new formula that integrates both cone and rod responses for photopic and mesopic vision conditions.

Furthermore, the thesis introduces a model of contrast matching functions, which attempts to explain suprathreshold contrast perception across luminance levels, based on novel data. This model extends to investigate the influence of rod photoreceptors on colour difference metrics, proposing a new formula that integrates both cone and rod responses for photopic

and mesopic vision conditions.

The key findings from this body of work include:

- A spatio-chromatic contrast sensitivity assessment under mesopic and photopic light levels, revealing critical insights into the human visual system's system's adaptation characteristics (Wuerger et al., 2020).
- An exploration of spatio-chromatic contrast sensitivity across the lifespan, delineating age-related variations and their implications for high dynamic range vision (Ashraf et al., 2020).
- The development of a colour difference formula that accounts for both cone and rod responses, bridging a gap in the understanding of contrast sensitivity under varying lighting conditions (Ashraf et al., 2022).
- An investigation into suprathreshold contrast matching, offering a new perspective on how different luminance levels affect contrast perception (Ashraf et al., 2022).
- A model detailing the contrast sensitivity of discs, contributing to the field of human vision and electronic imaging with practical applications (Ashraf et al., 2023).

The thesis attempts to offer a robust framework for understanding and modelling low-level human contrast vision, with implications for various fields, including vision science, computer graphics, display engineering, and image processing.

## CONTENTS

Acknowledgements . . . . .	iv
Abstract . . . . .	v
Contents . . . . .	vii
List of Figures . . . . .	xi
List of Tables . . . . .	xiv
Nomenclature . . . . .	xvi
Chapter 1: Introduction . . . . .	1
1.1 Research approach . . . . .	3
1.2 Thesis overview . . . . .	3
1.3 Published Content and Contributions . . . . .	5
Chapter 2: Background and Literature Review . . . . .	7
2.1 The Human Visual System (HVS) . . . . .	7
2.1.1 Ocular media . . . . .	7
2.1.2 The Retina . . . . .	8
2.2 Psychophysics . . . . .	10
2.2.1 Method of Adjustment . . . . .	10
2.2.2 Forced-choice Methods . . . . .	11
2.2.3 Method of limits . . . . .	11
2.2.4 Method of constant stimuli . . . . .	11
2.2.5 Psychometric functions . . . . .	12
2.3 Contrast vision . . . . .	12
2.4 Contrast sensitivity . . . . .	13
2.4.1 Spatial contrast vision . . . . .	14
2.4.2 Colour contrast vision . . . . .	15
2.4.3 Effect of luminance . . . . .	15
2.4.4 Effect of age . . . . .	16
2.4.5 Effect of size . . . . .	17
2.4.6 Interplay of different factors affecting CSF . . . . .	17
2.5 Suprathreshold contrast vision . . . . .	17
2.5.1 Measuring Suprathreshold Contrast . . . . .	18
2.5.2 Contrast constancy . . . . .	19
2.5.3 Effect of age . . . . .	21
2.6 Stimuli in Vision Science Experiments . . . . .	21
2.6.1 Gabor patches . . . . .	21
2.6.2 Additional Stimuli in Visual Psychophysics . . . . .	23
Chapter 3: Methodology . . . . .	25
3.1 Apparatus . . . . .	25

## CONTENTS

3.1.1	HDR screen . . . . .	25
3.2	Colour and contrast spaces . . . . .	27
3.2.1	LMS Colour Space . . . . .	28
3.2.2	DKL colour space . . . . .	29
3.2.3	Cone contrast space . . . . .	30
3.3	Stimuli . . . . .	31
3.4	Experimental setup . . . . .	32
3.4.1	Contrast detection experiments . . . . .	32
3.4.2	Contrast matching experiments . . . . .	33
3.5	Observers' recruitment . . . . .	34
Chapter 4: Contrast sensitivity functions . . . . .		36
4.1	Experiment 1: Effect of spatial frequency, chromatic direction and luminance . . . . .	37
4.1.1	Stimuli . . . . .	37
4.1.2	Procedure . . . . .	39
4.1.3	Observers . . . . .	40
4.1.4	Results and Discussion . . . . .	40
4.2	Experiment 2: Effect of Age . . . . .	47
4.2.1	Observers . . . . .	47
4.2.2	Statistical analysis . . . . .	48
4.2.3	Results . . . . .	49
4.2.4	Discussion . . . . .	50
4.3	Experiment 3: Contrast sensitivity of disc stimuli . . . . .	51
4.3.1	Displays . . . . .	52
4.3.2	Stimuli . . . . .	52
4.3.3	Experimental procedure . . . . .	53
4.3.4	Participants . . . . .	54
4.3.5	Results . . . . .	54
4.4	Summary of chapter . . . . .	55
Chapter 5: Modelling CSFs . . . . .		56
5.1	General model of CSF . . . . .	57
5.1.1	Spatio-chromatic contrast sensitivity function envelope . . . . .	57
5.1.2	Luminance Intrusion . . . . .	59
5.1.3	Contrast sensitivity as a function of mean luminance . . . . .	62
5.1.4	CSF as the function of the stimulus size . . . . .	66
5.1.5	Comparison with other datasets . . . . .	67
5.2	Contrast sensitivity as a function of age . . . . .	69
5.2.1	Empirical model . . . . .	72
5.2.2	Luminance reduction . . . . .	74
5.2.3	Pupil size reduction . . . . .	77
5.2.4	Lens transmission . . . . .	78
5.2.5	Optical factors . . . . .	80
5.2.6	Results . . . . .	81
5.3	Disc CSFs . . . . .	82

## CONTENTS

5.3.1	Contrast energy models . . . . .	83
5.3.2	Model fitting and practical considerations . . . . .	84
5.3.3	Multiple detector models . . . . .	88
5.3.4	Results . . . . .	91
5.4	Summary of chapter . . . . .	93
Chapter 6: Contrast matching functions . . . . .	94	
6.1	Experiment: Contrast matching across luminances . . . . .	95
6.1.1	Observers . . . . .	95
6.1.2	Procedure . . . . .	95
6.2	Statistical Analysis . . . . .	97
6.3	Results . . . . .	98
6.3.1	Failure of contrast constancy . . . . .	100
6.3.2	Low luminance matches require higher contrast . . . . .	102
6.3.3	Differences in near-threshold and suprathreshold matching . . . . .	102
6.3.4	Effect of age . . . . .	103
6.3.5	Modelling CMF . . . . .	104
6.4	Discussion . . . . .	104
6.5	Summary of chapter . . . . .	106
Chapter 7: Modelling CMFs . . . . .	107	
7.1	Additive model (Kulikowski's) . . . . .	108
7.2	Multiplicative model (Peli's) . . . . .	110
7.3	Empirical modelling of CMF . . . . .	113
7.3.1	Luminance-adaptive CMF . . . . .	116
7.4	Discussion . . . . .	118
7.4.1	Future work and applications . . . . .	119
7.5	Summary of chapter . . . . .	120
Chapter 8: Rod vision . . . . .	122	
8.1	Introduction . . . . .	122
8.2	Related work . . . . .	123
8.3	Colour difference metrics . . . . .	127
8.3.1	Validation with contrast sensitivity datasets . . . . .	128
8.4	Results . . . . .	130
8.4.1	Metric 1: Euclidean LMS distance ( $\Delta E_{LMSR}$ ) . . . . .	130
8.4.2	Metric 2: CIEDE2000 ( $\Delta E_{2000}^{LMS}$ ) . . . . .	131
8.4.3	Metric 3: CIEDE2000 + rod intrusion ( $\Delta E_{2000}^{L'M'S'}$ ) . . . . .	132
8.4.4	Metric 4: CIEDE2000 + rod intrusion + adaptation . . . . .	133
8.4.5	Perceptual uniformity . . . . .	134
8.5	Summary of chapter . . . . .	135
Chapter 9: Conclusions . . . . .	136	
9.1	Research highlights . . . . .	136
9.2	Future work recommendations . . . . .	139
References . . . . .	141	
Appendix A: Table of Ageing CSF studies . . . . .	164	

## CONTENTS

Appendix B: Data variability . . . . .	166
Appendix C: Optometry data for older observers . . . . .	168
Appendix D: CSF statistical tests . . . . .	171
D.1 Achromatic CSF . . . . .	171
D.2 Red-green CSF . . . . .	174
D.3 Yellow-violet CSF . . . . .	176
Appendix E: CMF statistical tests . . . . .	179
E.1 Achromatic contrast matching . . . . .	179
E.2 Red-green contrast matching . . . . .	182
E.3 Yellow-violet contrast matching . . . . .	185
Appendix F: Contrast matching modelling parameters . . . . .	189
Appendix G: CMF model statistical tests . . . . .	190
G.1 Modelling slopes of contrast matching . . . . .	190
G.1.1 Achromatic contrast matching . . . . .	190
G.1.2 Red-green contrast matching . . . . .	191
G.1.3 Yellow-violet contrast matching . . . . .	191
G.2 Modelling intercept of contrast matching . . . . .	192
G.2.1 Achromatic contrast matching . . . . .	192
G.2.2 Red-green contrast matching . . . . .	192
G.2.3 Yellow-violet contrast matching . . . . .	193

## LIST OF FIGURES

<i>Number</i>		<i>Page</i>
2.1 Structure of human eye . . . . .		8
2.2 Neural convergence of retinal photoreceptor . . . . .		10
2.3 Example psychometric function . . . . .		12
2.4 Examples of high and low contrast in sinusoidal gratings . . . . .		14
2.5 Example CSFs . . . . .		15
2.6 Examples of fixed-size and fixed-cycles Gabor patches at different spatial frequencies . . . . .		22
2.7 Examples of Gabor patches with different background colours and chromatic modulations . . . . .		23
3.1 HDR display experimental setup . . . . .		26
3.2 Spectral power distributions of the HDR displays. . . . .		27
3.3 DKL colour space with the three modulation directions used in the experiments		29
3.4 Gabor patch stimuli . . . . .		32
3.5 Photograph of the real contrast matching experiments setup . . . . .		33
3.6 Top view of contrast matching experiments setup . . . . .		34
4.1 Example 4AFC trial . . . . .		39
4.2 Contrast sensitivity as a function of spatial frequency . . . . .		41
4.3 Contrast sensitivity as a function of luminance. . . . .		42
4.4 CSF changes with retinal illuminance . . . . .		43
4.5 Additional CSF measurements to test for incomplete adaptation . . . . .		44
4.6 Additional chromatic CSF measurements for lower spatial frequencies . . . . .		45
4.7 Contrast sensitivity as a function of size . . . . .		46
4.8 Linear decrease in log contrast with the increase in log area of the stimulus .		46
4.9 Age distribution of observer groups . . . . .		47
4.10 Mean contrast sensitivity functions from older and younger observer groups.		50
4.11 Example disc stimuli . . . . .		53
4.12 Disc CSF measurements . . . . .		54
5.1 The results of fitting parabolic CSF models to the data . . . . .		58
5.2 Channel summation model with 11 free parameters . . . . .		61
5.3 The relationship between the fitted CSF parameters and luminance . . . . .		63

## LIST OF FIGURES

5.4	Luminance-dependent model of CSF . . . . .	64
5.5	Summary of the luminance and area-dependent model of CSF . . . . .	67
5.6	Predictions of the proposed model for the ColorFest dataset from Wuerger <i>et al.</i> [181] . . . . .	68
5.7	Predictions of the proposed model for the Mantiuk <i>et al.</i> [179] dataset . . . . .	69
5.8	Predictions of the proposed model for the Kim <i>et al.</i> [180] dataset . . . . .	69
5.9	Change in log-parabola CSF parameters with age . . . . .	70
5.10	Model predictions for contrast sensitivity functions of older and younger observer groups. . . . .	74
5.11	Age-dependent luminance reduction model of CSF . . . . .	76
5.12	Age-dependent pupil size reduction model of CSF . . . . .	78
5.13	Pokorny's lens transmission function . . . . .	79
5.14	Age-dependent lens transmission model of CSF . . . . .	80
5.15	Age-dependent optical changes model of CSF . . . . .	81
5.16	Decomposition of disk stimuli into sinusoids in Fourier space . . . . .	84
5.17	Decomposition of disk stimuli into Gabor patches in Fourier space . . . . .	87
5.18	Disc stimuli represented as partial square waves . . . . .	90
5.19	Measurements of the disc contrast sensitivity and the predictions of contrast energy models. . . . .	92
5.20	Measurements of the disc contrast sensitivity and the multiple detector models	93
6.1	An example contrast matching trial . . . . .	97
6.2	Mean measurements for contrast matching across luminance levels for the younger group . . . . .	99
6.3	Mean measurements for contrast matching across luminance levels for the older group . . . . .	100
6.4	Contrast matching across luminance levels for achromatic Gabor patches . .	101
6.5	Contrast matching across luminance levels for red-green Gabor patches . .	102
6.6	Contrast matching across luminance levels for yellow-violet Gabor patches .	103
7.1	Kulikowski's CMF model predictions for younger observers . . . . .	109
7.2	Kulikowski's CMF model predictions for older observers . . . . .	110
7.3	Peli's CMF model predictions for younger observers . . . . .	112
7.4	Peli's CMF model predictions for older observers . . . . .	113
7.5	Contrast matching linear function . . . . .	114
7.6	Proposed CMF model predictions for younger observers . . . . .	117
7.7	Proposed CMF model predictions for older observers . . . . .	118

## LIST OF FIGURES

7.8	Example of a retargeted image from high to low luminance . . . . .	121
8.1	Demonstration of Purkinje shift using the modified photoreceptor response model . . . . .	124
8.2	Values of rod contribution parameters as functions of retinal illuminance . .	126
8.3	Number of data points across luminance levels in each dataset . . . . .	128
8.4	Gabor patch stimulus . . . . .	129
8.5	$\Delta E_{LMSR}$ error predictions for 1 JND colour difference data points . . . .	131
8.6	$\Delta E_{2000}^{LMS}$ error predictions for 1 JND colour difference data points . . . .	132
8.7	$\Delta E_{2000}^{L'M'S'}$ error predictions for 1 JND colour difference data points . . . .	133
8.8	$\Delta E_{2000}^G$ error predictions for 1 JND colour difference data points . . . .	134
C.1	Cataract grading system. The figure is from Shaheen and Akram [136]. . . .	168

## LIST OF TABLES

<i>Number</i>	<i>Page</i>
2.1 Comparison of Rods and Cones in the Human Retina . . . . .	8
4.1 Slopes of log threshold contrast vs log retinal illuminance (trolands) in linear range . . . . .	43
4.2 Mean variation in disc CSF data . . . . .	55
5.1 Parameters for log-parabola fit with truncation parameters for chromatic channels	59
5.2 Parameters for the channel summation fit. . . . .	62
5.3 Summary of nested models . . . . .	65
5.4 Errors from per-luminance level model predictions in older observers . . . . .	76
5.5 Summary of ageing models . . . . .	82
5.6 Coefficients of sinc function for Gabor patch conversion . . . . .	86
5.7 Parameters and fitting errors for disc CSF models . . . . .	91
7.1 Optimised values of parameters for the proposed CMF model . . . . .	116
7.2 Summary of CMF models . . . . .	119
8.1 Summary of datasets . . . . .	128
8.2 Performance comparison of modified rod response-dependent colour difference metrics . . . . .	135
A.1 Summary of ageing CSF datasets from literature . . . . .	164
B.1 $CV_{mean}$ of log contrast sensitivity averaged across all spatial frequencies . . .	166
B.2 $CV_{mean}$ of log contrast sensitivity averaged across all spatial frequencies and luminance levels . . . . .	166
B.3 $CV_{mean}$ of matched test contrast averaged across all luminance levels . . . . .	167
B.4 $CV_{mean}$ of matched test contrast averaged across all luminance levels and spatial frequencies . . . . .	167
C.1 Clinical cataract grading system Shaheen and Akram [136]. . . . .	168
C.2 ataract grading for the tested observers . . . . .	169
C.3 Pupil sizes with dark and light adaptation . . . . .	169
C.4 Visual acuity test . . . . .	170
C.5 Contrast sensitivity measured with VectorVision (CSV-1000) chart with and without glare . . . . .	170
D.1 CSF data transforms and pre-processing . . . . .	171
D.2 Achromatic CSF statistical modelling results . . . . .	171
D.3 Red-green CSF statistical modelling results . . . . .	174

## LIST OF TABLES

D.4	Yellow-violet CSF statistical modelling results . . . . .	176
E.1	CMF data transforms and pre-processing . . . . .	179
E.2	Achromatic CMF statistical modelling results . . . . .	180
E.3	Red-green CMF statistical modelling results . . . . .	183
E.4	Yellow-violet CMF statistical modelling results . . . . .	185
F.1	Slopes and intercepts from fitted lines of matching contrast . . . . .	189
G.1	CMF modelling parameters transforms and pre-processing . . . . .	190
G.2	Achromatic CMF slope parameter statistical modelling results . . . . .	190
G.3	Red-green CMF slope parameter statistical modelling results . . . . .	191
G.4	Yellow-violet CMF slope parameter statistical modelling results . . . . .	191
G.5	Achromatic CMF intercept parameter statistical modelling results . . . . .	192
G.6	Red-green CMF intercept parameter statistical modelling results . . . . .	192
G.7	Yellow-violet CMF intercept parameter statistical modelling results . . . . .	193

## NOMENCLATURE

### ABBREVIATIONS.

- AFC.** Alternative Forced-Choice.
- CMF.** Contrast Matching Function.
- CSF.** Contrast Sensitivity Function.
- DKL.** Derrington-Krauskopf-Lennie.
- DLP.** Digital Light Processing.
- FOV.** Field Of View.
- HDR.** High Dynamic Range.
- HVS.** Human Visual System.
- ipRGC.** Intrinsically Photosensitive Retinal Ganglion Cell.
- JND.** Just Noticeable Difference.
- JOD.** Just Observable Difference.
- LCD.** Liquid Crystal Display.
- LMEM.** Linear Mixed-Effect Model.
- LMS.** Long, Medium, and Short wavelength-sensitives cones.
- MLE.** Maximum Likelihood Estimation.
- ND.** neutral density.
- RGC.** Retinal Ganglion Cell.
- RMSE.** Root Mean Squared Error.
- SEM.** Standard Error of Mean.
- VDP.** Visual Difference Predictor.

### GLOSSARY.

## LIST OF TABLES

**Deutanopia.** Red-green colour deficiency.

**Fovea.** The central 1° part of the retina.

**High-level vision.** involves complex cognitive processes, including recognition, categorisation, and interpretation of objects and scenes, integrating sensory input with memory, knowledge, contextual information and attention in the brain's more advanced visual areas.

**L cones.** Long wavelength-sensitive cones.

**Low-level vision.** refers to the initial stages of visual processing that involve basic features such as contrast, brightness, and colour, primarily handled by the retina and early visual cortex, without the influence of higher cognitive functions.

**M cones.** Medium wavelength-sensitive cones.

**Mesopic vision.** Ranges from approximately 0.001-3 cd/m<sup>2</sup>. Both rods and cones are active at these light levels. The colours are dim. Peak sensitivity can range from 507-555 nm.

**Photopic vision.** High light level vision. Ranges from 3 cd/m<sup>2</sup> and upwards. Cones are active in this light range and thus colour vision is functional. Peak sensitivity is at 555 nm.

**Psychophysics.** The study of the quantitative relationships between physical stimuli and their perceived sensory experiences.

**S cones.** Short wavelength-sensitive cones.

**Scotopic vision.** Low light or night vision. Ranges from 0.001 cd/m<sup>2</sup> and below. Only rods are activated at these light levels and so colours cannot be distinguished. Peak sensitivity is at 507 nm.

## UNITS.

**cd.** candela. SI unit of luminous intensity. Luminous flux per unit solid angle.

**cd/m<sup>2</sup>.** candela per square metre. SI unit of luminance. Luminous flux per unit solid angle per unit projected source area. Also known as nits.

**cpd.** cycles per visual degree. Unit of spatial frequency.

**td.** trolands. Unit of retinal illuminance, calculated as a product of retinal illuminance and pupillary area..

## *C h a p t e r* 1

### INTRODUCTION

For centuries, the human visual system has remained a source of inspiration and intrigue for scientists and artists. From the ancient camera obscura, to the modern virtual/augmented reality (VR/AR) technologies, we have tried to replicate, retain and reproduce the various attributes of our visual system. Thus, advancements in understanding human vision go hand in hand with improvements in imaging and display technologies. The multifaceted functioning of visual perception offers a wealth of inspiration for enhancing algorithms and hardware across a spectrum of applications, including image and video processing, quality assessments, display design, graphics rendering, and the optimisation of augmented and virtual reality technologies. Among these aspects, contrast vision stands out as a particularly influential factor. Accurate modelling of contrast vision—the ability of the human visual system to discern differences in luminance or colour between an object and its background—can significantly benefit the aforementioned applications. By understanding and replicating how humans perceive and process contrast, engineers can develop more effective and efficient systems that align with human visual capabilities, thereby improving user experience and system performance in various digital environments.

Among the various mechanisms of the human visual function, contrast vision is considered one of its fundamental building blocks. Contrast perception is the first processing stage for several critical daily functions such as detection of edges and boundaries within a visual scene, which are essential for object recognition and spatial orientation. The visual acuity which is effectively the spatial resolving power of the eye is also closely tied to contrast vision. Contrast vision also plays a crucial role in motion detection and depth perception. The detection of motion relies on temporal changes in contrast, and the visual system's ability to interpret these changes is vital for navigating dynamic environments [1]. Similarly, variations in contrast provide cues for depth perception, enabling the brain to construct a three-dimensional understanding of the world from two-dimensional retinal images.

In the classical sense, contrast vision is thought of as the ability to detect variations in luminance or brightness in areas of stimuli. However, the ability to perceive variations between colours or hues, independent of luminance, represents a less-explored aspect of

## CHAPTER 1. INTRODUCTION

contrast vision. While colour vision involves the detection of different ranges of wavelengths along the visible light spectrum, the contrast between different colours (chromatic contrast) enhances the perception of colour boundaries and enriches the visual experience. Research in colour vision has demonstrated that the LMS (long, medium, and short wavelength) cones in the retina contribute to contrast sensitivity for both luminance and colour, and the responses from these cones are passed on to later stages of visual processing, including the opponent-colour mechanisms [2].

In the context of visual impairments and ageing, contrast sensitivity often declines before other visual functions, making it a critical parameter for early detection and diagnosis of eye diseases. Conditions such as cataracts, glaucoma, and age-related macular degeneration can significantly reduce contrast sensitivity, impacting an individual's ability to perform everyday tasks and reducing their quality of life [3]. Contrast sensitivity is one of the measures of quantifying this decline in visual function.

The focus of this thesis is the study of contrast sensitivity functions (CSFs) and contrast matching functions (CMFs), which offer quantitative insights into the processing of visual information. Contrast sensitivity functions represent the sensitivity of the human visual system to stimuli varying along various parameters, including spatial, temporal, chromatic and luminance dimensions. Contrast matching functions, on the other hand, are concerned with the equivalent contrast perception of visual stimuli when the contrast is much higher than the minimum threshold, allowing for the mapping of perceived to actual contrast levels. Both CSFs and CMFs are crucial in understanding various visual tasks, including reading, object recognition, and navigation, which rely on the ability to perceive contrasts at different spatial scales. These functions are also key to understanding how contrast is encoded and processed in the brain, revealing the non-linearities in visual perception [4].

This thesis presents a comprehensive analysis of both achromatic and chromatic contrast sensitivity and matching data. While much of the literature has focused on achromatic stimuli, the visual system's response to colour and how chromaticity affects contrast perception are relatively less well-explored, especially for a wide range of luminance levels. Chromatic contrast sensitivity is particularly important for tasks that rely on colour vision and has implications for design, signage, and visual ergonomics [5]. The computational models proposed in this work are designed to account for a variety of factors that influence contrast perception, including the observer's age. Age-related changes in the eye and neural processing significantly impact contrast sensitivity, with older adults typically exhibiting reduced sensitivity, especially at higher spatial frequencies [3]. The models are informed by both psychophysical

## CHAPTER 1. INTRODUCTION

data and physiological knowledge of the visual system, ensuring they are rooted in empirical evidence while providing predictive power across different populations.

### 1.1 Research approach

This thesis aims to bridge gaps in the current understanding and provide a unified framework for modelling contrast perception. The extensive datasets and models presented here not only contribute to the academic field of vision science but also have practical applications in areas ranging from display technology to the diagnosis of visual impairments. The thesis begins with an extensive literature review, laying the groundwork by examining the Human Visual System (HVS), focusing on ocular media, the retina, visual pathways, and the visual cortex. Building on this, a deeper exploration into the literature about contrast sensitivity is conducted, detailing the effects of various factors such as spatial frequency, colour, luminance, age, and temporal dynamics on contrast perception. This investigation is expanded into suprathreshold contrast vision, examining its dependencies on various external and internal contributors. A detailed presentation of the methods used to collect achromatic and chromatic contrast data follows. Psychophysical methods were employed to probe the perceptual aspects of contrast sensitivity, utilising methods of adjustment and forced-choice to gather empirical data. The experimental setup is carefully designed, with a range of apparatus and stimuli with a large number of observers tested to ensure robustness and reliability. The thesis also bases its findings on the colour and contrast spaces relevant to the HVS, such as LMS (Long, Medium, and Short wavelength-sensitives cones), DKL (Derrington-Krauskopf-Lennie) [2], and cone contrast spaces, to provide a common framework for interpreting the psychophysical data. Subsequent chapters discuss the findings and trends from the data and then go on to develop and validate the proposed computational models while discussing the implications of these models for understanding visual perception in different age groups.

### 1.2 Thesis overview

The summary of each subsequent chapter and the novel contributions are highlighted below:

- Chapter 2: Background and Literature Review - A thorough review of the existing scholarly work on the human visual system is provided. The fundamental theories and existing findings related to the perception of contrast across light levels and colour modulations, and the processing of these perceptions by the visual system, are introduced, establishing a foundation for the research questions the thesis will address.

## CHAPTER 1. INTRODUCTION

The gaps in the literature are identified for CSF and CMF datasets spanning wide luminance ranges. The literature was also lacking in quantitatively characterising chromatic contrast vision.

- Chapter 3: Methodology - This chapter outlines the methodological approach taken in the empirical research, detailing the psychophysical techniques and experimental setups used in data collection. The specific instruments and tests conducted to gather data on contrast perception are described.
- Chapter 4: Contrast sensitivity functions - This chapter reports on the empirical findings from a series of experiments designed to measure the sensitivity of the human visual system to contrasts of different spatial frequencies, colours, and luminance levels as well as different stimulus shapes. It also examines the effects of age on contrast sensitivity, contributing valuable insights into the variability of visual perception across the lifespan. The chapter presents novel datasets of contrast sensitivity for many different stimulus, environmental, and observer conditions.
- Chapter 5: Modelling CSFs - This chapter introduces and explains the construction of several new computational models that simulate how humans perceive the contrast of basic visual stimuli, such as Gabor patches and discs. The models account for a range of factors, including the spatial scale of the stimuli, the influence of light intensity and the physiological changes that occur with ageing, and offer predictions that are tested against empirical data.
- Chapter 6: Contrast matching functions - The focus of this chapter is on how individuals compare and match suprathreshold contrasts across luminance levels for different stimuli. It investigates how these contrast matching abilities change with age and what this reveals about the adaptability of the visual system. The new measurements challenge widely-held theories about contrast constancy and the measured data quantifies the extent of deviation from contrast constancy for matching at different light levels.
- Chapter 7: Modelling CMFs - Building on the previous chapters, this part of the thesis first test two CMF models from the literature and then proposes a new model that predicts how the HVS judges differences in contrast appearance across very different luminance levels. The new model builds upon ideas from literature and adequately explains features of the measured CMF dataset.

## CHAPTER 1. INTRODUCTION

- Chapter 8: Rod vision - Dedicated to exploring the part of the visual system that allows us to see in dim light, this chapter proposes new colour different metrics in the context of rod vision. It utilises contrast sensitivity datasets to validate the performance of the proposed colour metrics.
- Chapter 9: Conclusions - The concluding chapter synthesises the findings from the empirical and modelling work. It highlights the main findings from the original research presented throughout the thesis, the implications of the study for both theory and practice, suggested pathways for future research, and the novel contributions of the thesis to the field of human visual perception.

### 1.3 Published Content and Contributions

The following publications are included as part of this thesis. Most of the work presented in this thesis has been produced in collaborative projects and I have indicated my own and my colleagues' contributions.

S. Wuerger, M. Ashraf, M. Kim, J. Martinovic, M. Perez-Ortiz, and R. K. Mantiuk, “Spatio-chromatic contrast sensitivity under mesopic and photopic light levels,” *Journal of Vision*, vol. 20, no. 4, pp. 1–26, 2020. doi: 10.1167/jov.20.4.23.

SW, RM and JM designed the experiment. RM built the HDR displays used in the experiment. MA collected the data in Liverpool with help from research assistants; RM and MK managed the data collection in Cambridge. MA and MK analysed the data and made the figures. MA developed the computational model with help from RM and MK with input from SW and JM. All authors contributed to the writing and proofreading.

Some contents of this paper are reproduced and incorporated in Chapters 2, 3, 4, and 5.

---

M. Ashraf, S. Wuerger, M. Kim, J. Martinovic, and R. K. Mantiuk, “Spatio-chromatic contrast sensitivity across the lifespan: Interactions between age and light level in high dynamic range,” in *Color and Imaging Conference*, Society for Imaging Science and Technology, vol. 2020, 2020, pp. 65–69. doi: 10.2352/issn.2169-2629.2020.28.10.

MA analysed the data and was the main contributor to the manuscript. All other co-authors proofread the manuscript and offered advice and feedback throughout the project.

## CHAPTER 1. INTRODUCTION

Some contents of this paper are reproduced and incorporated in Chapters 2, 4, and 5.

---

M. Ashraf, R. K. Mantiuk, J. Martinovic, and S. Wuerger, “Suprathreshold contrast matching between different luminance levels,” in *Color and Imaging Conference*, Society for Imaging Science and Technology, vol. 2022, 2022. doi: 10.2352/CIC.2022.30.1.38.

MA designed the psychophysical experiment and collected data in Liverpool with help from research assistants. RM managed data collected in Cambridge. MA analysed the data and was the main contributor to the manuscript. All other co-authors proofread the manuscript and offered advice and feedback throughout the project.

Some contents of this paper are reproduced and incorporated in Chapters 2, 3, and 6.

This paper received the Best Paper Award at CIC’22.

---

M. Ashraf, R. K. Mantiuk, G. Finlayson, A. Kucuk, and S. Wuerger, “Colour Difference Formula for Photopic and Mesopic Vision Incorporating Cone and Rod Responses,” in *London Imaging Meeting*, Society for Imaging Science and Technology, vol. 2022, 2022, pp. 79–83. doi: 10.2352/lim.2022.1.1.18.

MA analysed the data and was the main contributor to the manuscript. All other co-authors proofread the manuscript and offered advice and feedback throughout the project.

Contents of this paper are reproduced and incorporated in Chapter 8.

---

M. Ashraf, R. K. Mantiuk, and A. Chapiro, “Modelling contrast sensitivity of discs,” in *Human Vision and Electronic Imaging*, Society for Imaging Science and Technology, vol. 2023, 2023. doi: 10.2352/EI.2023.35.10.HVEI-246.

MA designed the psychophysical experiment and collected data in Liverpool. RM managed data collected in Cambridge. MA analysed the data and produced the figures, MA and RM developed the computational models and wrote the manuscript. All co-authors proofread the manuscript and offered advice and feedback throughout the project.

Some contents of this paper are reproduced and incorporated in Chapters 4, and 5.

## BACKGROUND AND LITERATURE REVIEW

### 2.1 The Human Visual System (HVS)

Human visual perception is an incredibly complex and non-linear system. Light is transduced into perceptually meaningful sensory input after passing through various stages of the visual system. The different sites comprising the visual system can be classified into four main categories: i) the ocular media, ii) the retina, iii) the post-retinal and pre-cortical visual pathways, and iv) the visual cortex. Here in this section, the components of the visual system included in the optical system and the retina are included as the data presented in the thesis is presented in the context of low-level vision. Higher-order post-retinal and cortical mechanisms are not explicitly included in the models presented in this thesis.

#### 2.1.1 Ocular media

Any input to the visual system first passes through the various ocular media, i.e., the transparent substances in the eye. These include the cornea, aqueous humour, pupil, lens, and vitreous humour. The optical elements of the eye can be thought of as the hardware responsible for physically collating, focusing and regulating the amount of light to be received by the retina. The functions performed by these optical components can be summarised as follows:

- *Focusing:* The cornea, aqueous humour, and the crystalline lens are all convex lenses that collect the light entering the eye from the entire field of view (FOV) and focus it on the retina. The curvature of the cornea and the lens as well as the change in the refractive index as light passes from air to the aqueous humour help in achieving this.
- *Flux regulation:* The pupil is the opening between the aqueous humour and the lens which determines the amount of light entering the eye. The size of the pupil is controlled by the iris (the coloured part of the eye) which, in general, expands in dim light and contracts in bright light. The diameter of the pupil can change from approximately 1mm to 9mm.
- *Accommodation:* The lens in the HVS can change shape (via ciliary muscles) and consequently change its focal length. This ability to selectively focus at different

## CHAPTER 2. BACKGROUND AND LITERATURE REVIEW

viewing distances is called accommodation.

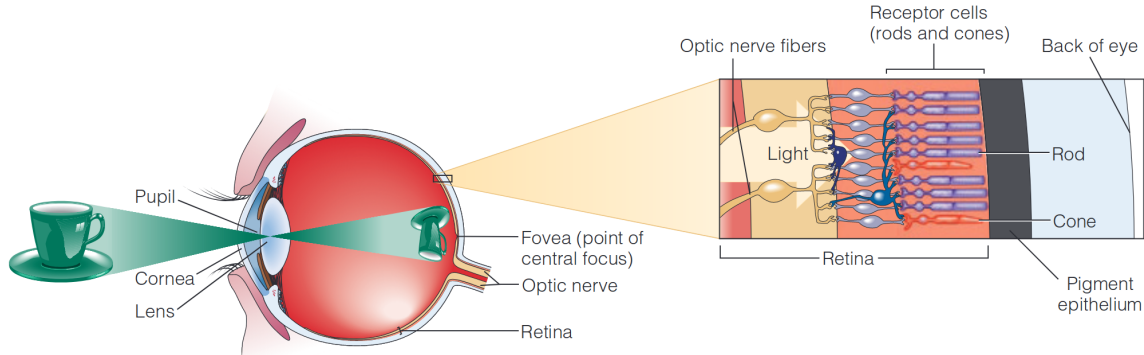


Figure 2.1: The optical media and the retinal structure in the human eye. Figure source: Goldstein and Cacciamani [6].

### 2.1.2 The Retina

Light, after passing through the optical components, reaches the retina where an array of photoreceptors convert it into electrical (neural) signals. There are two main types of photoreceptors; rods and cones. Their main physiological and functional characteristics are summarised in Table 2.1:

Table 2.1: Comparison of Rods and Cones in the Human Retina

<i>Rods</i>	<i>Cones</i>
Are composed of rhodopsin protein.	Are composed of three different types of photopsins; red-opsin, green-opsin, and blue-opsin.
Can respond to even a single photon [7] and are consequently much more sensitive than cones. Rods have a much higher pigment concentration and a much lower baseline noise level (dark light).	Need more photons to produce a response because the concentration of pigments as well as the magnitude of signal amplification in cones is lower. Additionally, the magnitude of dark light noise produced by cones is higher than the response produced by single photons.

## CHAPTER 2. BACKGROUND AND LITERATURE REVIEW

Produce monochromatic response.	Produce chromatic (colour) response, roughly corresponding to red (L: long wavelength-sensitive cones), green (M: medium) and blue (S: short).
Are only operational under low (scotopic: $<0.001 \text{ cd/m}^2$ ) to medium (mesopic: $0.001 \text{ cd/m}^2 \sim 3 \text{ cd/m}^2$ ) light conditions [8].	Are operational under medium (mesopic) to high (photopic: $>3 \text{ cd/m}^2$ ) light conditions [8].
Make up 95% of the photoreceptors in the retina and are mainly present in the parafoveal and peripheral regions.	Make up only 5% of the photoreceptors and are mainly concentrated in the fovea.
Have a low spatial acuity as a large number of rod responses are pooled in the same interneuron.	Have very high spatial acuity as only a few cones feed their responses to a single ganglion cell.
Have a slow temporal response and the signal takes longer to integrate.	Have very fast temporal response (100 Hz and higher [9]) and the signal integration time is much shorter.
Show slower light adaptation following the square-root law [10].	Show rapid light adaptation following Weber's law [11].
Start to saturate at mesopic light levels and become fully deactivated in photopic conditions because of bleaching of the rhodopsin pigment.	Saturate transiently at high light levels but rapidly recover.
Have lower contrast sensitivity.	Have higher contrast sensitivity.
Have a higher recovery time from bleaching.	Recover much more rapidly after full bleaching [12].
Can catch photons incident from any direction.	Can only detect photons at specific angles of incidence [13].

The light incident on the retinal photoreceptors is then transduced or turned into electrical signals which are then passed on to postreceptoral mechanisms. Figure 2.2 shows some

## CHAPTER 2. BACKGROUND AND LITERATURE REVIEW

examples of synaptic connections facilitating signal transmission from rods and cones to the retinal ganglion cells (RGCs).

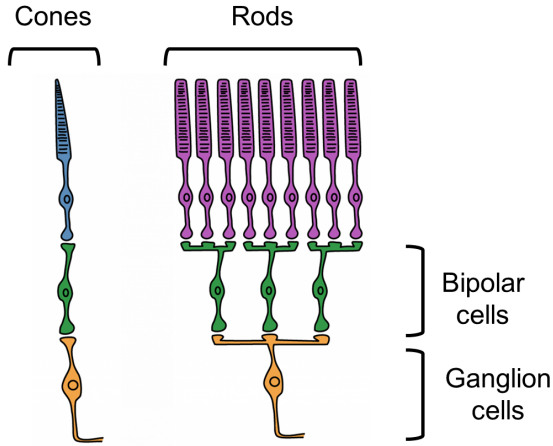


Figure 2.2: Synaptic convergence of rods vs. cones photoreceptors. Rods have higher convergence, i.e., the responses of more individual rod photoreceptors are pooled to fewer bipolar cells and subsequently to the retinal ganglion cells. Cones, on the other hand, have a much lower convergence ratio and in fovea, most cones have one-to-one convergence with the corresponding ganglion cells. Figure adapted from Henley [14].

### 2.2 Psychophysics

Psychophysics is a sub-branch of experimental psychology, the foundations of which are attributed to the polymath scientist and philosopher, Gustav Fechner [15]. It can be described as the investigation of quantitative relationships between physical stimuli and the corresponding responses of our perceptual systems (vision, hearing, smell, etc.). Psychophysical methods encompass the various techniques of presenting the stimuli, varying the stimuli along their specific physical parameters and measuring the responses of the perceptual systems. In contrast to neurophysiological measures, such as EEG, psychophysics does not focus on the specific sites of sensation but records the behavioural response. All the work included in this thesis uses psychophysical methods.

#### 2.2.1 Method of Adjustment

The method of adjustment is a psychophysical technique where the participant adjusts a stimulus until it reaches a certain threshold, such as just noticeable difference (JND) or the point of subjective equality (PSE). This method allows for direct interaction with the stimulus, providing an intuitive measure of perceptual thresholds [16]. However, it is subject to variability due to the reliance on the participant's response time and decision-making

## CHAPTER 2. BACKGROUND AND LITERATURE REVIEW

strategy [17].

### 2.2.2 Forced-choice Methods

Forced-choice methods require the participant to choose between two or more alternatives, often used in conjunction with adaptive procedures to efficiently and quickly estimate the threshold. One of the most prominent forced-choice adaptive methods is QUEST [18], which uses a Bayesian strategy to estimate the threshold based on the participants' responses. It adjusts the difficulty level of successive trials to quickly converge on the most likely threshold estimate.

### 2.2.3 Method of limits

The method of limits is often used to measure an individual's sensory thresholds. In this method, a stimulus is gradually increased or decreased until the participant can or cannot perceive it, respectively. The process involves presenting a series of stimuli in ascending and descending sequences. In the ascending sequence, the stimulus intensity is increased from below the threshold level until the participant reports detection. Conversely, in the descending sequence, the stimulus intensity starts above the threshold and is reduced until the participant can no longer detect it. The threshold is typically determined by taking the average of the values at which the participant's responses change from 'no detection' to 'detection' (in ascending trials) and from 'detection' to 'no detection' (in descending trials). This method is known for its efficiency but can be influenced by the participant's anticipation or adaptation to the stimuli [16].

### 2.2.4 Method of constant stimuli

Instead of progressively changing the stimulus intensity like in the method of limits, this method involves presenting the participant with a set of stimuli of fixed intensities, randomly ordered across trials. These intensities span both below and above the presumed threshold level. The participant's task is to indicate whether they can detect the stimulus in each trial. Unlike the Method of Limits, the stimulus intensity is not adjusted based on the participant's responses. After a sufficient number of trials, the proportion of 'detection' responses is calculated for each stimulus intensity. A psychometric function is then plotted, representing the detection probability as a function of stimulus intensity. The threshold is often defined as the intensity at which detection occurs 50% of the time. This method is less susceptible to the effects of anticipation and adaptation but requires more trials to achieve reliable results [19].

### 2.2.5 Psychometric functions

Psychometric functions are fundamental tools in psychophysics, used to describe the relationship between the physical characteristics of stimuli and the psychological responses they evoke in observers. These functions typically plot the probability of a given perceptual response as a function of some variable stimulus characteristic, such as intensity, frequency, or contrast. A psychometric function may take various forms but often follows a sigmoid shape, reflecting the probabilistic nature of sensory and perceptual processes. The most common model used to describe psychometric functions is the cumulative distribution function of a normal distribution, known as the cumulative Gaussian function. This model captures the idea that as the stimulus intensity increases, the probability of detecting or correctly identifying the stimulus also increases, following a smooth, S-shaped curve. The slope of the psychometric function reveals the participant's sensitivity to changes in the stimulus, and thresholds are estimated at the desired probability of detection. [20].

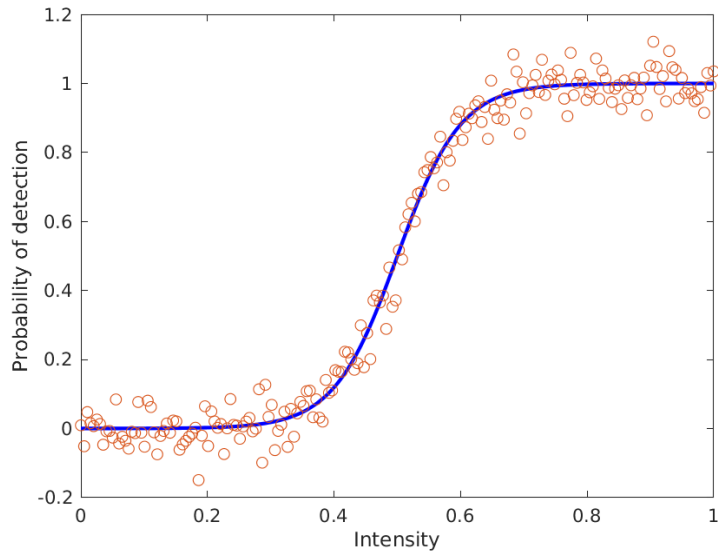


Figure 2.3: Example psychometric function fitted to the data from psychophysical trials.

### 2.3 Contrast vision

Contrast is defined as the perceived difference between the intensity of two adjacent areas. Figure 2.4 shows examples of sinusoidal gratings with high and low contrasts. The top two images depict the contrast between the light and dark areas of the image, also known as luminance contrast. When the stimulus is only modulated along the lightness/brightness axis, the colour (hue) remains unaffected, and thus this kind of modulation can also be called

## CHAPTER 2. BACKGROUND AND LITERATURE REVIEW

achromatic contrast. The bottom two images show colour differences with respect to a neutral background, also known as chromatic contrast. For chromatic contrast, the luminance of both the coloured areas (red and green) is kept constant (isoluminance) to avoid the brightness component and measure pure colour contrast discrimination. The different mathematical representations of contrast are later described in more detail in Section 3.2.

### 2.4 Contrast sensitivity

The visual system's capacity to interpret and understand the environment is highly sophisticated, encompassing a range of mechanisms that operate across various levels of light intensity, at different spatial and temporal scales, at various positions on the retina, and for a spectrum of colours, among various other environmental and stimulus properties. Threshold contrast vision is concerned with the minimum intensity difference between an object and its background necessary for detection. It is the baseline at which stimuli become visible, a concept that has been extensively studied in early psychophysical research. Threshold vision is crucial for the initial detection of stimuli, serving as the gateway for all subsequent visual processing. They are typically derived by measuring the minimum detectable contrast of sinusoidal gratings at various spatial frequencies, revealing the bandwidth of visual processing. The CSF peaks at intermediate spatial frequencies and falls off towards higher and lower frequencies, reflecting the visual system's filtering properties [21]. The mathematical inverse of the measured threshold contrast is called 'contrast sensitivity'. Quantitatively, higher contrast sensitivity means that the stimulus can be detected at low physical contrast values. Similarly, lower contrast sensitivity means that higher contrast values are required to be able to perceive that stimulus. Figure 2.5 shows examples of achromatic CSFs for different luminance levels.

There have been several studies reporting contrast sensitivity functions across a range of parameters including spatial frequency [21]–[23], chromatic directions [24], [25], luminance [26]–[28], eccentricity [29], [30], temporal frequency [22], [23], stimulus size [31], age [32], [33], etc. In the following subsections, the current state-of-the-art of the contrast sensitivity literature for different visual parameters is described.

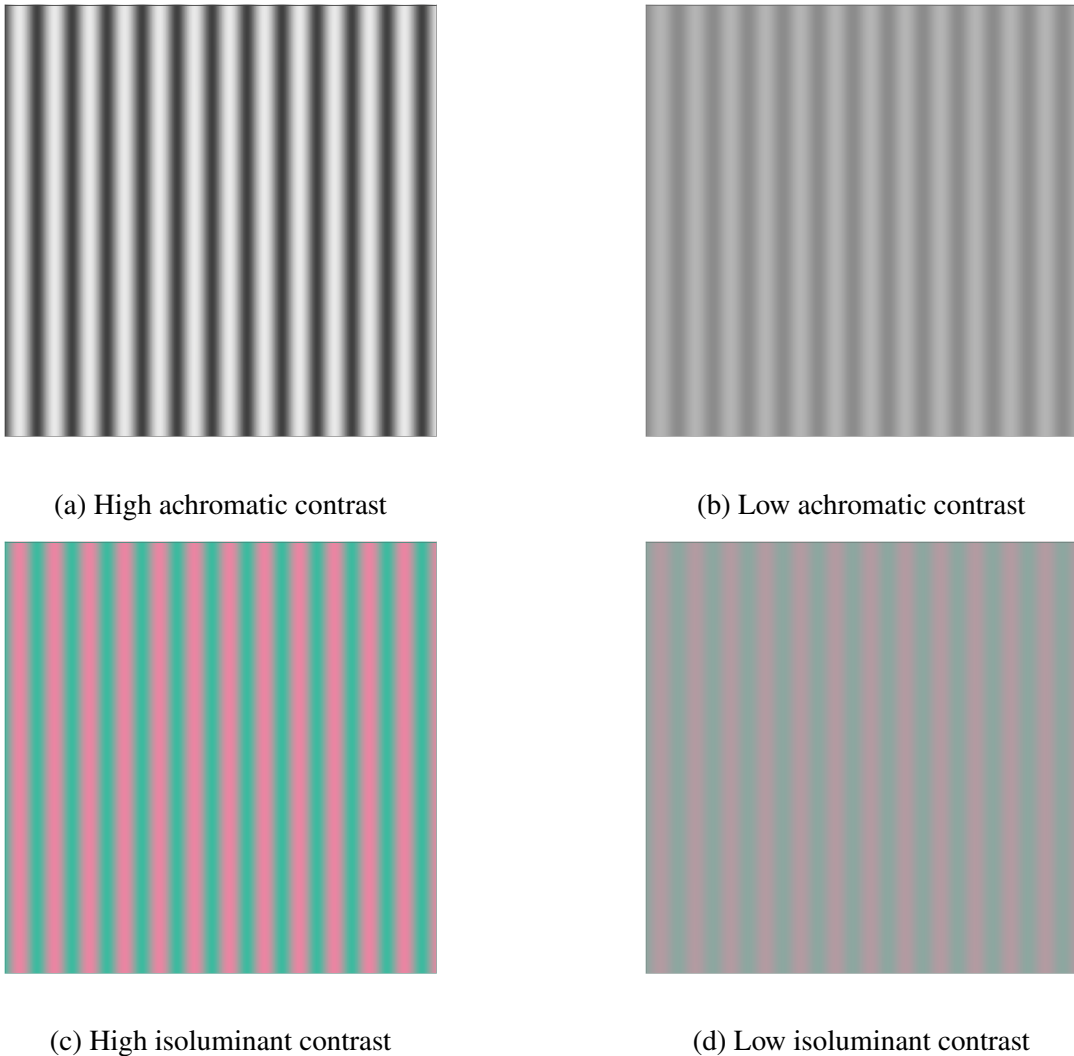


Figure 2.4: Sinusoidal gratings representing high and low contrast examples for achromatic and isoluminant chromatic stimuli.

#### 2.4.1 Spatial contrast vision

Spatial contrast sensitivity is one of the most basic measures of visual performance: it determines the minimum contrast required for observers to detect spatial patterns at different spatial scales. Spatial contrast sensitivity functions (CSFs) have applications in clinical settings as well as in optimising display technologies based on the known limitations of the human visual system. For that reason, CSFs have been studied extensively since the seminal paper by Campbell and Robson [21]. Early measurements of spatial visual sensitivity have focused on spatial resolution and spatial acuity (*e.g.*, [34]) and summation of signals across space (Ricco's law; [35]). Campbell and Robson [21] were the first to use principles of

## CHAPTER 2. BACKGROUND AND LITERATURE REVIEW

Fourier analysis to study spatial sensitivity and introduced the contrast sensitivity function, which is the reciprocal of the threshold contrast over a range of spatial frequencies. Progress has been made in our understanding of how spatial sensitivity varies with eccentricity [29], pattern size [31], [36], spatial orientation [37] and mean luminance level [26], [27]. The majority of these studies have focused on contrast sensitivity for achromatic image variations and a comprehensive model for achromatic spatial detection mechanisms has been proposed by Watson and Ahumada [38].

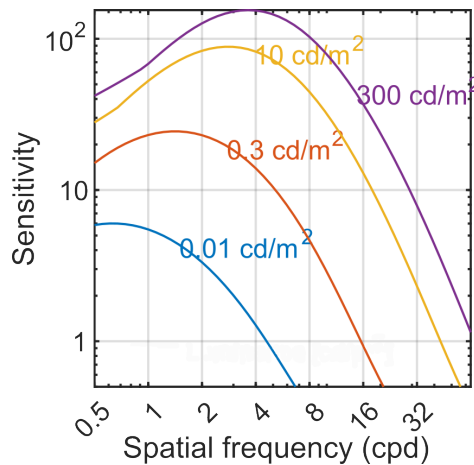


Figure 2.5: Example CSFs for different luminance levels, adapted from Ashraf *et al.* [39].

### 2.4.2 Colour contrast vision

The contrast sensitivity function for chromatic modulations has been studied to a lesser degree, with some notable exceptions [40]–[49]. The most extensive set of chromatic contrast sensitivity measurements come from Mullen [24] and Anderson *et al.* [30], who have assessed the contrast sensitivity for isoluminant red-green and S-cone isolating (lime-violet) gratings with individually adjusted isoluminant points to isolate chromatic channels and silence the luminance-driven mechanisms. Sekiguchi *et al.* [50] employed interference fringes to measure chromatic and luminance contrast sensitivity, thereby eliminating optical blur in addition to chromatic aberration; their contrast sensitivity data are in agreement with the measurements by Anderson *et al.* [30].

### 2.4.3 Effect of luminance

The majority of CSF studies have focused on contrast sensitivity at modest photopic light levels (usually ranging from about 10 to 50  $\text{cd}/\text{m}^2$ ). In the natural environment, our visual system needs to operate over a large dynamic range, from starlight to bright sunlight. This is achieved by light adaptation within the retina which ensures a useful dynamic range in

## CHAPTER 2. BACKGROUND AND LITERATURE REVIEW

the cone photoreceptor system [8]. Van Nes and Bouman [26] measured spatial contrast sensitivity over a wide range of retinal illuminances (from 0.0009 to 5,900 trolands) and observed that contrast sensitivity increases steadily with ambient illumination, up to about 900 trolands, where the sensitivity seems to saturate, reflecting light adaptation in the cone receptors. Secondly, contrast sensitivity for low spatial frequencies saturates earlier (at around 0.09 trolands) than for higher spatial frequencies, probably reflecting a decrease in spatial integration with increasing light levels. Adaptation to light and darkness is a remarkable feature of the human visual system, allowing it to operate over a vast range of luminance levels. Light adaptation involves the adjustment of the eye to bright conditions, reducing the sensitivity to prevent oversaturation, as suggested by Wald [51]. Dark adaptation, in contrast, sees the visual system increase its sensitivity in low light, enabling the detection of stimuli in darker conditions, a process extensively detailed by Hecht *et al.* [7].

### 2.4.4 Effect of age

Ageing in humans, as in most organisms, is accompanied by the deterioration of a number of physiological functions including vision [52]–[55]. Ageing affects the human visual system in a myriad of ways and at multiple stages, from degradation of the optics to a decline in various sensory and perceptual processing mechanisms. Some of the physiological factors that govern functional losses in vision with ageing are loss of photoreceptor cells [56], [57], loss of axons in the optic nerve [58], as well as changes in post-receptoral neural processing [59]. Age-related optical factors include an increase in ‘lens absorption (density and pigment discolouration) [60] and an increase in the light scattered in the eye, resulting in lower retinal illuminance and lower perceived contrast respectively, both of which consequently decrease contrast sensitivity [61], [62].

The optics of the eye is a limiting factor for contrast sensitivity at higher spatial frequencies, and age-related optical changes play a major role in explaining the decline in contrast sensitivity with age [54], but it is likely that the loss of neurons or decreased neural efficiency are also contributing to age-related contrast sensitivity losses [63]–[66]. Another factor associated with an age-related reduction in retinal illuminance is senile miosis, that is, at low (mesopic) light levels, the pupil size of older adults is significantly reduced. However, senile miosis does not underlie the age-related sensitivity loss, as shown by Sloane *et al.* (1988) who measured contrast sensitivity functions with natural and dilated pupils at different light levels for young and old observers. A smaller pupil may indeed be beneficial by limiting the optical aberrations in the presence of age-induced increased intraocular light scatter [67], and may to a small extent counteract the age-related optical changes.

## CHAPTER 2. BACKGROUND AND LITERATURE REVIEW

### 2.4.5 Effect of size

The contrast sensitivity for periodic stimuli is known to depend on the number of cycles displayed [68]. Gratings with fewer cycles result in higher contrast thresholds, suggesting summation across cycles and/or spatial extent [69] until a critical summation area has been reached [70]. The effect of stimulus area and number of cycles has been studied both in the fovea and the periphery, primarily for achromatic gratings [71]. Studies using chromatic stimuli reported sub-threshold spatial summation to be similar for achromatic and red-green gratings [50], but show a different dependence on eccentricity [72] and larger integration areas for S-cone isolating gratings [73].

### 2.4.6 Interplay of different factors affecting CSF

The peak sensitivity of CSFs or the stimulus that the eyes see best at different combinations of stimulus and environmental factors can reveal the spatial-chromatic receptive field structure of the visual neurones that detect that stimulus. Watson *et al.* [74] searched a large parameter space and concluded that, for achromatic sinusoidal modulations presented on a high luminance background ( $340\text{ cd/m}^2$ ), the optimal spatial frequency was at 6 cpd and could be detected at a threshold contrast of 1.44%. Chaparro *et al.* [75] generalised their study by including chromatic and achromatic stimuli of various stimulus sizes and durations, presented on a bright yellow background (3000 trolands). The optimal duration and stimulus size was greater for the chromatic spots compared to the achromatic ones, consistent with greater temporal and spatial summation. However, even for the non-optimal parameter settings, the threshold contrasts for chromatic variations were consistently lower (by a factor of 5-9) than for achromatic spots. The lowest threshold contrast was 0.7% for chromatic stimuli and 3% for achromatic variations.

## 2.5 Suprathreshold contrast vision

The previous section discussed the literature on different aspects of contrast sensitivity or the threshold contrast vision of the human visual system. However, most of our daily visual experiences do not occur at this borderline of visibility; they occur well above it, in what is known as suprathreshold contrast vision. Unlike simple detection, suprathreshold sensitivity measures the ability to perceive and characterise (spatial, chromatic, temporal, etc.) contrasts when stimuli are well above the level at which they can be just barely seen. This level of vision encompasses the vast majority of our visual experiences, where the contrast between objects and their background is significantly greater than the minimum detectable levels. Suprathreshold contrast vision is integral to tasks that require the discrimination of details

## CHAPTER 2. BACKGROUND AND LITERATURE REVIEW

within the visual scene, such as texture segregation, edge detection, and pattern recognition, which are essential for complex visual tasks like reading, face recognition, and navigating through our environment. In the following subsections, the literature regarding different techniques of measuring contrast matching, the concept of contrast constancy, and how suprathreshold vision is affected by the ageing of the visual system is discussed.

### 2.5.1 Measuring Suprathreshold Contrast

Suprathreshold contrast vision is typically measured using various psychophysical techniques that require observers to evaluate and respond to visual stimuli of different contrast levels that are clearly above their threshold of detection. These techniques can be broadly classified into methods focusing on direct comparison and those based on adaptive adjustments.

#### *Direct Comparison Methods*

- **Contrast Matching (Subtype of Pairwise Comparison):** In contrast matching tasks, observers adjust the contrast of a variable stimulus until it matches the perceived contrast of a fixed reference stimulus. This method is a specialized form of pairwise comparison where one stimulus remains constant while the other is adjusted to match it. This paradigm is used in our suprathreshold contrast studies, discussed in more detail in Section 3.4.2.
- **Contrast Discrimination (Subtype of Pairwise Comparison):** This technique involves presenting observers with pairs of stimuli at slightly different contrast levels and asking them to identify the stimulus with the higher contrast. This method determines the smallest perceivable difference in contrast, known as the just noticeable difference (JND). It's another form of pairwise comparison focusing on detecting minute differences between stimuli.
- **Pairwise Comparison:** In this general approach, observers are shown pairs of stimuli in quick succession and asked to report which of the two appears more contrasted. This method ranks stimuli by perceived contrast and creates psychometric functions. Contrast matching and discrimination can be seen as specific applications of this broader technique.
- **Magnitude Estimation:** Observers assign numerical values to the perceived contrast of different stimuli. The provided numbers are proportional to the subjective experience of contrast, enabling the construction of a perceived contrast scale. This

## CHAPTER 2. BACKGROUND AND LITERATURE REVIEW

method relies on the observer's ability to quantify their perception, offering a different dimension of contrast evaluation compared to pairwise methods.

### *Adaptive Methods*

- **Staircase Procedures:** Adaptive methods, such as the staircase procedure, are used to converge on a contrast level that corresponds to a specific point on the psychometric function, like the threshold for contrast detection or the point of subjective equality. These methods adjust the stimulus contrast based on the observer's responses, refining the level until the target contrast is determined accurately.

Each of these techniques can be modified to assess different aspects of suprathreshold contrast vision, such as the influence of spatial frequency, viewing distance, color, adaptation state, and ambient lighting conditions. The choice of technique depends on the specific aspect of contrast vision being investigated and the desired precision of the measurements.

### **2.5.2 Contrast constancy**

Georges and Sullivan coined the term 'contrast constancy' in their seminal work [76]. They found that at suprathreshold levels, the contrast of the stimuli matched across different spatial frequencies, orientation, and retinal eccentricities was perceptually the same when the physical contrast (e.g., Michelson contrast) had the same value. Similar results are reported in other studies [77]–[79]. Kulikowski proposed a simple mathematical model and explanation for the contrast constancy phenomenon in matching across spatial frequency. Kulikowski's contrast matching model postulates that the difference in perceived contrast can be explained by the difference in contrast detection thresholds between two luminance levels. Specifically,

$$C_1 - C'_1 = C_2 - C'_2 \quad (2.1)$$

where,  $C_1$  and  $C_2$  are the suprathreshold contrasts of the two stimuli at two different luminance levels, and  $C'_1$  and  $C'_2$  are the contrast detection thresholds at the corresponding luminance levels. If  $C_1$  and  $C_2$  are sufficiently large (high suprathreshold contrasts) then the difference between their thresholds can be considered negligible and Equation 2.1 becomes  $C_1 \approx C_2$ . The model predicts the across-spatial frequency contrast matching functions quite well [79].

Kulikowski's work showed that the model represented in Equation 2.1 was also valid for contrast matching of a 5 cpd grating across a 2 log unit luminance range for multiple suprathreshold levels. Hess' work also showed similar results qualitatively for a smaller

## CHAPTER 2. BACKGROUND AND LITERATURE REVIEW

luminance range [80]. For low luminance backgrounds or low contrast stimuli, their lines of matching contrasts appear to deviate from the constancy line but the quantitative deviation in terms of threshold differences is not reported. Later studies by Peli *et al.* showed that the assumption of contrast constancy while matching across luminance levels was not valid for a wider luminance range under natural viewing [81], [82]. They attributed the deviation from constancy to differences in viewing conditions; differences between theirs and Kulikowski's results disappeared when similar methodologies (haploscopic viewing with longer adaptation times) were employed. However, the relevant data points only spanned 1 log unit range of luminances (Figure 6 in [82]). A later study by Peli showed that the shape of across-luminance contrast matching lines also depended on spatial frequency [83]. Although they used natural viewing conditions (no adaptation period and both eyes could see both stimuli simultaneously), their results implied that a more complex model of contrast matching was required, also taking the spatial configuration of stimuli into account.

All the aforementioned studies dealt with suprathreshold contrast in achromatic channels only. A study by Tiippuna *et al.* [84] demonstrated that the principle of contrast constancy also held for chromatic contrasts when matching across spatial frequencies. Delahunt *et al.* [85] confirmed that contrast constancy in chromatic matches across spatial frequencies holds true for different luminance levels as well. However, their work did not investigate chromatic contrast constancy when matching across different luminance levels. In the present literature no work was found, that investigates contrast matching across luminance for chromatic stimuli.

Some work has been done to integrate models of contrast matching and contrast sensitivity in image retargeting algorithms. Wanat and Mantiuk [86] proposed a cross-luminance simulation framework for complex images. The model uses analytical contrast sensitivity and contrast matching functions. The contrast matching functions across luminance are adapted from Kulikowski [79]'s model in a log contrast space. However, the model is not verified experimentally on a dataset. Their model takes contrast thresholds of the stimuli into account and although the threshold values are different for different spatial patterns, the same contrast matching function model is assumed regardless of spatial configuration. The model also takes only achromatic contrast mechanisms into account. Ensuing work by Rezagholizadeh *et al.* [87] uses Shin *et al.* [88]'s mesopic vision model to retarget images between different luminance levels and their framework applies to all colour channels. However, their methodology assumes no spatial dependence and only considers colour values in isolation. Therefore, our study can empirically verify the current contrast matching

## CHAPTER 2. BACKGROUND AND LITERATURE REVIEW

functions widely used in the literature and provide a dataset that can act as the basis for a more accurate data-driven model.

### 2.5.3 Effect of age

Age-related optical and neural changes affect both colour and spatial vision, but differently for threshold and supra-threshold stimuli. While the perception of hue [89], [90] and perceived saturation [91] is fairly constant across the lifespan, chromatic discrimination sensitivity declines with an increase in age [92], [93]. This constancy across the lifespan has been explained by compensatory mechanisms for supra-threshold stimulus levels, and similar mechanisms might be at work for contrast sensitivity at the threshold and perceived supra-threshold contrast. For spatio-temporal contrast vision, perceived contrast at supra-threshold levels is unaffected by ageing [94], while the spatio-temporal contrast sensitivity declines with advanced age, with the decline being primarily due to the loss in spatial frequency sensitivity.

## 2.6 Stimuli in Vision Science Experiments

Psychophysical experiments serve as a bridge between the subjective experience of vision and the objective measurements of the visual system's capabilities. These experiments designed to investigate human visual processing often employ a diverse array of stimuli that mimic or abstract the various components and stages of the visual system's processing pipeline, ranging from the detection and discrimination of simple patterns to the perception of complex, real-world scenes. These stimuli are designed to activate specific aspects of visual perception, allowing us to independently understand the underlying mechanisms that govern how visual information is encoded, processed, and interpreted by the brain.

### 2.6.1 Gabor patches

A primary example of such stimuli is the Gabor patch, named after the seminal work by the illustrious scientist D. Gabor [95]. These are essentially sine/cosine modulated signals of specific spatial (or temporal) frequency enveloped with a Gaussian function. The one-dimensional Gabor signal is represented in [96] as follows:

$$S(x) = e^{-(x-x_m)^2/4\sigma^2} \cos(2\pi\rho_n(x - x_m)), \quad (2.2)$$

where  $x_m$  is the centre of the spatial location,  $\rho_n$  is the spatial frequency, and  $\sigma$  is the standard deviation of the Gaussian envelope of the signal. Figure 2.6 shows some example Gabor patch stimuli with a 2D Gaussian envelope and sinusoidal modulation of luminance along the horizontal axis.

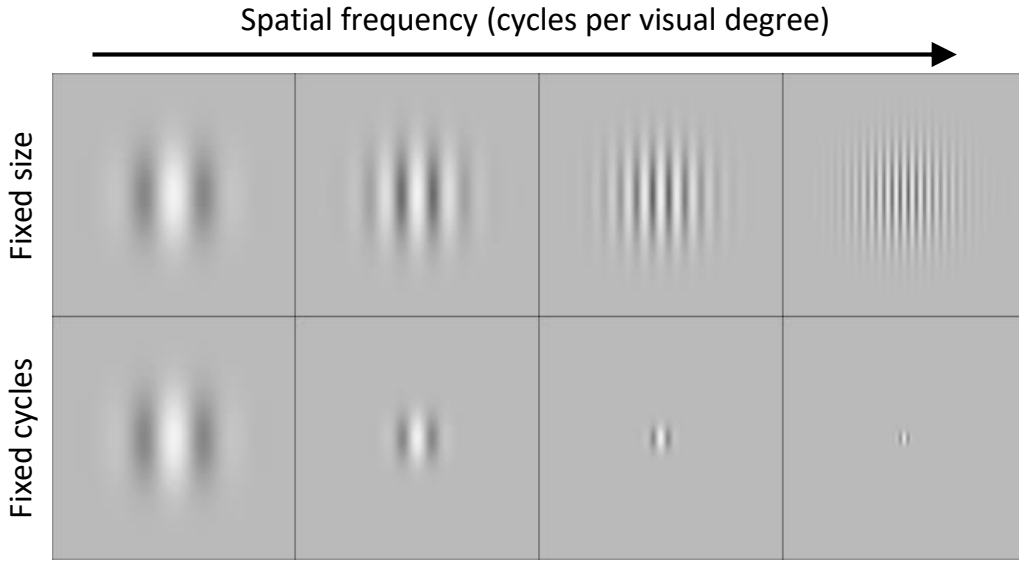


Figure 2.6: Achromatic Gabor patches with increasing spatial frequencies (left to right). The first row shows Gabor patches with fixed spatial size, while the second row shows stimuli with a fixed number of visible cycles with the size of the Gaussian envelope inversely related to the spatial frequency.

The structure of a Gabor patch closely resembles the spatially selective receptive fields of neurons within the visual cortex [96], [97], making them an ideal tool for investigating the visual system’s response to spatial information. The sine-wave modulation of Gabor patches across different spatial frequencies enables the isolation of the response of neurons that are selectively tuned to specific spatial frequencies and highlights the spatial frequency filtering properties of the visual system [21], [98].

When modulated along the luminance axis, Gabor patches undergo variations in intensity while maintaining a constant hue or colour that can elicit responses from the luminance-sensitive neurons in the visual pathway. Conversely, isoluminant Gabor patches maintain a constant luminance across the stimulus, with the sinusoidal modulation driving the colour variations. This is particularly useful in isolating the opponent-colour processing mechanisms, with red-green and yellow-violet isoluminant stimuli frequently employed to tap into the so-called cardinal colour directions, which are foundational to colour perception and discrimination tasks (more details later in Section 3.2). When these colour modulations are properly isolated, the response of chromatic mechanisms can be studied without the confounding influence of luminance changes. Figure 2.7 shows Gabor patches modulating along achromatic, red/green and yellow/violet colour directions for different background colours.



Figure 2.7: Gabor patches modulated along luminance and chromatic directions. The first row shows stimuli along a neutral grey background. The last two rows show stimuli with colour backgrounds. Note that the stimuli in the first column are still considered achromatic when the background is not grey as the variation is along the luminance axis (dark pink to light pink, for example).

### 2.6.2 Additional Stimuli in Visual Psychophysics

Beyond Gabor patches, psychophysical experiments employ a range of other stimuli to investigate different aspects of visual contrast perception. Discs, for example, offer a simple, geometric shape that can be used in various detection and discrimination tasks and are especially useful for measuring sensitivity to sharp edges. Landolt rings, characterised by their circular shape with a small gap, serve as a standard stimulus for assessing visual acuity and spatial resolution. The orientation of the gap can be varied to test the observer's

## CHAPTER 2. BACKGROUND AND LITERATURE REVIEW

sensitivity to orientation changes, providing insights into the orientation selectivity of the visual system. Sinusoidal or square wave gratings, presented within apertures of various shapes (such as circular, rectangular, or elliptical), are employed to investigate the visual system's response to different spatial frequencies and orientations, similar to Gabor patches but without the Gaussian envelope. The Modelfest dataset includes a large variety of the different stimuli used to study the human contrast vision [99].

## METHODOLOGY

This chapter presents the common experimental framework and the analytical techniques used in the data collection and modelling projects included in this thesis. The chapter starts with a detailed description of the apparatus, specifically the state-of-the-art high-dynamic-range (HDR) screens, and the rigorous calibration processes they underwent to ensure precision in the stimuli presentation. Then the theoretical foundations and practical applications of colour and contrast spaces—including LMS (Long, Medium, Short wavelength light), DKL (Derrington, Krauskopf, and Lennie space), and cone contrast spaces are described. Next, the stimuli used and the experimental setups are described, outlining the design and execution of contrast detection and matching experiments including recruitment strategies for observers.

### **3.1 Apparatus**

This section introduces the apparatus and the calibration methodology used in the experiments included in this thesis. Central to the research are two custom-built high-dynamic-range (HDR) displays located in Liverpool and Cambridge. The purpose-built HDR displays provided us with complete control of the stimuli which is critical for vision science studies like ours. The displays were capable of generating very high contrast for both luminance and chromatic stimuli. The working and calibration of the displays are described in the following sections.

#### **3.1.1 HDR screen**

The stimuli were displayed on two custom-built high-dynamic-range (HDR) displays: one in Liverpool (peak luminance:  $4,000 \text{ cd/m}^2$ ) and one in Cambridge (peak luminance:  $15,000 \text{ cd/m}^2$ ). As the two displays were otherwise identical in construction, the display in Cambridge is described and the differences are highlighted. The HDR display consisted of an LCD panel (9.7",  $2048 \times 1536 \text{ px}$  iPad 3/4 retina display; product code: LG LP097QX1) and a DLP projector (Optoma X600 in Cambridge, Acer P1276 in Liverpool; both  $1024 \times 768 \text{ px}$ ). The backlight of the LCD was removed and the DLP acted as the replacement backlight [100]. Because it was possible to modulate both the pixels on the LCD and on the DLP, the maximum contrast that could be achieved was a product of the

## CHAPTER 3. METHODOLOGY

contrast of each display; given 1,000:1 contrast of the LCD and 1,000:1 contrast of the DLP, the maximum contrast of the display was 1,000,000:1.

Several steps were taken to improve the light efficiency and therefore the brightness of the display. The DLP had its colour wheel removed, increasing its brightness by a factor of 3. The colour wheel was unnecessary as the LCD panel was responsible for forming a colour image. The image from the DLP is projected on a diffuser and further modulated by an LCD panel with its backlight removed. A Fresnel lens with the focal length of 32 cm was introduced behind the LCD panel to ensure that most of the light was directed towards the observer.

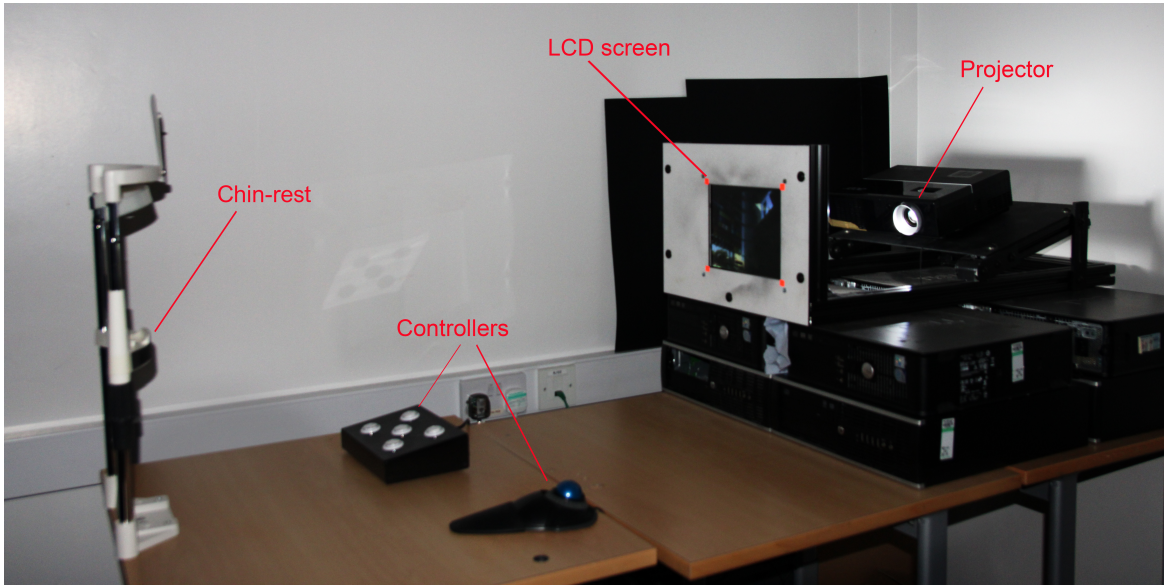


Figure 3.1: HDR display experimental setup in Liverpool.

### *HDR calibration*

The display was calibrated and driven by custom-made software, written in MATLAB and relying on Psychtoolbox and MATLAB OpenGL (MOGL) extensions [101]. The calibration involved displaying a series of grids consisting of dots, individually on the LCD and DLP, photographing them with a DSLR camera (Canon 550D) and finding both homographic and mesh-based transformations between DLP and LCD pixel coordinates. This step ensured an accurate alignment between LCD and DLP pixels.

The colour calibration was performed by measuring display's spectral emission, individually for LCD and DLP, using a spectroradiometer (JETI Specbos 1211 in Cambridge, PhotoResearch PR-670 in Liverpool). CIE 2006 cone fundamentals [102] were used to calculate the

## CHAPTER 3. METHODOLOGY

L, M, and S cone responses as follows:

$$\begin{aligned} L &= 0.689903 \int_{\lambda} l_2(\lambda) E(\lambda) d\lambda, \\ M &= 0.348322 \int_{\lambda} m_2(\lambda) E(\lambda) d\lambda, \\ S &= 0.0371597 \int_{\lambda} s_2(\lambda) E(\lambda) d\lambda, \end{aligned} \quad (3.1)$$

where  $l_2$ ,  $m_2$  and  $s_2$  are  $2^\circ$  cone fundamentals<sup>1</sup> and  $E$  is the measured spectral radiance emitted from the display. The  $l_2$  and  $m_2$  spectra were scaled such that the sum corresponded to luminance and the sensitivity of the S cones was set so that  $s_2(\lambda)/V(\lambda)$  peaks at 1 [102]. All the calculations were based on photopic luminance, including the lowest luminance level of  $0.02 \text{ cd/m}^2$  which was at the lower end of the mesopic range [8].

The responses were fitted to the gain-offset-gamma display model [103] for the LCD and a 1-dimensional look-up table was used for the DLP (since it was achromatic after removing the colour wheel); see Figure 3.2 for the spectral emission of the two HDR displays.

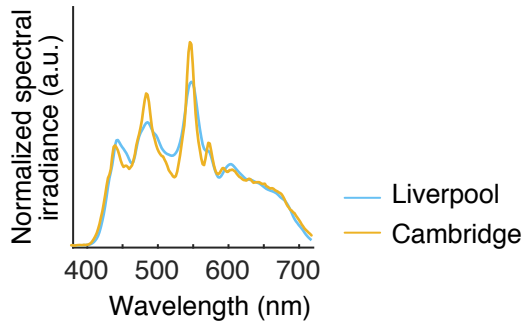


Figure 3.2: Spectral power distributions of the HDR displays.

### 3.2 Colour and contrast spaces

Colour vision is a complex facet of human perception, allowing us to distinguish objects based on the wavelengths of light they reflect or emit. Central to the understanding of colour vision are the colour spaces that provide frameworks for quantifying and describing these visual experiences. In this section, the critical colour and contrast spaces that have been instrumental in understanding colour contrast perception: LMS (Long, Medium, Short wavelength cones) colour space, DKL (Derrington-Krauskopf-Lennie) colour space, and cone contrast space, are discussed.

---

<sup>1</sup>Tabulated cone fundamentals can be found at <http://cvrl.ucl.ac.uk/>

## CHAPTER 3. METHODOLOGY

Before moving on to the description of the colour and contrast spaces used in this work, it is important to address the choice of not isolating chromatic mechanisms for individual observers. Contrast sensitivity function (CSF) models reflecting the visual system of a standard observer afford the generality necessary for practical applications. Due to this, the current study approaches the characterisation of chromatic contrast sensitivity slightly differently from Mullen [24]. Truly isoluminant stimuli are difficult to achieve even when using a heterochromatic flicker paradigm [104]. There are many possible sources of luminance intrusion, including inter-observer variations in  $V(\lambda)$  [105], retinal illuminance [106], chromatic aberration [107], and the variation of the isoluminance point across the visual field [108]. Therefore, rather than experimentally controlling for luminance intrusion, the experiments included in this thesis allowed for the possibility that the stimuli are not perfectly isoluminant for each observer, and included luminance intrusion in the models of chromatic channels. Since the aim here is to provide a model of chromatic contrast sensitivity for an average (standard) observer which would be applicable to complex spatio-chromatic images (*e.g.*, [109]), it is not useful to optimise stimulus parameters for a small set of individual observers.

### 3.2.1 LMS Colour Space

The LMS colour space is a chromatic representation based on the physiological response of the three types of cones in the human retina: Long (L), Medium (M), and Short (S) wavelength-sensitive cones. This colour space is fundamental in vision science as it closely matches the initial stage of colour encoding in the human visual system [110]. Changes in the LMS space can simulate the colour signals that would be sent to the brain, making it a powerful tool for studying colour perception and contrast [111].

The LMS colour space is used to represent the modulation of the three cone classes such that the cone contrasts are identical. This modulation is essential for isolating mechanisms in the visual system and studying how they contribute to colour perception and discrimination. By modulating along the red-green axis and keeping the sum of L and M cone responses constant, researchers can isolate the S cone responses and investigate the underlying mechanisms of colour vision [112].

The LMS space is defined not only by its physiological relevance but also by its ability to be adapted to different conditions and backgrounds, such as the D65 illuminant used in the experiments [113]. This versatility allows for experiments that can closely mimic the variety of visual experiences in everyday life, providing a more accurate understanding of human

## CHAPTER 3. METHODOLOGY

colour vision.

### 3.2.2 DKL colour space

In terms of the stimulus properties, changes along the achromatic direction resulted in all three cone classes being modulated such that the cone contrasts are identical; modulations along the red-green axis leave the excitation of the S cones constant and the excitation of the L and M cones co-varies as to keep their sum constant. Along the third, the yellow-violet direction, only the S cones are modulated. These modulations in colour space are designed to isolate a set of three hypothesised mechanisms: a luminance mechanism ( $R_{\mathcal{L}+\mathcal{M}}$ ), and two cone-opponent colour mechanisms ( $R_{\mathcal{L}-\mathcal{M}}$ ,  $R_{\mathcal{S}-(\mathcal{L}+\mathcal{M})}$ ) as shown in Figure 3.3 [2], [114].

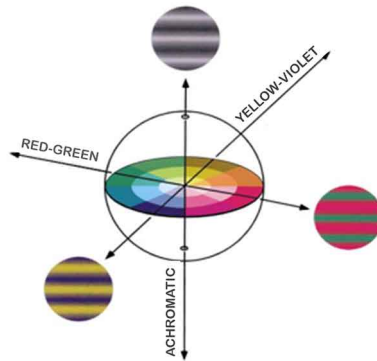


Figure 3.3: DKL colour space with the three modulation directions used in the experiments

The chromatic properties are described in the matrix below (Equation 3.2). The first mechanism, ( $R_{\mathcal{L}+\mathcal{M}}$ ), is the luminance mechanism, which adds up the L and M cone responses (which are normalised such that the sum corresponds to  $V(\lambda)$ ). The second mechanism, ( $R_{\mathcal{L}-\mathcal{M}}$ ), is an L/M opponent mechanism and takes the differences between the weighted incremental L and M cone signals. The third mechanism, ( $R_{\mathcal{S}-(\mathcal{L}+\mathcal{M})}$ ), is another cone-opponent mechanism taking the difference between the incremental S cone signal and the sum of the incremental L and M cones.

$$\begin{bmatrix} \Delta R_{\mathcal{L}+\mathcal{M}} \\ \Delta R_{\mathcal{L}-\mathcal{M}} \\ \Delta R_{\mathcal{S}-(\mathcal{L}+\mathcal{M})} \end{bmatrix} = \begin{bmatrix} 1 & 1 & 0 \\ 1 & -\frac{L_0}{M_0} & 0 \\ -1 & -1 & \frac{L_0+M_0}{S_0} \end{bmatrix} \begin{bmatrix} \Delta L \\ \Delta M \\ \Delta S \end{bmatrix} \quad (3.2)$$

where  $L_0$ ,  $M_0$  and  $S_0$  are the cone responses corresponding to the grey background. Stimuli were modulated around this neutral grey (white) background of a D65 metamer (CIE 1931 x, y = 0.3127, 0.3290).

## CHAPTER 3. METHODOLOGY

The inverse of the above matrix defines the stimulus modulations in LMS space that are required to achieve selective stimulation of the hypothesised mechanisms and is shown below (Equation. 3.3) as explained in Brainard [114]. For example, to isolate the luminance mechanism ( $R_{\mathcal{L}+\mathcal{M}}$ ), the mechanism output vector was set to [1 0 0], which results in changes in all three cone signals. To isolate the cone-opponent mechanism ( $R_{\mathcal{L}-\mathcal{M}}$ ), the response vector was set to [0 1 0] which results in equal L and M cone modulations, but of opposite sign. Finally, to isolate the third opponent mechanism ( $R_{\mathcal{S}-(\mathcal{L}+\mathcal{M})}$ ), the response vector is set to [0 0 1], resulting only in S cone modulations. The matrix that maps the mechanisms' output into the LMS modulations depends on the chromaticity of the background. Equation. 3.4 shows the matrix used in the experiments. The desired LMS modulations can then be converted to linearized RGB.

$$\begin{bmatrix} \Delta L \\ \Delta M \\ \Delta S \end{bmatrix} = \begin{bmatrix} \frac{L_0}{L_0+M_0} & \frac{M_0}{L_0+M_0} & 0 \\ \frac{M_0}{L_0+M_0} & -\frac{M_0}{L_0+M_0} & 0 \\ \frac{S_0}{L_0+M_0} & 0 & \frac{S_0}{L_0+M_0} \end{bmatrix} \begin{bmatrix} \Delta R_{\mathcal{L}+\mathcal{M}} \\ \Delta R_{\mathcal{L}-\mathcal{M}} \\ \Delta R_{\mathcal{S}-(\mathcal{L}+\mathcal{M})} \end{bmatrix} \quad (3.3)$$

$$\begin{bmatrix} \Delta L \\ \Delta M \\ \Delta S \end{bmatrix} = \begin{bmatrix} 0.6981 & 0.3019 & 0 \\ 0.3019 & -0.3019 & 0 \\ 0.0198 & 0 & 0.0198 \end{bmatrix} \begin{bmatrix} \Delta R_{\mathcal{L}+\mathcal{M}} \\ \Delta R_{\mathcal{L}-\mathcal{M}} \\ \Delta R_{\mathcal{S}-(\mathcal{L}+\mathcal{M})} \end{bmatrix} \quad (3.4)$$

To achieve comparable response units in these three mechanisms, the responses could be scaled such that the response for each mechanism is unity for a stimulus of unit pooled cone contrast. However, all these scaling procedures are to a large extent arbitrary [115]. Therefore, the length in cone contrast space (Equation. 3.5) was used as a measure of stimulus contrast since it allows comparison across different colour directions [5]. The rationale for measuring contrast sensitivity along these three modulation directions in colour space was twofold. First, these modulations were likely to preferentially stimulate early post-receptoral mechanisms. While it was unlikely that cortical mechanisms could be isolated with these colour modulations [116], it still allowed us to characterise the contrast sensitivity for salient and, to some degree, independent mechanisms. Second, it constituted a device-independent definition of the chromatic stimulus modulations and allowed comparisons with previously obtained CSF measurements.

### 3.2.3 Cone contrast space

The cone contrast space is defined by the normalised changes in the cone responses relative to a background, and it is instrumental for quantifying how the human visual system perceives

## CHAPTER 3. METHODOLOGY

colour differences. This space utilises the contrasts of the L, M, and S cones, normalised to the background to define a metric for colour contrast [5]. The use of this space is particularly advantageous as it aligns with the physiological processes of the visual system, allowing for the assessment of contrast sensitivity and other aspects of colour vision [24].

The mathematical representation of the cone contrast space is often given in terms of the differential cone responses  $\Delta L$ ,  $\Delta M$ , and  $\Delta S$ , which are the increments or decrements from the background cone absorptions  $L_0$ ,  $M_0$ , and  $S_0$  respectively [5]. These values are then used to compute the threshold contrast, which provides a measure of the smallest detectable colour difference in the visual system [117] (Equation. 3.5):

$$C_t = \frac{1}{\sqrt{3}} \sqrt{\left(\frac{\Delta L}{L_0}\right)^2 + \left(\frac{\Delta M}{M_0}\right)^2 + \left(\frac{\Delta S}{S_0}\right)^2} \quad (3.5)$$

$C_t$  = Threshold cone contrast

$\Delta L, \Delta M, \Delta S$  = Incremental L,M,S cone absorptions

$L_0, M_0, S_0$  = L,M,S absorptions of the display background

### 3.3 Stimuli

The main stimuli used in all the experiments were Gabor patches created by multiplying a sinusoidal grating with a Gaussian envelope. The Gabor patches were odd-symmetric, that is, the phase was adjusted so that the zero-crossing was exactly in the centre of the stimulus. Achromatic, red-green, or yellow-violet Gabor patches were created by modulating the gratings along one of the three cardinal colour axes in DKL space (Figure 3.3) [2]. Modulations in this colour space can either be described by the stimulus properties reflecting the appearance (achromatic, red-green, yellow-violet) or by the chromatic properties of a set of hypothesised mechanisms that are isolated by these stimulus modulations [114].

The width of the Gaussian envelope relative to the spatial frequency of a Gabor patch is used to generate either fixed-cycle or fixed-size stimuli as shown in Figure 2.6. In the experiments presented in this thesis, the standard deviation of the Gaussian envelope was set to be half of the spatial wavelength ( $\sigma = 0.5 \cdot \frac{1}{f}$  [deg]). Figure 3.4 shows Gabor patches of spatial frequencies 0.5, 1, 2, 4, or 6 cycles per degree of visual angle (cpd). The  $\pm 2\sigma$  region of these Gabor patches subtended  $4^\circ \times 4^\circ$ ,  $2^\circ \times 2^\circ$ ,  $1^\circ \times 1^\circ$ ,  $0.5^\circ \times 0.5^\circ$ , and  $0.33^\circ \times 0.33^\circ$ , respectively.

## CHAPTER 3. METHODOLOGY

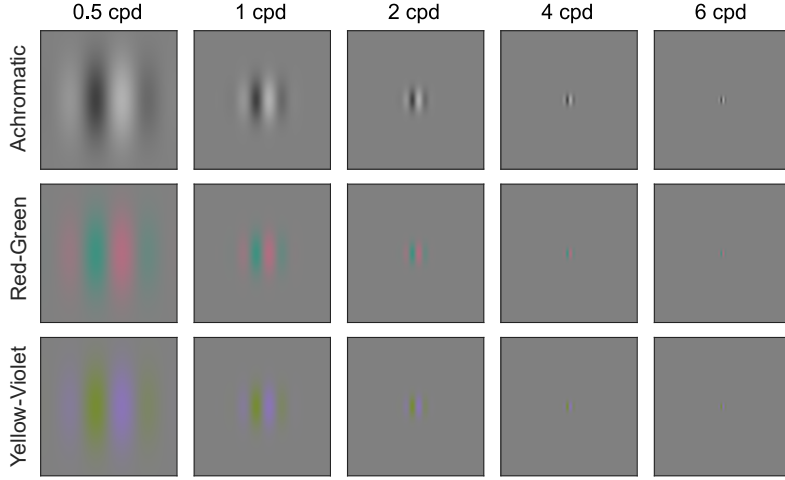


Figure 3.4: Fixed-cycles stimuli used in contrast sensitivity and contrast matching experiments. The width of the Gaussian envelope was set to be half of the wavelength,  $\sigma = (0.5/f)^\circ$ .

### 3.4 Experimental setup

This section outlines the configurations and methodologies employed across two distinct types of experiments: contrast detection and contrast matching. The two types of experimental setups investigate contrast vision and threshold and at suprathreshold levels respectively. This setup was designed to isolate specific variables of interest while ensuring a high degree of experimental control and replicability.

#### 3.4.1 Contrast detection experiments

The participants observed the stimuli binocularly in natural viewing conditions at a distance of 91 cm from the display. Observers used a chin rest to ensure the viewing angle was correct. The whole apparatus was placed in a dark room and the only light source in the room was the display. For contrast detection, the goal was to measure the lowest possible contrast that could be detected by the observers. This is the threshold contrast, the inverse of which is the contrast sensitivity. All the CSF measurements included in this work used a 2-step contrast detection procedure. First, the observer was asked to adjust the contrast of the stimuli used in the experiment (once for each stimulus) using the method of adjustment. The values from this step were then passed on to the next adaptive stage of the experiment. A 4-AFC (Alternate Forced Choice) experiment asked the observer to choose the quadrant which contained the stimulus. The correct or wrong response was recorded for each trial and then used to estimate the threshold using psychometric fitting procedures.

## CHAPTER 3. METHODOLOGY

### 3.4.2 Contrast matching experiments

For contrast matching experiments, the apparatus consisted of two screens separated by a black opaque screen as shown in Figures 3.5-3.6. This configuration allowed haploscopic viewing, i.e. each eye could only see one screen at a time. The left eye only saw the HDR screen (described in Section 3.1.1), while the right eye only saw a standard dynamic range (SDR) screen with a fixed mean luminance of  $200 \text{ cd/m}^2$ . The SDR display is a Retina iPad screen interfaced with an Adafruit display port kit with  $400 \text{ cd/m}^2$  peak luminance. Both the displays were luminance and colour calibrated as detailed in Section 3.1.1. The SDR display needed to be configured at an angle because of the viewing angle limitation of the HDR displays. The angle was adjusted such that the viewing distance from the centre of the screens to the observer's respective eye was the same.

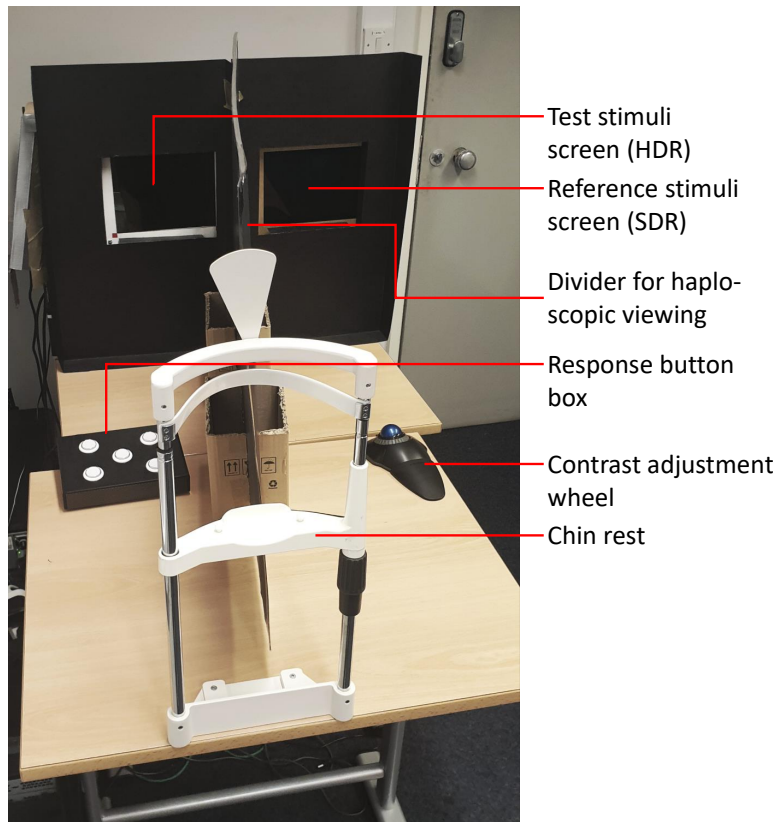


Figure 3.5: Contrast matching experiment setup in Liverpool photographed from observers' point of view. The test display (HDR screen) and the reference display (SDR screen) were separated by an opaque black screen. The button and trackball are the input devices to record observers' responses.

In a typical contrast matching experiment, an observer is presented with two visual stimuli:

## CHAPTER 3. METHODOLOGY

a test stimulus on one display and a reference stimulus on another. The objective is for the observer to adjust the contrast of the test stimulus until it perceptually matches the contrast of the reference stimulus. In the apparatus, the observer could adjust the contrast of the stimulus displayed on the HDR screen to match the contrast on the reference SDR screen using a trackball. The apparatus setup, as shown in Figure 3.5, ensures that each eye views one display independently, thereby facilitating the comparison of contrasts between two different luminance conditions—high dynamic range (HDR) and standard dynamic range (SDR). The observers were instructed to alternately view one screen at a time using one eye while closing the other eye.

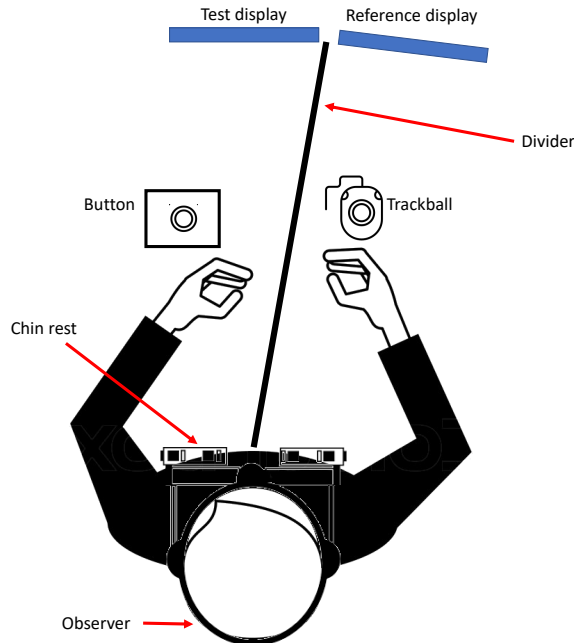


Figure 3.6: Contrast matching experiment setup. The observers' line of sight needs to be perfectly perpendicular to the HDR display for the content to be seen correctly. The reference display has no such issue so it was set at an angle such that the viewing distances between both displays and the corresponding eyes are equal.

### 3.5 Observers' recruitment

Observers provided informed consent prior to participation, in accordance with the ethical approval of respective University Ethics Committees. All naïve observers were reimbursed for their time. All observers had normal or corrected-to-normal visual acuity. All observers had normal colour vision, verified using the Cambridge Colour Test for the CRS ViSaGe

### CHAPTER 3. METHODOLOGY

System [118] or Ishihara's Tests for Colour Deficiency, 38-plates edition. Observers were asked to use their normal corrections (glasses or contact lenses), where applicable.

## CONTRAST SENSITIVITY FUNCTIONS

With the advent of high-dynamic range displays, it is vital to understand how the visual system operates at very high and very low luminance levels. For achromatic contrast modulations, Van Nes and Bouman [26] and Mustonen *et al.* [27] characterised the dependence of the contrast sensitivity on light levels up to 5,900 trolands. There are no corresponding measurements for chromatic contrast sensitivity. In the experiments detailed in this chapter, the contrast thresholds for three directions in colour space are measured. The stimuli were either modulated along an achromatic direction (ACH), a red-green direction (RG) or an S-cone-isolating, lime-violet direction (YV) for younger and older observers, resulting in a comprehensive set of measurements reflecting the vision of a standard observer. Thresholds were measured as a function of spatial frequency (0.5, 1, 2, 4, and 6 cpd) under steady-state adaptation to low mesopic ( $0.02 \text{ cd/m}^2$ ) and high photopic ( $7000 \text{ cd/m}^2$ ) light levels. Additional data points to rule out incomplete adaptation, to characterise chromatic sensitivity at very low spatial frequencies, and to model the spatial summation were measured for a subset of observers. In addition to Gabor patches, sensitivity data for disc stimuli at different luminance levels and colours was also measured to investigate the relationship between sensitivity for spatially-isolated Gabor patches and sharp edges of discs.

The chapter is divided into three main sections detailing: i) contrast sensitivity measurements for younger observers for a large range of parameters, ii) contrast sensitivity measurements for older observers, and iii) contrast sensitivity measurements for disc stimuli.

Section 4.1 of this chapter is adapted from the publication:

S. Wuergler, M. Ashraf, M. Kim, J. Martinovic, M. Perez-Ortiz, and R. K. Mantiuk, “Spatio-chromatic contrast sensitivity under mesopic and photopic light levels,” *Journal of Vision*, vol. 20, no. 4, pp. 1–26, 2020. doi: 10.1167/jov.20.4.23.

Section 4.2 is adapted from the publication:

## CHAPTER 4. CONTRAST SENSITIVITY FUNCTIONS

M. Ashraf, S. Wuerger, M. Kim, J. Martinovic, and R. K. Mantiuk, “Spatio-chromatic contrast sensitivity across the lifespan: Interactions between age and light level in high dynamic range,” in *Color and Imaging Conference*, Society for Imaging Science and Technology, vol. 2020, 2020, pp. 65–69. doi: 10.2352/issn.2169-2629.2020.28.10.

Section 4.2 also includes unpublished results from statistical analysis focusing on the effect of age. The statistical models reported here were developed with the assistance of my coauthors JM and SW.

Section 4.3 is adapted from the publication:

M. Ashraf, R. K. Mantiuk, and A. Chapiro, “Modelling contrast sensitivity of discs,” in *Human Vision and Electronic Imaging*, Society for Imaging Science and Technology, vol. 2023, 2023. doi: 10.2352/EI.2023.35.10.HVEI-246.

### 4.1 Experiment 1: Effect of spatial frequency, chromatic direction and luminance

In Experiment 1, the effect of background light level on contrast sensitivity to both achromatic and chromatic contrast modulations was tested. The contrast thresholds for Gabor patches at mean luminances ranging from 0.02 cd/m<sup>2</sup> (low mesopic range) to 7000 cd/m<sup>2</sup> (high photopic range) were measured.

#### 4.1.1 Stimuli

The mean luminance of the stimuli was one of 0.02, 0.2, 2, 20, 200, 2000, or 7,000 cd/m<sup>2</sup>; assuming pupil sizes from Watson and Yellott [119] unified pupillary model, these luminances were equivalent to 0.86, 7.83, 62.87, 416.80, 2,335.85, 13,245.57, and 36,560.55 trolands, respectively. For sessions at 0.02 and 0.2 cd/m<sup>2</sup>, observers adapted to the darkness for 5 to 10 minutes prior to starting the session and remained in the experiment room until the end of the session. Sessions at 7,000 cd/m<sup>2</sup> were conducted exclusively in Cambridge. For the main dataset in Experiment 1, Gabor patches of fixed stimuli and spatial frequencies 0.5, 1, 2, 4, and 6 cpd modulated along the three DKL axes were used. These stimuli are shown in Figure 3.4. Three sets of additional data points described as Sets A-C in the following sections were also measured.

#### *Set A: Control for incomplete adaptation*

The purpose of this additional dataset was to determine whether incomplete adaptation to the mean luminance level affected the contrast sensitivity measurements at high luminances

## CHAPTER 4. CONTRAST SENSITIVITY FUNCTIONS

( $> 200 \text{ cd/m}^2$ ). Though luminance adaptation is largely local and typically limited to a  $0.5^\circ$ -radius neighbourhood [120], the adaptation level can nonetheless be influenced by more distant parts of the visual field. As the main dataset was measured in a dark room and the display subtended only a small portion of the visual field, the possibility that the dark surroundings prevented observers from becoming fully adapted to the high luminance of the display was considered. The hypothesis was that such incomplete adaptation was responsible for the drop in sensitivity that was observed at luminance levels above  $200 \text{ cd/m}^2$ . To test this hypothesis, contrast sensitivities in bright surroundings were measured. The room light was kept on and additional light sources around the display were placed, in order to reduce the difference between the mean luminance of the display and of the region surrounding the display.

### *Set B: Low spatial frequencies*

The results from the main dataset showed that the contrast sensitivity curves for the red-green and yellow-violet modulations were low-pass in shape, that is, the peak sensitivity occurred at the lowest spatial frequency measured. The purpose of this additional dataset was to examine whether chromatic contrast sensitivity measurements at extremely low spatial frequencies would reveal a bandpass shape as observed for achromatic modulations. Additional low frequencies ranging from 0.125 to 6 cpd, at three luminance levels: 0.02, 200, and  $7,000 \text{ cd/m}^2$ , for red-green and lime-violet stimuli, were tested.

### *Set C: Effect of stimulus size*

The contrast sensitivity for periodic stimuli is known to depend on the number of cycles displayed [68]. Gratings with fewer cycles result in higher contrast thresholds, suggesting summation across cycles and/or spatial extent [69] until a critical summation area has been reached [70]. The effect of stimulus area and the number of cycles has been studied both in the fovea and the periphery, primarily for achromatic gratings [71]. Studies using chromatic stimuli reported subthreshold spatial summation to be similar for achromatic and red-green gratings [121] but show a different dependence on eccentricity [72] and larger integration areas for S-cone isolating gratings [73]. The purpose of this additional experiment was to predict contrast sensitivity for stimuli of different sizes from the fixed-cycles measurements from the main dataset.

### 4.1.2 Procedure

The experiment was grouped into multiple sessions by mean luminance level to ensure that observers were fully adapted to the display luminance during data collection. At the beginning of each session, a preliminary estimate of the contrast threshold using a method of adjustment task was obtained. This was used as an initial estimate for the QUEST procedure.

The main task was a 4AFC (Alternative Forced-Choice) detection task, in which observers indicated which quadrant of the display contained a Gabor patch. The stimulus was positioned  $3.77^\circ$  from the centre of the display: upper left, upper right, lower left, or lower right. The stimulus was displayed until the observer responded. Between trials, a mask was presented over the 4AFC stimulus region for 500 ms to neutralise adaptation to the previously seen Gabor. To create the mask, a matrix of random numbers from  $\mathcal{U}(-1, 1)$  per colour channel was sampled and the resulting image was blurred with a Gaussian kernel ( $\sigma = 4$  px).

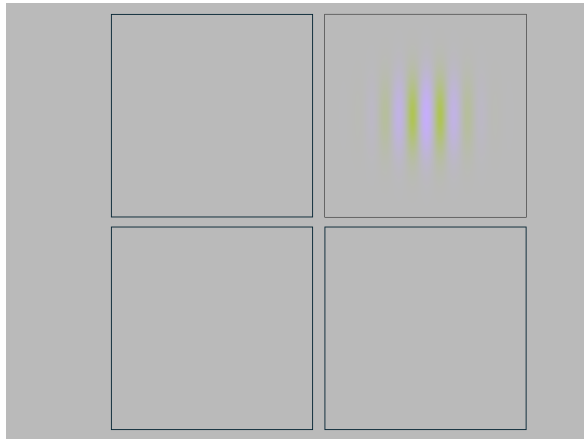


Figure 4.1: An example 4AFC trial for a yellow-violet Gabor patch with stimulus shown in the upper-right quadrant.

The stimulus contrast was determined using a QUEST procedure [18]. There was one QUEST staircase per spatial frequency and colour modulation combination, for a total of 21 staircases per session. Each staircase lasted for a minimum of 25 and a maximum of 35 trials. Within a session, observers saw Gabor patches of different spatial frequencies and colour modulation interleaved in random order. Since the Gabor orientation was not a stimulus dimension of interest, a vertical or horizontal orientation for each trial was chosen randomly. Observers had no information as to the spatial frequency, colour modulation, or orientation of the target Gabor patch. Each session lasted approximately 40 to 50 minutes. Some observers chose to omit sessions at  $7000 \text{ cd/m}^2$ , as the high luminance could be uncomfortable to view for an extended period of time.

## CHAPTER 4. CONTRAST SENSITIVITY FUNCTIONS

Observers were seated 91 cm from the HDR display such that the display subtended  $12.5^\circ \times 9.4^\circ$ . The effective spatial sampling of the LCD was 165 pixels per visual degree (ppd). The head position was fixed with a chin rest to the horizontal and vertical centre of the display. Observers were allowed to move their eyes in order to examine stimuli. All viewing was binocular. The rationale for unlimited viewing time and free scanning of the display was driven by two considerations. Firstly, since the aim of this study was to provide a dataset of contrast sensitivity that could be modelled for everyday viewing conditions, unlimited viewing time seemed to be the most appropriate choice. Secondly, in Experiment 2 (described in the next section), data from observers falling into an older age group (60+ y.o.a) is measured. For these observers, it is difficult to obtain robust data with very brief stimulus durations.

### 4.1.3 Observers

16 observers from the University of Liverpool and five observers from the University of Cambridge were recruited. Eleven of the observers were naïve to the purpose of the study (5 female, 11 male, mean age =  $26.8 \pm 7.7$ ); the rest were the experimenters (4 female, 1 male, mean age =  $40.4 \pm 12.6$ ). In order to verify that the experimental set-ups in the two locations were calibrated to the same standard, three observers repeated the experiment in both Cambridge and Liverpool. The data from these observers were found to be consistent across locations and so the pooled data from these observers is reported.

In addition to the main dataset, additional measurements were also recorded as described in the earlier *Stimuli* section. For additional measurements set A, four observers (three female, one male, mean age =  $29.0 \pm 8.2$ ) including two of the experimenters participated. For additional measurements set B, five observers (two male, three female, mean age =  $27.2 \pm 4.3$ ) including three of the experimenters participated. For additional measurements set C, 11 of the observers (four male, seven female, mean age =  $30.7 \pm 11.9$ ) who had also done the main experiment participated.

### 4.1.4 Results and Discussion

For each condition, the maximum likelihood estimate of the contrast sensitivity is estimated. Each threshold estimate is typically based on between 25 to 35 trials. Threshold contrast is defined as the normalised length in cone contrast space (Equation. 3.5):

Figure 4.2 shows the contrast sensitivities as a function of frequency for light levels ranging from  $0.02 \text{ cd/m}^2$  to  $7000 \text{ cd/m}^2$ . The achromatic modulations resulted in a classic band-

## CHAPTER 4. CONTRAST SENSITIVITY FUNCTIONS

pass response for medium to high luminance levels (from  $2 \text{ cd/m}^2$  onwards), with a peak response at medium spatial frequencies (ranging from 1 to 2 cpd). The gradual change from a low-pass shape at very low luminance levels ( $0.02 \text{ cd/m}^2$ ) to the typical band-pass shape at higher luminance levels is similar to the results of Van Nes and Bouman [26]. Red-green and yellow-violet modulations, on the other hand, resulted in low-pass contrast sensitivity curves at all light levels, with the peak sensitivity occurring at the lowest spatial frequency measured (0.5 cpd). Sensitivity was higher for the red-green stimuli than for the achromatic modulation when expressed as the inverse of the cone contrast, which is consistent with Kim *et al.* [46].

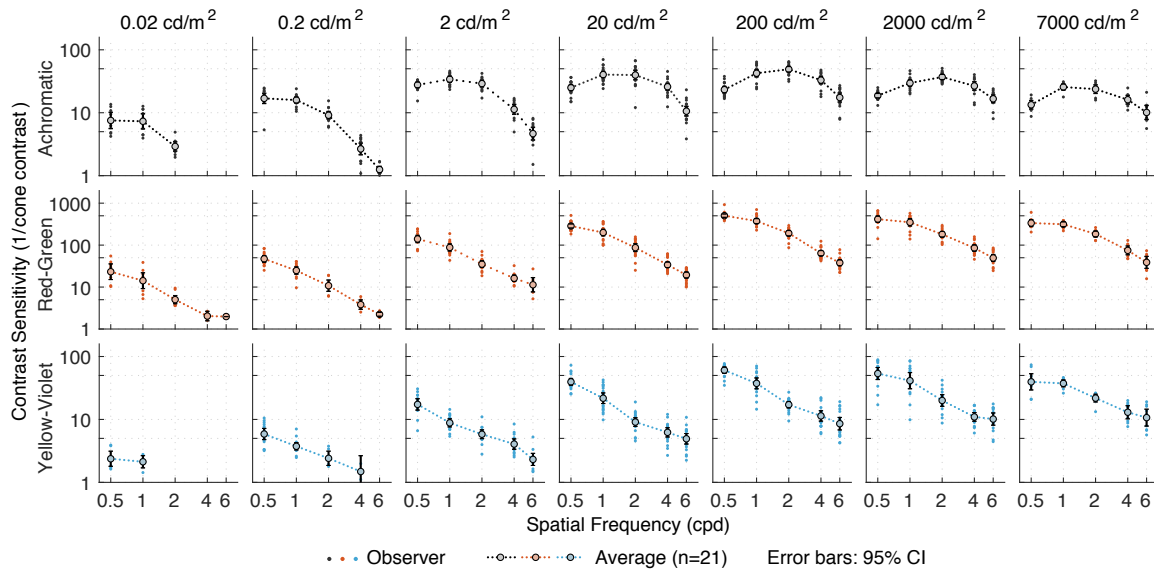


Figure 4.2: Contrast sensitivity as a function of luminance for the three colour directions: achromatic, red-green, and yellow-violet.

When contrast sensitivity data are replotted as a function of light level (Figure 4.3), sensitivity was not a monotonic function of luminance for achromatic modulations; rather, contrast sensitivity was lowest at  $0.02 \text{ cd/m}^2$  and rose steadily with increasing mean luminance till it reached a peak at  $20-200 \text{ cd/m}^2$  for low to medium frequencies, then decreased again beyond  $200 \text{ cd/m}^2$ . This luminance dependence interacted with spatial frequency, such that the overall maximum sensitivity occurred between  $20-200 \text{ cd/m}^2$  for 1-2 cpd where observers could reliably detect a Gabor patch of 2-3% contrast. For red-green and yellow-violet modulations, contrast sensitivity rose steadily as a function of luminance, reaching a maximum at around  $200 \text{ cd/m}^2$ . Only for the lowest frequency, a decrease in peak sensitivity was observed.

## CHAPTER 4. CONTRAST SENSITIVITY FUNCTIONS

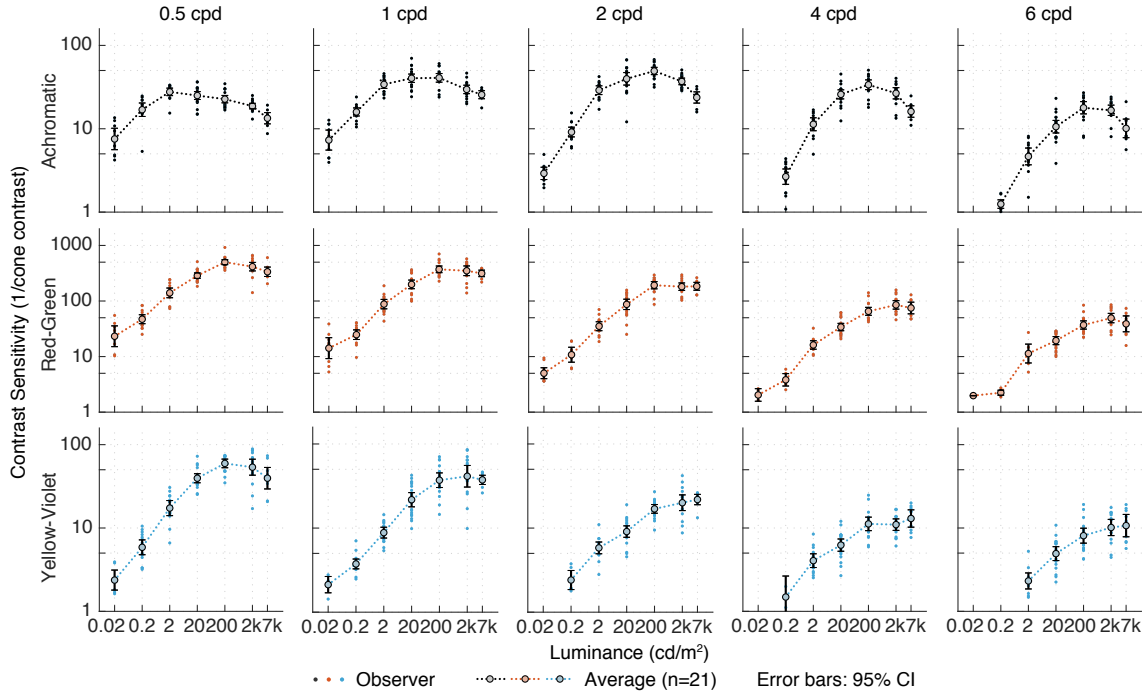


Figure 4.3: Contrast sensitivity re-plotted from Figure 4.2 as a function of luminance.

In Figure 4.4, thresholds are plotted as a function of retinal illuminance (trolands). For chromatic stimuli (*Red-Green*, and *Yellow-Violet*), contrast thresholds were independent of the retinal illuminance beyond about 2000 trolands, hence consistent with Webers' law, whereas for achromatic stimuli ( $L+M$ ) thresholds rose again for very high light levels. This failure of Weber-law behaviour in the high photopic range has not been reported by Van Nes and Bouman [26], probably due to the fact that they only investigated contrast sensitivity up to 5,900 trolands and the data show that Weber law only fails at retinal illuminances above 10,000 trolands.

For all three modulation directions, log threshold contrast decreased approximately linearly with log retinal illuminance for low and intermediate light levels, with slopes systematically a bit less than -0.5, (DeVries-Rose law; [122], [123]). Mean slopes were -0.42 and -0.36 for *Red-Green* and *Yellow-Violet*, respectively (Table 4.1) and independent of spatial frequency. For achromatic thresholds, the slopes were frequency-dependent and increased with spatial frequency, consistent with Mustonen *et al.* [27].

## CHAPTER 4. CONTRAST SENSITIVITY FUNCTIONS

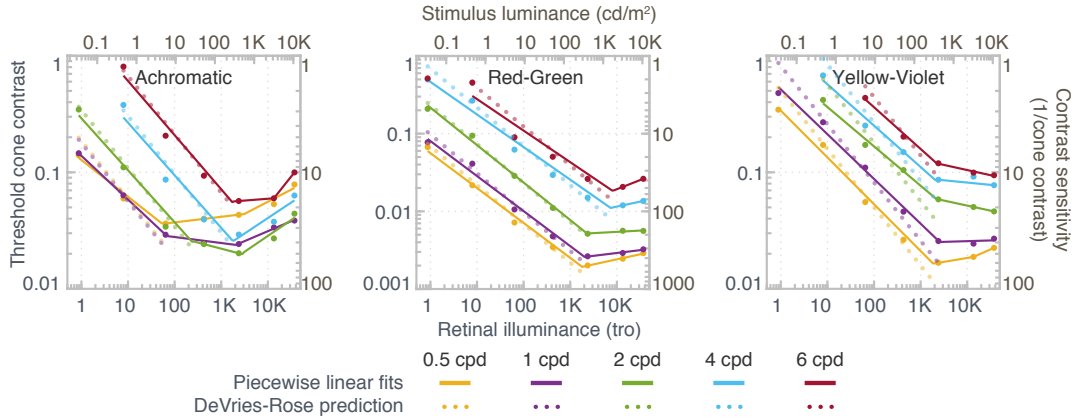


Figure 4.4: Logarithmic threshold cone contrast sensitivity as a function of log retinal illuminance.

The transition from the DeVries-Rose to Weber behaviour was independent of spatial frequency for chromatic modulations (Figure 4.4); for achromatic stimuli, on the other hand, the inflection point shifted to higher retinal illuminances when the spatial frequency was increased. Díez-Ajenjo and Capilla [124] and Valero *et al.* [49] reported a similar difference between chromatic and achromatic gratings: for achromatic gratings, the transition from DeVries-Rose to Weber-law behaviour was dependent on spatial frequency and occurred between 1 and 2 cd/m<sup>2</sup> for the lowest spatial frequency measured (0.5 cpd), consistent with the current findings. For chromatic modulations, threshold contrast decreased approximately linearly with background luminance in log-log space, without a clear transition point up to 100 cd/m<sup>2</sup>. Valero *et al.* [49] only investigated luminances up to 100 cd/m<sup>2</sup>, which is well below the maximum luminance range (7,000 cd/m<sup>2</sup>) of the apparatus used in this work; in the data presented here (Figure 4.4), the transition point occurred at around 200 cd/m<sup>2</sup> for chromatic stimuli.

Table 4.1: Slopes of log threshold contrast vs log retinal illuminance (trolands) in linear range

Modulation	Spatial frequency (cpd)					
	0.5	1	2	4	6	Mean
Achromatic	-0.313	-0.375	-0.421	-0.433	-0.455	-0.399
Red-Green	-0.436	-0.426	-0.470	-0.380	-0.400	-0.422
Yellow-Violet	-0.379	-0.372	-0.342	-0.357	-0.355	-0.361

## CHAPTER 4. CONTRAST SENSITIVITY FUNCTIONS

One of the major features of the data presented in this chapter is the superior sensitivity to red-green chromatic contrast variations (cf Figure 4.4). The lowest threshold contrast (0.2% cone contrast) is reached at 2000 trolands for a low spatial frequency (0.5 cpd) chromatic stimulus; for achromatic variations, the best detection performance (lowest threshold: 2%) is also achieved at 2,000 trolands, but at a medium spatial frequency (2cpd). The superior sensitivity to chromatic over achromatic variations (by a factor of 10 in our experiment) is consistent with the prevalence of retinal parvocellular neurones which are L/M cone-opponent. It is worth noting that the cone contrast measure used to compare chromatic and achromatic variations does not reflect the contrast variations found in natural scenes [125]; the high chromatic sensitivity of the visual system might rather compensate for the low chromatic contrasts typically occurring in our natural environment [75].

The failure of Weber law behaviour for very high luminances may be due to incomplete adaptation to the display background for luminances greater than 200 cd/m<sup>2</sup>. This possibility was investigated by the additional measurements (Set A) presented in Figure 4.5. For the stimulus conditions tested, No systematic differences in contrast sensitivity were found when observers were in a dark room or in a bright room with high ambient light levels. This suggests that incomplete adaptation alone cannot explain the drop in sensitivity at the luminance levels above 200 cd/m<sup>2</sup>.

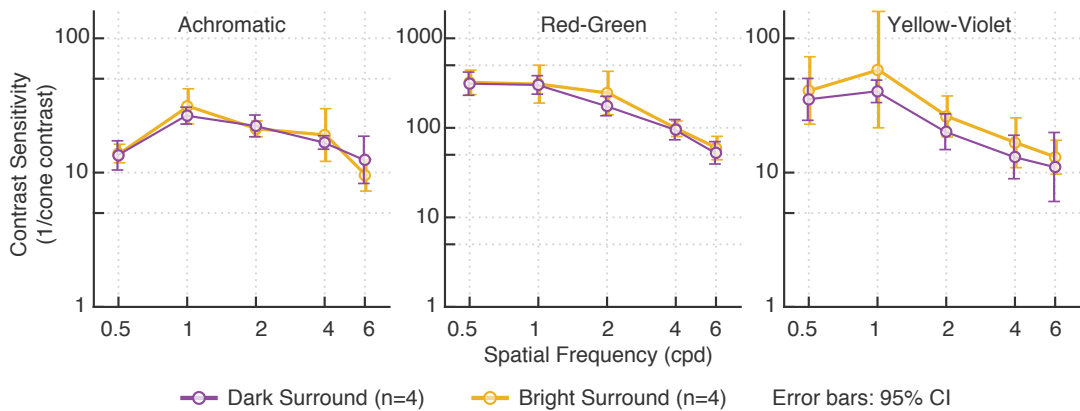


Figure 4.5: Contrast sensitivity measures in dark (dark symbols) and bright (bright symbols) surroundings. In the dark surround condition, only the HDR display emitted light ( $7000 \text{ cd/m}^2$ ). No systematic differences were found between these two conditions.

Looking at data from the additional measurements (Set B), no systematic reduction in contrast sensitivity was found at the very low frequency (0.125 cpd) at low and intermediate (0.02 and 20 cd/m<sup>2</sup>) luminance levels (Figure 4.6). For the highest luminances ( $7,000 \text{ cd/m}^2$ ),

## CHAPTER 4. CONTRAST SENSITIVITY FUNCTIONS

there was some evidence that the chromatic contrast sensitivity drops off as the achromatic sensitivity does. However, these differences are within measurement error and the data does not provide any strong evidence against the low-pass characteristics of the chromatic contrast sensitivity.

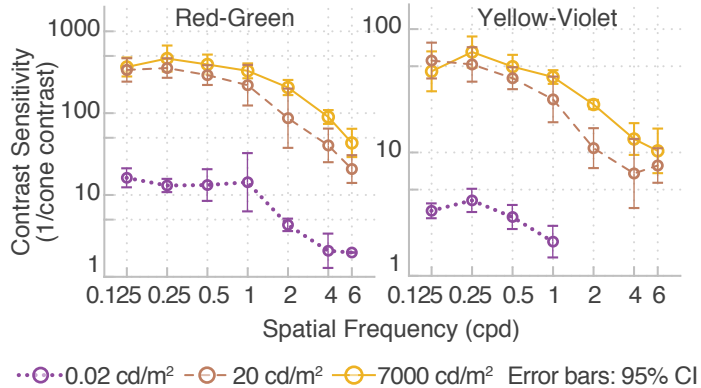


Figure 4.6: Chromatic contrast sensitivity extended to lower spatial frequencies from 0.125 cpd to 6 cpd.

The data from the additional measurements (Set C) show that contrast sensitivity increased with stimulus size (Figure 4.7). Due to display size restrictions, not all spatial frequencies could be measured at all three envelope sizes. However, the available data suggests that an increase in envelope size causes a fixed increase in sensitivity in log-log space. In Figure 4.8, contrast thresholds are replotted as a function of area for three different frequencies (2, 4, and 6 cpd) with slopes in log-log space varying from -0.29 to -0.47. Slopes of -0.5 are consistent with Piper's law [126] and can be modelled as a single-filter contrast energy model [71]; slopes in the region from -0.25 to -0.5 reflect probability summation between multiple filters or nonlinear summation mechanisms [127]. The dependency on stimulus size is revisited in the modelling chapter (Chapter 5).

## CHAPTER 4. CONTRAST SENSITIVITY FUNCTIONS

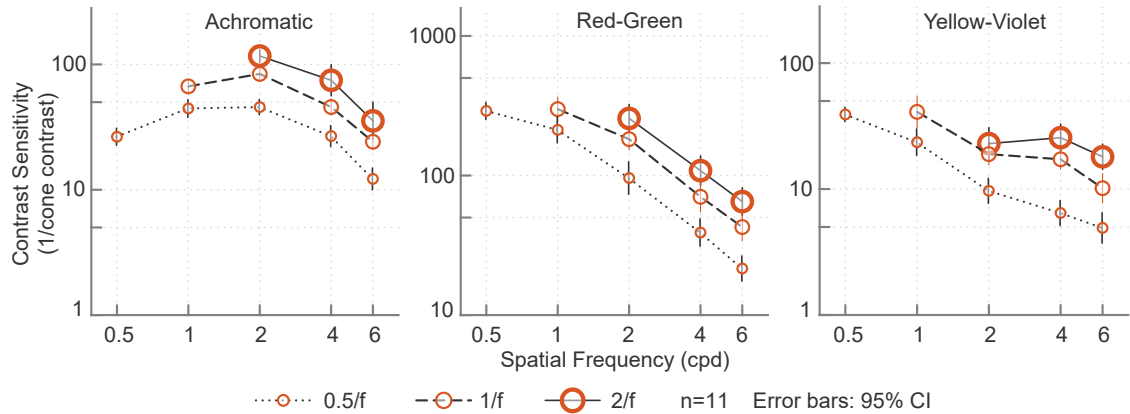


Figure 4.7: Each line represents the contrast sensitivity function for a series of stimuli with a different number of cycles and consequently different stimuli sizes. The size of the Gaussian envelope was fixed to 0.5, 1, and 2 times the wavelength (the inverse of spatial frequency).

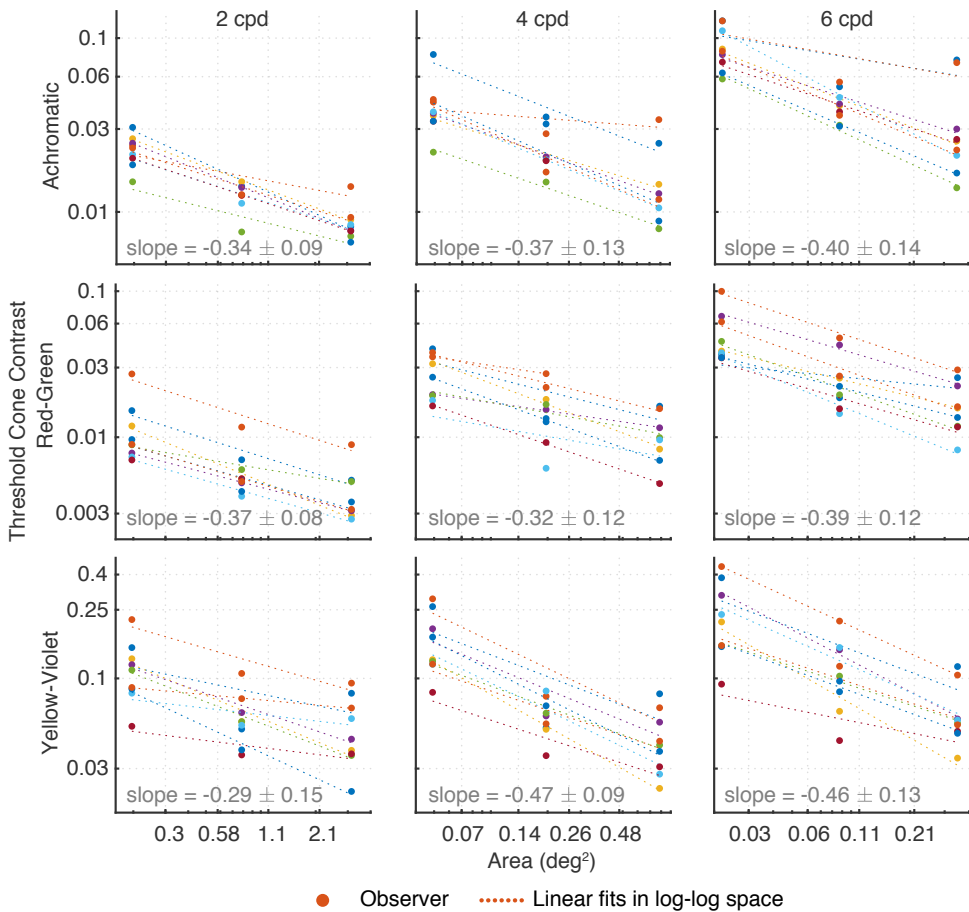


Figure 4.8: Linear decrease in log contrast with the increase in log area of the stimulus

## 4.2 Experiment 2: Effect of Age

The aim of this section is to characterise how age modulates achromatic and chromatic contrast vision for a wide range of light levels under steady-state adaptation. While the loss of contrast sensitivity for high spatial frequencies is well-established for modest lightness levels [32], [94], [128]–[130], the interaction between the adapting light level, age and spatial frequency has not been systematically investigated, despite its importance for a wide range of visual functions including reading and driving. Previous studies (see Appendix A) have reported age-related contrast sensitivity changes in a range from 2 to about  $120\text{ cd/m}^2$ , but only for achromatic stimuli with the notable exception of Hardy *et al.* [131], who also measured chromatic contrast sensitivity for a background luminance level of  $15\text{ cd/m}^2$ .

This section investigates age-related changes in contrast detection thresholds for chromatic and achromatic stimuli as a function of adapting light levels. The methodology is the same as in Section 4.1, but in this study, the contrast sensitivity measurements were extended to different age groups and focused on the general trends and correlation between factors that affect contrast sensitivity with normal ageing.

### 4.2.1 Observers

To compare the data obtained from the previous experiment (the younger observer group), older participants were recruited. The mean age of the 20 observers was 65 years. The distribution of the ages of both the younger group in the previous experiment and the older group in the current experiment is shown in Figure 4.9.

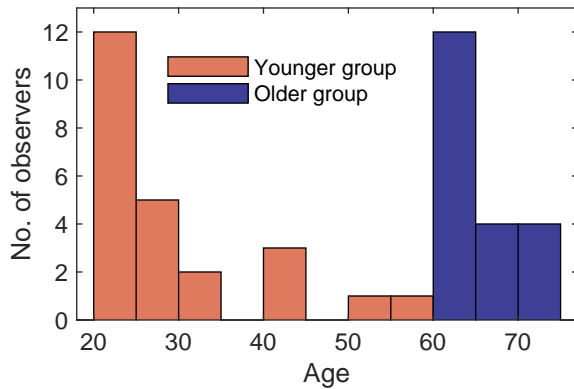


Figure 4.9: Age distribution of observer groups

Observers in the older group were asked to do a series of vision tests to rule out any optical disease. 11 of the older observers were tested by ophthalmic professionals. These tests were

## CHAPTER 4. CONTRAST SENSITIVITY FUNCTIONS

conducted a year and a half later than the CSF measurements due to COVID restrictions and it was not possible to get all the observers back. This means that unfortunately, the data from this optometry test cannot be used to find correlations between physiological vision health and CSF measurements. Nevertheless, the tests confirmed that all the older observers who took part in the study did not have any severe eye diseases that would impact the measurements. The tests included measuring vision and stereoacuity, contrast sensitivity, pupil size, anterior chamber angle grading, intraocular pressure, and slit lamp examination for cataract grading, in addition to taking a case history. The habitual and pinhole visual acuity as well as near visual acuity were tested using a Bailey-Lovie logMAR chart [132], [133]. The contrast sensitivity for 3, 12, and 18 cpd (sinusoidal grating with circular aperture of  $0.87^\circ$  diameter viewed at a distance of 2.5 m and a mean luminance of  $85 \text{ cd/m}^2$ ) with and without glare was also tested using a VectorVision CSV-1000 chart [134]. Frisby stereo tests were used to test stereoacuity [135]. Pupil sizes under dark and light conditions were recorded. All observers had normal intraocular pressure. Slit lamp examination was used to characterise cataracts using an integrated framework for grading nuclear, cortical and posterior cataracts [136]. 3 of the observers had since received cataract surgery. All the observers were deemed to have good visual health appropriate to their ages and did not have any acute ocular disorders. Detailed results from the tests can be found in Appendix C.

### 4.2.2 Statistical analysis

For each stimulus in each session, a psychometric function was fitted to the responses from the trials to obtain the threshold cone contrast. The contrast where the probability of correct guesses was 0.84 was recorded as the contrast threshold for the respective condition. The inverse of the threshold contrast (defined in Eq. 3.5) is the contrast sensitivity. For each observer, two datasets for the  $20 \text{ cd/m}^2$  luminance level were measured (the first and the last session). No differences were found between the first and last sessions and so the average of contrast sensitivity measures from the repeated  $20 \text{ cd/m}^2$  sessions for individual observers was used. Within each group (younger and older observers), the mean of all the observers was calculated to identify and quantify contrast sensitivity differences between the two groups. Conditions with less than 5 measurements were removed from the analysis. Figure 4.10 shows the contrast sensitivity averaged across observers for the younger and the older age groups. The error bars indicate the standard errors of the mean.

Our data set spanned two observer age groups, five spatial frequencies, six luminance levels, and three colour directions. To determine how these factors affected contrast sensitivity, linear mixed effect models (LMMs) were fitted to the data from each of the three colour

## CHAPTER 4. CONTRAST SENSITIVITY FUNCTIONS

directions.

The best-fitting linear mixed-effect models were determined by the backward procedure of removing the factors that did not contribute significantly. In other words, none of the remaining effects or interactions can be removed without reducing the variance explained. Post-hoc tests on any interactions in this final model were performed using omnibus paired t-tests ( $p < 0.05$ ).

The data was pre-processed using MATLAB and then all statistical analyses were performed in R using packages `lmerTest`, `caret`, `emmeans`, `performance`, and see [137]–[143]. For the full description of the best-fitting statistical models, please refer to the Appendix D.

### 4.2.3 Results

Our results section focuses on evaluating: (1) the impact of age on spatial contrast sensitivity for both achromatic and chromatic channels, (2) whether age-related sensitivity losses are frequency-specific, and (3) whether these sensitivity losses are modulated by the adapting light level. Supplementary analyses of other determinants of contrast sensitivity can be found in the statistical supplementary material.

Figure 4.10 shows the contrast sensitivity as a function of spatial frequency for the achromatic (row 1) and chromatic directions (rows 2-3), across all luminance levels (columns 1-6). For all three colour directions, there is a significant effect of age (achromatic:  $t(66.3) = -5.2, p < 0.001$ ), red-green ( $t(45.2) = -5.3, p < 0.001$ ), and yellow-violet ( $t(33.1) = -7.6, p < 0.001$ ). The spatial contrast sensitivity of older observers is lower or equal to that of the younger age group across all light levels. The age-related sensitivity loss is more pronounced at higher spatial frequencies, i.e. for achromatic stimuli presented at high light levels (above  $20 \text{ cd/m}^2$ ), contrast losses occur for frequencies above 2 cpd. For chromatic stimuli, age-related contrast losses are evident at all frequencies, with the exception of the lowest, the 0.5cpd stimuli, where both groups have similar contrast sensitivity for light levels above  $200 \text{ cd/m}^2$ . This interaction between age, spatial frequency, and luminance was significant for achromatic ( $t(955.3) = -2.2, p < 0.05$ ), and yellow-violet ( $t(769.2) = -3.9, p < 0.001$ ) stimuli, but did not reach statistical significance for red-green stimuli ( $\chi^2(2) = 5.4033, p = 0.0671$ ); in this case, only the interaction between age group and frequency was significant, indicating that the reduction of contrast sensitivity with increasing SF generalised across luminance levels ( $t(915.8) = -5.9, p < 0.001$ ).

## CHAPTER 4. CONTRAST SENSITIVITY FUNCTIONS

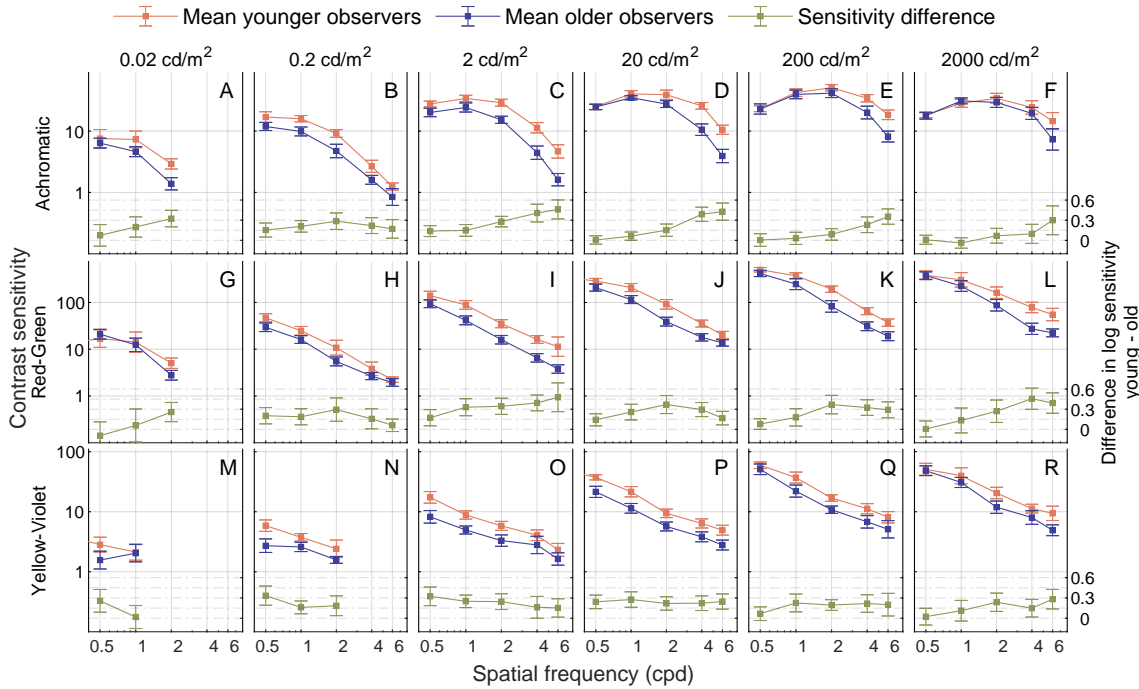


Figure 4.10: Mean contrast sensitivity functions from older and younger observer groups. The three rows present achromatic, red-green and yellow-violet CSFs respectively. The columns present CSFs at different background luminance levels from  $0.02 \text{ cd/m}^2$  to  $2000 \text{ cd/m}^2$ . The secondary axis (green curves) indicates the difference in population means of log sensitivity values from the two age groups (young - old) with a 95% confidence interval.

### 4.2.4 Discussion

The main finding is that there is a general decline in spatial contrast sensitivity in the older age group. This sensitivity loss is modulated by the adapting light level, for both achromatic and chromatic channels.

For achromatic stimuli (Figure 4.10, row 1), the contrast sensitivity for both age groups is low-pass at mesopic ( $0.02 \sim 2 \text{ cd/m}^2$ ) light levels and becomes bandpass at photopic ( $\geq 20 \text{ cd/m}^2$ ) levels. Under mesopic conditions, the age-related contrast sensitivity loss is constant across frequencies (Figure 4.10 (A-C)), i.e. lower spatial frequencies are also affected by ageing at mesopic light levels, hence corroborating previous findings [144]–[149]. In contrast, at photopic light levels (Figure 4.10 (D-F)) low spatial frequencies are spared and the sensitivity losses for older observers are more pronounced at relatively higher spatial frequencies ( $> 2 \text{ cpd}$ ), consistent with previous studies [32], [64], [67], [94], [128], [129], [150]–[157].

## CHAPTER 4. CONTRAST SENSITIVITY FUNCTIONS

Silvestre *et al.* [66] used an external noise method to characterise the source of the age-related decline in the achromatic CS. They concluded that an increase in photon noise (less efficient light absorption in the cones) limits the CS in the elderly age group at mesopic light levels; at higher light levels, CS is limited by late neural noise (after contrast is encoded). Only at fairly high spatial frequencies (above 4 cpd), optical factors such as intraocular scattering are predicted to affect the CS.

The contrast sensitivity for chromatic (red-green and yellow-violet) stimuli (Figure 4.10, rows 2 and 3) also show a loss of sensitivity with ageing [131], [158]. As for the achromatic CSFs, the reduction in chromatic CS is less dependent on spatial frequency under mesopic light levels (G-I; M-O), but under photopic conditions (J-L; P-R), the age-related sensitivity loss is more pronounced at higher spatial frequencies (Figure 4.10 (G-J, M-P)). The fact that contrast sensitivity does not decline uniformly across spatial frequencies indicates that it is not merely due to an age-related increase in lens absorption, which would lead to changes in retinal illuminance.

The decrease in sensitivity for luminance levels up to 20 cd/m<sup>2</sup> is more pronounced for the yellow-violet stimuli of the older observers. This differential age-related decrease in sensitivity for S-cone isolating stimuli is consistent with previous studies [159], [160]. The standard deviation of the estimated contrast thresholds is higher for the older age group as individual variability becomes more pronounced with advancing age [92], [152], [161].

### 4.3 Experiment 3: Contrast sensitivity of disc stimuli

Contrast sensitivity explains the visibility of low-contrast patterns and is an important indicator of the performance of the visual system. There have been multiple attempts to model an all-encompassing function of contrast sensitivity [162]–[166], which could predict the visibility thresholds for stimuli of a given spatial and temporal frequency, luminance, size, orientation, eccentricity and modulation along different directions in a colour space. To model all these dimensions, it is necessary to combine contrast sensitivity measurements from multiple sources, often obtained using different procedures and varying stimuli. The two dominant types of stimuli are Gabor patterns, typically used for the measurement of spatial contrast sensitivity, and discs, which are used to measure temporal contrast sensitivity. Combining spatial and temporal sensitivity data is problematic as there is no established model that can explain the detection of discs from Gabor data or vice-versa. The goal of this work was to propose such a model.

Numerous studies over the years have measured contrast sensitivity across a very large

## CHAPTER 4. CONTRAST SENSITIVITY FUNCTIONS

parameter space. It varies along spatial frequency, temporal frequency, luminance level, colour direction, stimulus size, retinal eccentricity, stimulus shape, etc. [21], [23], [24], [27], [28], [31], [167]–[169]. Many studies have presented contrast sensitivity data along different combinations of the aforementioned parameters but the measurements can be difficult to compare due to slight differences in methodology and the data covering a different part of the parameter space. Some of these differences in measurements can be compensated by a constant offset in sensitivity [166]. Differences in pupil diameter can be compensated using standard models [119]. However, when the stimuli differ considerably, a simple offset or multiplier cannot account for the differences.

Most achromatic and chromatic temporal contrast sensitivity studies have used a fixed-aperture flickering stimulus to measure the temporal contrast sensitivity [170]–[175]. In addition to contrast sensitivity, flicker sensitivity measurements are a widely used measure to characterise temporal vision. Most older studies investigating this used a simple backlight temporal modulation with a fixed aperture resulting in a disk-shaped stimulus [176]–[178]. To be able to compare these fixed-aperture stimuli with the more physiologically-motivated stimuli (e.g., Gabor patches), we need a model that can integrate the sensitivities from fundamental components to predict the thresholds of more complex stimuli.

### 4.3.1 Displays

The study was carried out using three different displays in Liverpool and Cambridge. The complete set of measurements was collected on an Eizo ColorEdge CS2740 27" 4K LCD monitor in Cambridge. This monitor could be calibrated with very high colour accuracy. To reproduce luminance levels below  $1\text{ cd/m}^2$ , the observers wore a modified pair of goggles with neutral density (ND) filters (Kodak Wratten Gelatin 2.0D). A few select conditions were measured by a larger number of participants on either a custom-HDR display (described in [28]) or an LG G2 55" OLED display in Liverpool. Goggles with a 2.1 ND filter were used to measure  $0.2\text{ cd/m}^2$  conditions on the OLED display. All displays were colour-calibrated prior to measurement. Three different displays were used to ensure that the measurements were consistent across different devices. A chin rest was used to control the viewing distance.

### 4.3.2 Stimuli

The stimuli were circular disks of different sizes, luminance levels and colour directions. Some examples of those are shown in Figure 4.11. The stimuli varied along the following parameters:

## CHAPTER 4. CONTRAST SENSITIVITY FUNCTIONS

- Luminances: 0.02, 0.2, 2, 20 and 200 cd/m<sup>2</sup>
- Sizes: 0.0833, 0.5 and 2 deg diameter disks
- Colour directions: luminance (C1), pinkish red (C2) and violet (C3) directions were the three cardinal colour directions in the DKL colour space [2]. C1 is an achromatic stimulus with contrast changing only along the luminance direction. C2 and C3 contrasts are isoluminant (with respect to the background) modulated along the positive directions of the DKL colour space.

The background for all stimuli was D65 grey with the corresponding mean luminance level and had the size of 31.2° × 17.9°.

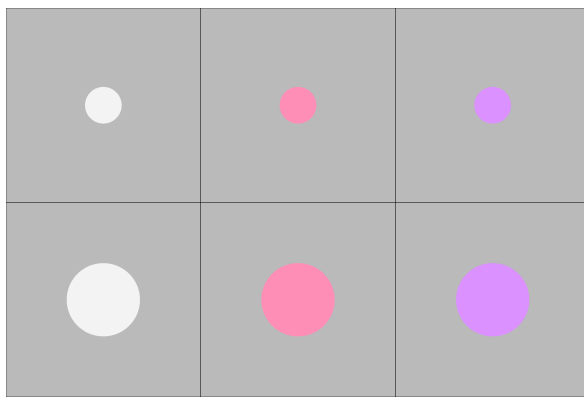


Figure 4.11: Example disc stimuli used in the experiment.

### 4.3.3 Experimental procedure

Initial estimates of contrast sensitivities were recorded via a method of adjustment where the observers were asked to adjust the contrast of each of the stimuli until they could just detect it. This initial estimate was the prior for the next adaptive 4AFC stage. In the 4AFC stage, the observers were shown a 2x2 grid, with only one quadrant containing the stimulus. The presentation time was not limited. The observers indicated which quadrant contained the stimulus and their responses drove the QUEST adaptive sampling method [18] implemented in PsychToolBox-3 [101]. The responses were fitted with a psychometric function and the contrast level with 0.84 probability of correct guesses was chosen as the threshold contrast for the specific stimulus.

A single luminance level was measured at a time. The observers were asked to adapt for 3 minutes to the lowest luminance (0.02 cd/m<sup>2</sup>), one minute to 0.2 cd/m<sup>2</sup> and 30 seconds for

## CHAPTER 4. CONTRAST SENSITIVITY FUNCTIONS

other luminance levels. The sizes and colour directions were randomised across the QUEST trials.

### 4.3.4 Participants

3 colour normal observers and one observer with deutanopia took part in the experiment in Cambridge. The deutan observer completed only the conditions for the achromatic disc. A further 6 observers participated in Liverpool for a reduced number of conditions.

### 4.3.5 Results

The individual measurements are in Figure 4.12. The means were computed only over the data collected in Cambridge as only a subset of conditions was measured in Liverpool. The inter-observer variability across the devices used in Cambridge and Liverpool was found to be comparable. Table 4.2 reports the standard deviations in dB for the data.

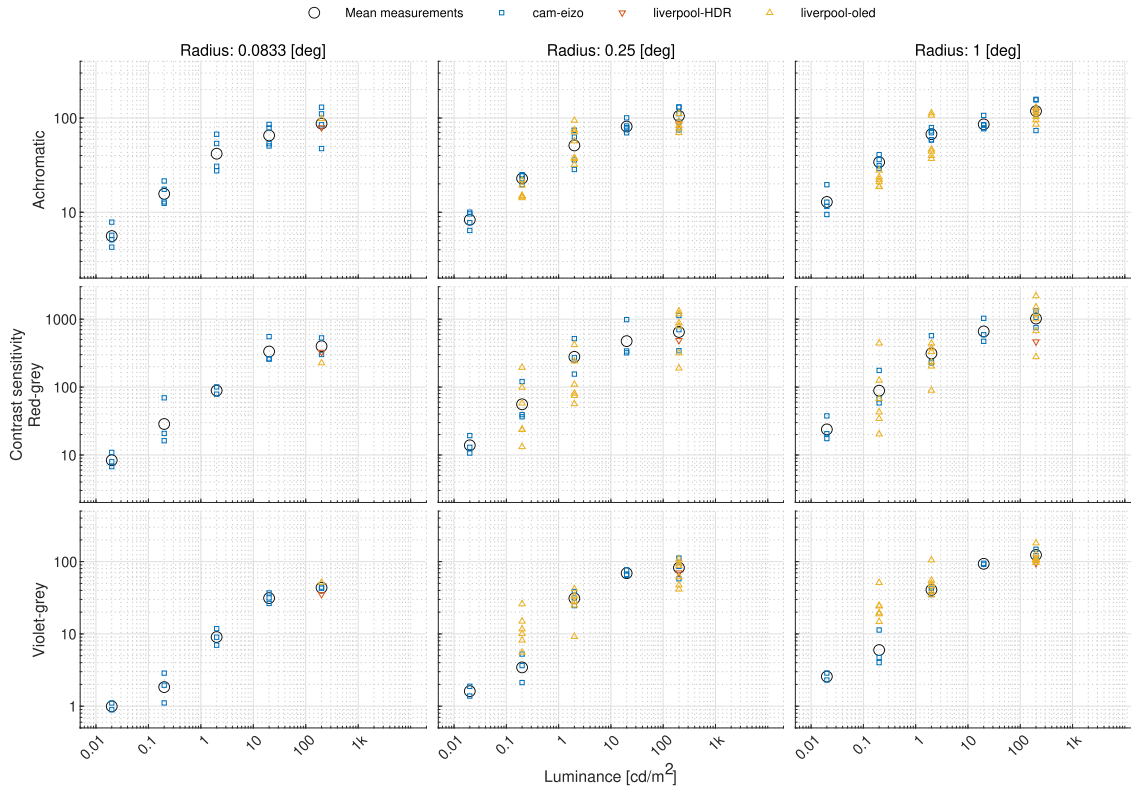


Figure 4.12: Measurements of the disc contrast sensitivity. The means (black circles) are computed over the data collected in Cambridge (cam-eizo). The sensitivity is plotted in the units of cone contrast [28].

## CHAPTER 4. CONTRAST SENSITIVITY FUNCTIONS

Table 4.2: Mean of inter-observer standard deviation for all stimuli. Standard deviations from two of the devices separately is also reported. Only one observer participated in experiment with the device *liverpool-HDR*, so the variance is not reported.

	All devices	Cam-Eizo	Liv-OLED
SD [dB]	2.9687	2.7678	2.7126

A one-way ANOVA was performed to test if there were significant differences in contrast measurements between the three devices. Luminance, spatial frequency, and stimulus size were random effects in the model. No statistically significant difference was found between the measurements from the difference devices ( $F(2, 283) = 0.1026, p = 0.9025$ ). The data shows that contrast sensitivity increases with luminance and the size of the disc for all measured colour directions. To test the statistical significance of these effects, a n-way ANOVA was performed with the log of luminance and size (along with their two-way interaction) as fixed effects and colour direction, device, and observers as random effects. The combined effect of luminance and size was found to be statistically significant ( $F(1, 282) = 6.3668, p < 0.05$ ).

### 4.4 Summary of chapter

The datasets presented in this chapter provide comprehensive insights into spatiochromatic contrast sensitivity under various lighting conditions, across different age groups, and with specific visual stimuli like discs. In the dataset from Section 4.1, the dataset encompasses measurements of contrast sensitivity at both mesopic and photopic light levels, revealing how the visual perception of spatial and colour contrasts varies under low and standard lighting. The dataset in Section 4.2, extends this investigation to include the effects of age, offering a detailed look at how contrast sensitivity, particularly in high dynamic range scenarios, is influenced by both the ageing process and ambient light levels. The data in Section 4.3 measures contrast sensitivity specifically for disc stimuli, providing a dataset that isolates the effects of shape and size on visual sensitivity to contrast. Together, these datasets highlight the joint role of light conditions, age, and stimulus characteristics in shaping contrast sensitivity.

## MODELLING CONTRAST SENSITIVITY FUNCTIONS

The goal of this chapter was to derive a spatio-chromatic contrast sensitivity function which could interpolate and extrapolate the collected data within an allowable range. All the data used to train the models in this chapter have been presented in Chapter 4. This chapter is divided into models of i) General CSF with spatial frequency, luminance, chromatic modulation and size, ii) CSF with observer age as a predictor, and iii) Disc CSF model derived from CSF models of Gabors.

Section 5.1 of this chapter is adapted from the publication:

S. Wuergler, M. Ashraf, M. Kim, J. Martinovic, M. Perez-Ortiz, and R. K. Mantiuk, “Spatio-chromatic contrast sensitivity under mesopic and photopic light levels,” *Journal of Vision*, vol. 20, no. 4, pp. 1–26, 2020. doi: 10.1167/jov.20.4.23.

The models presented in Sections 5.1.1-5.1.3 were mainly developed by me with input from all the collaborators, in particular MK who helped with the formatting of the figures. The model extension in Section 5.1.4 was proposed by my collaborator RKM. This part of the publication is summarised here for completion since this model is used in later parts of the thesis.

Section 5.2 introduces models of CSF as a function of age. These models are an extension of general CSF models in Section 5.1. The models presented in this section are currently being prepared as a publication.

Section 5.3 introduces some computational models that relate the CSF from Gabor patches to those of disc stimuli. This section is adapted from the publication:

M. Ashraf, R. K. Mantiuk, and A. Chapiro, “Modelling contrast sensitivity of discs,” in *Human Vision and Electronic Imaging*, Society for Imaging Science and Technology, vol. 2023, 2023. doi: 10.2352/EI.2023.35.10.HVEI-246.

7 different models are proposed in Section 5.3 with inputs from all the co-authors. In particular, RKM introduced and wrote the code and description of the ‘multiple detector

## CHAPTER 5. MODELLING CSFS

models'. They are included in this thesis for completion as the models had common shared features.

### 5.1 General model of CSF

This section presents a set of nested models, with each successive model being more restrictive and with fewer free parameters. In Model 5.1.1 (*Spatio-chromatic contrast sensitivity function*), the CSF was fitted separately for each colour direction and each luminance level. Model 5.1.2 (including *Luminance Intrusion*) restricts the fits by assuming that the CSF for chromatic stimuli is a mixture of a purely chromatic CSF and a luminance CSF for high spatial frequencies. In Model 5.1.3, a functional relationship between the model parameters and the adapting light level (*CSF as a function of adapting light level*) was introduced. Subsequently, contrast sensitivity measurements for different envelope sizes were used to generalise the model predictions from fixed-cycle stimuli to stimuli of arbitrary sizes and the extended Model 5.1.4 (*CSF as the function of the stimulus size*) and was used to predict previously published contrast sensitivity data [179]–[181] for validation.

#### 5.1.1 Spatio-chromatic contrast sensitivity function envelope

As a function of spatial frequency, the achromatic CSF is band-pass and the chromatic CSFs have a low-pass shape (Figure 4.2, 4.6). This behaviour is modelled using a truncated log-parabola [38], [46], [152], [182]:

$$\log_{10} S(f; S_{\max}, f_{\max}, b) = \log_{10} S_{\max} - \left( \frac{\log_{10} f - \log_{10} f_{\max}}{0.5 \cdot 2^b} \right)^2 \quad (5.1a)$$

$$S'(f; S_{\max}, f_{\max}, b, t) = \begin{cases} \frac{S_{\max}}{t}, & \text{if } f < f_{\max} \quad \text{and} \quad S(f; S_{\max}, f_{\max}, b) < \frac{S_{\max}}{t} \\ S(f) & \text{otherwise} \end{cases} \quad (5.1b)$$

Equation 5.1 has four parameters: peak frequency  $f_{\max}$ , peak sensitivity  $S_{\max}$ , bandwidth  $b$ , and an optional truncation parameter  $t$ .  $t$  describes the low-pass behaviour in sensitivity functions where the sensitivity saturates to a constant value for spatial frequencies below the peak frequency.

All the CSFs were first modelled as log-parabola without the truncation parameter and then the chromatic CSFs were modelled as truncated log-parabolas. The three colour channels and the seven luminance levels were modelled independently of each other. The average data for each of the 21 conditions (7 luminances and 3 colour channels) was fitted with either three ( $f_{\max}, S_{\max}, b$ ) or four ( $f_{\max}, S_{\max}, b, t$ ) free parameters.

## CHAPTER 5. MODELLING CSFS

The assumption that the contrast sensitivity of the chromatic stimulus modulations ('red-green', 'yellow-violet') is determined by the sensitivity of two putative chromatic mechanisms is made implicitly. While chromatic mechanisms favour low temporal and low spatial frequencies, it is unlikely that chromatic contrast variations at medium to high frequencies (4 and 6 cpd) are only seen by chromatic mechanisms (due to luminance artefacts; see Section 3.2 for details). Based on the data from Mullen [24], the nominally isoluminant chromatic data were fitted using only the spatial frequencies  $\leq 2$  cpd.

The results are shown in Figure 5.1 and Table 5.1. The log-parabola model fits the achromatic data well, but a truncated log-parabola model is needed to explain the chromatic data, especially at the lower frequencies, which were measured only at  $20\text{ cd/m}^2$ . The chromatic data shows a small dip in sensitivity at the extreme luminance levels of  $0.02\text{ cd/m}^2$  and  $7,000\text{ cd/m}^2$ . At this stage, it could not be confirmed whether the dip reflected a real effect or a measurement error.

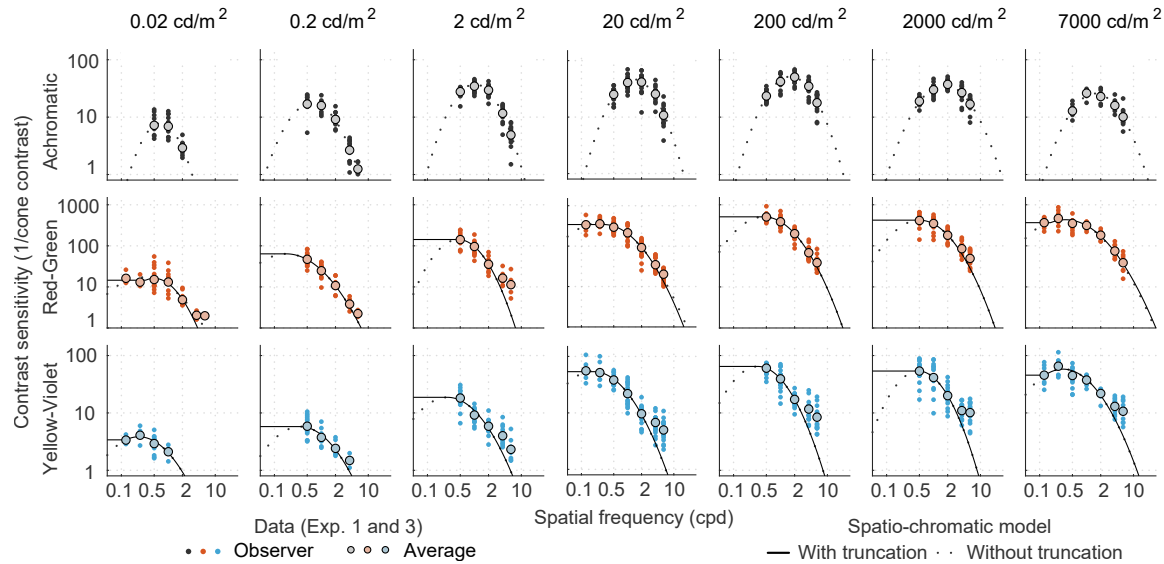


Figure 5.1: The results of fitting parabolic CSF models to the data, individually for each luminance level (columns) and colour direction (rows). Note that the frequencies below 0.5 cpd were only measured at  $20\text{ cd/m}^2$  and only for the chromatic colour channels.

Table 5.1: Parameters for log-parabola fit with truncation parameters for chromatic channels

<b>Para- meter</b>	<b>Channel</b>	<b>Luminance ( cd/m<sup>2</sup>)</b>						
		<b>0.02</b>	<b>0.2</b>	<b>2</b>	<b>20</b>	<b>200</b>	<b>2000</b>	<b>7000</b>
$f_{\max}$	<b>Achromatic</b>	0.6839	0.6371	1.023	1.372	1.624	1.689	1.540
	<b>Red-Green</b>	0.5704	0.2596	0.4536	0.3094	0.4422	0.5547	0.5501
	<b>Yellow-Violet</b>	0.2702	0.4407	0.3543	0.1679	0.3344	0.4783	0.3263
$S_{\max}$	<b>Achromatic</b>	7.825	17.63	37.45	46.46	50.89	36.44	25.80
	<b>Red-Green</b>	15.73	53.93	142.6	347.8	508.9	417.4	388.6
	<b>Yellow-Violet</b>	3.845	5.536	17.16	54.57	64.42	53.69	57.93
$b$	<b>Achromatic</b>	0.7809	0.9883	0.903	0.9082	0.9475	1.064	1.003
	<b>Red-Green</b>	0.8471	1.153	0.9108	1.17	1.123	1.015	1.055
	<b>Yellow-Violet</b>	1.159	1.156	1.155	1.356	1.126	1.041	1.271
$t$	<b>Red-Green</b>	0.0339	0.000	0.000	0.0132	0.000	0.0024	0.000
	<b>Yellow-Violet</b>	0.0576	0.000	0.000	0.000	0.000	0.000	0.1048

### 5.1.2 Luminance Intrusion

The CSF model in Figure 5.1 predicted lower sensitivities for the chromatic modulations (R-G, Y-V) at frequencies greater than 4 cpd than what was found in the experiments. This could be explained by the assumption of intrusion of a luminance mechanism at higher spatial frequencies [107], possibly because the stimuli were not made isoluminant for each observer using hetero-chromatic flicker photometry as explained in Section 3.2. This luminance intrusion was modelled by predicting chromatic sensitivity as the combination of responses of both luminance and chromatic mechanisms.

The achromatic sensitivity is modelled using the log-parabola model from Equation 5.1:

$$S_{\text{Ach}} = S(f; f_{\max}^{(\text{Ach})}, S_{\max}^{(\text{Ach})}, b^{(\text{Ach})}) \quad (5.2)$$

where  $f_{\max}^{(\text{Ach})}$ ,  $S_{\max}^{(\text{Ach})}$ ,  $b^{(\text{Ach})}$  are the peak frequency, peak sensitivity, and bandwidth of the achromatic channel, at a given luminance level. The sensitivity to the two chromatic directions is modelled as the Minkowski summation of both chromatic and achromatic

## CHAPTER 5. MODELLING CSFS

sensitivity:

$$S_{\text{Ach+RG}} = \left( \alpha_{RG}^\beta S_{Ach}^\beta(f; f_{\max}^{(\text{Ach})}, S_{\max}^{(\text{Ach})}, b^{(\text{Ach})}) + S'_{RG}^\beta(f; f_{\max}^{(\text{RG})}, S_{\max}^{(\text{RG})}, b^{(\text{RG})}, t^{(\text{RG})}) \right)^{1/\beta} \quad (5.3)$$

$$S_{\text{Ach+YV}} = \left( \alpha_{YV}^\beta S_{Ach}^\beta(f; f_{\max}^{(\text{Ach})}, S_{\max}^{(\text{Ach})}, b^{(\text{Ach})}) + S'_{YV}^\beta(f; f_{\max}^{(\text{YV})}, S_{\max}^{(\text{YV})}, b^{(\text{YV})}, t^{(\text{YV})}) \right)^{1/\beta} \quad (5.4)$$

where  $f_{\max}^{(\text{RG})}$ ,  $S_{\max}^{(\text{RG})}$ ,  $b^{(\text{RG})}$ ,  $t^{(\text{RG})}$ ,  $f_{\max}^{(\text{YV})}$ ,  $S_{\max}^{(\text{YV})}$ ,  $b^{(\text{YV})}$ ,  $t^{(\text{YV})}$  are the parameters of the two chromatic mechanisms, fitted independently for each luminance level. The parameters  $\alpha_{RG}$  and  $\alpha_{YV}$  control the amount of luminance intrusion. At each luminance level, all three sensitivity functions were fitted with 13 parameters in total (3 peak frequencies, 3 peak sensitivities, 3 bandwidths, 2 summation coefficients, and 2 achromatic channel gains). The optimisation was performed for the data of all 20 observers individually as well as the average CSF for all the observers. The fitting results for the average CSF data are presented in Figure 5.2. The log-parabola fits (truncated in cases of chromatic channels) are shown as dotted lines in Figure 5.2. The model assumes that the achromatic stimuli are picked up solely by a luminance channel (upper row) and can be completely specified by Equation 5.2. For chromatic stimuli, it was assumed that a luminance channel also contributes to the overall contrast sensitivity. In the second and third rows of Figure 5.2, the dotted lines represent the contributing luminance channel which adds to the chromatic sensitivity via probability summation and determines the response at higher spatial frequencies. The effect is more evident for the lime-violet stimuli.

## CHAPTER 5. MODELLING CSFS

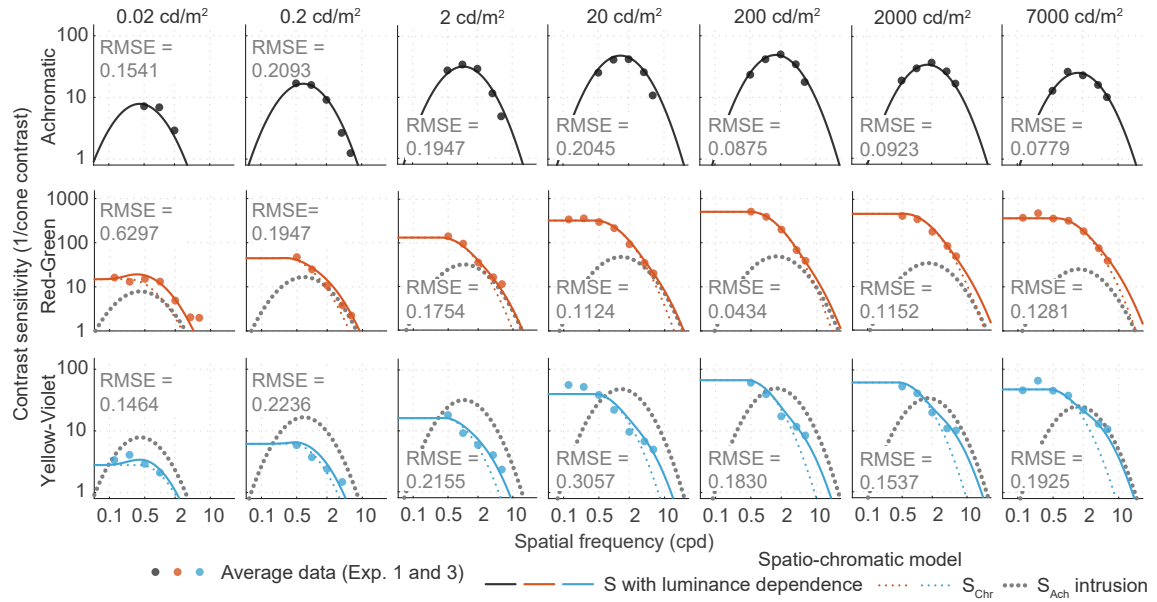


Figure 5.2: Channel summation model with 11 free parameters; see Table 5.2 for fitted parameters. Including luminance intrusion improves the model prediction for chromatic channels at higher frequencies. Filled dots represent the measured data for contrast sensitivities. Solid lines are the resultant model predictions while the dotted lines, in cases of chromatic contrast sensitivities, represent the pure chromatic and the luminance intrusion components.

The fitted parameters for the model are listed in Table 5.2. The values for  $\alpha_{RG}$  are much higher than for  $\alpha_{YY}$ , which is due to the sensitivity values for *Red – Green* being higher than for *Yellow – Violet* or *Achromatic* channels. This difference in sensitivity is partly due to the way contrast is defined (Equation (3.5)). A quick investigation of the table reveals that many of the parameters are related to the logarithmic value of luminance. In the next section, such a functional relationship is modelled so that the predictions can be generalised to any luminance level within the measured range.

Table 5.2: Parameters for the channel summation fit.

Para-meter	Channel	Luminance (cd/m <sup>2</sup> )						
		0.02	0.2	2	20	200	2000	7000
$f_{\max}$	<b>Achromatic</b>	0.5052	0.6368	1.016	1.349	1.652	1.701	1.547
	<b>Red-Green</b>	0.4735	0.2907	0.3889	0.3690	0.5028	0.5506	0.5622
	<b>Yellow-Violet</b>	0.2463	0.5571	0.5226	0.2410	0.3849	0.4831	0.4314
$S_{\max}$	<b>Achromatic</b>	7.138	17.63	37.29	41.43	47.29	36.02	25.16
	<b>Red-Green</b>	14.44	45.85	128.3	335.4	501.6	415.6	387.3
	<b>Yellow-Violet</b>	3.595	4.973	13.60	52.53	63.39	54.09	51.43
$b$	<b>Achromatic</b>	1.158	0.9886	0.9086	1.02	1.025	1.08	1.031
	<b>Red-Green</b>	0.9825	1.221	1.201	1.052	1.016	1.023	1.038
	<b>Yellow-Violet</b>	1.055	1.216	1.274	1.067	0.9617	0.9754	1.029
$\alpha$	<b>Red-Green</b>	2.858	1.089	1.315	1.037	1.527	2.750	3.120
	<b>Yellow-Violet</b>	0.3480	0.2646	0.2672	0.2443	0.3513	0.5305	0.8683

### 5.1.3 Contrast sensitivity as a function of mean luminance

Figure 5.3 shows the relationship between the fitted CSF parameters and the logarithmic luminance. The plots clearly show that some parameters, such as  $f_{\max}$ ,  $S_{\max}$  and the inverse of  $\alpha$ , are strongly related to log-luminance, while the relation of  $b$  is less clear given the data.

## CHAPTER 5. MODELLING CSFS

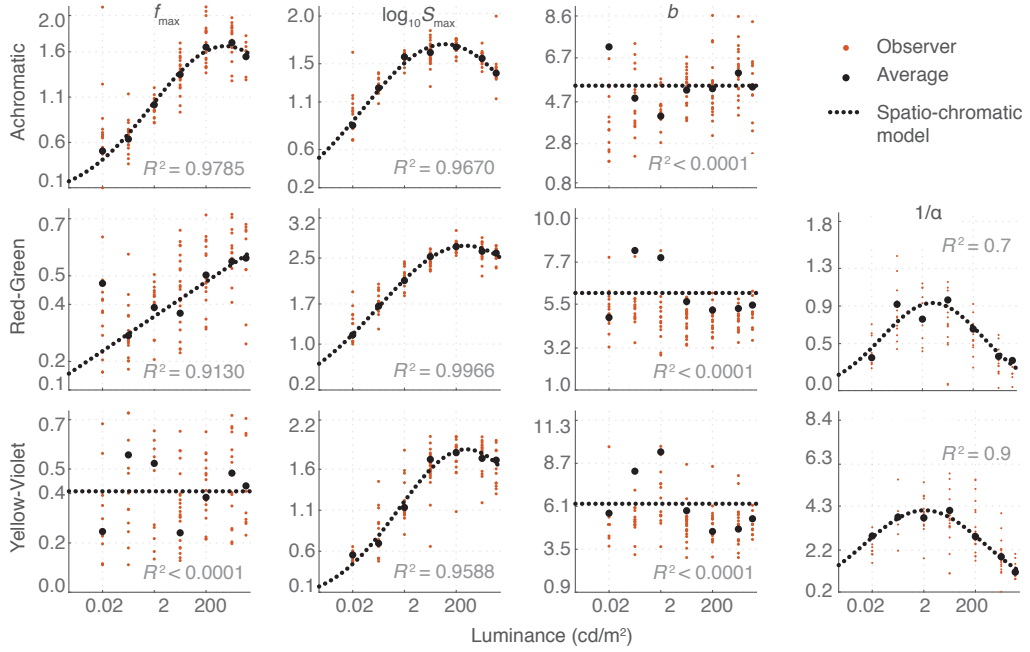


Figure 5.3: The relationship between the fitted CSF parameters and luminance. The orange dots indicate parameters fitted for individual observers and the black dots are the parameters fitted for the average observer. The dashed lines show the functions that were fitted to the parameters from average observer data to build a luminance-dependent CSF. The adjusted  $R^2$  values of the fits to the average observer are reported.  $b$  (in octaves) for all channels and  $f_{\max}$  for the lime-violet channel did not fit well to a simple function and were thus fixed to the median value across luminance levels. Left: Log-parabola parameters; peak frequency  $f_{\max}$ , peak sensitivity  $S_{\max}$ , and bandwidth  $b$ . Right: Achromatic channel gain  $\alpha$  used in the Minkowski summation.

To be able to generalise the model to different luminance levels (between  $0.02 \text{ cd/m}^2$  and  $7,000 \text{ cd/m}^2$ ), the functions for the CSF parameters that show a strong relationship with luminance were fitted and the constant values for the parameter  $b$  were found, as listed in the equations below:

$$f_{\max} = \begin{cases} 1.663\phi(\log l; 3.045, 2.834), & \text{Achromatic} \\ 0.06069 \log l + 0.3394, & \text{Red-Green} \\ 0.4095, & \text{Yellow-Violet} \end{cases} \quad (5.5a)$$

$$\log_{10} S_{\max} = \begin{cases} 1.705\phi(\log l; 1.867, 3.142), & \text{Achromatic} \\ 2.715\phi(\log l; 2.663, 3.364), & \text{Red-Green} \\ 1.843\phi(\log l; 2.696, 2.608), & \text{Yellow-Violet} \end{cases} \quad (5.5b)$$

## CHAPTER 5. MODELLING CSFS

$$b = \begin{cases} 1.036, & \text{Achromatic} \\ 1.085, & \text{Red-Green} \\ 1.097, & \text{Yellow-Violet} \end{cases} \quad (5.5c)$$

$$\frac{1}{\alpha} = \begin{cases} 0.9323\phi(\log l; 0.6986, 1.998), & \text{Red-Green} \\ 4.099\phi(\log l; 0.3328, 2.336), & \text{Yellow-Violet} \end{cases} \quad (5.5d)$$

where  $\phi$  is a Gaussian function:  $\phi(x; \mu, \sigma) = \exp\left(\frac{-(x - \mu)^2}{2\sigma^2}\right)$ . The summation coefficient  $\beta$  was fixed to 3.5. Figure 5.4 shows model predictions for the achromatic (Equation 5.2) and two chromatic (Equation 5.3 and 5.4) components of the model when the parameters are predicted by the functions and constants from Equation 5.5 above. Despite the approximations made to predict luminance-dependent parameters, the model provides a good fit to the data.

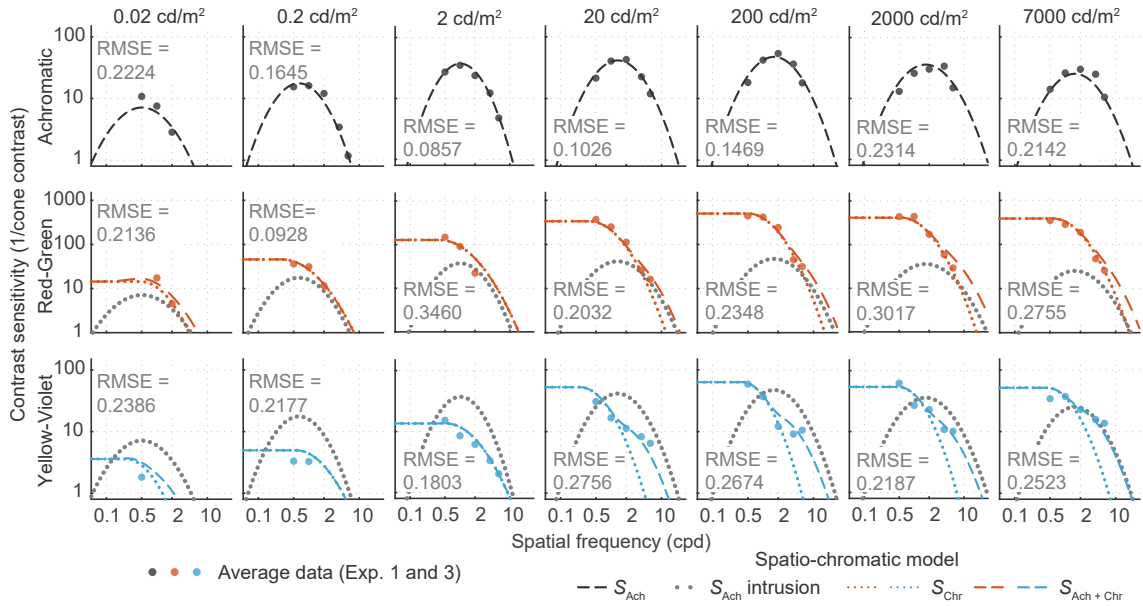


Figure 5.4: Model predictions including luminance intrusion and parameters as a function of the light level, based on equations 5.2 to 5.5

The three models (5.1.1-5.1.3) and their root-mean-squared-error (RMSE) are compared in Table 5.3. Model 5.1.1 was fitted individually for each measured luminance level and colour direction. Model 5.1.2 was fitted for each luminance level, but jointly for all colour directions. Model 5.1.3 was fitted for seven luminance-dependent parameters and can generalise predictions to any arbitrary luminance level at the cost of higher RMSE.

## CHAPTER 5. MODELLING CSFS

Table 5.3: Summary of nested models

<b>Model No.</b>	<b>Model de-scrip-tion</b>	<b>Summary</b>	<b>Equations</b>	<b>Mean RMSE</b>	
1	Log-parabola	Optimisation with 3 free parameters for Ach; $f_{\max}^{(Ach)}, S_{\max}^{(Ach)}, b^{(Ach)}$ , 4 free parameters for RG; $f_{\max}^{(RG)}, S_{\max}^{(RG)}, b^{(RG)}, t^{(RG)}$ , and 4 free parameters for YV; $f_{\max}^{(YV)}, S_{\max}^{(YV)}, b^{(YV)}, t^{(YV)}$	Eq. 5.1 fitted separately for each colour and luminance	<i>Achromatic</i>	0.0463
				<i>Red-Green</i>	0.0347
				<i>Yellow-Violet</i>	0.0529
2	Model 5.1.1 + Luminance intrusion	Optimisation with 13 free parameters; $f_{\max}^{(Ach)}, S_{\max}^{(Ach)}, b^{(Ach)}, f_{\max}^{(RG)}, S_{\max}^{(RG)}, b^{(RG)}, f_{\max}^{(YV)}, S_{\max}^{(YV)}, b^{(YV)}, \alpha^{RG}, \alpha^{YV}, \beta^{RG}, \beta^{YV}$ , and 2 fixed parameters: $t^{(RG)}, t^{(YV)}$	Eqs. 5.2 - 5.4 fitted simultaneously for all colours, independently for each luminance	<i>Achromatic</i>	0.0701
				<i>Red-Green</i>	0.1155
				<i>Yellow-Violet</i>	0.1256
3	Model 5.1.1 + Model 5.1.2 + Luminance dependence	Coefficients in Eqs. 5.5 optimised with 3 free parameters (Gaussian), and 2 free parameters (linear)	Eqs. 5.2 - 5.4 with parameters from Eq. 5.5	<i>Achromatic</i>	0.1458
				<i>Red-Green</i>	0.1998
				<i>Yellow-Violet</i>	0.2029

### 5.1.4 CSF as the function of the stimulus size

When measuring stimuli of different frequencies in, the number of cycles was kept fixed. This made the stimulus size smaller as frequency increased. This approach was used because, for most applications, it is more important to know the exact threshold of a small pattern of high frequency rather than a large field of a high-frequency sine grating. But this choice also made the dataset harder to compare with other measurements, which were mostly done for stimuli of fixed size. In this section, the previous model is extended such that the predictions could be generalised to stimuli of arbitrary size and frequency so that model predictions could be compared with other data sets. The spatial integration model proposed by Rovamo *et al.* [183] was used, in which the extent of the spatial integration is increased with the stimulus area and saturates after reaching a critical area. This model from the literature was adapted to use the proposed Model 5.1.1 as follows:

$$S_A(f, a; S_{\max}, f_{\max}, b, a_0, f_0) = S(f; S_{\max}, f_{\max}, b) \cdot \sqrt{\frac{a f^2}{a_0 + a f_0 + a f^2}}, \quad (5.6)$$

where  $S(f)$  is the log-parabola model from Equation 5.1,  $f$  is the spatial frequency in cycles per degree and  $a$  is the area in  $\text{deg}^2$ . For the stimuli in the measured dataset, which were smoothly modulated by Gaussian envelopes,  $a$  is approximated with  $\pi \cdot \sigma^2$ ; the area of a disk of the same radius as the standard deviation of the Gaussian envelope.  $a_c$  and  $f_0$  are the two parameters of the stimulus size model. To generalise the area model to work at different luminance levels, the following model was proposed:

$$S_{AL}(f, l, a) = S_A(f, a) \cdot \frac{S_L(f, l)}{S_L(f, 20)} \quad (5.7)$$

where  $S_L$  is luminance-dependent chromatic/achromatic CSF from the previous section (Equations 5.2–5.4) and  $S_A$  is the area-dependent CSF from Equation 5.6. The  $S_L(f, 20)$  in denominator accounts for the fact that  $S_A$  was fitted to the data measured at  $20 \text{ cd/m}^2$ . Figure 5.5 shows the predictions from the model described in this section.

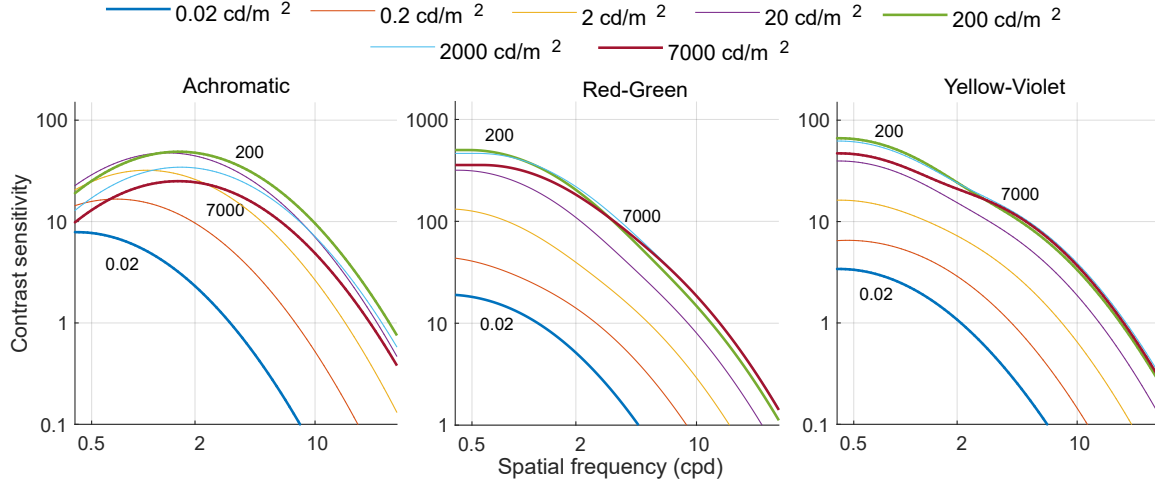


Figure 5.5: Predictions from Model 5.1.4 for spatio-chromatic contrast sensitivity at multiple luminance levels.

### 5.1.5 Comparison with other datasets

In the previous sections, it was shown that a relatively simple model can predict contrast sensitivity variation due to frequency, stimulus size and adapting luminance level, both for chromatic and achromatic gratings, as measured in the experiments. In this section, the predictions of the same model are demonstrated to be generalised and used to predict data from other experiments. Datasets from the literature that contained variability in luminance levels and/or included both chromatic and achromatic stimuli were selected for this validation.

First, the model from Equation 5.7 was used to predict the data from the ColorFest study [181]. It should be noted that the ColorFest study used stimuli of fixed size and stimuli were temporally modulated (Gaussian modulation with a standard deviation of 0.125 sec). The sensitivity in the ColorFest data is consistently higher by a factor of  $0.3 \log_{10}$  units compared to the measured data presented in the previous chapter, across all three colour directions. To obtain comparable sensitivity values, the sensitivity of the original data was reduced by this amount, which resulted in reasonably good fits (Figure 5.6). The difference in overall sensitivity could be explained by the differences in experimental procedures: while ColorFest data were collected sequentially for each stimulus variation so that the same pattern was presented in consecutive 2AFC trials, in the 4AFC measurements presented in this work, the stimuli of different frequency, colour direction or orientation were randomly selected in each trial.

## CHAPTER 5. MODELLING CSFS

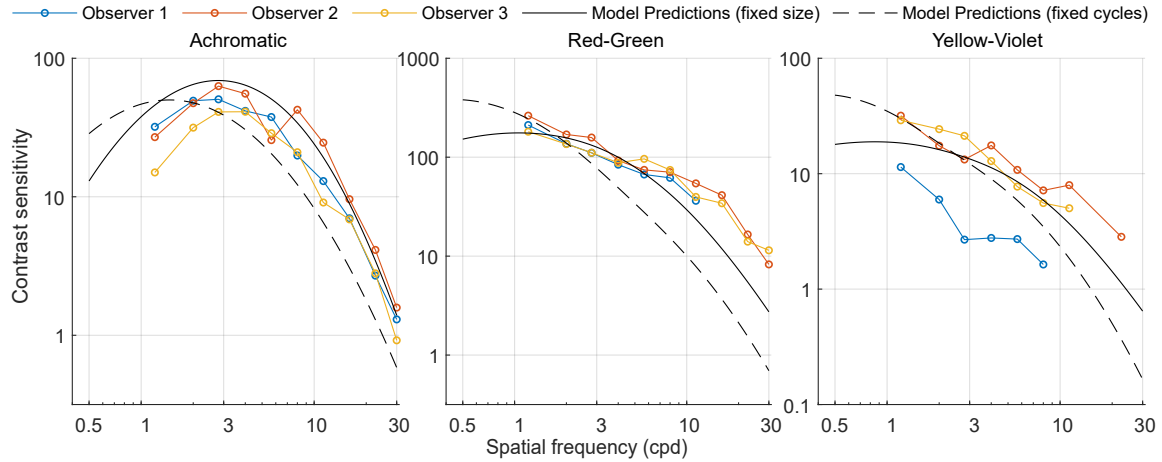


Figure 5.6: Comparison of the proposed model with the ColorFest dataset from Wuerger *et al.* [181]. The data is well explained by the continuous lines, showing the predictions for fixed-size stimuli, which were used in the original experiment.

Figure 5.6 shows the original data together with the model predictions. Predictions for that data are shown as solid lines (labelled 'fixed size'). In addition to that, the predictions for the stimuli with a fixed number of cycles (and varying size), similar to the stimuli used in the experiments presented in this work (labelled 'fixed cycles') are shown as dashed lines. The model from Equation 5.7 was used for both curves.

Finally, the proposed model is used to predict the data from the measurements of achromatic and chromatic gratings at luminance levels varying from  $0.002 \text{ cd/m}^2$  to  $200 \text{ cd/m}^2$  from Kim *et al.* [180]. Since the experimental procedure was the same as in Wuerger *et al.* [181] and different from the experiments reported in the current work, the contrast sensitivity of the data was reduced by the same amount of  $0.3 \log_{10}$  units. The predictions for achromatic gratings are shown in Figure 5.7 and for chromatic gratings in Figure 5.8. The same notation is used as before: solid lines for fixed-size stimuli used in Kim *et al.* [180] experiments, and dashed lines for the fixed-cycles stimuli used in the current work. The predictions of the model (solid lines) for achromatic gratings are close to the data except for the two lowest frequencies. This could be both due to the limitation of the simple log-parabola model used here and the lack of data for low-frequencies and achromatic gratings. The predictions for chromatic gratings (Figure 5.8) are reasonably accurate for the *Red-Green* colour direction, but slightly higher than the measurements for the *Yellow-Violet* colour direction. The cause of that difference could not be determined.

## CHAPTER 5. MODELLING CSFS

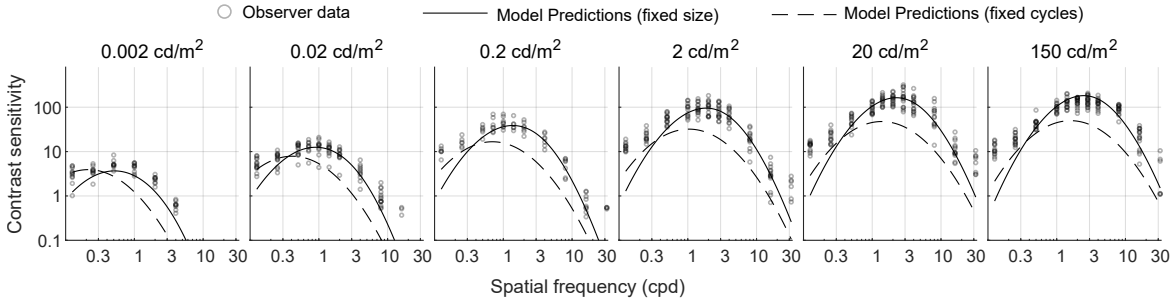


Figure 5.7: Comparison of the proposed model predictions with the achromatic contrast sensitivity measurements from Mantiuk *et al.* [179]. Solid lines represent the same stimuli as used for the measurements in the compared dataset.

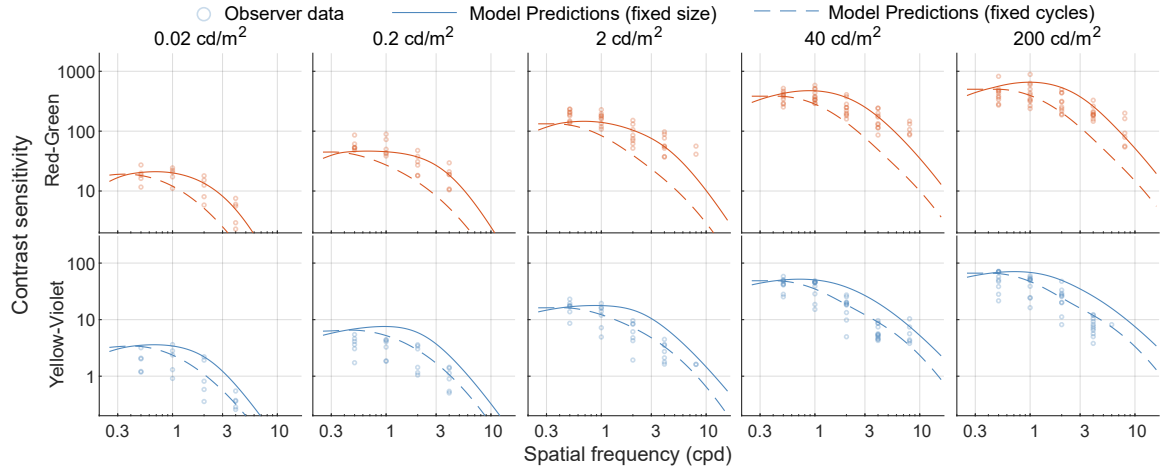


Figure 5.8: Comparison of the proposed model predictions with chromatic contrast sensitivity measurements from Kim *et al.* [180]. Solid lines represent the same stimuli as the ones used in the compared dataset.

## 5.2 Contrast sensitivity as a function of age

In this section, models of CSF as a function of observer age are evaluated based on the data presented in Section 4.2. CSFs from each observer are fitted as log-parabola functions using Equation 5.1. The parameters of interest are peak frequency  $f_{\max}$ , and peak sensitivity  $S_{\max}$  for each luminance and colour channel. The cut-off frequency  $f_c$  is calculated as the point where the contrast sensitivity predicted by the fitted CSF falls to zero. For each curve, the fitted values of peak frequency, peak sensitivity and cut-off frequency are obtained and are shown in Figure 5.9. Empty circles in the figure are optimised parameters; peak frequency, peak sensitivity, and the calculated cut-off frequency for each observer at multiple luminance levels plotted with respect to age. Solid lines are linear regression lines fitted to age versus the optimised values of the log parabola parameters with criteria  $P < 0.1$  and show the

## CHAPTER 5. MODELLING CSFS

approximate trend of change in parameter values with age.

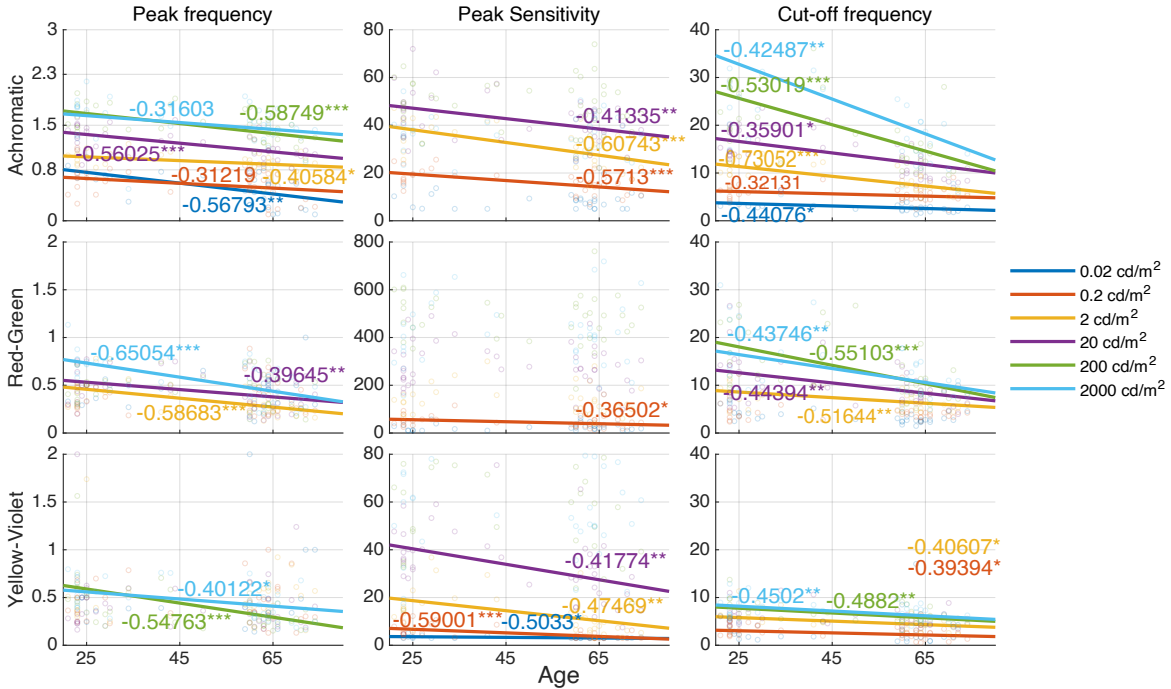


Figure 5.9: Change in log-parabola CSF parameters with age. Empty circles in the figure are optimised parameters: peak frequency, peak sensitivity, and cut-off frequency for each observer at multiple luminance levels plotted with respect to age. Solid lines are linear regression lines fitted to age vs. the optimised values of the three parameters. Peak sensitivity and cut-off frequency show a decrease with age, and the slopes of these lines appear to be luminance-dependent. Peak frequency decreases with age for achromatic contrast as well as for chromatic contrasts. Only the correlations for which the p-value is below 0.1 are shown here. \*( $P < 0.05$ ), \*\* ( $P < 0.01$ ), \*\*\* ( $P < 0.001$ )

For achromatic CSFs, peak frequencies of the functions are decreasing with age for all luminance levels, i.e., the peak of CSFs shifts towards lower frequencies with age. This is also clearly shown in Figure 4.10 (first row). The relationship is highly statistically significant ( $P < 0.001$ ) for luminance levels 20 and 200 cd/m<sup>2</sup>. Peak sensitivities for achromatic contrast also show a decrease with age for luminance levels ranging from 0.2 to 20 cd/m<sup>2</sup>. The cut-off frequency is calculated using the values of the optimised parameters for each individual. The values for cut-off frequency for achromatic stimuli appear to become more age-dependent with increasing luminance levels, as indicated by the increasing slope parameters with increasing luminance. This shows the differential effect of age on contrast sensitivity at higher frequencies.

## CHAPTER 5. MODELLING CSFS

McGrath et al. (1981) also showed similar trends for senescence of achromatic CSFs at  $2 \text{ cd/m}^2$  [130]. Similarly, Owsley et al. (1983) showed a large decrease in contrast sensitivity for higher spatial frequencies ( $> 2 \text{ cpd}$ ) at  $103 \text{ cd/m}^2$  [32]. Much of the age-dependent decrease in contrast sensitivity can be attributed to decreased retinal illuminance which largely results from changes in lens density and pupil constriction [67], [184]–[186]. From the data, it can be observed that achromatic CSFs are very much age-dependent for mid-range luminance levels ( $0.2 \sim 200 \text{ cd/m}^2$ ). As the luminance level increases, the decrease in sensitivity is observed in higher spatial frequencies only. This could be explained by the greater rate of age-dependent change in pupil size for lower luminance levels [67], [186]. Because the reduction in retinal illuminance is much stronger in low light, the sensitivity decreases with age almost uniformly across all spatial frequencies. Meanwhile, in high light-level conditions, this reduction in retinal illuminance impacts higher spatial frequencies only.

In terms of chromatic contrast, the decrease in peak frequency with age is predicted for luminance levels above  $2 \text{ cd/m}^2$  and  $200 \text{ cd/m}^2$  for red-green and yellow-violet colour directions respectively. The peak frequencies predicted for chromatic channels are around 0.5 cpd which is consistent with other studies [24], [44], [187], [188]. However, this is also the lowest spatial frequency that was measured. The fits from the data suggest that this peak frequency may decrease further with observers' age. More data needs to be collected for isoluminant chromatic stimuli at lower spatial frequencies ( $< 0.5 \text{ cpd}$ ) to verify this finding.

As shown in Figure 4.10, the peak sensitivity of the yellow-violet colour direction seems to be affected much more by age compared to the red-green colour direction. Figure 5.9 shows a significant change to red-green peak sensitivity with age only at  $0.2 \text{ cd/m}^2$ . Meanwhile, yellow-violet peak sensitivity decreases with age for luminance levels up to  $20 \text{ cd/m}^2$ . This disparate effect among the two chromatic directions can be explained by changes in lens density with age. Studies investigating the spectral characteristics of human lens ageing have shown that transmittance of the shorter end of the visible spectrum (blue/violet light) decreases much more rapidly with age compared to medium to long wavelengths [184]. Thus, while L and M cone responses are reduced with age, the ratio of these reductions is comparable in magnitude and so the age-dependent effect on red-green (L-M) contrast sensitivity is not very pronounced. On the other hand, S cone response is decreased much more with age compared to L and M cone responses, resulting in a much larger decrease in yellow-violet (S-(L+M)) contrast sensitivity. The study by Hardy et al. (2005) demonstrates that this large change in yellow-violet contrast sensitivity is in part due to the wavelength-

## CHAPTER 5. MODELLING CSFS

dependent filtering happening in the ocular media and it can be accounted for when the stimuli are equated at the retina [131].

The values for cut-off frequency for red-green stimuli appear to become more age-dependent with increasing luminance level which shows that the sensitivity at higher frequencies decreases more rapidly with age. For yellow-violet stimuli, the correlation between cut-off frequency and age is statistically significant but the slopes are close to zero. Therefore, higher frequencies are not disproportionately affected by age in yellow-violet stimuli.

### 5.2.1 Empirical model

Based on the trends shown in Figure 5.9, Model 5.1.4 was extended to add age as a factor in determining the peak frequency, peak sensitivity and the bandwidth of the log-parabola contrast sensitivity curves. The peak frequency of achromatic and red-green CSFs is modelled to decrease linearly with age. The peak frequency of yellow-violet CSFs is unaffected by age. Peak sensitivity is modelled as a quadratic polynomial function of age and log luminance for all three colour directions, i.e., the sensitivity decreases with age but the rate of this decline is dependent on the mean luminance as well. The bandwidth is modelled to decrease with age for all three colour directions. The age factor in the model is normalised to the mean age of the younger group. This is done to maintain consistency with Model 5.1.4 which was optimised for the younger group only. The following equations show the joint effect of luminance and age in the CSF model with the optimised parameters:

$$f_{\max} = \begin{cases} 1.857\phi(\log l; 5.589, 50.443) - 0.004(\text{age} - 27), & \text{Achromatic} \\ 0.004 \log l + 9.739 * 10^{-5} - 0.019(\text{age} - 27), & \text{Red-Green} \\ 3.127 * 10^{-5}, & \text{Yellow-Violet} \end{cases} \quad (5.8a)$$

$$\log_{10} S_{\max}' = \begin{cases} 2.362\phi(\log l; 2.141, 31.32), & \text{Achromatic} \\ 2.781\phi(\log l; 3.132, 27.474), & \text{Red-Green} \\ 2.961\phi(\log l; 3.46, 41.3), & \text{Yellow-Violet} \end{cases} \quad (5.8b)$$

$$S_{\max} = \begin{cases} S_{\max}' - 0.009(4 - \log l)(\text{age} - 27), & \text{Achromatic} \\ S_{\max}' + 0.034(4 - \log l)(\text{age} - 27), & \text{Red-Green} \\ S_{\max}' + 0.046(4 - \log l)(\text{age} - 27), & \text{Yellow-Violet} \end{cases} \quad (5.8c)$$

## CHAPTER 5. MODELLING CSFS

$$b = \begin{cases} 0.789 - 0.014(\text{age} - 27), & \text{Achromatic} \\ 1.326 + 0.020(\text{age} - 27), & \text{Red-Green} \\ 5.315 - 0.006(\text{age} - 27), & \text{Yellow-Violet} \end{cases} \quad (5.8d)$$

(5.8e)

where  $\phi$  is a Gaussian function:  $\phi(x; \mu, \sigma) = \exp\left(\frac{-(x - \mu)^2}{2\sigma^2}\right)$ .

The fitting results of this empirical model are shown in Figure 5.10. The shift in peak frequency and the narrower bandwidth (lower cut-off frequency) for achromatic contrast sensitivity curves in the older age group are correctly predicted by the model. The model also predicts the decrease in chromatic sensitivities for higher spatial frequencies as shown in the data. The mean error values (shown in Table 5.5) for younger and older observers are comparable. However, the model is strictly numerical and does not explicitly define the physiological changes in human vision brought upon by ageing. In the next few models, the various age-related changes in human vision were included and their relationship with changes in contrast sensitivity functions was investigated.

## CHAPTER 5. MODELLING CSFS

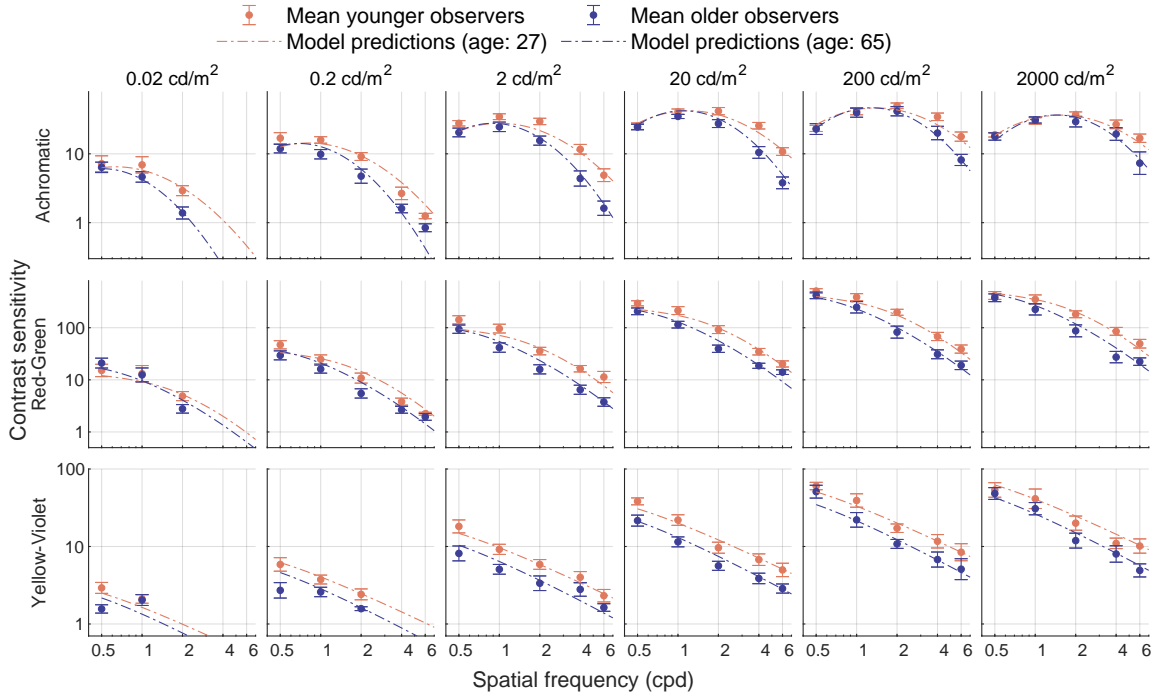


Figure 5.10: Mean contrast sensitivity functions from older and younger observer groups. The three rows present achromatic, red-green and yellow-violet CSFs respectively. The columns present CSFs at different background luminance levels from  $0.02$  to  $2000\text{ cd/m}^2$ . The secondary axis (green curves) indicates the difference in population means of log sensitivity values from the two age groups (young - old) with 95% confidence interval.

### 5.2.2 Luminance reduction

The amount of light entering the eyes of younger vs older observers differs due to physiological changes in the optical elements of the eye and the reduction in pupil size known as senile miosis. With ageing, the lens becomes yellower and blocks out short wavelengths more [184], [189]. Meanwhile, luminous efficiency curves shift towards shorter wavelengths with decreasing luminance [51], [190]. This causes a reduction in the amount of light reaching the retina and being absorbed by the photoreceptors [184], [191], [192]. Several ageing vision studies have tried simulating the optical characteristics of older visual systems in younger observers by reducing the amount of light that falls upon their retinas [32], [64]. If contrast sensitivity losses with ageing occur solely due to reduced retinal illumination, the data trends from younger observers with artificially lowered luminance stimuli should mimic the decline in contrast sensitivity for older observers.

Assuming that the main factor that affects the contrast sensitivity with respect to age is

## CHAPTER 5. MODELLING CSFS

luminance reduction, Model 5.1.4 can be used for young observers with the input mean luminance reduced to simulate this reduction of luminance in older observers. This model does not make any assumptions about the site of luminance reduction. Mathematically, the variable  $l$  (mean background luminance) in Equations 5.5 is reduced by a factor for older observers. The model was tested with luminance reduction factors of 3 and 10.

The fitting results in Figure 5.11 show the predictions for younger observers (without any luminance reduction) and two predictions for older observers with luminance reduction factors of 3 and 10. Table 5.4 compares the error values for the two reduced luminance transmittance values. For achromatic and red-green modulation directions, the scotopic/mesopic (low luminance) contrast sensitivity is better predicted when the luminance input to the model is one-third of that of the younger observers. The photopic contrast sensitivity for achromatic and red-green stimuli is better predicted when the luminance input to the model is one-tenth of that of younger observers (except 2000 cd/m<sup>2</sup> in achromatic CSF). This result might seem counter-intuitive at first because a larger luminance reduction factor would be expected for scotopic/mesopic regions as the difference between younger and older groups is larger in this region as well. However, we should keep in mind that the rate of change of sensitivity with respect to luminance is also much higher in the scotopic/mesopic region as compared to the photopic region (see the steep increment in sensitivity from 0.02 to 20 cd/m<sup>2</sup> as compared to higher luminances in Figure 4.3). This means that even a small change in luminance in the scotopic/mesopic region can cause a large change in the predicted sensitivity. On the other hand, since the sensitivities are largely independent of luminance in the photopic range, a much larger change in luminance would be required to cause any change in the predicted sensitivity for older observers. Similarly, at 2000 cd/m<sup>2</sup>, lowering the luminance in the model for older observers resulted in higher predicted contrast sensitivity compared to younger observers. This is because of the anomalous behaviour of CSF decreasing at very high luminance levels. Since, this model is agnostic towards the age group, lowering the luminance from 2000 to 670 cd/m<sup>2</sup> (when the reduction factor is 3) or 200 cd/m<sup>2</sup> (when the reduction factor is 10) results in increased sensitivity for older observers contrary to the data.

## CHAPTER 5. MODELLING CSFS

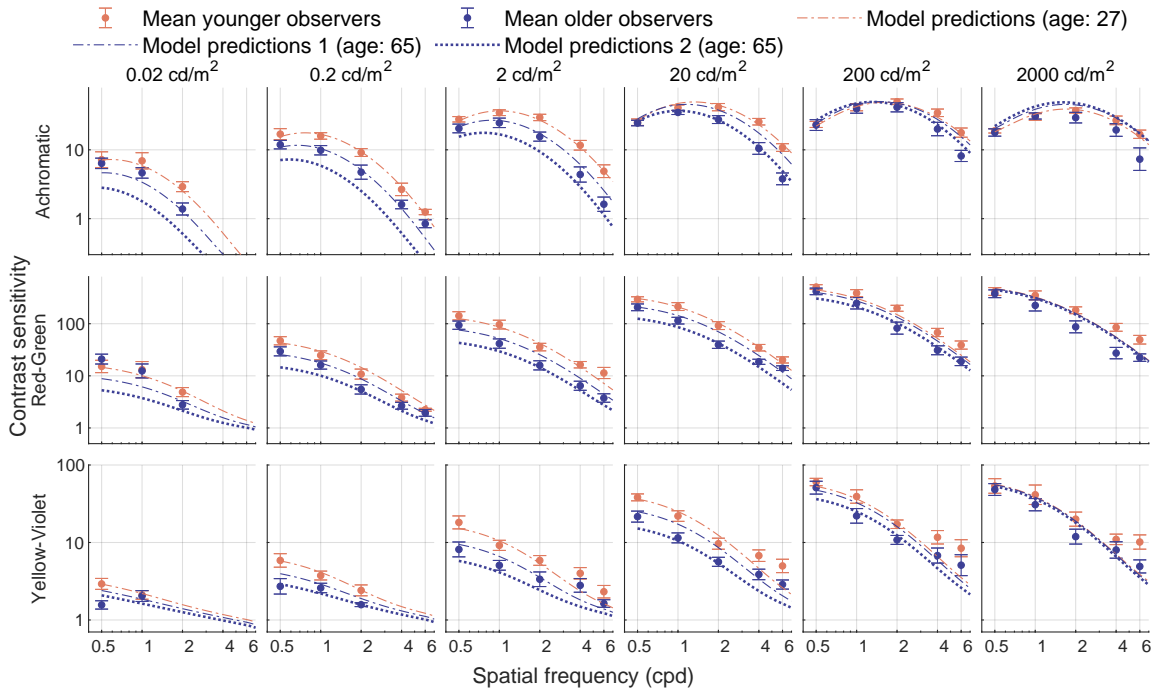


Figure 5.11: Age-dependent luminance reduction model of CSF. The description of the plots is the same as in Figure 5.10.

Table 5.4: Mean RMSE from model predictions for older observer group for each tested combination of luminance level and colour direction. The prediction errors for luminance reduction factors 3 and 10 are compared and the smaller errors in each comparison are highlighted.

Colour direction	Luminance reduction	Luminance( cd/m <sup>2</sup> )					
		0.02	0.2	2	20	200	2000
<i>Achromatic</i>	3	0.113	0.1	0.1125	0.2047	0.1442	0.2088
	10	0.376	0.3584	0.1709	0.0537	0.0946	0.2212
<i>Red-Green</i>	3	0.2822	0.1238	0.1413	0.1541	0.1245	0.1806
	10	0.4625	0.2136	0.2154	0.146	0.1045	0.1617
<i>Yellow-Violet</i>	3	0.1347	0.1085	0.077	0.1515	0.1406	0.1324
	10	0.1115	0.0444	0.129	0.0918	0.097	0.1141

In the case of yellow-violet stimuli, the higher luminance reduction factor of 10, explains the lower contrast sensitivity of older observers for both photopic and mesopic conditions

## CHAPTER 5. MODELLING CSFS

(except 2 cd/m<sup>2</sup>). From these observations, it can be concluded that simply reducing the luminance by a fixed factor does not explain the reduced sensitivity in older observers. If that were the case, the same reduction factor would explain the reduced sensitivity for all colour channels. Thus, instead of a simple luminance reduction factor, the age-related differences in optical transmission across the spectrum of visible light should be accounted for. Moreover, contrast sensitivity is affected differently in photopic versus mesopic/scotopic ranges in older observers which can not be predicted well with a simple reduced luminance model.

### 5.2.3 Pupil size reduction

As we age, the dilator and sphincter pupillary muscles, which control the amount of light entering the eye, weaken and cause the pupils to be constricted. This age-dependent reduction in pupil size, called senile miosis, is much larger for low luminance conditions. As luminance increases, the differences in pupil size between older and younger observers diminish [119], [193]. To illustrate, for a 1.5 cd/m<sup>2</sup> uniformly illuminated stimulus spanning a 30° × 30° visual area, the pupil diameters for 25 and 75 year old observers will be 5.6 and 4mm ( $\Delta = 1.6$  mm) respectively. For the same stimulus at 150 cd/m<sup>2</sup>, the pupil diameters for 25 and 75 years old observers will be 3.2 and 2.7mm ( $\Delta = 0.5$  mm) respectively (pupil sizes are calculated using Watson and Yellott [119]’s unified pupil size formula and the values are comparable to those reported in Nakamura *et al.* [193]). In other words, the age-dependent percentage reduction in retinal illumination roughly increases with decreasing light levels. Hence, at lower luminance, greatly reduced pupil diameter in older observers in addition to lower lens transmittance results in a much lower amount of light entering the eye.

In the previous model, a fixed luminance reduction factor was used to predict decreased contrast sensitivity in older observers. Here, the luminance input to older observers is reduced as a function of the ratio of pupil area between the younger and older observers. Mathematically, the variable  $l$  (mean background luminance) in Equations 5.5 becomes:

$$l' = l \frac{f(l, a, age)}{f(l, a, 27)} \quad (5.9)$$

where,  $f(l, a, age) = \pi p_s(l, a, age)^2$

where,  $f(l, a, age)$  is the function representing the pupil area calculated from a predicted pupil size ( $p_s$ ). Watson and Yellott’s unified pupil size model was used here, which takes the mean luminance, area of the visual field and age as its parameters. For any given condition, the pupil area of the younger observer (mean age: 27) is taken as reference and the ratio

## CHAPTER 5. MODELLING CSFS

between the pupil areas of the specified age group and the reference group is then calculated. The measured mean luminance value is recalculated accordingly and fed to the CSF model to predict contrast sensitivity.

Figure 5.12 shows that this model predicts lower sensitivity in older observers only for low luminance conditions. In photopic conditions, the pupil size difference between older and younger observers is not large enough to predict the corresponding contrast sensitivity differences. It can be surmised that while reduced luminance due to smaller pupil size may predict some of the reduced contrast sensitivity in older observers in mesopic/scotopic conditions, it does not explain the contrast sensitivity changes in photopic conditions.

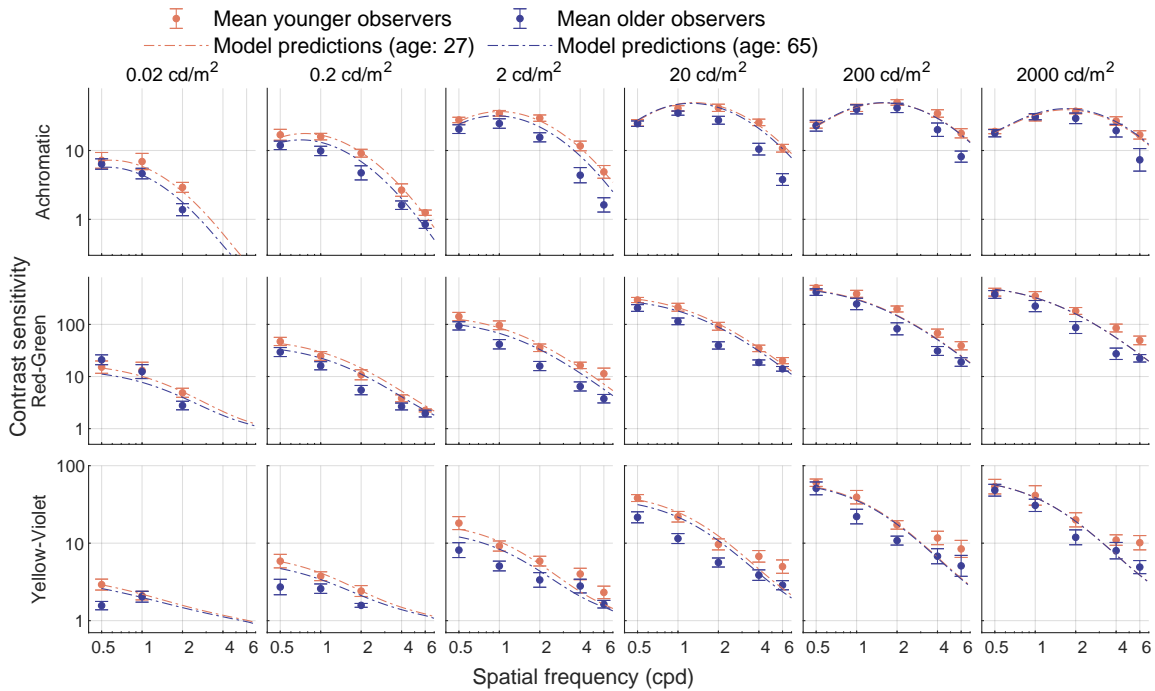


Figure 5.12: Age-dependent pupil size reduction model of CSF. The description of the plots is the same as in Figure 5.10.

### 5.2.4 Lens transmission

The optical density of the human lens changes as we age which also results in changes in its spectral transmittance function. Pokorny *et al.* [184] have shown that the transmittance in the shorter wavelength region of the visible spectrum is reduced much more than the longer wavelengths [184]. Figure 5.13 (left) shows the relative reduction in lens transmittance in the visible spectrum. Because of this, the response of the cones is also affected as less light

## CHAPTER 5. MODELLING CSFS

is reaching the retina. Figure 5.13 (right) shows the reduction in the cone responses with age. The S-cone response is much more affected with age compared to the L and M cones owing to the disproportionate reduction in short-wavelength transmittance.

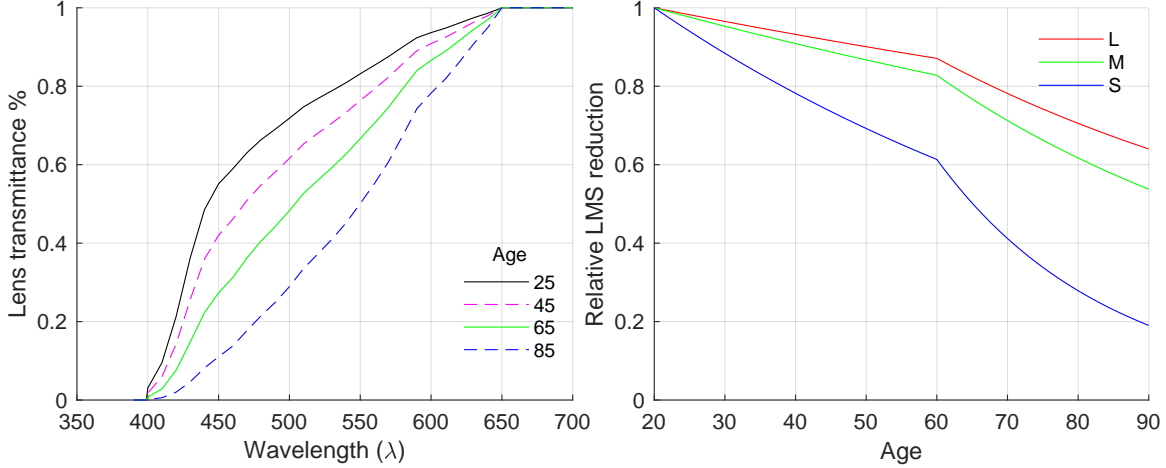


Figure 5.13: Pokorny's lens transmission function.

To model this effect, the mean cone response values for the background and the incremental difference in cone responses for the stimuli are weighed with a factor representing age-related cone response reduction.

$$\begin{aligned} L'_0 &= L_0 \frac{T_L(\text{age})}{T_L(27)}, & M'_0 &= M_0 \frac{T_M(\text{age})}{T_M(27)}, & S'_0 &= S_0 \frac{T_S(\text{age})}{T_S(27)}, \\ \Delta L' &= \Delta L \frac{T_L(\text{age})}{T_L(27)}, & \Delta M' &= \Delta M \frac{T_M(\text{age})}{T_M(27)}, & \Delta S' &= \Delta S \frac{T_S(\text{age})}{T_S(27)} \end{aligned} \quad (5.10)$$

$$T_{C \in \{L,M,S\}}(\text{age}) = \int_{\lambda} P(\lambda, \text{age}) F_{C \in \{L,M,S\}}(\lambda) d\lambda \quad (5.11)$$

where, the function  $P(\lambda, \text{age})$  is the lens transmittance function from Pokorny *et al.* [184] (reproduced in Figure 5.13 (left)) and  $F_{C \in \{L,M,S\}}(\lambda)$  are Stockman and Sharpe [110]'s cone fundamental functions for L, M and S cones.  $T_{C \in \{L,M,S\}}(\text{age})$  are the unscaled cone responses calculated by integrating the product of the aforementioned two functions over the entire visible wavelength range for different ages (result shown in Figure 5.13 (right) for ages 20 to 90). The ratio of these cone responses for any arbitrary age relative to the mean age (27) of the younger observer group is used to calculate the age-dependent cone responses (Equation 5.10), which in turn are used to estimate the age-dependent response of the hypothetical opponent colour mechanisms (Equation 3.2). These cone and opponent responses

## CHAPTER 5. MODELLING CSFS

are fed to Model 5.1.4 to predict changes in contrast sensitivity functions based on just the age-dependent lens transmission model. The results are shown in Figure 5.14

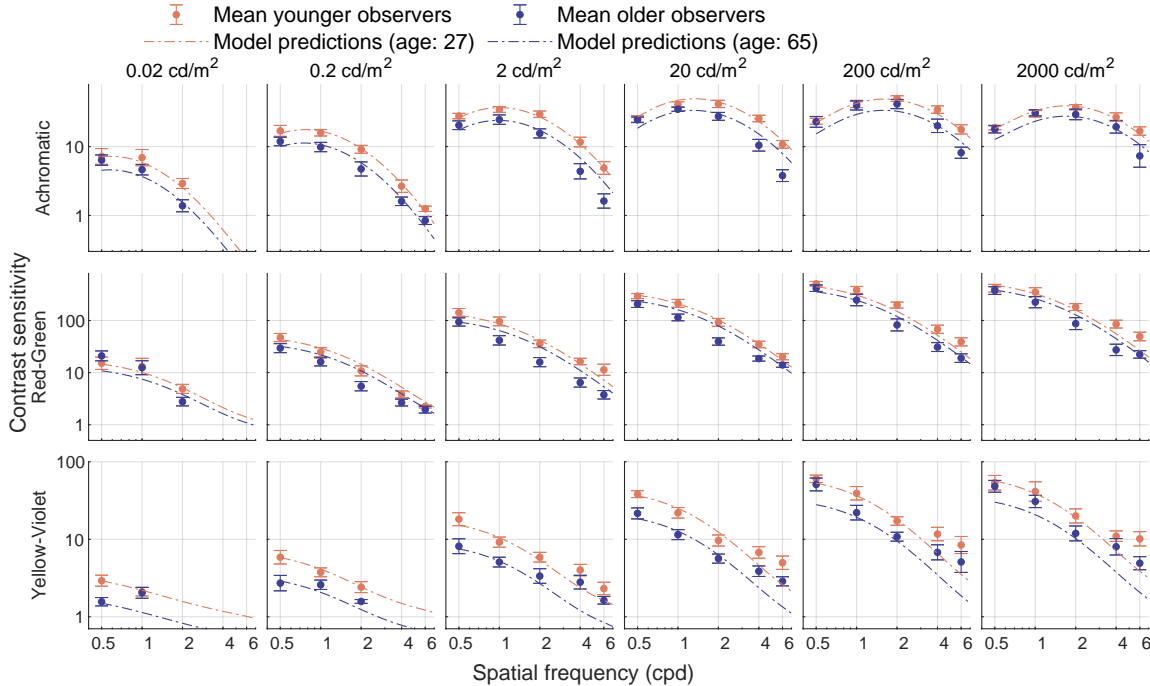


Figure 5.14: Age-dependent lens transmission model of CSF. The description of the plots is the same as in Figure 5.10.

The lens transmission model predicts the loss of sensitivity in high frequencies very well as shown in Figure 5.14 which is expected since the spatial frequency cutoff of CSF is heavily dependent on the properties of the optical system. The model overpredicts the loss of sensitivity for low spatial frequencies for photopic luminances. This could be because these losses are compensated for by higher neural mechanisms which are not included in this simple model.

### 5.2.5 Optical factors

The *Pupil size reduction* and the *Lens transmission* models evaluate the effect of ageing on the pupil and the ocular lens respectively. Both of these individual factors were able to predict part of contrast sensitivity loss in older observers. In this section, both of these models are combined to evaluate the joint effects of these physiological changes in the optical system of ageing humans. Both Equation (5.5) and 5.9 were integrated into the general CSF Model 5.1.4. Figure 5.15 shows the results from the combined *Optical factors* model.

## CHAPTER 5. MODELLING CSFS

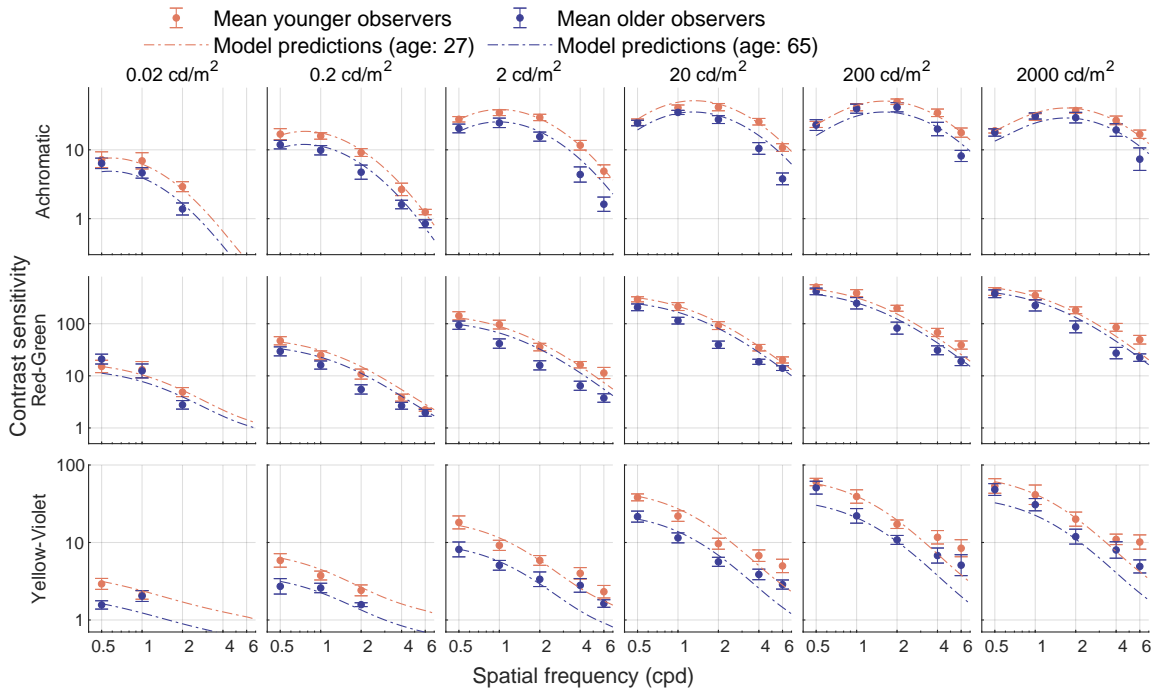


Figure 5.15: Age-dependent optical changes model of CSF. The description of the plots is the same as in Figure 5.10.

The results of this model are very similar to those from the *Lens transmission* model. This is because the *Pupil size reduction* predicted very small age-related differences in CSF as shown in Figure 5.12 and its contribution is fairly negligible when both the tested optical factors are combined.

### 5.2.6 Results

The prediction errors of all the evaluated age-dependent models are reported in Table 5.5. For the empirical model, the predictions of both the younger and older observers are the lowest compared to the preceding models. This is to be expected as the empirical model, though informed by the age-related changes in CSF, does not make any explicit assumptions about the mechanisms that bring about this change. The physiological models on the other hand attempted to explain the behavioural measurements using the decline in biological function of specific parts of the visual system. The proposed empirical model is recommended to predict age-related changes in CSF.

## CHAPTER 5. MODELLING CSFS

Table 5.5: Summary of ageing models. The empirical model was fitted for both younger and older observer groups. The physiological models were not refitted for the young observers and show the model predictions for the Model 5.1.4 without any additional age-related factors. The physiological models for older observers are extensions of Model 5.1.4 for specific age-related changes in the visual system.

<b>Model</b>	<b>Summary</b>	<b>Equations</b>	<b>Mean RMSE</b>	
Empirical	Optimisation with both older and younger groups data with age as a parameter	Eq. 5.8	Younger group	0.0798
			Older group	0.0933
Luminance reduction	No optimisation	N/A	Younger group	0.0879
			Older group	0.1464 (3x luminance reduction), 0.1759 (10x luminance reduction)
Pupil size reduction	No optimisation	Eq. 5.9	Younger group	0.0879
			Older group	0.1732
Lens transmission	No optimisation	Eqs. 5.10-5.11	Younger group	0.0879
			Older group	0.1612
All optical factors	No optimisation	Eqs. 5.9-5.11	Younger group	0.0879
			Older group	0.1693

### 5.3 Disc CSFs

Since the visual system is composed of channels that are tuned to different spatial frequencies and orientations [21], [194], the combined sensitivities of these individual channels can be used to predict sensitivities of more complex stimuli. In their seminal work, Campbell and Robson (1968) proposed the spatially-selective multi-channel model of the human vision system by comparing contrast thresholds from sine and square wave gratings and also proposed a simple relationship between contrast sensitivities of high-frequency square and sine waves [21]. This is extended by testing this simple model on disk stimuli. Watson and Ahumada (2005) proposed a relatively simple energy summation model to predict the contrast sensitivity of different spatial stimuli [169]. Their model performs very well for a variety of different achromatic spatially-varying stimuli. However, the model has not

## CHAPTER 5. MODELLING CSFS

been demonstrated to work across luminance levels, stimulus sizes and chromatic contrast modulation. This work validates the energy model for such a variety of conditions.

### 5.3.1 Contrast energy models

First, a family of contrast energy models [169] is reviewed that attempts to predict the sensitivity to a disk. The contrast energy model assumes that a pattern is detected when the energy of that pattern exceeds a predetermined threshold. The energy is computed as:

$$E = \int_{\rho_x} \int_{\rho_y} (I(\rho_x, \rho_y) S(\rho_x, \rho_y))^2 d\rho_x d\rho_y, \quad (5.12)$$

where  $\rho_x$  and  $\rho_y$  are the horizontal and vertical spatial frequencies in cycles per degree (cpd),  $I$  is the Fourier transform of a signal (Fourier transform of a luminance map) and  $S$  is a contrast sensitivity function.

To model the frequency decomposition of a disc, we can take its cross-section, which forms a rectangular function as shown in Figure 5.16. The analytical Fourier transform of a rectangular function is a sinc function:

$$D(\rho; r) = r \operatorname{sinc}(2\rho r) \quad (5.13)$$

where  $r$  is the radius of the disc in visual degrees and  $\rho$  is the spatial frequency in cycles per degree. To avoid integration in both spatial dimensions, as done in Equation (5.12), the energy can be integrated in the polar coordinates ( $\rho = \sqrt{\rho_x^2 + \rho_y^2}$ ,  $\theta$ ):

$$\begin{aligned} E(r, L_b, c) &= \int_0^{2\pi} \int_\rho (c D(\rho; r) S(\rho, L_b, a))^2 \rho d\rho d\theta \\ &= 2\pi c^2 \int_\rho (D(\rho; r) S(\rho, L_b, a))^2 \rho d\rho, \end{aligned} \quad (5.14)$$

where  $S()$  is the contrast sensitivity as the function of spatial frequency  $\rho$ , luminance of the background  $L_b$  and area  $a$ . The last term  $\rho$  serves as the Jacobian determinant.  $c$  is the contrast of the disc expressed as a Weber ratio,  $\Delta L/L_b$ . The disc is detected when the energy exceeds the threshold energy,  $E_{\text{thr}}$ , therefore the detection threshold can be found as:

$$c_{\text{thr}} = \sqrt{\frac{E_{\text{thr}}}{E(r, L_b, 1)}} \quad (5.15)$$

The contrast sensitivity is computed as the inverse of the detection threshold,  $s = 1/c_{\text{thr}}$ .

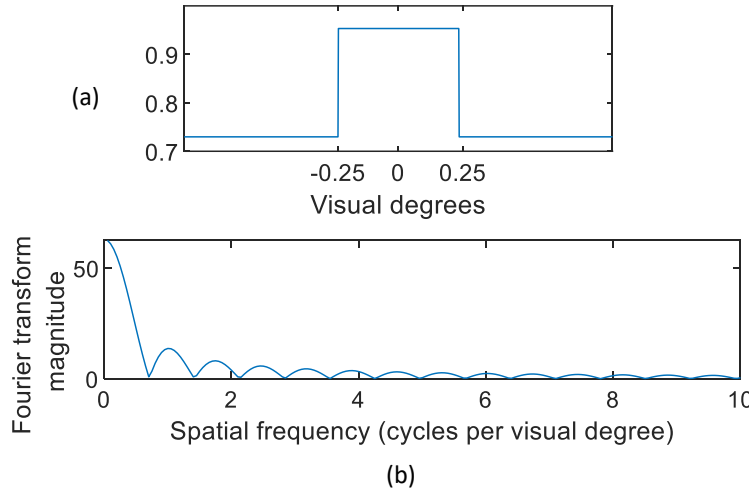


Figure 5.16: Decomposition of disk stimuli into sinusoids in Fourier space. (a) 1D representation of disk stimulus in the spatial domain; (b) Fourier transform magnitude of the disk stimulus in the spatial frequency domain. The transform of the rectangular pulse is the sinc function.

The spatio-chromatic CSF from [165] is used as a function  $S()$ . This model relies on data from 5 separate datasets, measured from  $0.0002 \text{ cd/m}^2$  to  $10,000 \text{ cd/m}^2$ , and is capable of predicting contrast sensitivity for modulation in any direction in the colour space. The colour direction is queried corresponding to the achromatic or chromatic contrast of the disc. This CSF does not model the effect of orientation, and therefore the energy summation in Equation (5.14) is assumed to be orientation-independent.

### 5.3.2 Model fitting and practical considerations

The integral from Equation (5.14) is approximated by a numerical integration between 0 and 32 cpd. It was found that the predictions are stable at 128 samples. To fit each model described below, the prediction error is minimised:

$$20 \sqrt{\frac{1}{N} \sum_{i=1}^N (\log S_{\text{predicted}}[i] - \log S_{\text{measured}}[i])^2} \quad [\text{dB}] \quad (5.16)$$

for  $N$  data points. For  $S_{\text{measured}}$ , the mean of the data measured across the three displays and all observers is used. For all models, the threshold energy is fitted separately for the achromatic and two chromatic colour directions.

One difficulty with the energy model from Equation (5.14) is the choice of the area parameter for the contrast sensitivity function. Several models are reviewed below, which vary in the method by which stimuli are integrated over spatial area.

## CHAPTER 5. MODELLING CSFS

### *Disc area*

If it is assumed that the detection of a disc is largely governed by its low-frequency components, then the detection should be dependent on the size of the disc. Therefore, the area parameter of the CSF could be set to be proportional to the area of the disc:  $a \propto \pi r^2$ . Unfortunately, the proportionality could not be optimised, as the area parameter was too strongly correlated with  $E_{\text{thr}}$  parameters (optimisation results in very large areas). Instead, it was assumed that  $a = \pi r^2$ .

### *Constant area*

It can be argued that the area parameter is irrelevant for the contrast energy model as the model itself accounts for spatial pooling by integrating over the area. This is because the integration over the frequency domain in Equation (5.14) is equivalent to an integration over the spatial area (Plancherel theorem).

A constant-area model was attempted to be fitted by optimising for the area parameter of the CSF, but this resulted in an implausible large value ( $900 \text{ deg}^2$ ). Therefore, this parameter was instead set to 1.

### *Sinc local extrema*

One major inconvenience of modelling a disc as a sinc function is that it requires a numerical solution to an integral from Equation (5.14). A more convenient model was tested, in which the integral is approximated by summing up the CSF-weighted energy only for the local minima and maxima of the sinc function.

### *Sum of Gabor*s

Most CSF models, including the one used in this work, explain the sensitivity to Gabor patches rather than to isolated spatial frequencies. The sensitivity to isolated frequency can only be measured for an infinite-size grating. The Fourier transform of a Gabor patch is a Gaussian function in the frequency domain — it occupies a band of frequencies rather than a single frequency in the Fourier domain. This raises the question, of whether the sinc function can be approximated with a sum of Gabor, or a sum of Gaussian functions in the frequency domain.

## CHAPTER 5. MODELLING CSFS

Figure 5.17 shows that indeed the sinc function can be well approximated as a sum of multiple Gaussian curves. The sinc function from Equation 5.13 can be expressed as a series:

$$D_g(\rho; r) = \sum_{n=0}^{\infty} h_n \exp\left(-\frac{\left(\rho - \frac{\rho_n}{2r}\right)^2}{2\left(\frac{\sigma_n}{2r}\right)^2}\right), \quad (5.17)$$

The peak ( $\rho_n$ ), deviation ( $\sigma_n$ ) and height ( $h_n$ ) of the Gaussian functions are fixed and the first few values are listed in Table 5.6.

Table 5.6: Base values of Gaussian curves parameters for the central and the next 5 sinc function lobes as depicted in Figure 5.17a.

Sinc lobe ( $n$ )	0	1	2	3	4	5
$\rho_n$	0	1.43	2.46	3.47	4.48	5.48
$\sigma_n$	0.5	0.37	0.36	0.35	0.35	0.34
$h_n$	1	-0.22	0.13	-0.09	0.07	-0.06

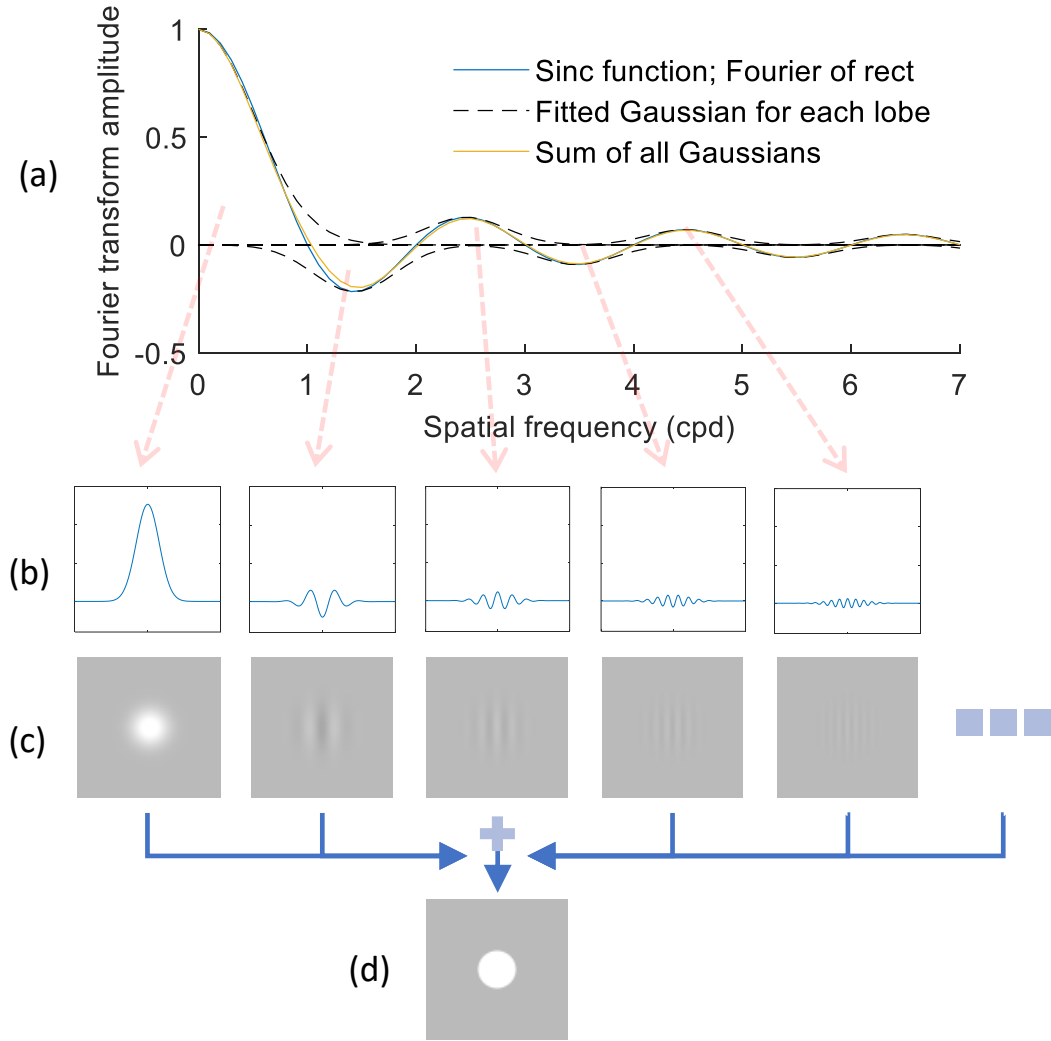


Figure 5.17: Decomposition of disk stimuli into Gabor patches in Fourier space. (a) Sinc function as a sum of Gaussian curves; (b) Sinusoids modulated with a Gaussian envelope are the 1D spatial domain representation for each sinc lobe (Gaussian curve). The position of the peak in the Fourier space represents the spatial frequency of the sinusoid, the height of the Gaussian is the amplitude of the sinusoid and the standard deviation of the Fourier Gaussian represents the width of the Gaussian envelope in the spatial domain; (c) Representative Gabor patches for each lobe of the Fourier transform in (a); (d) 2D achromatic disk stimulus.

## CHAPTER 5. MODELLING CSFS

The total contrast energy for this model can be represented as a numerical integral with respect to the spatial frequencies corresponding to the peaks of the sinc lobes. Equation 5.14 then becomes:

$$E(r, L_b, c) = c^2 \sum_{n=0}^{\infty} \frac{f(n-1) + f(n)}{2} \Delta\rho_n,$$

where,  $f(n) = (D_g(\rho_n; r) S(\rho_n, L_b, a_n) \rho_n)^2$ , (5.18)

$$a_n = \pi \left( \frac{r}{\pi \sigma_n} \right)^2 = \frac{1}{\pi} \left( \frac{r}{\sigma_n} \right)^2$$

$a_n$  is the area of the corresponding patch which is directly proportional to the radius of the disk and inversely proportional to the standard deviation of the Gaussian curve in the Fourier domain.

### 5.3.3 Multiple detector models

Foley et al. demonstrated that the detection of Gabor patches of different sizes, shapes (circular, collinearly and orthogonally elongated) and phases can be explained by detection by one or more mechanisms that are characterised by a receptive field that sums contrast linearly followed by a nonlinear transformation to a response [195]. The idea has been extended in this work to model the detection of discs. Rather than modelling an array of receptive fields as conducted in previous work, an analytical detection model for a disc has been derived.

It is assumed that the detection of a disc is primarily based on its edge. Let's assume that a single piece of such an edge is detected by a single hypothetical edge detector. When a disc radius is increased, the edge gets larger and more detectors have a chance to detect it. Such contribution of multiple detectors is typically modelled as probability summation, which corresponds to a generalised (see "Luminance intrusion" in Section 5.1.2):

$$s_{\text{all}} = \left( s_1^\beta + s_2^\beta + s_3^\beta + \dots + s_N^\beta \right)^{1/\beta}, \quad (5.19)$$

where  $s_1, \dots, s_N$  are the sensitivities of individual detectors.  $\beta$  is the exponent of the psychometric function, typically between 3 and 4. For convenience, it was assumed that the edge detectors are identical and the visual system performs summation in the continuous domain. Therefore, if all detectors along the circumference of a disc with the radius  $r$  contribute, the sensitivity is:

$$s_{\text{all}} = \left( 2\pi r s_{\text{ed}}^\beta \right)^{1/\beta} = (2\pi r)^{1/\beta} s_{\text{ed}}, \quad (5.20)$$

## CHAPTER 5. MODELLING CSFS

where  $s_{\text{ed}}$  is the sensitivity of a single edge detector. Below several candidate models were considered for the individual edge detector.

### *Fundamental frequency*

Campbell and Robson demonstrated that the detection of the square wave can be explained by the detection of the fundamental frequency of that square wave [21]. Although the detection of discs is of interest here rather than square waves, it could be assumed that a single edge detector in a multiple-detector model detects a pattern similar to a square wave. This is because the cross-section of a disk is a rectangular function, and a square wave consists of tiled copies of rectangular functions.

The Fourier series representation of a square wave is composed of a set of sine waves with decreasing amplitude and increasing frequency. For a 50% duty cycle square wave of a specified spatial frequency, the Fourier series representation would be the fundamental component (sine wave) with the same spatial frequency as the square wave and a series of odd harmonics with spatial frequencies in odd multiples (3x, 5x, 7x, ...) of the fundamental. Campbell and Robson (1968) have shown that for higher spatial frequencies, the sensitivity of a square is  $4/\pi$  times the sensitivity of a sine wave with the same spatial frequency. This relationship remains valid as long as the third harmonic component is of a high enough spatial frequency to remain below the threshold, as the contrast sensitivity of our visual system decreases rapidly for higher spatial frequencies. Given that, the multiple detector model can be expressed as:

$$S_{\text{disc}}(L_b, r) = S_c (2\pi r)^{1/\beta} \frac{4}{\pi} S\left(\frac{1}{4r}, L_b, a\right), \quad (5.21)$$

The spatial frequency,  $1/4r$ , is selected so that the rectangular function formed by the cross-section of the disc corresponds to a square wave (Figure 5.18). Variations of the model where the area is either a function of the radius of the disc  $a = \pi r^2$ , set to a constant value  $a = 1$  or fitted as a parameter of the model were tested. The model with different  $\beta$  values was also tested. The model provided the best predictions when both the area and the  $\beta$  parameter were optimised in conjunction. However, the optimised value of  $\beta = 1.24$  is not realistic for a Weibull psychometric function. So, the  $\beta$  value was fixed to 3.5 and fitted the area and the  $S_c$  parameters; the fitted values are reported in Table 5.7.

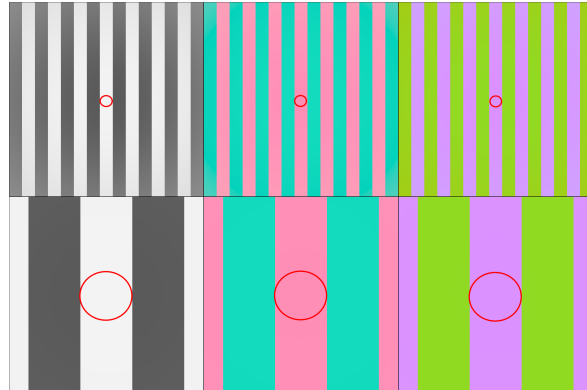


Figure 5.18: Disc stimuli (in red circles) represented as partial square waves. Smaller radii correspond to higher spatial frequencies.

#### *Peak Spatial CSF*

Edge contrast sensitivity has been shown to be an indicator of the most sensitive contrast vision channel [196], [197]. In other words, the peak of the contrast sensitivity envelope (across spatial frequencies) is proportional to the edge sensitivity of the visual system. Since a disc forms a circular edge, the peak-sensitivity assumption can be combined with the multiple-detectors model to predict the disc sensitivity as:

$$S_{\text{disc}}(L_b, r) = S_c \max_\rho(S(\rho, L_b, a_0)) (2\pi r)^{1/\beta}, \quad (5.22)$$

where  $S_c$  is the fitted base sensitivity for a particular colour direction, listed in Table 5.7.

#### *Multiple contrast energy detectors*

The multiple detector model can be combined with the energy model. Assuming that the inner integral of Equation (5.14) represents an individual edge detector:

$$E(r, L_b, c) = c^2 (2\pi r)^{1/\beta} \int_\rho (D(\rho; r) S(\rho, L_b, a_0))^2 \rho d\rho, \quad (5.23)$$

where  $a$  is the nominal (fitted) area, so that  $S(\rho, L_b, a_0)$  models the sensitivity of a single edge detector ( $s_{\text{ed}}$ ).  $\beta$  was optimised as a parameter of the model.

Table 5.7: Parameters and error of fitting each model. The threshold energy,  $E_{\text{thr}}$  is reported for achromatic, red-grey and violet-grey colour directions. The error is reported in the units of dB.

Model	$E_{\text{thr}}^{\text{ach}}$	$E_{\text{thr}}^{\text{rg}}$	$E_{\text{thr}}^{\text{vg}}$	a	Error
Disc area	0.1639	0.0826	0.0864	n/a	6.78
Constant area	0.4805	0.2533	0.1758	1	4.99
Multiple detectors	2.1066	0.7460	0.4044	3.63	4.39
Sinc local extrema	0.1925	0.0917	0.0502	1	6.74
Sum of Gabors	0.3213	0.1495	0.1353	n/a	5.62
	$S_{\text{ach}}$	$S_{\text{rg}}$	$S_{\text{vg}}$		
Fundamental frequency	0.6967	0.8040	1.1020	6.94	6.01
Peak spatial CSF	0.5641	0.9429	1.2404	2.42	4.54

### 5.3.4 Results

The numerical errors and the fitted parameters for our models are summarised in Table 5.7. In terms of numerical error, the *disc area* model is the worst performing, while the *constant area* model has the lowest prediction error among the four contrast energy models. The predictions, shown in Figure 5.19, demonstrate that the sensitivity to disc type stimuli does not increase with the disc radius as rapidly as predicted by the *disc area* model. Therefore, the hypothesis that the detection of the disc is mostly mediated by the detection of the low-frequency signal formed by a disc can be discarded. The *constant area* model predicts the data better than the disc area model. However, this model does not account for the small increase of sensitivity with the radius of the disc. In the case of the *sinc local extrema* model, the summation over a discrete set of frequencies poorly predicts the sensitivity to discs. And our last contrast energy model, *sum of gabors* does not predict the data as well as the *constant area* model despite the theoretical premise that a disc can be approximated by a series of Gabors.

Figure 5.20 and Table 5.7 show the fitting results for the three proposed multiple detectors models. Numerically, the *fundamental frequency* multiple detectors model, performs worse than the *constant area* and *sum of gabors* models but better than *disc area* and *sinc local extrema* models. Qualitatively, the fitting results of the *fundamental frequency* model show that the shape of the CSF with respect to luminance is distorted as the radius of the disc stimuli increases, as depicted in the top-right panel in Figure 5.20. The assumption that the contrast sensitivity of a disc could be approximated as a function of square wave contrast sensitivity could be valid for smaller-sized disc stimuli only.

*Multiple c.e. detectors* and *peak spatial CSF* models have the lowest two error values

## CHAPTER 5. MODELLING CSFS

respectively among all our proposed models. Increasing the size of a disc has a small effect on sensitivity that is well modelled assuming probability summation across multiple detectors, shown in Equation (5.20). This is the strategy used in both our best-performing models. The fitting errors of both models (4.39 and 4.54 dB) are comparable, as well as the curves shown in Figure 5.20. The available data cannot sufficiently discriminate between both models. Therefore, the simpler *peak spatial CSF* model is recommended.

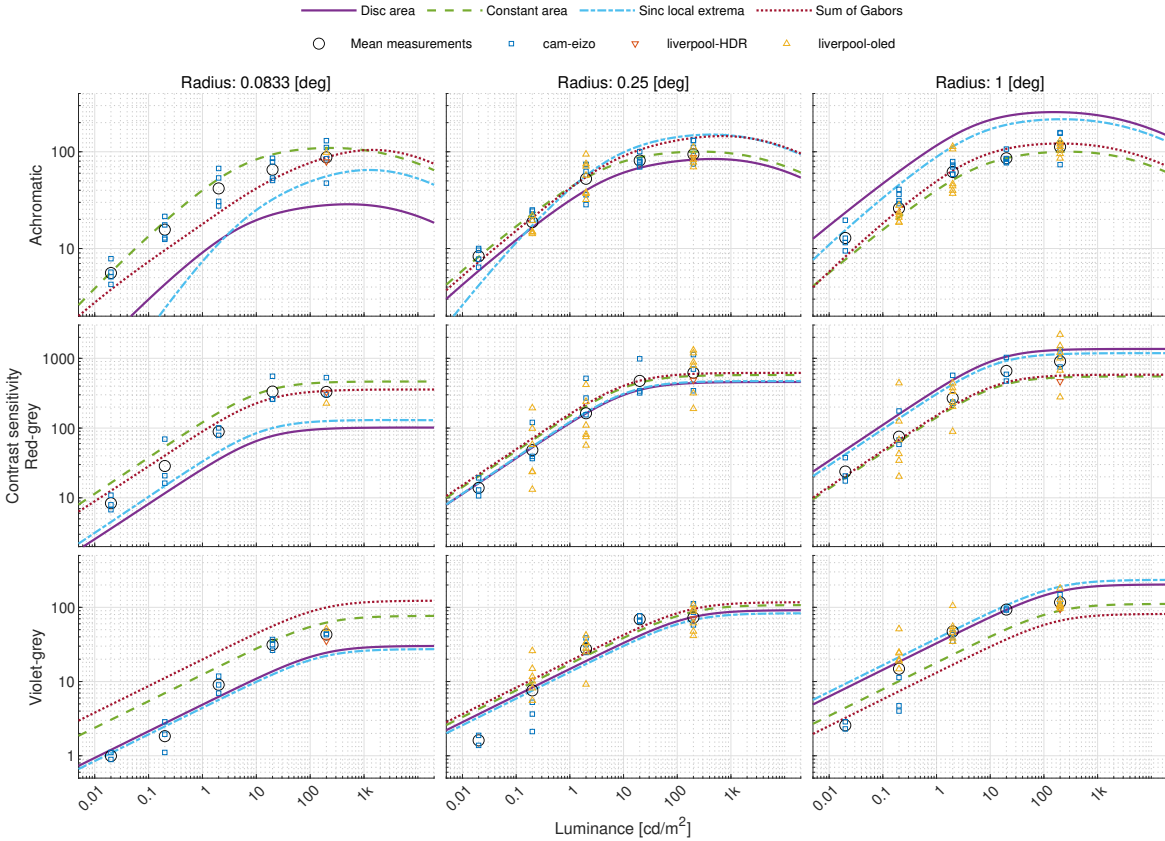


Figure 5.19: Measurements of the disc contrast sensitivity and the predictions of four contrast energy models. The means (black circles) are computed over the data collected in Cambridge (cam-eizo). The sensitivity is plotted in the units of cone contrast [28].

## CHAPTER 5. MODELLING CSFS

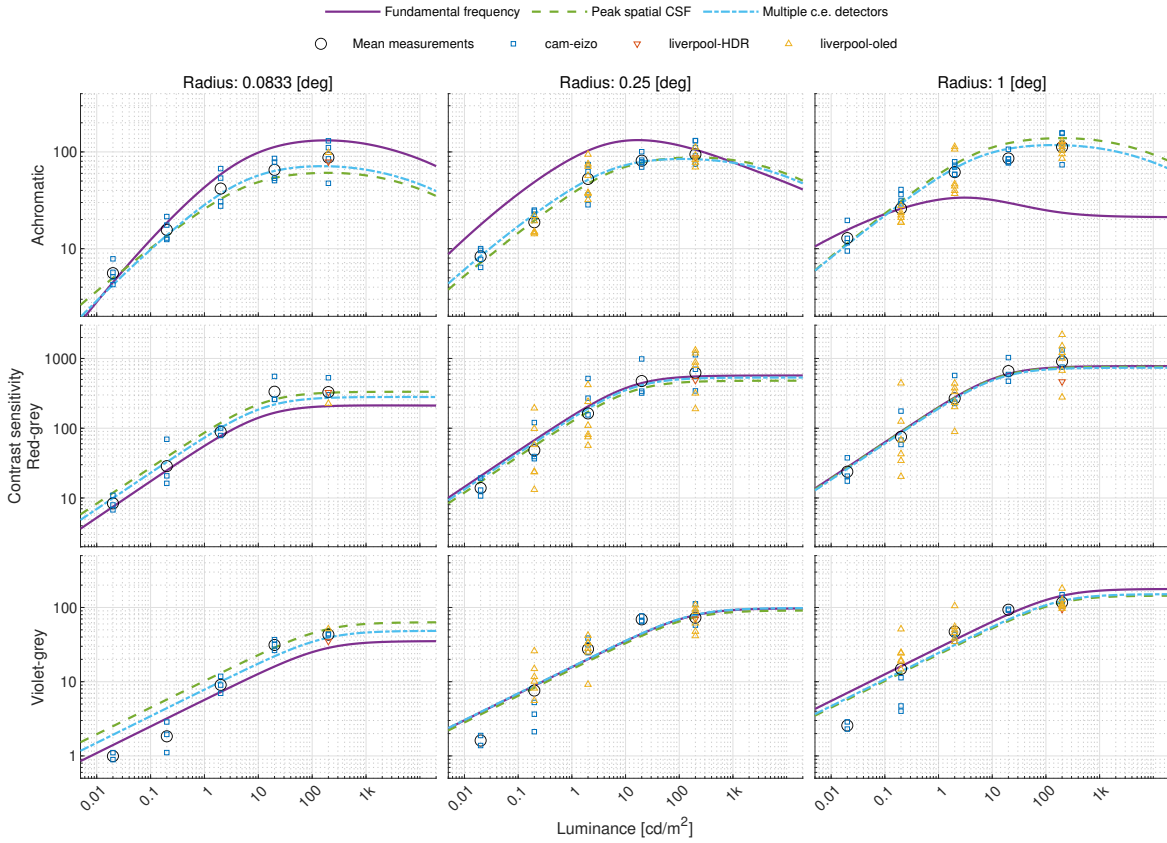


Figure 5.20: Measurements of the disc contrast sensitivity and the three multiple detector models.

### 5.4 Summary of chapter

The models presented in this work offer new approaches to understanding and predicting spatiochromatic contrast sensitivity under varied conditions. In Section 5.1, a computational model was developed to describe how contrast sensitivity functions adapt to different light levels, specifically under mesopic and photopic conditions, emphasising on the different roles of spatial and chromatic contrasts in visual perception. The next Section 5.2, introduced an empirical model that incorporates age as a critical factor. A series of physiologically-based models were also presented to understand how different optical parts of the visual system affect CSF. In Section 5.3, several models focused on the contrast sensitivity for disc stimuli are presented, highlighting how the visual processing of different shapes is related and can be influenced by factors such as size and luminance.



## CONTRAST MATCHING FUNCTIONS

These contrast sensitivity functions (CSFs), as discussed in Chapter 4, provide valuable information about the limits of the human visual system. Human vision at higher contrast levels (also known as suprathreshold contrast vision), however, cannot be explained by contrast sensitivity functions. Studies have shown that when the contrast is sufficiently high, the response of the visual system becomes largely independent of the threshold contrast of the respective stimulus [76]. For example, once physical contrast is sufficiently high, low and high spatial frequency patterns are perceived as having equal contrast, regardless of large differences between their respective threshold contrasts. This phenomenon is known as contrast constancy [76]. Contrast constancy across different spatial frequencies is an established phenomenon [76], [79], [198]. It shows that the limitations in pre-cortical mechanisms that affect contrast at the threshold might be compensated for at post-receptoral sites. Hence, the mechanisms governing contrast vision at threshold and suprathreshold contrast levels might be very different from each other.

In normal everyday conditions, the input to our visual system mostly consists of suprathreshold contrasts. It is therefore very important to characterise contrast perception at these high contrast levels to gain a better understanding of our visual system. The assumption of contrast constancy would be valid in most cases and would thus provide a convenient model for retargeting images across different conditions. However, there is not enough unambiguous evidence to support this hypothesis for matching across very different luminance levels. Studies investigating contrast constancy across luminance levels report quite different results depending on the methodology and the range of luminance levels used [79]–[81]. In this chapter, the issue of contrast constancy, or the lack thereof, across a wide range of luminance levels is investigated by measuring contrast matching functions for different stimuli and viewing conditions for two age groups.

The chapter is divided into four sections detailing: i) contrast matching measurements for younger and older observer groups, ii) statistical analysis of the significant factors affecting the contrast matching data, iii) detailed results describing the trends in the contrast matching data, iv) general discussion of the results from the dataset.

## CHAPTER 6. CONTRAST MATCHING FUNCTIONS

The data and contrast matching results for the younger observers group presented in this chapter have been adapted from a published article which won the 2022 Best Paper award at *Color and Imaging Conference (CIC)*:

M. Ashraf, R. K. Mantiuk, J. Martinovic, and S. Wuerger, “Suprathreshold contrast matching between different luminance levels,” in *Color and Imaging Conference*, Society for Imaging Science and Technology, vol. 2022, 2022. doi: 10.2352/CIC.2022.30.1.38.

### 6.1 Experiment: Contrast matching across luminances

The contrast matching functions were measured using the apparatus described in Section 3.4.2 for a younger and an older observer group. Briefly, the apparatus used comprised of two screens separated by a black opaque partition, enabling haploscopic viewing where each screen is visible to only one eye. The left eye was exposed to the high-dynamic-range (HDR) screen, while the right eye viewed a standard dynamic range (SDR) screen set to a fixed mean luminance. Calibration of both displays was meticulously conducted to ensure luminance and colour accuracy. For the experiments, observers were presented with visual stimuli on both screens, with the task of adjusting the HDR screen’s contrast to match that of the reference stimulus on the SDR screen, facilitated by input devices. This setup, allowed independent viewing by each eye, and for comparing contrasts under different luminance conditions.

#### 6.1.1 Observers

Two groups of observers participated in the contrast-matching experiments. The older group consisted of the same observers who participated in the contrast sensitivity experiments in Section 4.2. The younger group consisted of 27 observers below the age of 60 (mean age: 28 years). All the older observers performed the contrast matching experiment at Liverpool. The younger observer group was tested at both sites (Liverpool and Cambridge).

#### 6.1.2 Procedure

The stimuli were Gabor patches of spatial frequencies 0.5, 2, and 4 cpd visual angle and showed 2 cycles of a sinusoidal grating, as described in Section 3.3. Such fixed-cycle stimuli result in higher spatial frequency patterns being smaller in size. Three colour directions (achromatic, red-green and lime-violet) were used. Three suprathreshold contrasts were tested, which are referred as *high*, *medium*, and *low* contrast conditions.

Contrast matching was done across luminance levels. Each session consisted of test stimuli

## CHAPTER 6. CONTRAST MATCHING FUNCTIONS

displayed at either 0.02, 0.2, 2, 20, 200, or 2,000 cd/m<sup>2</sup> on the left (HDR display). The reference stimulus was displayed on the right (SDR display) at a mean luminance of 200 cd/m<sup>2</sup> for all the sessions. An example of the stimuli configuration in a single trial is shown in Figure 6.1. Ideally, the reference and test contrast should be alternated between the right and the left randomly during the experiment but the displays used in this experiment are not interchangeable. Moreover, the display configuration could not be physically randomised because the HDR display system was carefully calibrated both geometrically and colourimetrically and thus does not allow for movement.

The trials were not time-limited and were scheduled in blocks with the same test and reference luminance, to ensure that the observers were fully adapted to test and reference background luminance levels. In low luminance test conditions (0.02, 0.2, and 2 cd/m<sup>2</sup>) five-minute dark adaptation period was mandated before the start of the experiment. The participants were asked to quickly alternate between the two eyes to ensure that both eyes were adapted to their respective luminance levels. Within each session, stimuli of all three spatial frequencies, three suprathreshold contrast levels, and all three chromatic directions were randomly interleaved. The test and reference stimuli were of identical spatial frequency and colour direction but rendered at different luminance luminances (except for the test = 200 cd/m<sup>2</sup> condition, which matched the reference luminance level). The contrast of the reference stimulus was fixed at any of the *high*, *medium*, and *low* reference contrast conditions, while the contrast of the test stimulus could be manipulated by the observer. The initial test contrast was assigned a random value that was either higher or lower than the reference contrast. The lower initial value was the threshold contrast of the corresponding stimulus, while the higher initial value was the highest contrast that the display was able to produce at that viewing condition. The test contrast was allowed to exceed the value of 1 (resulting in asymmetric contrast within the stimuli) which indicates that a suitable match within the display gamut was not achieved. Observers could also skip a trial if they failed to obtain a close match.

## CHAPTER 6. CONTRAST MATCHING FUNCTIONS

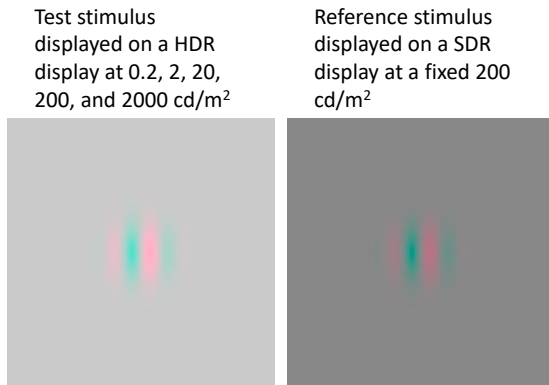


Figure 6.1: An example contrast matching trial. The same stimulus is shown at two luminance levels and the observer is asked to adjust the contrast of the test stimulus until both stimuli have the same perceived contrast.

The method of adjustment was used to measure the point of subjective equality between the test and reference contrast. The observers were asked to increase or decrease the test contrast until they perceived both stimuli as equal in contrast relative to their respective background luminances. Once the observers were satisfied with the match, they pressed a button and moved on to the next trial. For some extreme conditions where a match was not possible, the observers were able to skip to the next condition. As contrast matching is a subjective task, no feedback was given to the observer after their response. Each pair of test and reference contrast was measured 3 to 5 times depending on the variance between measurements for each observer. The measurement of a condition was concluded when either the (within-observer) target standard deviation of 0.1 units was achieved or when the condition was measured 5 times.

### 6.2 Statistical Analysis

The same statistical analysis approach as the one described in Section 4.2.2 was used here. The dataset spanned two observer age groups, five spatial frequencies, six luminance levels, and three colour directions as well as three different supra-threshold contrast levels. Separate LMEMs were fitted to the data from the three colour directions. Only the data points where the matched test contrast was below 1 (i.e. within the display gamut) were used for the statistical modelling. Again, luminance and frequency values were log10 and log2 transformed, respectively, and entered into LMEMs as continuous predictors. Age group (younger and older) and standard contrast levels (low, medium and high) were entered as categorical

## CHAPTER 6. CONTRAST MATCHING FUNCTIONS

predictors. A maximal random effects structure that allowed for goodness-of-fit was used. It included random intercepts for different subjects, frequencies and luminance levels. The best-fitting model was selected via a step-wise regression method which iteratively eliminates effects and interactions to determine the model that best explains the data. The full details of the LMEM analysis can be found in Appendix E.

### 6.3 Results

The mean results from the younger and older observers group are summarised in Figures 6.2-6.3 respectively. Figures 6.4, 6.5, and 6.6 show the same data but the younger and older group data are shown together which highlights the age-specific difference in matching curves. The three columns represent data from the three spatial frequencies. The rows represent the three colour directions. The log contrast matches are shown as a function of log background luminances of the test stimuli. Each panel has three matching curves corresponding to *high*, *medium*, and *low* suprathreshold contrast conditions. For each suprathreshold matching curve, the corresponding reference contrast line is also shown. The grey dotted lines represent the contrast thresholds across luminance levels for the corresponding spatial frequency pattern from the data presented in Chapter 4. Matched contrast values above 1 indicate that the observers were not able to achieve a perceived contrast match within the display gamut and the contrast envelope of the Gabor patch was no longer symmetric. Incremental values were displayed while decrements were clipped. Although these data points were not included in the statistical analyses, they are shown in the results figures since they are still informative about perceived contrast at very low background luminances ( $0.02$  and  $0.2\text{ cd/m}^2$ ).

## CHAPTER 6. CONTRAST MATCHING FUNCTIONS

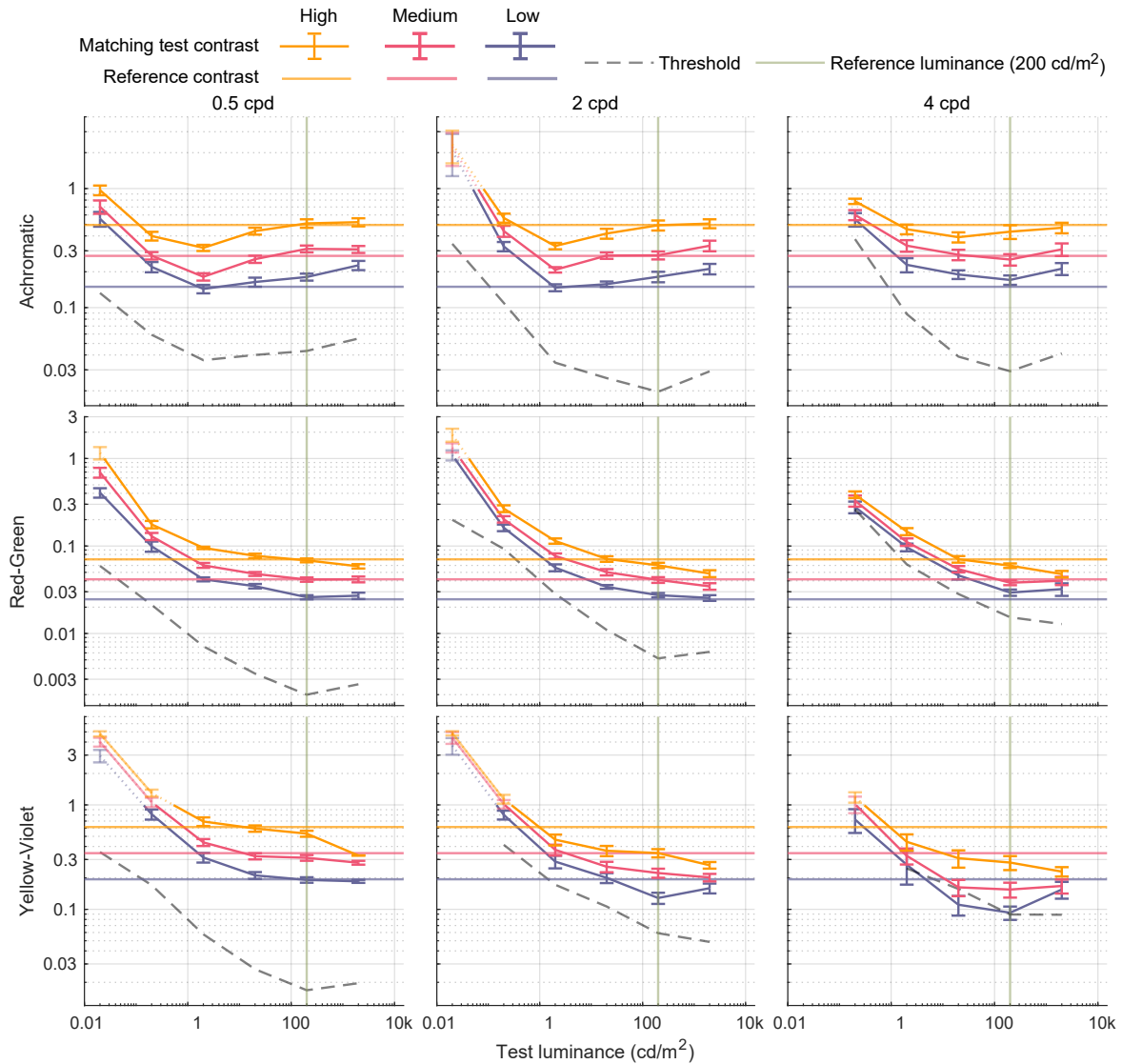


Figure 6.2: Mean measurements for contrast matching across luminance levels for the younger age group. Error bars are  $\pm\text{SEM}$  (standard error of the mean). Fixed reference stimuli at  $200 \text{ cd}/\text{m}^2$  are perceptually matched with equivalent test stimuli. The matching pairs span multiple spatial frequencies, colour directions and suprathreshold contrast levels and are presented at different luminance levels. The matched contrasts greater than 1 are denoted by dotted lines, since the stimuli become asymmetrical (in terms of contrast) once this limit is passed.

## CHAPTER 6. CONTRAST MATCHING FUNCTIONS

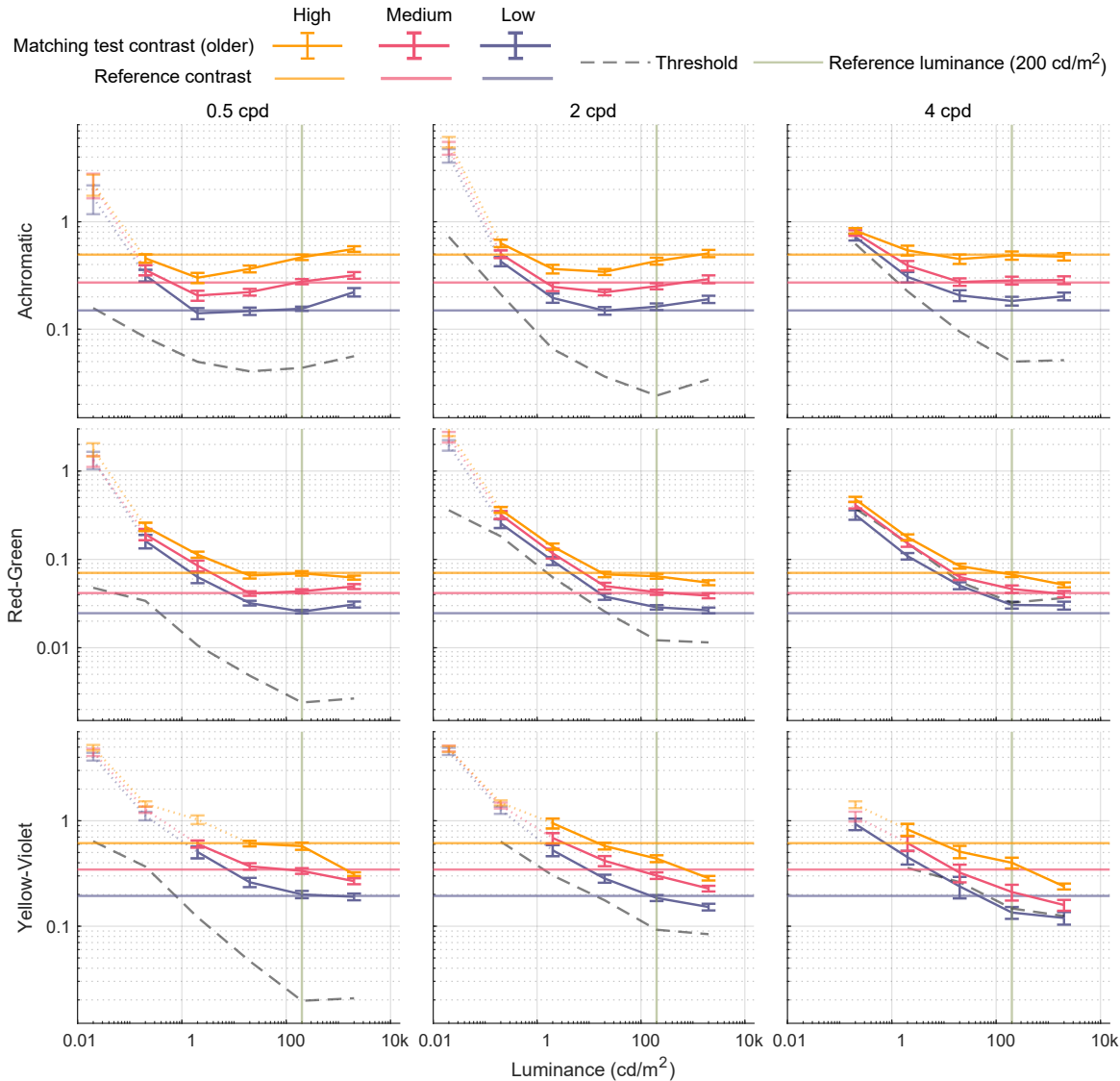


Figure 6.3: Mean measurements for contrast matching across luminance levels for the older age group. The description of the plots is the same as in Figure 6.2.

### 6.3.1 Failure of contrast constancy

Figures 6.2-6.6 show that the matched contrast varies with the background luminance for all three colour directions (achromatic:  $t(32.2) = -4.4, p = 0.001$ ; red-green:  $t(32.9) = -23.6, p < 0.0001$ ; yellow-violet:  $t(33.6) = -14.7, p < 0.001$ ). Hence, to a first approximation, it can be concluded that contrast constancy does not hold over large luminance ranges. This is apparent from the lines of matching test contrast from the figure, which deviate strongly from horizontal. If the phenomenon of contrast constancy was valid for matching

## CHAPTER 6. CONTRAST MATCHING FUNCTIONS

across luminance levels, test contrast magnitude would equal reference contrast magnitude regardless of the mean luminance. This is not the case in these measurements. Although contrast constancy is not achieved for the full luminance range, regions of constancy were observed in the data. Between 20 - 2000 cd/m<sup>2</sup> approximate contrast constancy was observed for most cases. For achromatic *medium* and *high* suprathreshold stimuli, the lines of matching contrast almost fully coincide with the reference contrast, indicating contrast constancy. This is also generally the case with red-green and yellow-violet stimuli at all three suprathreshold levels, with the exception of high spatial frequencies, for which the sensitivity is also lower.

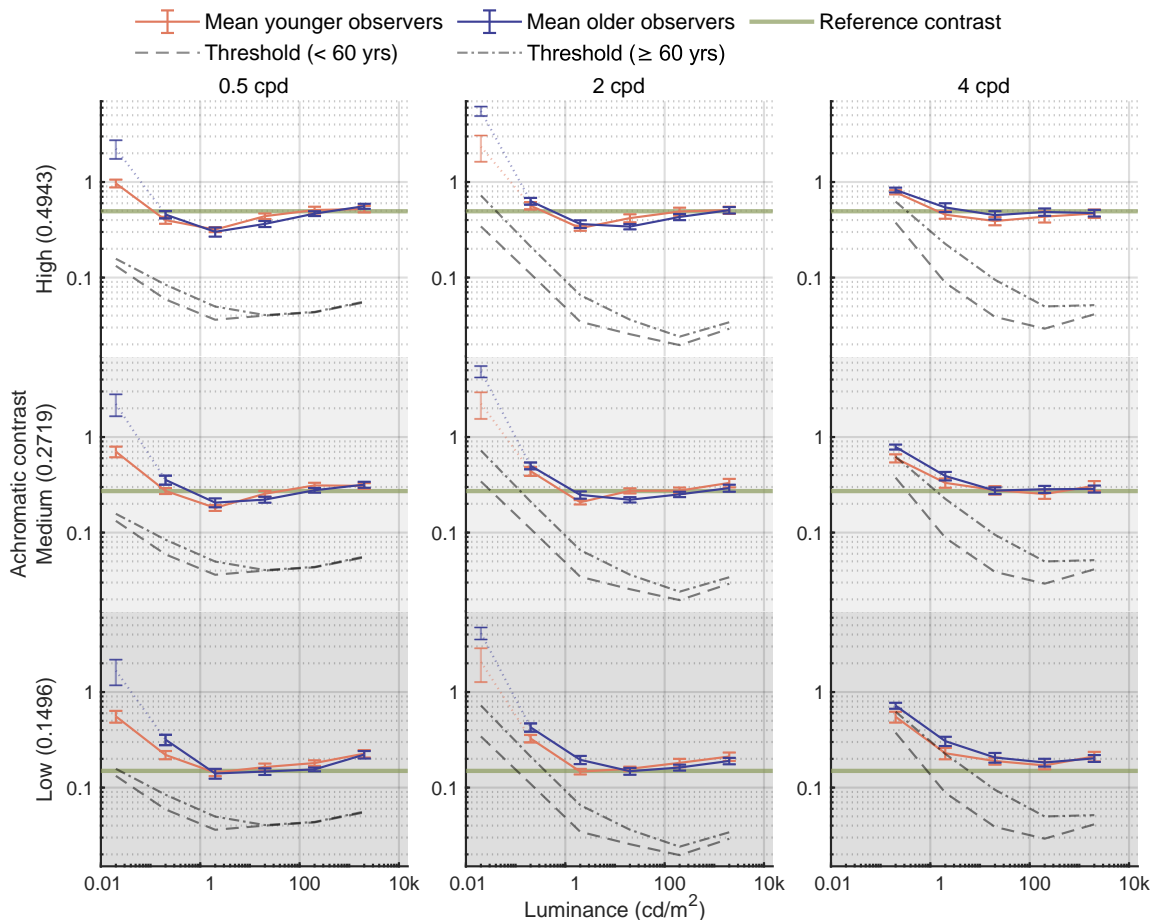


Figure 6.4: Contrast matching across luminance levels for achromatic Gabor patches for both younger and older observers. Error bars are  $\pm SEM$  (standard error of the mean). The thresholds for both younger and older observer groups are shown as grey dashed lines. The three rows represent the high, medium and low contrast respectively. The matched contrasts greater than 1 are denoted by dotted lines since the stimuli become asymmetrical (in terms of contrast) once this limit is passed.

### 6.3.2 Low luminance matches require higher contrast

For all conditions, the low luminance stimuli are matched at a much higher contrast compared to the reference. The findings are not surprising since the tested low luminance levels coincide with the DeVries-Rose region. It also indicates that for matching across luminance levels, the factors that limit contrast sensitivity are not fully compensated for in the suprathreshold region. It should also be noted that the differences between reference and low luminance matched test contrast are much higher for red-green and yellow-violet stimuli. Chromatic mechanisms lose contrast sensitivity at a higher rate with decreasing luminance, and this continues to be the case at suprathreshold levels.

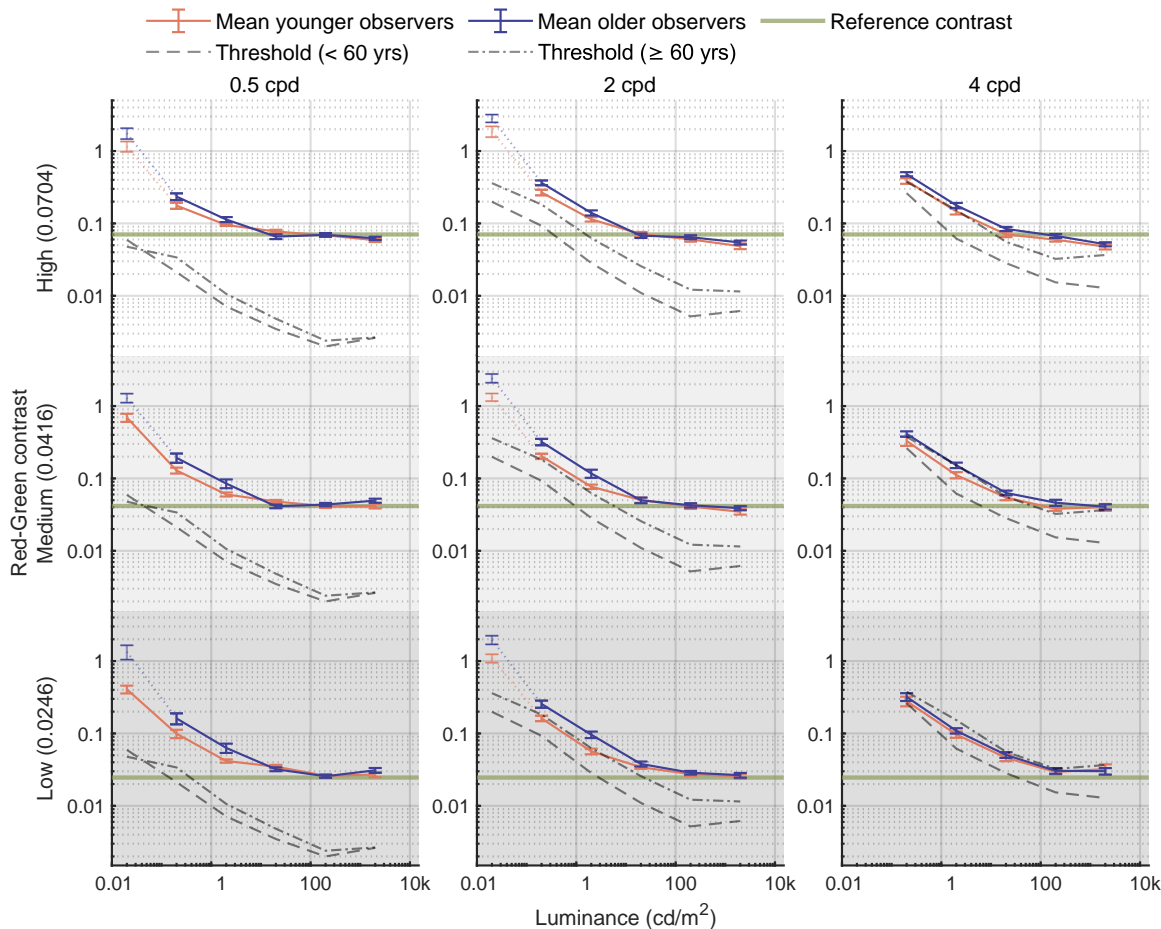


Figure 6.5: Contrast matching across luminance levels for red-green Gabor patches for both older and younger observers. The description of the plots is the same as in Figure 6.4.

### 6.3.3 Differences in near-threshold and suprathreshold matching

Low contrast suprathreshold stimuli show slightly different trends for the achromatic direction. For 0.5 and 2 cpd stimuli, the test contrasts at 2 and 20 cd/m<sup>2</sup> are matched well with the

## CHAPTER 6. CONTRAST MATCHING FUNCTIONS

reference stimuli, while the higher photopic stimuli at 2,000 cd/m<sup>2</sup> require higher contrasts to match with the reference. This resembles the trend in high luminance achromatic contrast sensitivity functions for lower sensitivity (i.e. increased threshold contrast) with increasing luminance beyond 200 cd/m<sup>2</sup>. One explanation could be that since the *low* suprathreshold level is closer to the threshold, it is possible that the matching for these conditions is mediated by both threshold and suprathreshold physiological mechanisms. However, the same can not be said for chromatic stimuli. For both red-green and yellow-violet stimuli, despite the increase in the threshold at very high luminance levels, no such increase in matched test contrast is observed even at *low* suprathreshold levels.

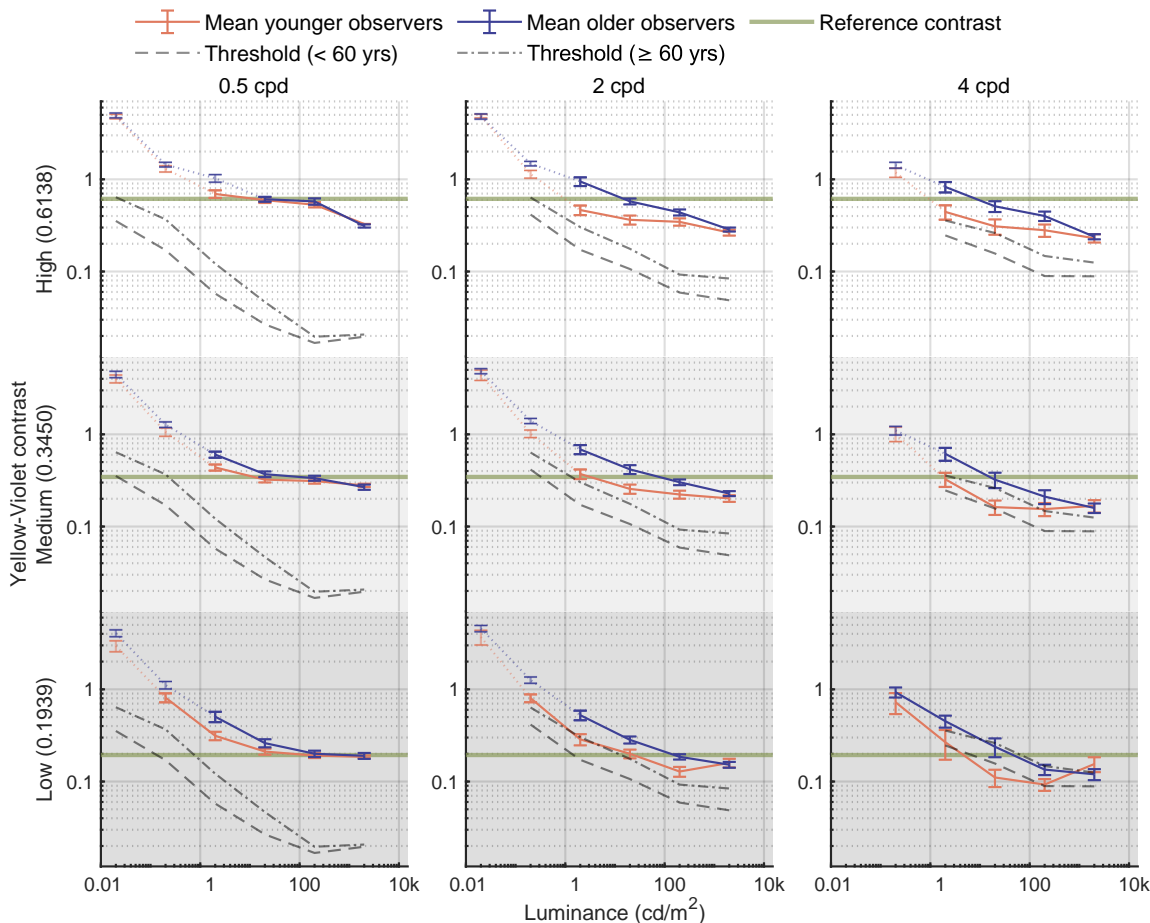


Figure 6.6: Contrast matching across luminance levels for yellow-violet Gabor patches for both younger and older observers. The description of the plots is the same as in Figure 6.4.

### 6.3.4 Effect of age

The effect of age on suprathreshold contrast matching was not significant for achromatic and red-green stimuli. The matching curves for older and younger observers almost always

## CHAPTER 6. CONTRAST MATCHING FUNCTIONS

overlap except at very low luminance levels ( $0.02\text{ cd/m}^2$ ) and for low and medium spatial frequencies, 0.5 and 2cpd (Figures 6.4 and 6.5) where older observers require considerably higher contrast to achieve a contrast match with the reference stimuli; these out-of-gamut data points, were, however not entered into the statistical analysis.

For stimuli that isolate the short-wavelength-sensitive cones (yellow-violet stimuli: Figure 6.6), contrast matches are affected by age ( $(t(29.9) = 2.7, p = 0.0116)$ ), in particular at medium (2 cpd) and higher spatial frequencies (4 cpd), which is reflected in the significant interaction ( $(t(29.3) = 2.4, p = 0.0228)$ ). Age-related contrast matching effects also interact with the adapting light levels ( $(t(31.9) = -2.2, p = 0.0385)$ ): for light levels up to  $200\text{ cd/m}^2$ , older observers require a higher contrast than younger observers to match the reference contrast presented at  $200\text{ cd/m}^2$ .

### 6.3.5 Modelling CMF

The relationship between the threshold and suprathreshold matching curves is not a one-size-fits-all model. As shown in Figure 6.2, for the 0.5 cpd condition, the matching curves are separated from the threshold curves by an approximately constant offset (in log scale) across the whole luminance range. However, as spatial frequency increases, this log-offset relationship between the threshold and the matching curves no longer holds. To adequately characterise contrast matching across luminance levels, a more sophisticated model is needed instead of simple threshold difference-based models [79]. This is explored later in Chapter 7.

## 6.4 Discussion

If contrast constancy was held across all tested parameters, contrast matches would be equivalent to the reference contrast. At moderate to high photopic light levels the contrast matching curves indeed converge towards reference contrast, in particular for achromatic and red-green modulations. These results agree with Peli *et al.* [81] who observed contrast constancy across luminance levels for achromatic stimuli only when luminance exceeded  $8\text{ cd/m}^2$ . Another interesting feature exhibited in the achromatic matching data is the 'dipper curve' for the lower spatial frequencies when matches are made to a reference stimulus of sufficiently high contrast (above 0.345%). This dip in the matching curves can be clearly observed in Figure 6.4 in the *high* and *medium* contrast data for 0.5 cpd, and the *high* contrast data for 2 cpd. The dip occurs at  $2\text{ cd/m}^2$  which is a luminance level where both rods and cones are likely active and their overlapping response might create a sweet spot for higher contrast perception. The lowering of matched test contrast means that the lower luminance stimulus is perceived to be of higher contrast than the much brighter reference stimulus

## CHAPTER 6. CONTRAST MATCHING FUNCTIONS

which could be made possible if the rod response augments and boosts the cone response in the achromatic channel creating a high contrast appearance. The theory of rod intrusion is also supported by the fact that this dip feature only appears in achromatic data and for only lower spatial frequencies.

In contrast to red-green and achromatic vision, age strongly affects contrast matches for S-cone-isolating stimuli (yellow-violet). When observers are asked to match yellow-violet stimuli to the fixed reference at lower light levels, older adults require more contrast. The contrast matching curves for the old age group are above those of the young age group for all reference contrasts (rows in Figure 6.6) and spatial frequencies (columns in Figure 6.6). Yellow-violet matched contrast was close to the threshold for the lower contrast reference (Rows 2-3, Figure 6.6). In conjunction with the known age-related optical changes in the lens, this may have been a further contributory factor to the age-dependency of yellow-violet matches.

Contrast matches for yellow-violet stimuli are in general more difficult and less reliable than those for achromatic and red-green stimuli, which is reflected in their higher variability (Coefficient of Variation for yellow-violet: 0.11; red-green: 0.084; achromatic: 0.087; see Appendix B for more details). Furthermore, observers were not able to provide veridical yellow-violet contrast matches: when the background luminance on both the HDR and the reference display is set to  $200 \text{ cd/m}^2$ , both young (Figure 6.2) and older observers (Figure 6.3) adjust the test contrast on the HDR to a lower level than the contrast displayed on the reference display; this bias occurs at medium and higher frequencies (2 and 4 cpd) at all three reference contrasts. To a smaller degree, this effect can also be observed for the highest contrast red-green stimuli at 4cpd. Since the underestimation is not observed for the lowest frequency, it can be speculated that it may have been due to an intrusion of luminance contrast, as opposed to a calibration issue.

While the contrast matching curves partly follow the general shape of the CSFs (dashed lines in Figures 6.2 and 6.3), they are flatter than them. When the reference contrast is close to the threshold, as is the case for the chromatic 4cpd stimuli, the contrast matching curves follow the CSFs very closely. The deviation from reference contrast reduces as suprathreshold contrast increases from low to medium to high, which is consistent with contrast constancy studies demonstrating that at higher reference contrasts the matching contrast is relatively independent of threshold-level differences [76]. Suprathreshold contrast constancy also decreases at 4 cpd. The contrast matching curves deviate more from the reference contrast line as spatial frequency increases (cf. Columns 1-3 in Figures 6.4 - 6.6). This is similar to

## CHAPTER 6. CONTRAST MATCHING FUNCTIONS

findings in Peli *et al.* [83].

For the effect of age, the main finding is that suprathreshold contrast perception for achromatic and red-green stimuli is very similar for the young and the old age group (Figures 6.4- 6.5). Differences in the contrast matching curves are only apparent when observers are asked to adjust the contrast for low and medium spatial frequency stimuli (0.5 and 2cpd) while adapted to very low light levels; at these mesopic ( $0.02$  and  $0.2\text{ cd/m}^2$ ) and low photopic light levels ( $2\text{ cd/m}^2$ ), older observers require more contrast than younger observers to match the reference contrast. This is consistent with Mei *et al.* [199] who measured suprathreshold contrast matching at a fixed adapting light level of  $60\text{ cd/m}^2$  for achromatic sinusoids and failed to identify marked age-related deficits when the reference contrast was sufficiently high (i.e., above 13.6%). McCourt *et al.* [200] also found no significant effect of age on suprathreshold matching contrast between two gratings in lower and upper visual fields. When the results of the lower and upper visual fields were analysed separately, they found that for test stimuli in the lower visual field, there was a significant effect of age.

This is not to say that the stimuli contrast appearance is the same for younger and older observers. The contrast sensitivity data indicates that there is a high likelihood that the suprathreshold stimuli appear to be of lower contrast to older eyes compared to younger ones. However, the contrast matching between a test and reference stimuli is not affected by ageing and both stimuli would undergo the same change in their contrast appearance.

### 6.5 Summary of chapter

The CMF datasets presented in this chapter focus on suprathreshold contrast matching across different luminance levels for different age groups. This dataset is specifically designed to explore how observers perceive and match contrasts above their detection threshold when presented with stimuli set against backgrounds of varying luminance. It was found that the contrast constancy assumptions underestimate the contrast required to perceive low-luminance stimuli at the same level. The data also revealed that the contrast matching abilities of older observers, relative to their own visual system, is not affected by ageing and older observers were able to maintain the same level of contrast perception at the same rate as younger observers.



## MODELLING CONTRAST MATCHING FUNCTIONS

Suprathreshold contrast vision refers to the ability of the human visual system to perceive differences in luminance or colour when presented with stimuli above the detection threshold. Suprathreshold contrast vision is typically measured and characterised using contrast matching experiments, where observers adjust the contrast of a test stimulus until it matches the reference stimulus. In the previous chapter (Chapter 6), a comprehensive dataset of contrast matching was presented, which described the non-linear behaviour of the visual system when matching across two luminance levels and the joint effect of spatial frequency and luminance levels for observers of two age groups. This dataset can be used to further our understanding of contrast perception and model the contrast appearance at higher contrast levels for real-world stimuli as it focuses not just on achromatic contrast but chromatic contrasts as well. The contrast vision for younger as well as older observer groups was measured which provided vital information about human visual changes with age.

Literature on suprathreshold contrast vision is extensive as summarised in Section 2.5. In this chapter, the focus is on computational modelling of suprathreshold contrast which involves developing a mathematical framework that can predict the perceived contrast based on the physical parameters of the stimulus and the context in which it is viewed. A robust model needs to account for the complexities of human contrast perception, which is influenced by factors such as luminance, spatial frequency, chromatic modulation, temporal properties, etc. The visual system's sensitivity at the threshold level can be extrapolated to predict contrast perception at higher levels but the relationship is likely non-linear. This chapter is a step towards proposing a unified contrast vision model as it aims to establish a relationship between the mathematical models of contrast sensitivity proposed in Chapter 5 and spatiochromatic contrast vision at suprathreshold levels.

In this chapter, the contrast matching data from Chapter 6 is used to: (i) test the additive model of suprathreshold contrast introduced by Kulikowski [79], (ii) test the multiplicative model inspired by work from Peli *et al.* [83], (iii) fit values of matched contrast as a linear function of reference contrast and evaluate the statistical significance of the model, and (iv) propose a new model that combines the additive and multiplicative models with model

parameters as functions of contrast sensitivity. The work presented in this chapter is being prepared for publication.

### 7.1 Additive model (Kulikowski's)

Kulikowski [79]'s model is based on the contrast sensitivity assumption in the linear contrast domain. It is assumed that the perceived contrast of both the reference and the test suprathreshold contrasts would be equal to the difference between the corresponding physical contrast and the threshold (minimum required contrast to perceive that stimulus). For suprathreshold levels that are high enough, the difference introduced by the threshold values is negligible and thus the perception of the two matching stimuli is equivalent. This was shown to be true for matching across different luminance levels as well. However, the range of luminances tested in Kulikowski's work is less than 2 log units. While the contrast matching data presented in the Chapter 6 of this work span 6 log units. Whether Kulikowski's constancy model holds for this wide range of luminance is tested in this section.

The Equation (2.1) can be rearranged to predict the matched contrast of the test stimuli to the reference contrast.

$$C_{test} = C_{ref} + \Delta C^t, \quad (7.1a)$$

$$\Delta C^t = C_{test}^t - C_{ref}^t. \quad (7.1b)$$

The threshold contrasts  $C^t$  are predicted by the contrast sensitivity model in Section 5.2.1. Equation (7.1) is essentially an equation of the straight line with a slope of 1 and the intercept as the difference between the threshold contrasts for reference and test stimuli. The predictions from Kulikowski's model for younger and older observers are shown in Figures 7.1-7.2. The model predictions faithfully follow the shape of the trends from the measured data points at higher luminances. For matching at lower test luminances, the model underpredicts the required test contrast needed for equivalent perception of the two contrasts. The prediction of contrast when the test stimulus is at a higher luminance level ( $2,000 \text{ cd/m}^2$ ) than the reference ( $200 \text{ cd/m}^2$ ) is also underpredicted for achromatic stimuli. The CSF data presented in Section 4.1, showed a decrease in achromatic sensitivity at very high light levels. This feature is also present in achromatic contrast matching data but is not well-predicted by the model. The model also shows higher prediction errors for higher frequency yellow-violet stimuli for both older and younger observers.

## CHAPTER 7. MODELLING CMFS

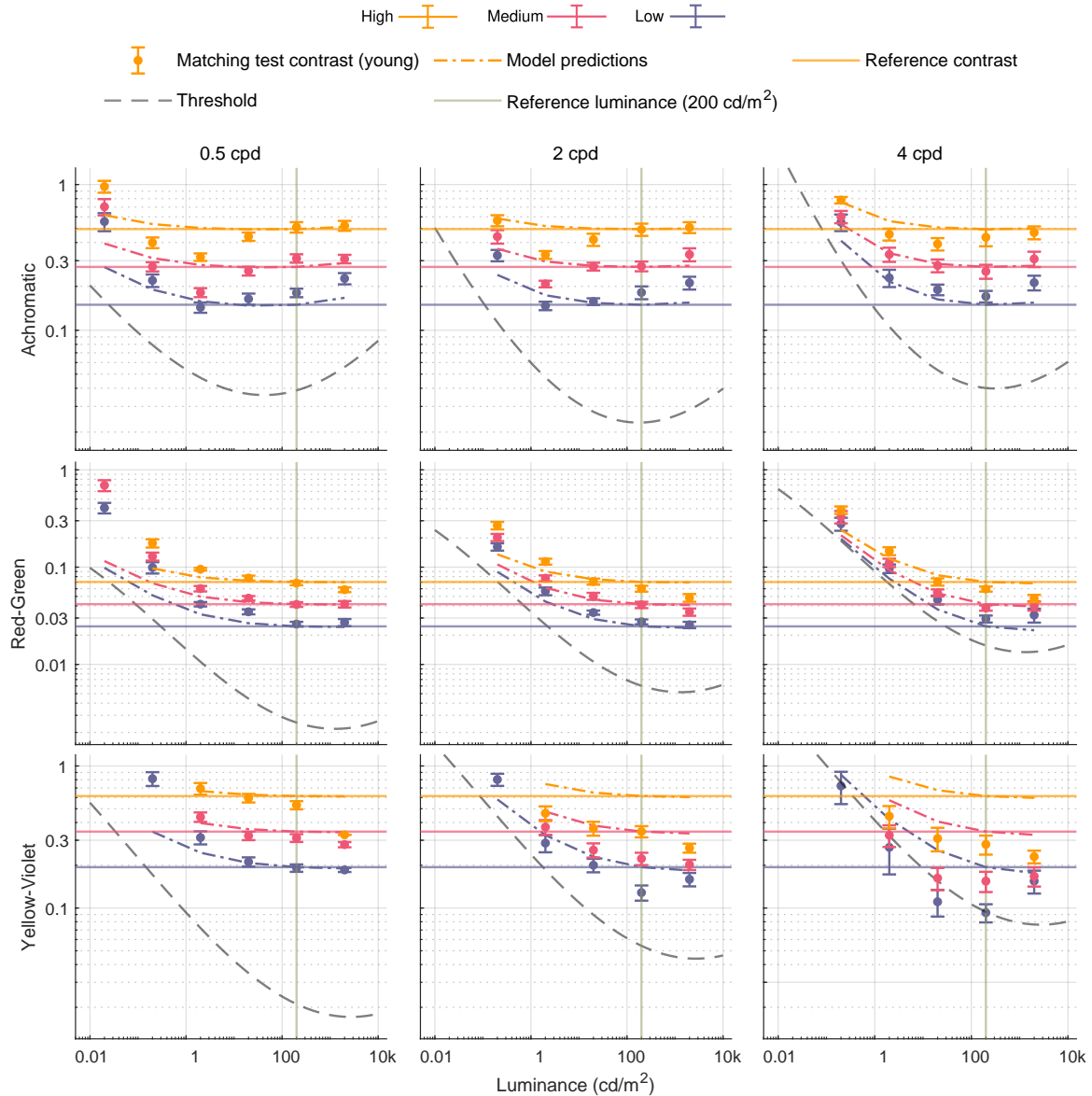


Figure 7.1: Kulikowski's CMF model predictions for younger observers. The coloured data points with  $\pm SEM$  error bars are the measured data points for different suprathreshold contrast levels. The corresponding dashed lines are the model predictions. The grey dashed lines show the threshold contrasts predicted from the age-dependent CSF (Model 5.2.1).

## CHAPTER 7. MODELLING CMFS

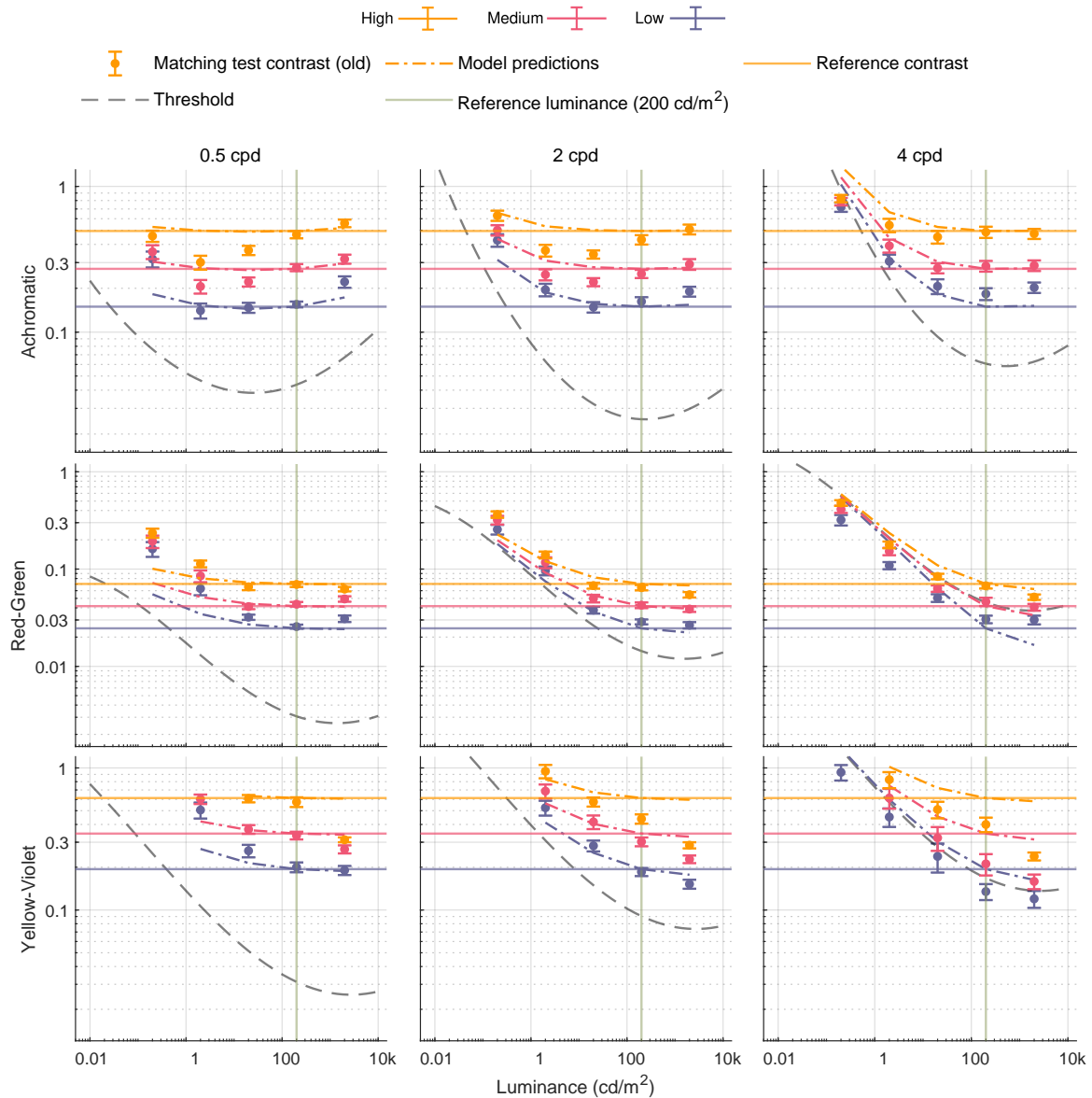


Figure 7.2: Kulikowski’s CMF model predictions for older observers. The description of the plots is the same as in Figure 7.1.

### 7.2 Multiplicative model (Peli’s)

The contrast matching studies presented in Peli *et al.* [81] and Peli *et al.* [83] do not explicitly introduce a mathematical CMF model, but they have shown their data following the contrast matching predictions in log contrast space. The contrast matching data presented in this work also spans only 2 log units of luminance. In a model inspired by Peli *et al.*’s work, the test and reference contrast are related in the log space and Equation (7.1) becomes:

## CHAPTER 7. MODELLING CMFS

$$\log_{10}(C_{test}) = \log_{10}(C_{ref}) + \log_{10}(C_{test}^t) - \log_{10}(C_{ref}^t), \quad (7.2a)$$

$$C_{test} = r^t C_{ref}, \quad (7.2b)$$

$$r^t = \frac{C_{test}^t}{C_{ref}^t}. \quad (7.2c)$$

Equation (7.2) models the matched test contrast as linearly proportional to the reference contrast with the ratio of the test and reference threshold contrasts as the gradient of this relationship. The predictions from Peli's model for younger and older observers are shown in Figures 7.3-7.4. The lines of matching contrast for different suprathreshold levels (*high*, *medium*, and *low*) are predicted with a constant offset in the log contrast axis. The shape of these curves along luminance is similar to the DeVries-Rose to Weber region transition curves shown in Figure 4.4. The model predictions are well-aligned with the higher required test contrast for lower luminance levels for lower suprathreshold contrasts (purple curves in Figures 7.3-7.4), but overpredict the test contrast for medium to high suprathreshold contrasts. This model is also able to predict the increase in test contrast for high-luminance matches. The predictions from Kulikowski's and Peli's models are suited for different ranges of the stimuli parameter space and thus, combining the strengths of both models is needed to predict the full range of stimuli tested in this work.

## CHAPTER 7. MODELLING CMFS

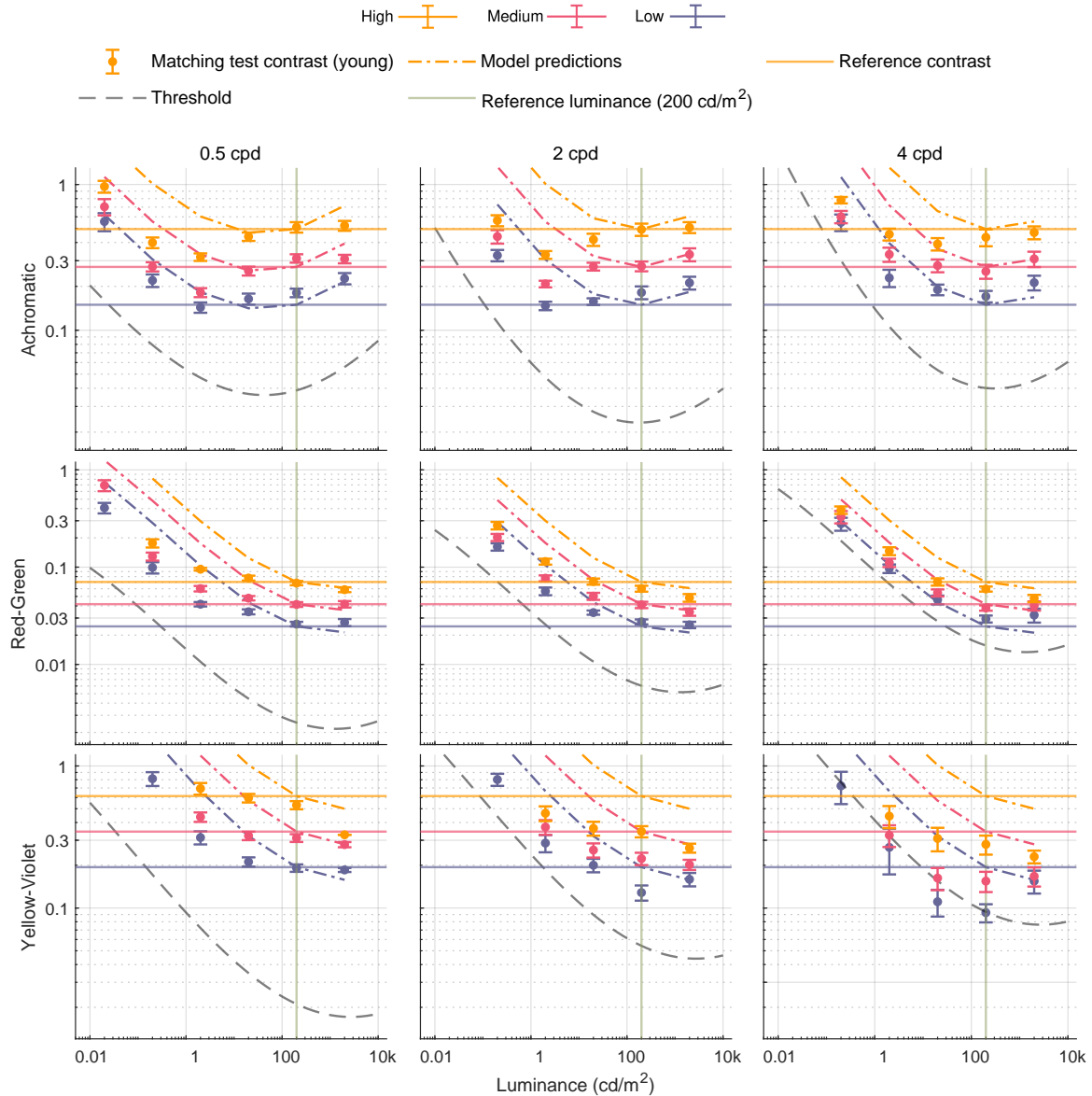


Figure 7.3: Peli's CMF model predictions for younger observers. The description of the plots is the same as in Figure 7.1.

## CHAPTER 7. MODELLING CMFS

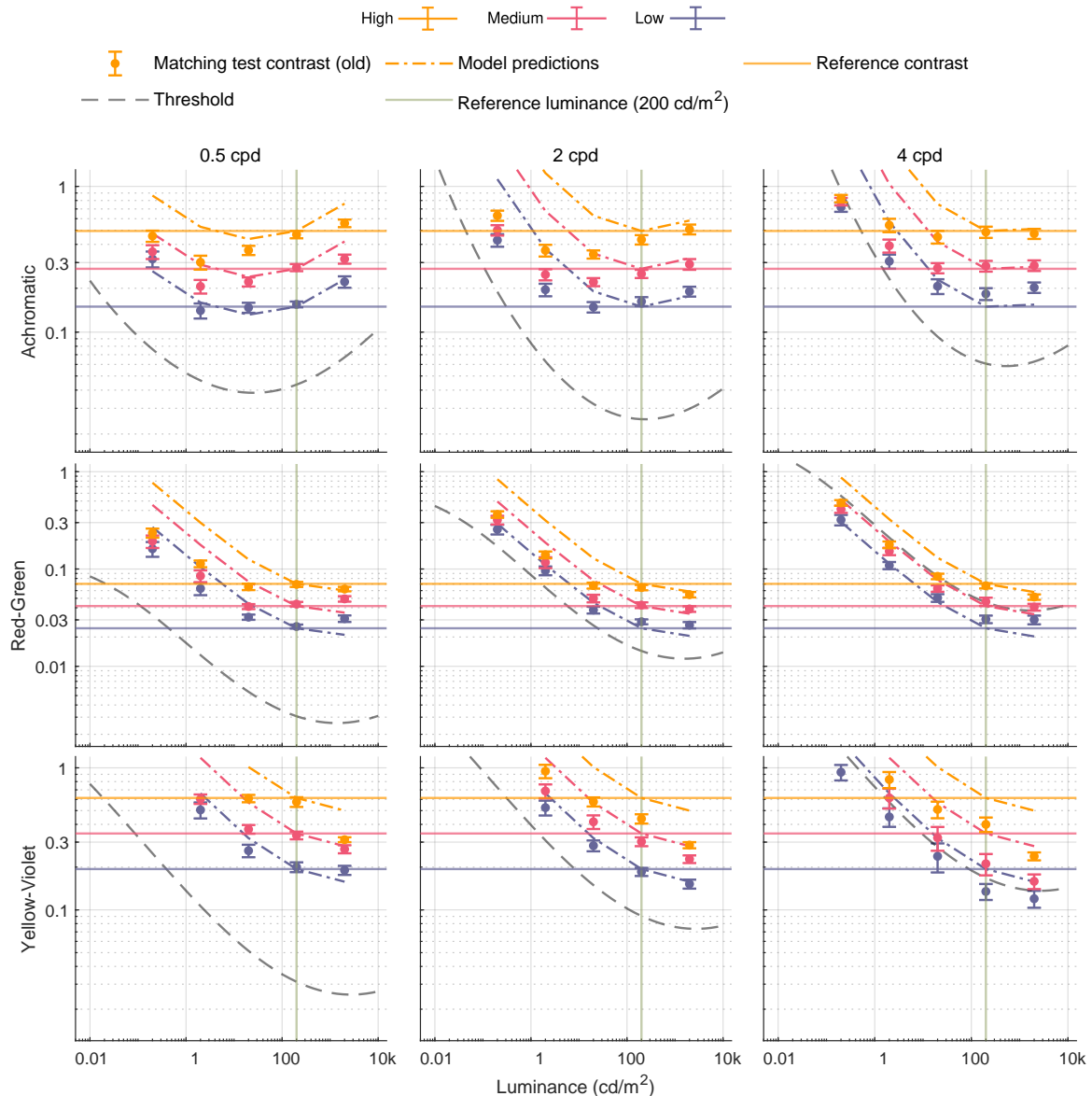


Figure 7.4: Peli’s CMF model predictions for older observers. The description of the plots is the same as in Figure 7.1.

### 7.3 Empirical modelling of CMF

Neither the additive (Kulikowski [79]) nor the multiplicative (Peli *et al.* [83]) models from the literature could fully explain the contrast matching trends across luminance levels from the measured contrast matching data. Figure 7.5 shows the matched test contrasts with respect to the reference contrasts for the mean data from the younger observer group. The relationship between the two contrasts is linear for each combination of spatial frequency and luminance

## CHAPTER 7. MODELLING CMFS

level for all three colour directions but with different slopes and offsets, similar to the results in Biondini and De Mattiello [201]. To investigate this relationship, a straight line was fitted to the matching curves and the best-fitted values of slope and intercept were estimated for each observer in the younger group.

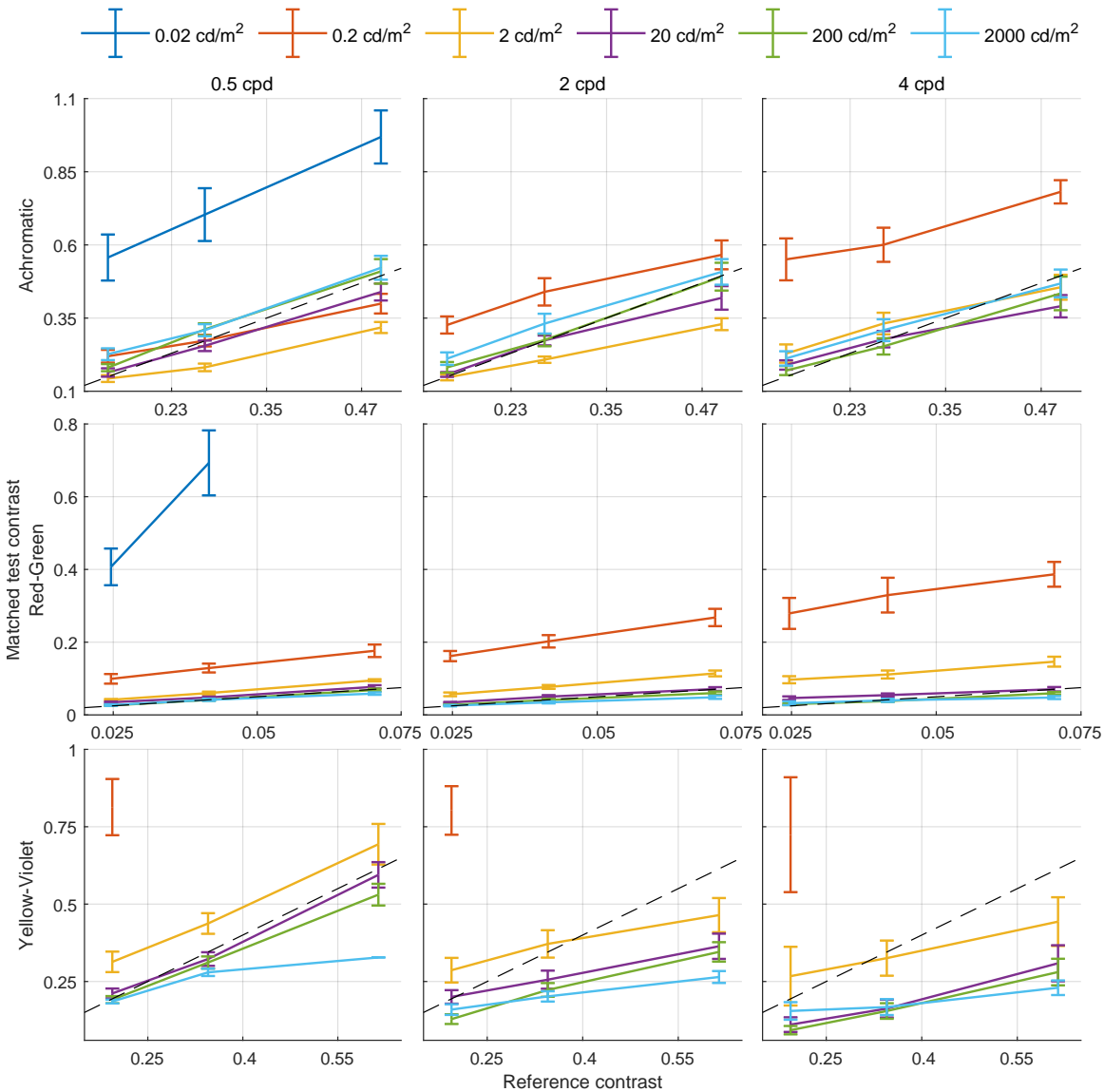


Figure 7.5: Linear relationship of contrast matching data for younger observers. The linear function between the matched test and the reference contrast data is shown for different spatial frequencies and luminance levels. From the data, it is clear that the two contrast values are linearly related and the slope and intercept of these matches depend on the spatial frequency and the luminance of the stimuli.

## CHAPTER 7. MODELLING CMFS

The `polyfit` function in MATLAB was used to fit the following equation for individual observers:

$$C_{test} = \delta C_{ref} + \alpha, \quad (7.3)$$

where  $\delta$  is the slope and  $\alpha$  is the intercept of the linear function between test and reference contrast. The mean fitted slope and intercept values for each combination of spatial frequency and test luminance are listed in Appendix F. In Appendix E, no effect of age group was shown in the statistical analysis of contrast matching data except for the yellow-violet colour direction. The effect of age on yellow-violet contrast matching can be explained by the higher loss of yellow-violet contrast sensitivity in older observers as discussed in Section 4.2. Thus, a model that depends on the threshold contrasts of reference and test stimuli, should be able to adequately compensate for these differences. To test this, the data from only the younger group was used in this contrast matching modelling analysis and the results were validated on the data from the older observer group.

With the per-observer fitted slopes and intercept values, a multiple linear regression analysis was performed within each colour group to find the statistical significance of the effect of spatial frequency, luminance difference, the difference in threshold contrasts ( $\Delta C^t$ ), and the ratio of the threshold contrasts ( $r^t$ ) on the fitted values of slope and intercept. The data spanned three spatial frequencies, six luminance levels, and three colour directions. To determine how these factors affected the slope and intercept of contrast matching, a linear mixed effect model (LMM) was fitted to data from each of the three colour directions. The model included the main effects of the four independent variables as well as their two-way and three-way interaction terms. The best-fitting linear mixed-effect model was determined by a backward procedure of removing the factors that did not contribute significantly. In other words, none of the remaining effects or interactions can be removed without reducing the variance explained. The statistical analyses were performed in R using packages `lmerTest`, `caret`, `performance`, and see [137]–[143]. For the full description of the best-fitting models and the statistical significance, please refer to Appendix G. The threshold ratio variable was found to be significant on average both as the main effect and in interaction terms for the matching slope values. Similarly, the effect of threshold difference and its interaction terms were significant for the intercept values. Following this analysis, a model is proposed that combines the strengths of both the additive and the multiplicative models of contrast matching to better predict the matching data across different luminance levels.

### 7.3.1 Luminance-adaptive CMF

A new model of contrast matching was proposed where the test contrast is a power function of the reference contrast, taking inspiration from Steven's power law which stipulates that the strength of perception is a power function of the physical intensity of the stimulus [202]. In the case of contrast matching, the magnitude of the test contrast represents the response or the perception and the reference contrast represents the intensity of the stimulus. The multiplier ( $\delta(\cdot)$ ) is a function of the threshold ratio ( $r^t$  in Equation (7.2)), and the intercept ( $\alpha(\cdot)$ ) is a function of the threshold differences ( $\Delta C^t$  in Equation (7.1)).

$$C_{test} = \delta(r^t)(C_{ref})^\gamma + \alpha(\Delta C^t), \quad (7.4a)$$

$$\delta(r^t) = \delta_m r^t + \delta_i, \quad (7.4b)$$

$$\alpha(\Delta C^t) = \alpha_m \Delta C^t + \alpha_i, \quad (7.4c)$$

where  $\gamma$ ,  $\delta_m$ ,  $\delta_i$ ,  $\alpha_m$ , and  $\alpha_i$  are the parameters of the model with different values for each colour direction.  $\gamma$  represents the value of the exponent to correct for the non-linearity between the two matched contrasts. The  $\delta(\cdot)$  function represents a scaling factor of the 'gamma-corrected' reference contrast as a function of the threshold ratio with  $\delta_m$ , and  $\delta_i$  as the slopes and the intercepts of the linear relationship respectively. Finally, the  $\alpha(\cdot)$  function scales the contribution of an additional term - the difference in thresholds - with  $\alpha_m$ , and  $\alpha_i$  as the slopes and the intercepts of the linear relationship respectively.

The parameter values were optimised using `fminsearch` in MATLAB with the RMSE error, between the measured test contrast values from the data and the predicted values from Equation (7.4), as the objective function. The data used for optimisation was the mean contrast matching data from the younger observer group. The optimised values of the parameters are listed in Table 7.1 and the predicted test contrasts are shown in Figures 7.6-7.7.

Table 7.1: Optimised values of parameters for the proposed CMF model

<b>Color direction</b>	$\delta_m$	$\delta_i$	$\alpha_m$	$\alpha_i$	$\gamma$
<i>Achromatic</i>	-0.0116	2.6194	1.9299	-2.0204	0.0940
<i>Red-Green</i>	0.0300	0.1490	0.2525	-0.0876	0.1367
<i>Yellow-Violet</i>	0.1164	8.4239	-0.4673	-8.1108	0.0211

## CHAPTER 7. MODELLING CMFS

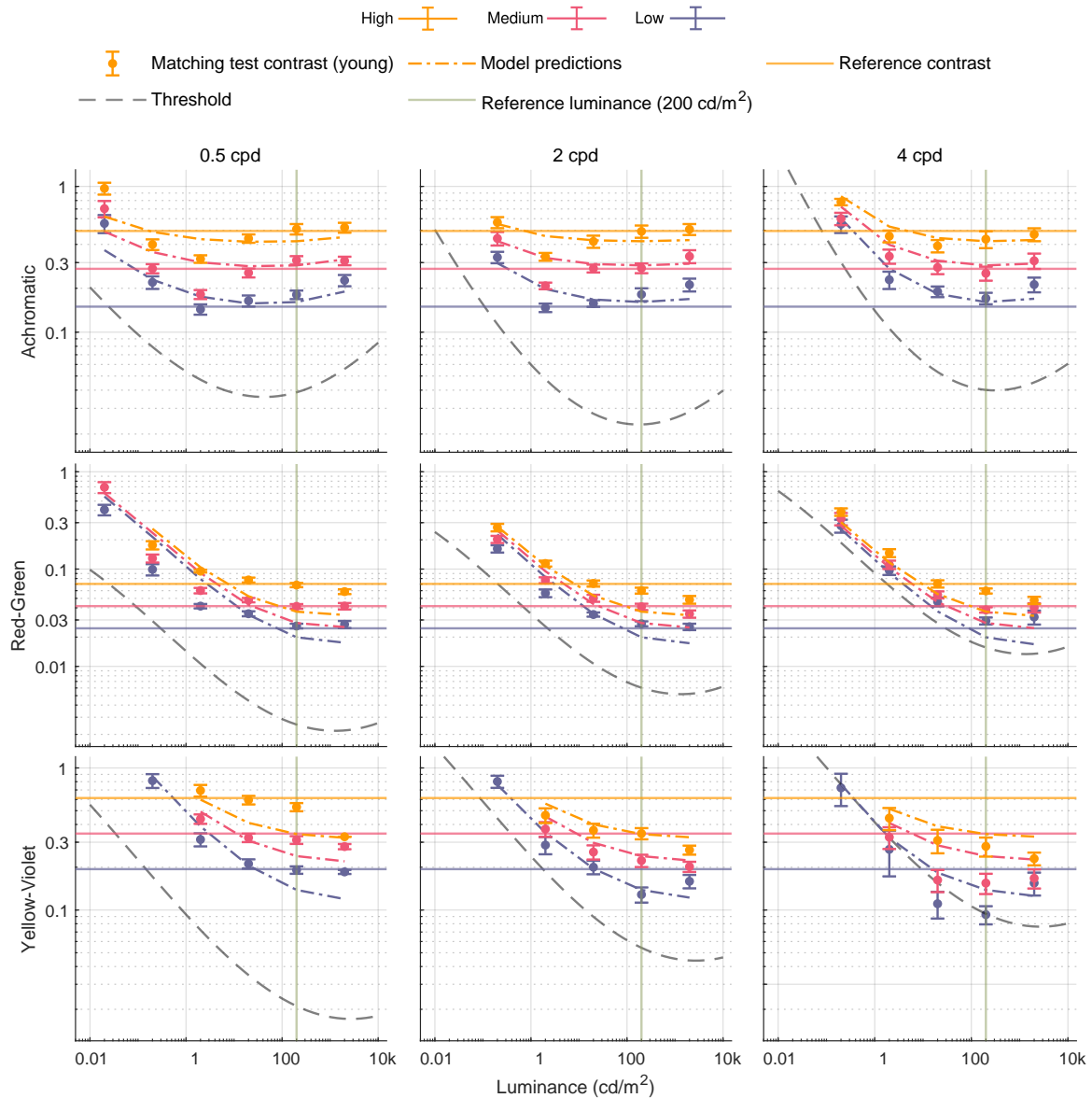


Figure 7.6: Proposed CMF model predictions for younger observers. The description of the plots is the same as in Figure 7.1.

## CHAPTER 7. MODELLING CMFS

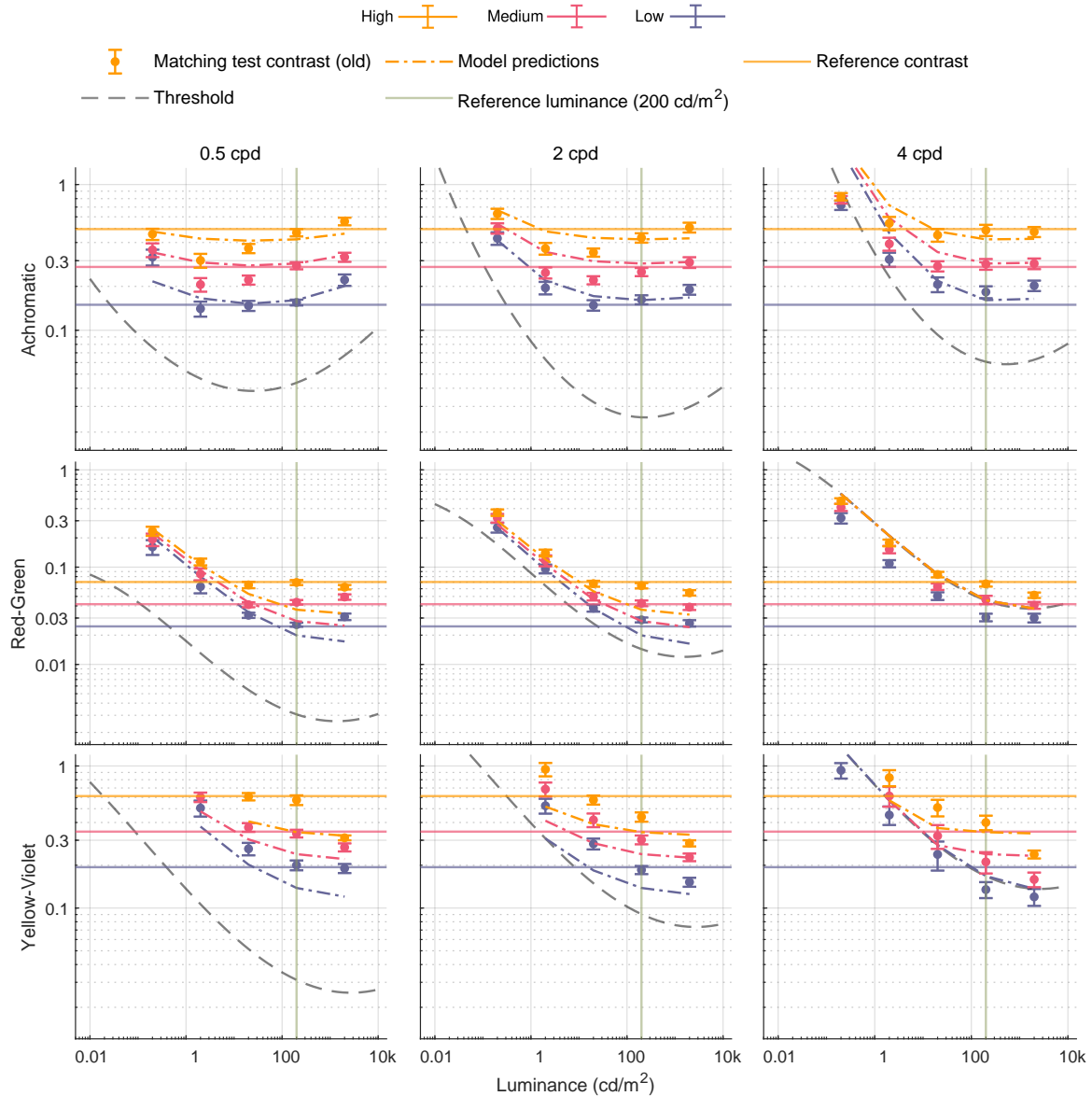


Figure 7.7: Proposed CMF model predictions for older observers. The description of the plots is the same as in Figure 7.1.

### 7.4 Discussion

The numerical errors from predictions of all the tested models are shown in Table 7.2 for both younger and older observers. The predictions from Kulikowski's and Peli's model were only dependent on the thresholds predicted by the CSF model and no parameters were optimised. For these models from the literature, the prediction errors for older observers were smaller compared to younger observers. It should be noted that for older observers,

## CHAPTER 7. MODELLING CMFS

more low luminance data points were removed as the observers were not able to match the test contrast within the display gamut and this is not accounted for in the mean RMSE value.

Table 7.2: Summary of CMF models

<b>Model</b>	<b>Summary</b>	<b>Equations</b>	<b>Mean RMSE</b>	
Kulikowski	No optimisation	Eq. 7.1	Younger group	0.4725
			Older group	0.3930
Peli	No optimisation	Eq. 7.2	Younger group	0.8303
			Older group	0.6354
Proposed	Optimisation with 15 free parameters listed in Table 7.1	Eq. 7.4	Younger group	0.3399
			Older group	0.3979

In the proposed CMF model, 5 free parameters for each of the three colour directions were optimised and the model was trained for younger observers only. The proposed model has the lowest prediction error among the three tested models for younger observers. This is not surprising as the model parameters are fitted to the training set. Qualitatively, the shape of the matching curves predicted by the proposed model follows the measurements quite closely as shown in Figures 7.6-7.7. The elevated test contrast for both very low and very high luminance matching was predicted well especially for achromatic contrasts. The mean error in predictions for the unseen older observer data is comparable but slightly larger than that from Kulikowski's model. This could also be due to the model feature where the values of the predicted test contrasts are capped at the corresponding threshold values, while naive models like Kulikowski's allow for test contrast to be predicted lower than the threshold, or in the sub-threshold region.

### 7.4.1 Future work and applications

The proposed model shows a promising direction to unify suprathreshold and threshold contrast models for very large dynamic ranges. Future works could aim to measure similar datasets for higher spatial and temporal frequencies as well to test the validity of the hybrid additive + multiplicative model. Currently, the three colour directions are treated independently of each other; another very interesting venue for future research would be the matching of contrast appearance across different colour directions. As correctly pointed out by Switkes and Cognale [203], the quantitative measurement of qualitative chromatic contrast perception can be quite tricky but very useful for applications such as chroma-subsampling.

## CHAPTER 7. MODELLING CMFS

A comprehensive model of contrast matching across luminance is very useful for various image processing applications. One of the direct applications of this work would be in image retargeting for different luminance levels [86], [87]. Ultimately, the aim would be to develop a cross-luminance retargeting algorithm for complex images. For example, an HDR movie shot for a  $1,000 \text{ cd/m}^2$  display when screened at a  $50 \text{ cd/m}^2$  cinema screen would need to be retargeted accordingly. Figure 7.8 shows a high-luminance image retargeted for a low-luminance display. If contrast constancy is assumed, no change is made to the physical contrasts of the rendered low luminance image as the perceived contrast is assumed to be the same across luminances. But when viewing the image, we can see that the perceived contrast of the content is much lower (middle) than the original image (top). The bottom image shows an enhanced version of the dim image where contrast constancy is not assumed and the contrasts for the lower mean luminance image are increased much more than what a contrast constancy algorithm would forecast. With the increasing popularity of high dynamic range (HDR) content and technologies, the need for better algorithms for making the content adaptable to different viewing conditions is imperative.

### 7.5 Summary of chapter

This chapter first investigates theoretical frameworks for CMFs, starting with an additive model inspired by Kulikowski's approach, followed by a multiplicative model based on Peli's principles. The models from the literature were not adequately able to explain the data and so an empirical model of CMF was proposed, with a specific focus on predicting matched contrast as functions of the corresponding threshold contrasts of the stimuli.



Figure 7.8: Example of a retargeted image from high to low luminance. Top: Original high luminance image. Middle (to be viewed through a ND (neutral density) 2.0 filter): Image rendered to a low luminance level assuming contrast constancy. Bottom (to be viewed through a ND 2.0 filter): Desired rendition of low luminance retargeted image with contrasts preserved (digitally manipulated). The lower two images should be viewed with a ND 2.0 filter at a distance of approximately 0.5 m and the images zoomed to be about 5 inches on the screen. When compared with the top image, the luminance and chromatic contrast perception of the bottom rendition is preserved much better than the middle rendition at low luminance levels.



## ROD VISION

In the preceding chapters of this thesis, contrast vision at many different luminance levels including very low scotopic and mesopic levels is shown to be successfully modelled and validated, albeit without explicitly defining the role of rod responses. The cone contrast definitions, the LMS and DKL colour spaces all only consider cone responses even at low luminance levels, even though rods are active up to  $3\text{ cd/m}^2$ . While this approach makes for simpler models, the explicit introduction of rod responses might improve prediction accuracy in low luminance ranges. In this chapter, the data from Section 4.1, along with two other datasets from the literature are used to test the performance of some proposed colour difference metrics which include the effect of rod response. The four novel metrics are extensions of well-established existing colour difference metrics. The content of this chapter is adapted from the publication:

M. Ashraf, R. K. Mantiuk, G. Finlayson, A. Kucuk, and S. Wuerger, “Colour Difference Formula for Photopic and Mesopic Vision Incorporating Cone and Rod Responses,” in *London Imaging Meeting*, Society for Imaging Science and Technology, vol. 2022, 2022, pp. 79–83. doi: 10.2352/lim.2022.1.1.18.

### 8.1 Introduction

Max Schultze’s seminal *duplicity theory of vision* dictates that rods and cones govern two independent visual mechanisms [204], [205], with the rods mediating only low luminance achromatic vision (scotopic vision), while the cones mediating high luminance vision with better spatial resolution (photopic vision) with some overlap in the respective luminance ranges (mesopic vision). Rods become active as luminance levels decrease and completely take over in scotopic luminance levels after complete dark adaptation. The assumption of different types of photoreceptors explains phenomena like the well-known Purkinje effect where a brightness match obtained between two colours in a light-adapted state may no longer hold after dark adaptation [206]. This change in relative brightness between light and dark-adapted states could not be explained by earlier trichromatic theories of vision alone.

The role of rods is not just limited to coarse achromatic vision. The perception of colours in

## CHAPTER 8. ROD VISION

dim lights is also altered, including changes in brightness perception [207], [208], changes in the gamut of perceived colours [209], desaturation of test colours [210]. These colour changes can be explained by the fact that rods and cones have different spectral responses in addition to different luminance operating ranges (Figure 8.1 (top-right)) [51], [190], [211], [212]. Rod response favours shorter wavelength stimuli while the photopic luminous efficiency function mediated by long and medium (L, M) cones peaks at higher wavelengths. This results in different wavelength ranges dominating the contribution to the visual system for photopic, mesopic and scotopic ranges. The luminance-dependent shift in peak wavelength of spectral response results in changes in both chromatic and achromatic visual responses which indicates the role of rods in supplementing cone responses in low luminances.

The contribution of rods to human vision is not modelled by most colour spaces despite evidence of rods providing input to cones [213] and even providing stand-alone chromatic responses below small and medium cone thresholds [214]. The LMS colour spaces are based on the responses of long, medium, and short (L, M, and S) cones and only represent photopic vision [215]. Similarly, the XYZ colour spaces are linear transforms of the corresponding LMS cone spaces [216] and do not take into account the rod responses or the shifts in colour perception at low luminance levels. CIELAB colour difference error metrics  $\Delta E_{76}$  [217],  $\Delta E_{94}$ , [218] and  $\Delta E_{2000}$  [219] also work for colour differences under photopic luminances only. Widely used colour appearance models such as CIECAM02 [220] and iCAM06 [221] are also limited to predict effects relevant to medium to high luminance image appearance only. Because most of the applications of these colour models are in higher light levels, modelling rod contributions have not been a priority. However, advances in high dynamic range imaging allow displaying content at both very high photopic levels and low mesopic and scotopic levels; consequently, a faithful representation of low luminance scenes requires accurately capturing and relaying rod responses as well.

The aim of this work is to develop a colour difference formula that accounts for rod contribution to colour perception. Three colour difference formulas that incorporate different stages of Cao et al. rod intrusion model [213] are proposed and their perceptual uniformity in terms of STRESS and PF/3 metrics is tested.

### 8.2 Related work

A number of researchers have developed algorithms and tone-mapping operators to predict image appearances in low light levels based on physiological and psychophysical data [86], [222]–[225]. The scope of this work is to propose simple error metrics (comparable to

## CHAPTER 8. ROD VISION

CIELAB colour difference metrics) for L, M, S, and R (cones and rod) responses. So the models that quantify rod responses to vision at receptoral and early post-receptoral levels will be used here.

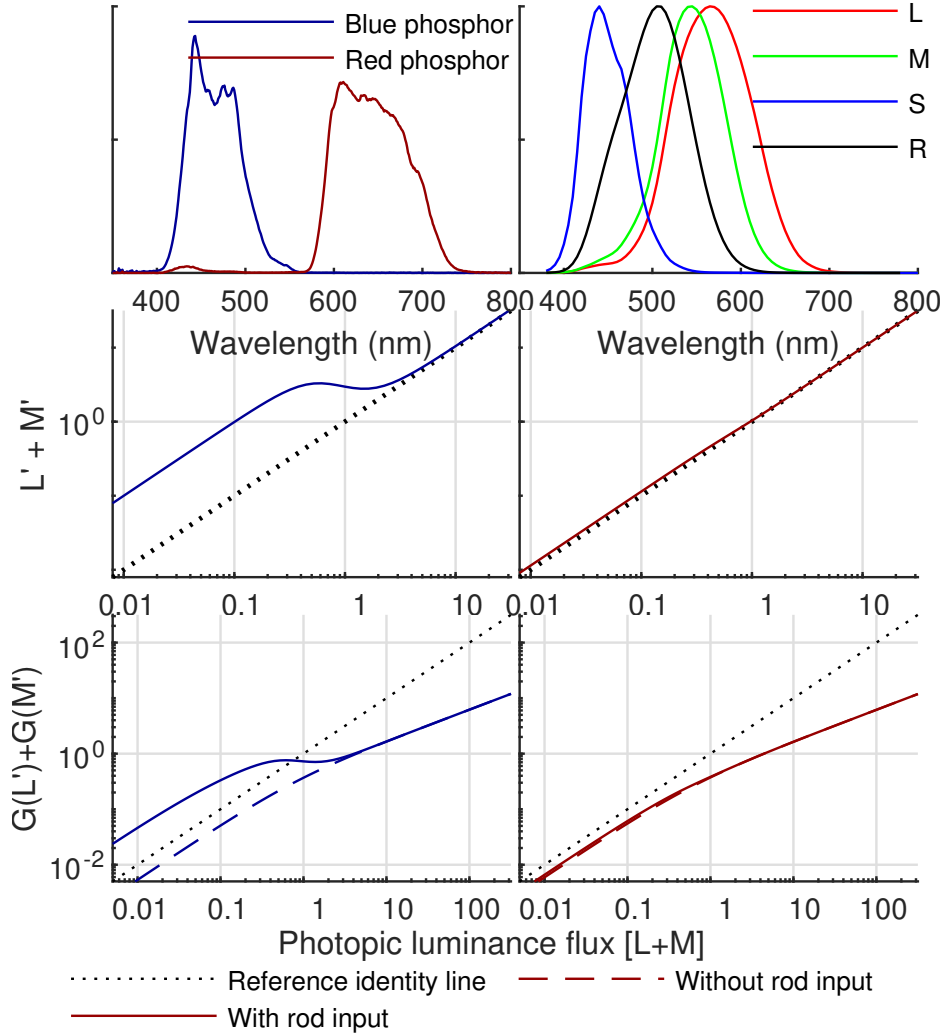


Figure 8.1: Demonstration of Purkinje shift using the modified photoreceptor response model. The blue and red coloured lines correspond to responses for blue and red display primary respectively. Top row (left): Emission spectra of blue and red display primaries. Top row (right): Spectral sensitivities of cones and rods. Middle row: Luminance from modified long and medium cone response  $L' + M'$  from Equation (8.1). Bottom row: Luminance from regulated long and medium cone response  $G(L') + G(M')$  from Equation (8.3).

Rods and cones feed into the same neural pathways [226] despite differences in anatomical structure, density distribution over the retina and different light activation range [227]. That is, the light incident upon the retina is transduced by rods and the three different types of cones (long, medium, and short wavelength), then combined and converted into post-receptoral

## CHAPTER 8. ROD VISION

signals which are then passed on to the higher-order visual mechanisms. Rods' contribution to cone responses has been modelled and quantified using perceptual matching where rod contrasts were matched with the equivalent cone contrasts [213]. Cao *et al.* [213] have determined the combined cone and rod responses through contrast matching psychophysical functions as follows:

$$L' = \frac{L + \alpha_1(l_{tr})R}{l_{max}}, \quad M' = \frac{M + \alpha_1(l_{tr})R}{m_{max}}, \quad S' = \frac{S + \alpha_2(l_{tr})R}{s_{max}} \quad (8.1)$$

where  $L$ ,  $M$ , and  $S$  are the cone troland responses based on Smith and Pokorny cone fundamentals [211], [228] and  $R$  is the response from the CIE 1951 standard scotopic luminous efficiency function  $V'$  [212, p.259].  $l_{max}$ ,  $m_{max}$ , and  $s_{max}$  are the weights of the Smith and Pokorny cone fundamentals [211]. The strength of rod input to the cone responses is modelled by the parameters  $\alpha_1$  and  $\alpha_2$  in Eq. Equation (8.1). The mean of data points from Figure 3 in Cao et al. [213] was used to fit a logistic function to obtain equations of  $\alpha_1$  and  $\alpha_2$  as functions of retinal illuminance,  $l_{tr}$ :

$$\alpha_i(l_{tr}) = \frac{y_i}{1 + e^{b_i(l_{tr}-0.62)}}, \quad i \in 1, 2 \quad (8.2)$$

where,  $y_1 = 0.2053$  and  $y_2 = 0.7247$  represent the maximum values and  $b_1 = 6.065$  and  $b_2 = 8.465$  are the rates of change of rod weighting parameters  $\alpha_1$  and  $\alpha_2$  respectively. Note that the weight of rods' contribution to both L and M cones is equal to  $\alpha_1$  for any given retinal illuminance, while that to the S cones is  $\alpha_2$ . Figure 8.2 shows the original data points along with the obtained fits.

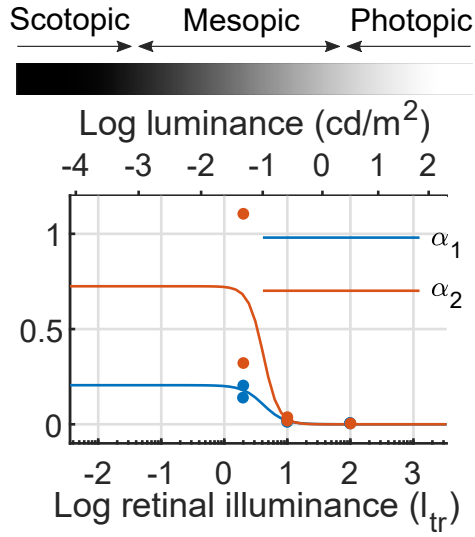


Figure 8.2: Values of rod contribution parameters as functions of retinal illuminance in trolands.  $\alpha_1$  is the weight of rod contribution to L and M cones.  $\alpha_2$  is the weight of rod contribution to S cones. The solid lines are fitted logistic functions. Data points are from Figure 3 in Cao et al. [213] for two observers. The mean of the values was used to fit the logistic function.

The cone responses undergo a sensitivity regulation before passing to the higher-order opponent colour mechanisms [225], [229], [230]. This gain parameter amplifies the low luminance responses and suppresses high luminance responses. The product of cone responses (with rod contributions) from Equation (8.1) and the regulation parameter is:

$$G(P') = \frac{P'}{(1 + k_1 P'_A)^{k_2}}, \quad P' \in L', M', S', \\ P'_A \in L'_A, M'_A, S'_A \quad (8.3)$$

where  $P'$  represents the cone responses of the stimuli with rod response added (Equation (8.1)), and  $P'_A$  the corresponding coordinates (adapting luminance and chromaticity) for the background. Here,  $P'_A = P_A$  is assumed, given the interest in very small, just noticeable colour differences. The commonly used values of  $k_1$  is 0.33 (trolands) and for  $k_2$  is 0.5 (unit-less) [213], [229]. The modified LMS+R responses from Equations (8.1)-(8.3) are used for the proposed colour difference formulae as they represent the perceptual response of the human visual system.

One of the measures of performance of a perceptual colour difference metric is its consistency with equivalent visual data. Some of the commonly used metrics to measure the correlation between colour difference formulae and perceptual error difference include the PF/3 [231]–

## CHAPTER 8. ROD VISION

[233],  $V_M$  [234], and STRESS [235].  $PF/3$  and the STRESS index are used to evaluate the proposed LMSR error metric. The range of  $PF/3$  is  $[0, \infty]$ , and that of STRESS is  $[0, 1]$ . For both uniformity metrics, a value of 0 indicates perfect agreement with visual performance. The values increase with increased deviation from perceptual data.

### 8.3 Colour difference metrics

To illustrate the effect of rod contribution, the achromatic response ( $L' + M'$  from Equation (8.1)) for red and blue colours are plotted in Figure 8.1, corresponding to the two display primaries. The display primaries' spectral response was scaled to obtain photopic luminance from 0.01-100 cd/m<sup>2</sup>, covering mesopic and photopic light levels. Each of the scaled spectral responses was converted to the corresponding LMSR responses. The modified L', M', and S' responses were calculated using Equations (8.1)-(8.3) with the rods contribution taken into account. The modified L', M', and S' responses were also calculated while keeping  $R = 0$  (assuming no rod response). The results are shown in Figure 8.1 (b-c). Adding rod input did not make any difference to the output of the red primary. However, for the blue primary at low luminance, the responses with and without the rod input clearly deviated from each other. The responses with rod addition had higher luminance output for low light levels. The model clearly predicts the Purkinje shift, according to which the luminous efficiency curve shifts towards short wavelengths with decreasing luminance levels. Consequently, short wavelength stimuli appear brighter in low luminance once the dark adaptation is complete. The model assumes full dark adaptation. The following error metrics are proposed based on the model in Equations (8.1)-(8.3):

$$\Delta E_{LMSR} = \sqrt{(\Delta G(L'))^2 + (\Delta G(M'))^2 + (\Delta G(S'))^2} \quad (8.4)$$

$$\Delta E_{2000}^{LMS} = \Delta E_{2000}(f(L_1, M_1, S_1), f(L_2, M_2, S_2)) \quad (8.5)$$

$$\Delta E_{2000}^{L'M'S'} = \Delta E_{2000}(f(L'_1, M'_1, S'_1), f(L'_2, M'_2, S'_2)) \quad (8.6)$$

$$\begin{aligned} \Delta E_{2000}^G = & \Delta E_{2000}(f(G(L'_1), G(M'_1), G(S'_1)), \\ & f(G(L'_2), G(M'_2), G(S'_2))) \end{aligned} \quad (8.7)$$

where,

$$\Delta G(P') = G(P'_1) - G(P'_2), \quad P' \in L', M', S' \quad (8.8)$$

$$\text{and, } f(L, M, S) = M_{\text{LMS} \rightarrow \text{XYZ}}[L \ M \ S]^T = [X \ Y \ Z]^T \quad (8.9)$$

$\Delta E_{LMSR}$  in Equation (8.4) is a RMSE metric for the regulated cone+rod responses in Equation (8.3). Equations (8.5)-(8.7) use either an unmodified  $\Delta E_{2000}$  colour difference formula ( $\Delta E_{2000}^{LMS}$  in Equation (8.5)), modified  $L^*a^*b^*$  values transformed using Equation (8.1)

Table 8.1: Summary of datasets

Dataset	Luminance (cd/m <sup>2</sup> )	Spatial frequency (cpd)	Size (deg <sup>2</sup> )	Back- grounds	Colour directions
HDR CSF [28]	0.002- 10,000	0.125, 0.25, 0.5	0.78- 50.26	1 (D65 grey)	3 (black-white, red-green, lime-violet)
HDRVDP CSF [179]	0.002-150	0.125, 0.25, 0.5	7.07	1 (D65 grey)	1 (black-white)
CC CSF [237]	8.8-72	0.06, 0.12, 0.24, 0.48	271.72	5 (grey, red, blue, green, yellow, blue)	6 (0, 40, 70, 100, 120, and 150 ° in <i>u'v'</i> space)

( $\Delta E_{2000}^{L'M'S'}$  in Equation (8.6)), and modified regulated  $L^*a^*b^*$  values transformed using Equation (8.3) ( $\Delta E_{2000}^G$  in Equation (8.7)).

### 8.3.1 Validation with contrast sensitivity datasets

Since traditional colour difference datasets based on patches [236] are missing samples at mesopic light levels, the proposed metrics were tested instead on three contrast sensitivity datasets. The three datasets are listed in Table 8.1 and the number of data points at each luminance is presented in Figure 8.3.

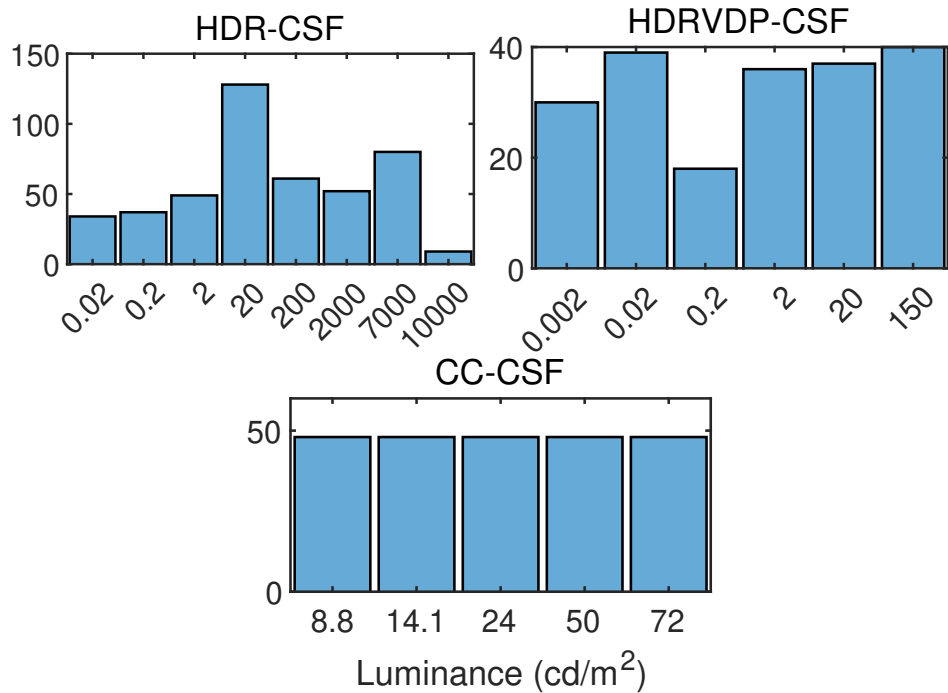


Figure 8.3: Number of data points across luminance levels in each dataset

## CHAPTER 8. ROD VISION

Contrast sensitivity is the inverse of cone contrast threshold, which is the minimum required contrast for the stimuli to be just visible. The cone contrast is used to represent contrasts in cardinal colour directions (as opposed to only achromatic Michelson contrast). It is the magnitude of the vector of individual L, M, and S-cone Michelson contrasts (Equation (3.5)). The stimuli used in the datasets are sine-wave gratings with a Gaussian window as shown in Figure 8.4. It was assumed that the colour difference between the peak and the trough of a Gabor patch at the detection threshold forms a unit just noticeable difference (JND) in colour. For validation purposes, the low spatial frequency stimuli (as referenced in Table 8.1) were used, owing to the interest in developing a colour metric for large stimuli. This choice is also important for comparison purposes, as the proposed metric was tested against  $\Delta E_{2000}$ , which is a metric designed for larger stimuli.

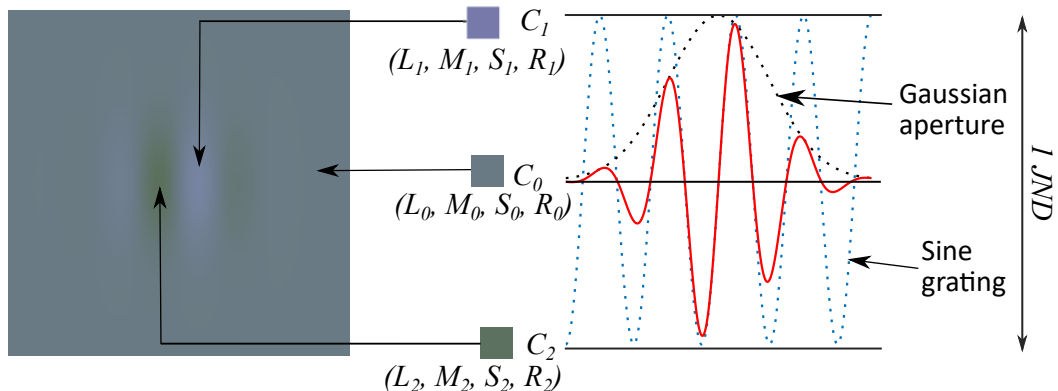


Figure 8.4: Left: An example CSF stimulus modulated in lime-violet direction against a grey background. Right: 1D representation of the stimulus on the left. The peaks of the red curve depict the contrast of blue and yellow areas of the grating against the background.

The spectral response of the displays was used to measure each dataset to calculate the LMSR coordinates of the background colour,  $C_0$ , using Smith and Pokorny cone fundamentals and CIE V'. The threshold contrast is a function of the change in LMSR coordinates with respect to the background coordinates. The change in LMSR was calculated to obtain the LMSR coordinates of the peak and trough of the stimulus as follows:

$$\begin{aligned} C_1 &= [L_0 + \Delta L, M_0 + \Delta M, S_0 + \Delta S, R_0 + \Delta R], \\ C_2 &= [L_0 - \Delta L, M_0 - \Delta M, S_0 - \Delta S, R_0 - \Delta R] \end{aligned} \quad (8.10)$$

where,  $L_0, M_0, S_0, R_0$  are the background coordinates,  $\Delta L, \Delta M, \Delta S$  and  $\Delta R$  are the differences in cone and rod responses corresponding to the threshold contrast, and  $C_1$  and  $C_2$  are pairs of LMSR coordinates with 1 JND perceptual difference.

## CHAPTER 8. ROD VISION

Each pair of  $C_1$  and  $C_2$  in all three datasets is converted to the modified photoreceptor responses using Equations (8.1)-(8.3), transformed to the equivalent  $L^*a^*b^*$  responses and then plugged in the error difference formulae in Equations (8.4)-(8.7) accordingly. It was assumed that the background of the stimuli is shown at the mid-grey level of a display, which corresponds to the luma value of 0.5. In linear units, the background luminance becomes  $0.5^{2.2} = 0.2176$  which is about 5 times lower than the luminance value of the display white point. Thus, the white point of  $\Delta E_{2000}$  formulae was set as a D65 white with 5 times higher luminance than the pairs tested. The  $PF/3$  and  $STRESS$  indices were calculated for the error results. The perceptual difference was assumed to be 1 unit for all colour pairs.

### 8.4 Results

The performances of the colour difference metrics defined in Equations (8.4)-(8.7) were evaluated using the three datasets described in Table 8.1.

#### 8.4.1 Metric 1: Euclidean LMS distance ( $\Delta E_{LMSR}$ )

Figure 8.5 shows the error distributions across luminance levels from  $\Delta E_{LMSR}$  for all the datasets. A well-performing colour difference metric should result in possibly similar colour difference predictions both within and across the luminance levels. The predicted  $\Delta E_{LMSR}$  colour differences values vary greatly between low and high luminance levels. The errors and their spread increase with increasing luminance levels for all three datasets. For the high dynamic range datasets, HDR-CSF and HDRVDP-CSF, the differences between the low and high luminance stimuli are particularly large as shown in Figure 8.5. This suggests that  $\Delta E_{LMSR}$  does not account for the effect of luminance on colour discrimination.

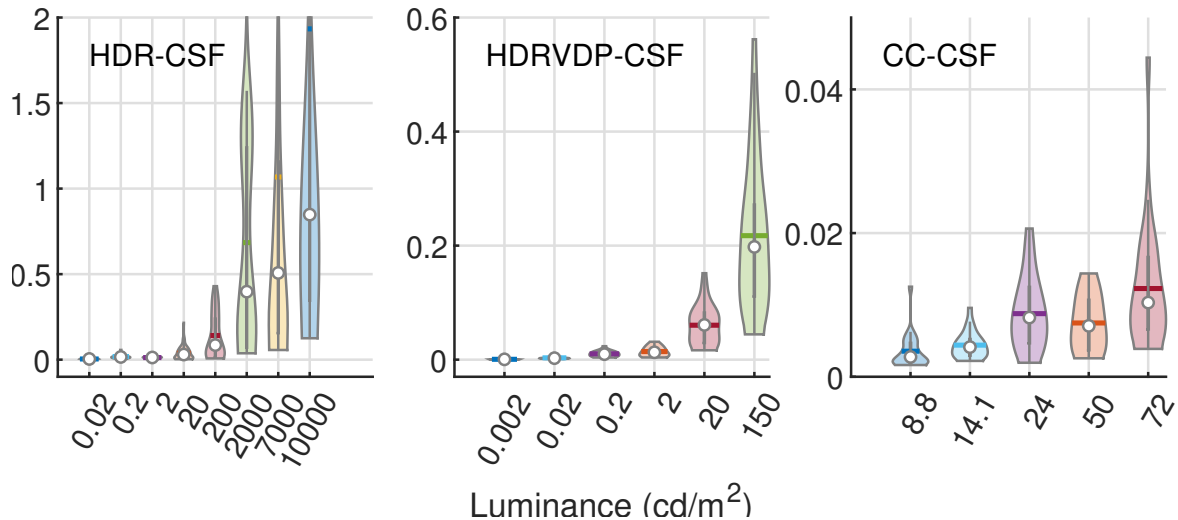


Figure 8.5:  $\Delta E_{LMSR}$  error predictions for 1 JND colour difference data points from the three dataset. The violin shapes show the smoothed kernel density at each error value. The white circles are the median and the horizontal lines are the mean values. The vertical grey lines show the interquartile range of the errors. The same notation is used in the subsequent violin plots. A well-performing colour difference metric should result in similar error values across the luminance levels.

#### 8.4.2 Metric 2: CIEDE2000 ( $\Delta E_{2000}^{LMS}$ )

The colour differences from  $\Delta E_{2000}^{LMS}$  metric are shown in Figure 8.6. Contrary to the previous metric  $\Delta E_{LMSR}$ , the predicted colour differences are much larger for low luminance stimuli. The colour differences are much more consistent across photopic and high mesopic luminance levels ( $\geq 2 \text{ cd/m}^2$ ). This is expected as  $\Delta E_{2000}$  was fitted to mostly photopic data and was not meant to be used for low luminance colours. The colour difference values are the most consistent for the CC-CSF dataset, which contains only stimuli at the photopic luminance levels.

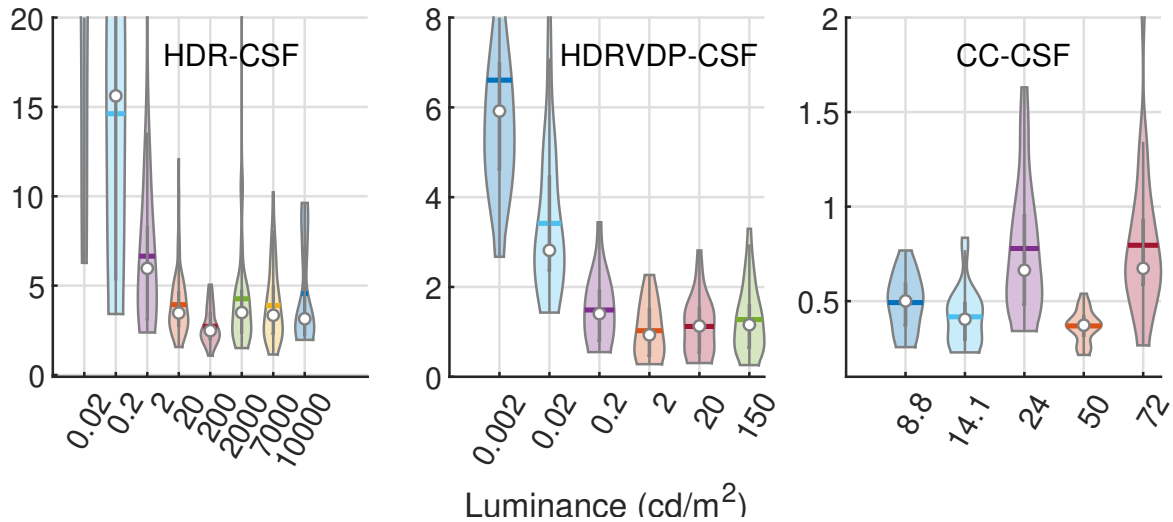


Figure 8.6:  $\Delta E_{2000}^{LMS}$  error predictions for 1 JND colour difference data points from the three datasets, using the same notation as Figure 8.5

#### 8.4.3 Metric 3: CIEDE200 + rod intrusion ( $\Delta E_{2000}^{L'M'S'}$ )

The  $\Delta E_{2000}^{L'M'S'}$  metric differs with  $\Delta E_{2000}^{LMS}$  in only the low luminance range. Therefore, the performance of  $\Delta E_{2000}^{L'M'S'}$  at photopic levels (Figure 8.7) is the same as  $\Delta E_{2000}^{LMS}$  (Figure 8.6) because the rod inputs in Equation (8.1) only contribute to cone responses in the scotopic range. The modified scotopic errors are much more consistent for this metric than for  $\Delta E_{2000}^{LMS}$  showing that the modelled rod intrusion can much improve colour predictions in the scotopic range. This can be observed for low luminance level colour differences in both HDR-CSF and HDRVDP-CSF datasets. There is no difference in performance between  $\Delta E_{2000}^{LMS}$  and  $\Delta E_{2000}^{L'M'S'}$  for CC-CSF dataset since the dataset has photopic stimuli only and there is no rod contribution.

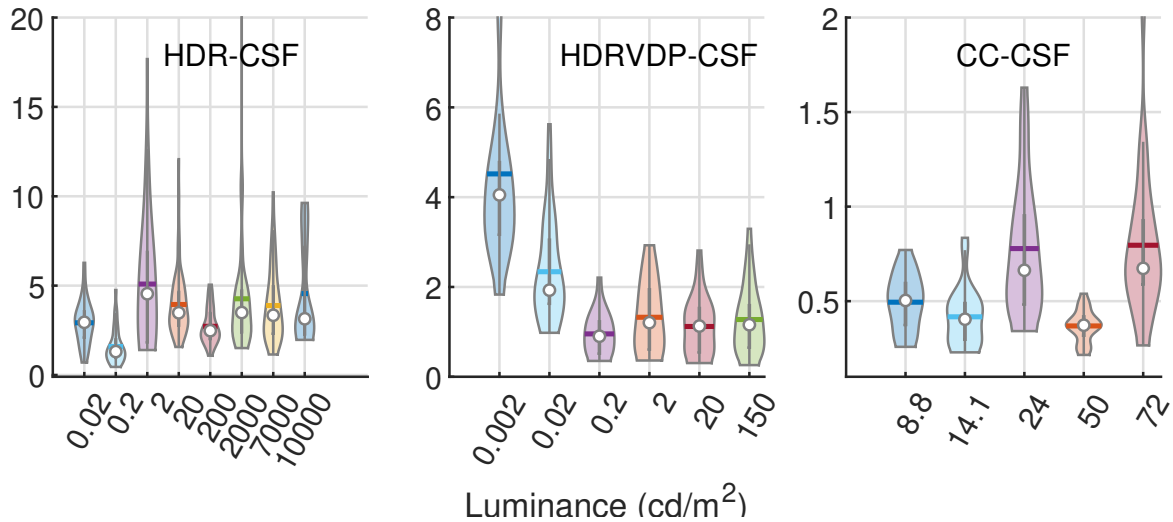


Figure 8.7:  $\Delta E_{2000}^{L'M'S'}$  error predictions for 1 JND colour difference data points from the three datasets, using the same notation as Figure 8.5

#### 8.4.4 Metric 4: CIEDE2000 + rod intrusion + adaptation

$\Delta E_{2000}^G$  is based on the gain-regulated cone responses which are suppressed for high luminances and amplified for low luminances. Such suppression results in worse consistency across the luminance levels. The effect is clearly shown in Figure 8.8 for the datasets HDR-CSF and HDRVDP-CSF. This is most likely because  $\Delta E_{2000}$  formula already accounts for the change in colour sensitivity across photopic luminance levels. Because the range of luminance of stimuli in CC-CSF dataset is relatively small, no marked difference in performance was observed for different luminance levels.

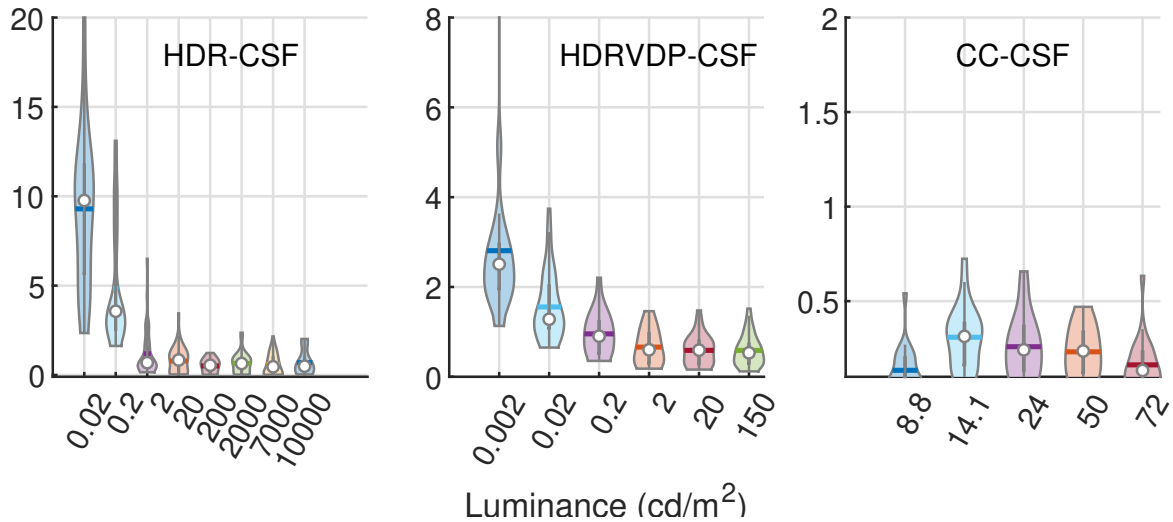


Figure 8.8:  $\Delta E_{2000}^G$  error predictions for 1 JND colour difference data points from the three datasets, using the same notation as Figure 8.5

#### 8.4.5 Perceptual uniformity

The perceptual uniformity of all four tested colour spaces is measured in terms of  $PF/3$  and  $STRESS$  indices and reported in Table 8.2.  $\Delta E_{2000}^{L'M'S'}$  shows the best performance (smallest indices) across all the datasets both in terms of  $PF/3$  and  $STRESS$  values. This indicates that  $\Delta E_{2000}^{L'M'S'}$  is the best predictor of 1 JND colour differences from the CSF datasets. For CC-CSF dataset,  $\Delta E_{2000}^{LMS}$  and  $\Delta E_{2000}^{L'M'S'}$  show the exact same performance, which is expected because the dataset only consists of photopic stimuli, and the two metrics are effectively the same for high luminance levels. The metric  $\Delta E_{LMSR}$  shows the worst performance in terms of perceptual uniformity almost across all conditions. This is a relatively simple metric based on RMSE of modified cone and rod responses and can not compete with more sophisticated  $\Delta E_{2000}$  based colour difference metrics which take a number of human perceptual attributes into account.

## CHAPTER 8. ROD VISION

Table 8.2: Performance comparison of the four metrics with respect to  $PF/3$  and  $STRESS$  uniformity measures. The values are compared for each column and the best and the worst performing metrics are highlighted with green and red colours respectively.

Colour difference metric	Datasets					
	HDR-CSF		HDRVDP-CSF		CC-CSF	
	$PF/3$	$STRESS$	$PF/3$	$STRESS$	$PF/3$	$STRESS$
$\Delta E_{LMSR}$	380.3	0.93	359	0.86	84.5	0.63
$\Delta E_{2000}^{LMS}$	126.1	0.83	117	0.73	53.9	0.48
$\Delta E_{2000}^{L'M'S'}$	68.1	0.55	95.5	0.66	53.9	0.48
$\Delta E_{2000}^G$	295.7	0.86	104	0.69	106	0.58

### 8.5 Summary of chapter

The proposed modification of the standard  $\Delta E_{2000}$  colour difference formula tackles its limitation in the low luminance levels. The modification of L\*a\*b\* coordinates for low luminance levels to include rod contributions was proposed. The rod contribution model by Cao et al. [213], based on colour matching data, also shows good predictions for threshold discrimination data from the CSF datasets. It was demonstrated that the Purkinje shift and the change from photopic to mesopic and scotopic luminous efficiency curves are well-captured by the model. The  $\Delta E_{2000}^{L'M'S'}$  colour difference formula shows improved colour difference predictions in mesopic and scotopic luminance ranges.

The metric currently does not account for chromatic adaptation, which is a potential future direction for this work. It does not take the time scale of adaptation into account either, which could be interesting given the different adaptation speeds of rods and cones.  $\Delta E_{2000}^{L'M'S'}$  could be used as a custom loss function for tasks that require matching or reproduction of low luminance colours. It is also a good tool to evaluate colour reproduction at low luminance levels, for example, in the case of HDR displays.



## CONCLUSIONS

The goal of this thesis was to provide a detailed investigation of the human contrast vision and mathematical modelling of contrast response for a variety of different conditions. This work was specifically focused on the aspects of vision that can be incorporated into practical applications in display technologies and computer graphic algorithms. To that end, human contrast vision was studied for a wide range of luminance levels reflecting the dynamic range of newer and future display technologies and HDR content. Similarly, the relatively less studied chromatic contrast vision was also investigated because accurate characterisation of chromatic contrast can be very useful for technologies where efficient as well as realistic representation of colour is important.

### 9.1 Research highlights

In this section, I summarise some important insights as well as the novel contributions from my work.

#### *Novel spatiochromatic contrast sensitivity data and models*

The spatiochromatic contrast sensitivity measurements presented in Chapter 4 bridge a gap in the literature for CSF measurements spanning both mesopic and photopic lighting conditions and for achromatic as well as chromatic modulations. The data offers insights on CSF extending beyond the typically studied photopic range. The research integrates both spatial and chromatic factors in the analysis of contrast sensitivity. While previous studies have often focused on either spatial or chromatic contrast sensitivity in isolation, this work examines the interaction between spatial frequencies and colour contrast.

Moreover, the spatiochromatic models presented in Chapter 5 were the first combined computational models that could predict contrast sensitivity as a joint function of spatial frequency, luminance, size and chromatic modulation. This work has already been extended to models that can predict CSF for even more stimulus parameters [39], [166], [238]–[240]. CSFs are directly applicable to applications such as visual difference predictors (VDP) models. A later iteration of the model presented here has recently been used as part of such a VDP [241].

## CHAPTER 9. CONCLUSIONS

Additionally, contrast sensitivity data measured at very high luminance levels reveals a decrease in sensitivity, rather than remaining constant, which does not conform to Weber's law. This effect has been systematically demonstrated for a large number of observers and for different spatial frequencies and sizes, representing a novel contribution. Although no explanation for this phenomenon has been identified, the finding is significant and warrants further investigation.

### *New insights on inter-luminance contrast constancy*

Contrast constancy - the equal perception of high contrast stimuli across many different stimulus properties - is a well-established property of contrast vision. However, very few works have attempted to verify this for matching across luminance levels. The few studies that have studied matching across luminance levels have done so for a limited luminance range. The CMF data presented in Chapters 6 is the only dataset that has spanned a luminance range of 6 log units and the only dataset to investigate chromatic contrast matching across luminance levels. When designing the study, it was hypothesised that the data would deviate from the constancy assumption but the magnitude of this deviation was much higher than expected and a new contribution to the research area.

The CMF model proposed in Chapter 7 borrows ideas from contrast models in the literature and combines different theoretical perspectives in its approach to predict the new CMF dataset across different luminances and colours. The model leverages the non-linearities of the human visual system and proposes new ways of using threshold predictions to scale up to suprathreshold levels.

These findings have direct implications for the design and calibration of display technologies. By understanding how contrast perception varies with luminance, display designers, for example, can optimise image rendering for various lighting conditions, enhancing viewer experience across different devices and environments.

### *Quantification of age-dependent change in contrast vision*

The CSF and CMF measurements for older observers presented in Chapters 4 and 6 respectively make up the only datasets in the current literature that span spatiochromatic space as well as a wide range of luminance levels. Because of the parallel dataset collected for younger observers measured for the same stimuli and conditions, it was made possible to pinpoint and quantify the exact changes in contrast perception that occur with age.

## CHAPTER 9. CONCLUSIONS

The age-dependent CSF models presented in Chapter 5 showed the empirical change in CSF parameters as well as the physiological change in the optics of the human visual system. The empirical model can accurately predict the CSF data for different age groups. No effect of age was found for contrast matching data which implies that the vision adapts with age and develops some compensatory mechanisms to cancel the physiological impacts of the ageing visual system.

The findings have significant implications for the design of visual displays and interfaces, especially for ageing populations. Understanding how contrast sensitivity changes with age and lighting can inform the development of more accessible and effective visual technologies. The data and models can also inform design decisions for more accessible real-world environments to prevent falls, for example [242].

### *New models to relate CSFs from Gabors and disc stimuli*

Unlike many studies that explore contrast sensitivity using more traditional stimuli like sinusoidal gratings or Gabor patches, this work focused on disc stimuli, which are less commonly used for spatial CSFs but commonly employed for chromatic and temporally-modulated stimuli. The long-term goal of the studies included in this thesis is to create a unified model of contrast vision that can predict sensitivity to all sorts of stimuli. The disc CSF data presented in Chapter 4 was used to explore any relationship with the CSFs measured from Gabor patches.

In Chapter 5, several novel models of disc CSF were proposed and validated with the measured dataset. The models employed several different approaches to predict disc CSF data using the general model trained on Gabor datasets. Future studies can build on these findings to explore contrast sensitivity for other non-traditional stimuli under different viewing conditions.

### *Inclusion of rod response for predicting colour difference*

This part of the thesis presented in Chapter 8 uniquely combined the rod intrusion model by Cao *et al.* [213] with the CIEDE2000 colour difference formula and proposed another way of looking at colour differences. The standard colour difference formulas typically focus only on cone responses and ignore the influence of rods on colour perception, especially under low luminance levels where rods are more active. By incorporating rod responses into the

## CHAPTER 9. CONCLUSIONS

colour difference calculation, the new formulae were demonstrated to improve the perceptual uniformity of colour spaces at low luminance levels.

The accuracy of the new formula using three contrast sensitivity datasets was validated, ensuring that the proposed model is grounded in empirical evidence. The results from this work are particularly important for applications in night-time lighting, display design and multimedia content for low light levels, and environments where mesopic vision predominates.

### 9.2 Future work recommendations

The models of CSF and CMF proposed in this thesis provide a solid foundation for further explorations of these topics. The modelling of contrast sensitivity, as seen in the studies involving discs and colour difference formulas, provides a promising approach to predicting overall visual performance. Future efforts should focus on refining these models with machine learning algorithms and incorporating more complex visual stimuli to enhance their predictive accuracy and applicability in real-world scenarios. Another approach that has already begun to be used is the incorporation of other datasets to train more general models. The current literature already contains hundreds of different datasets investigating different portions of the parameter space. Standardising these disjointed datasets into unified coherent measurements is proving to be a promising approach for future contrast vision modelling [39], [166], [240].

The insights from these studies can be applied to optimise the design displays, particularly for devices used in low-light conditions and to improve the appearance of content meant to be displayed in variable environments. By tailoring display technologies and rendering algorithms to align with human spatiochromatic contrast sensitivity, manufacturers can improve visibility, reduce eye strain and fatigue, and enhance the overall user experience. The findings can also be extended to improve the design of AR and VR environments, making them more accessible and reducing the potential for visual discomfort or disorientation.

Future research could aim to extend the presented measurements and models to include rods and ipRGCs as well. Incorporating rod response can be very useful for low-light environments. While ipRGCs are a relatively new research area and have already been shown to affect the contrast vision [243]. Including these photoreceptors in contrast vision modelling may provide new insights into the workings of our visual system.

Investigating the interaction between visual contrast sensitivity and other sensory modalities (e.g., auditory, tactile, olfactory) could offer novel insights into multisensory integration

## CHAPTER 9. CONCLUSIONS

and how it affects perception under varying light conditions. This line of research could have implications for understanding sensory processing in mixed-reality environments (VR, AR, XR, etc.). While significant advancements have been made in understanding contrast sensitivity under static mesopic and photopic conditions, it might be an interesting research avenue to explore these sensitivities under dynamically changing lighting conditions, which more closely mimic real-world scenarios where light levels fluctuate rapidly.

## REFERENCES

- [1] R. J. Snowden and O. J. Braddick, “The temporal integration and resolution of velocity signals,” *Vision research*, vol. 31, no. 5, pp. 907–914, 1991 (cit. on p. 1).
- [2] A. M. Derrington, J. Krauskopf, and P. Lennie, “Chromatic mechanisms in lateral geniculate nucleus of macaque.,” *The Journal of physiology*, vol. 357, no. 1, pp. 241–265, 1984 (cit. on pp. 2, 3, 29, 31, 53).
- [3] D. B. Elliot, K. C. Yang, and D. Whitaker, “Visual acuity changes throughout adulthood in normal, healthy eyes: seeing beyond 6/6,” *Optometry and vision science*, vol. 72, no. 3, pp. 186–191, 1995 (cit. on p. 2).
- [4] E. Peli, J. Yang, and R. B. Goldstein, “Image invariance with changes in size: The role of peripheral contrast thresholds,” *JOSA A*, vol. 8, no. 11, pp. 1762–1774, 1991 (cit. on p. 2).
- [5] G. R. Cole, T. Hine, and W. McIlhagga, “Detection mechanisms in L-, M-, and S-cone contrast space,” *Journal of the Optical Society of America A*, vol. 10, no. 1, pp. 38–51, 1993 (cit. on pp. 2, 30, 31).
- [6] E. B. Goldstein and L. Cacciamani, *Sensation and perception*. Cengage Learning, 2021 (cit. on p. 8).
- [7] S. Hecht, S. Shlaer, and M. H. Pirenne, “Energy, quanta, and vision,” *The Journal of general physiology*, vol. 25, no. 6, pp. 819–840, 1942 (cit. on pp. 8, 16).
- [8] J. Barbur and A. Stockman, “Photopic, mesopic and scotopic vision and changes in visual performance,” in *Encyclopedia of the Eye*, D. A. Dartt, Ed., Oxford: Academic Press, 2010, pp. 323–331, ISBN: 978-0-12-374203-2 (cit. on pp. 9, 16, 27, 166).
- [9] C. W. Tyler and R. D. Hamer, “Analysis of visual modulation sensitivity. IV. Validity of the Ferry–Porter law,” *Journal of Optical Society of America A*, vol. 7, no. 4, pp. 743–758, 1990 (cit. on p. 9).
- [10] H. B. Barlow, “Dark and light adaptation: psychophysics,” in *Visual psychophysics*, Springer, 1972, pp. 1–28 (cit. on p. 9).
- [11] D. A. Burkhardt, “Light adaptation and photopigment bleaching in cone photoreceptors in situ in the retina of the turtle,” *Journal of Neuroscience*, vol. 14, no. 3, pp. 1091–1105, 1994 (cit. on p. 9).

## REFERENCES

- [12] S. Hecht, C. Haig, and A. M. Chase, “The influence of light adaptation on subsequent dark adaptation of the eye,” *The Journal of general physiology*, vol. 20, no. 6, pp. 831–850, 1937 (cit. on p. 9).
- [13] W. S. Stiles and B. Crawford, “The luminous efficiency of rays entering the eye pupil at different points,” *Proceedings of the Royal Society of London. Series B, Containing Papers of a Biological Character*, vol. 112, no. 778, pp. 428–450, 1933 (cit. on p. 9).
- [14] C. Henley, “Vision: The Retina,” in *Foundations of neuroscience*, Michigan State University Libraries, 2021 (cit. on p. 10).
- [15] G. T. Fechner, *Elemente der psychophysik*. Breitkopf u. Härtel, 1860, vol. 2 (cit. on p. 10).
- [16] G. A. Gescheider, *Psychophysics: the fundamentals*. Psychology Press, 2013 (cit. on pp. 10, 11).
- [17] M. R. Leek, “Adaptive procedures in psychophysical research,” *Perception & Psychophysics*, vol. 63, no. 8, pp. 1279–1292, 2001 (cit. on p. 11).
- [18] A. B. Watson and D. G. Pelli, “QUEST: A Bayesian adaptive psychometric method,” *Perception & psychophysics*, vol. 33, no. 2, pp. 113–120, 1983 (cit. on pp. 11, 39, 53).
- [19] N. Prins *et al.*, *Psychophysics: a practical introduction*. Academic Press, 2016 (cit. on p. 11).
- [20] F. A. Wichmann and N. J. Hill, “The psychometric function: I. Fitting, sampling, and goodness of fit,” *Perception & psychophysics*, vol. 63, no. 8, pp. 1293–1313, 2001 (cit. on p. 12).
- [21] F. W. Campbell and J. G. Robson, “Application of Fourier analysis to the visibility of gratings,” *The Journal of physiology*, vol. 197, no. 3, p. 551, 1968 (cit. on pp. 13, 14, 22, 52, 82, 89).
- [22] J. G. Robson, “Spatial and temporal contrast-sensitivity functions of the visual system,” *Journal of the Optical Society of America*, vol. 56, no. 8, pp. 1141–1142, 1966 (cit. on p. 13).
- [23] D. Kelly, “Visual contrast sensitivity,” *Optica Acta: International Journal of Optics*, vol. 24, no. 2, pp. 107–129, 1977 (cit. on pp. 13, 52).

## REFERENCES

- [24] K. T. Mullen, “The contrast sensitivity of human colour vision to red-green and blue-yellow chromatic gratings.,” *The Journal of physiology*, vol. 359, no. 1, pp. 381–400, 1985 (cit. on pp. 13, 15, 28, 31, 52, 58, 71).
- [25] J. M. Rovamo, M. I. Kankaanpää, and H. Kukkonen, “Modelling spatial contrast sensitivity functions for chromatic and luminance-modulated gratings,” *Vision research*, vol. 39, no. 14, pp. 2387–2398, 1999 (cit. on p. 13).
- [26] F. L. Van Nes and M. A. Bouman, “Spatial Modulation Transfer in the Human Eye,” *Journal of the Optical Society of America*, vol. 57, no. 3, pp. 401–406, Mar. 1967 (cit. on pp. 13, 15, 16, 36, 41, 42).
- [27] J. Mustonen, J. Rovamo, and R. Näsänen, “The effects of grating area and spatial frequency on contrast sensitivity as a function of light level,” *Vision research*, vol. 33, no. 15, pp. 2065–2072, 1993 (cit. on pp. 13, 15, 36, 42, 52).
- [28] S. Wuerger, M. Ashraf, M. Kim, J. Martinovic, M. Perez-Ortiz, and R. K. Mantiuk, “Spatio-chromatic contrast sensitivity under mesopic and photopic light levels,” *Journal of Vision*, vol. 20, no. 4, pp. 1–26, 2020. doi: 10.1167/jov.20.4.23 (cit. on pp. 13, 52, 54, 92, 128).
- [29] J. G. Robson and N. Graham, “Probability summation and regional variation in contrast sensitivity across the visual field,” *Vision research*, vol. 21, no. 3, pp. 409–418, 1981 (cit. on pp. 13, 15).
- [30] S. J. Anderson, K. T. Mullen, and R. F. Hess, “Human peripheral spatial resolution for achromatic and chromatic stimuli: limits imposed by optical and retinal factors.,” *The Journal of physiology*, vol. 442, no. 1, pp. 47–64, 1991 (cit. on pp. 13, 15).
- [31] J. Rovamo, O. Luntinen, and R. Näsänen, “Modelling the dependence of contrast sensitivity on grating area and spatial frequency,” *Vision research*, vol. 33, no. 18, pp. 2773–2788, 1993 (cit. on pp. 13, 15, 52).
- [32] C. Owsley, R. Sekuler, and D. Siemsen, “Contrast sensitivity throughout adulthood,” *Vision research*, vol. 23, no. 7, pp. 689–699, 1983 (cit. on pp. 13, 47, 50, 71, 74, 164).
- [33] M. Ashraf, S. Wuerger, M. Kim, J. Martinovic, and R. K. Mantiuk, “Spatio-chromatic contrast sensitivity across the lifespan: Interactions between age and light level in high dynamic range,” in *Color and Imaging Conference*, Society for Imaging Science and Technology, vol. 2020, 2020, pp. 65–69. doi: 10.2352/issn.2169-2629.2020.28.10 (cit. on p. 13).

## REFERENCES

- [34] S. Shlaer, “The relation between visual acuity and illumination,” *The Journal of general physiology*, vol. 21, no. 2, pp. 165–188, 1937 (cit. on p. 14).
- [35] C. H. Graham and R. Margaria, “Area and the intensity-time relation in the peripheral retina,” *American Journal of Physiology-Legacy Content*, vol. 113, no. 2, pp. 299–305, 1935 (cit. on p. 14).
- [36] C. Noorlander, M. G. Heuts, and J. J. Koenderink, “Influence of the target size on the detection threshold for luminance and chromaticity contrast.,” *Journal of the Optical Society of America*, 1980, ISSN: 00303941 (cit. on p. 15).
- [37] F. W. Campbell, J. J. Kulikowski, and J. Levinson, “The effect of orientation on the visual resolution of gratings,” *The Journal of Physiology*, vol. 187, no. 2, pp. 427–436, 1966 (cit. on p. 15).
- [38] A. B. Watson and A. J. Ahumada, “A standard model for foveal detection of spatial contrast,” *Journal of Vision*, vol. 5, no. 9, pp. 717–740, 2005, ISSN: 15347362 (cit. on pp. 15, 57).
- [39] M. Ashraf, R. K. Mantiuk, A. Chapiro, and S. Wuerger, “castleCSF — A Contrast Sensitivity Function of Color, Area, Spatio-Temporal frequency, Luminance and Eccentricity,” *Journal of Vision*, vol. (in press), 2024 (cit. on pp. 15, 136, 139).
- [40] D. G. Green, “The contrast sensitivity of the colour mechanisms of the human eye,” *The Journal of Physiology*, vol. 196, no. 2, pp. 415–429, 1968 (cit. on p. 15).
- [41] M. Lucassen, M. Lambooij, D. Sekulovski, and I. Vogels, “Spatio-chromatic sensitivity explained by post-receptoral contrast,” *Journal of Vision*, vol. 18, no. 5, pp. 13–13, May 2018, ISSN: 1534-7362 (cit. on p. 15).
- [42] S. J. Cropper, “Detection of chromatic and luminance contrast modulation by the visual system,” *J. Opt. Soc. Am. A*, vol. 15, no. 8, pp. 1969–1986, Aug. 1998 (cit. on p. 15).
- [43] B. W. Andrews and D. A. Pollen, “Relationship between Spatial-frequency Selectivity and Receptive-field Profile of Simple Cells,” *Journal of Physiology*, vol. 287, pp. 163–176, 1979 (cit. on p. 15).
- [44] E. M. Granger and J. C. Heurtley, “Visual chromaticity-modulation transfer function,” *J.Opt.Soc.Amer.*, vol. 63, no. 9, pp. 1173–1174, 1973, ISSN: 0030-3941. doi: 10.1364/JOSA.63.001173 (cit. on pp. 15, 71).

## REFERENCES

- [45] G. J. Van der Horst and M. A. Bouman, “Spatiotemporal chromaticity discrimination,” *Journal of Optical Society of America*, vol. 59, no. 11, pp. 1482–1488, 1969 (cit. on p. 15).
- [46] Y. J. Kim, A. Reynaud, R. F. Hess, and K. T. Mullen, “A normative data set for the clinical assessment of achromatic and chromatic contrast sensitivity using a qCSF approach,” *Investigative ophthalmology & visual science*, vol. 58, no. 9, pp. 3628–3636, 2017 (cit. on pp. 15, 41, 57).
- [47] D. J. McKeefry, I. J. Murray, and J. J. Kulikowski, “Red-green and blue-yellow mechanisms are matched in sensitivity for temporal and spatial modulation,” *Vision Research*, vol. 41, no. 2, pp. 245–255, 2001, ISSN: 00426989 (cit. on p. 15).
- [48] W. H. Swanson, “S-cone spatial contrast sensitivity can be independent of pre-receptoral factors,” *Vision Research*, vol. 36, no. 21, pp. 3549–3555, 1996, ISSN: 0042-6989 (cit. on p. 15).
- [49] E. M. Valero, J. L. Nieves, J. Hernández-Andrés, and J. A. García, “Changes in contrast thresholds with mean luminance for chromatic and luminance gratings: A reexamination of the transition from the DeVries–Rose to Weber regions,” *Color Research & Application*, vol. 29, no. 3, pp. 177–182, 2004 (cit. on pp. 15, 43).
- [50] N. Sekiguchi, D. R. Williams, and D. H. Brainard, “Efficiency in detection of iso-luminant and isochromatic interference fringes,” *Journal of the Optical Society of America A*, vol. 10, no. 10, p. 2118, 1993, ISSN: 1084-7529 (cit. on pp. 15, 17).
- [51] G. Wald, “Human vision and the spectrum.,” *Science*, vol. 101, no. 2635, pp. 653–658, 1945 (cit. on pp. 16, 74, 123).
- [52] R. A. Weale, “Aging and vision.,” *Vision Research*, 1986 (cit. on p. 16).
- [53] J. S. Werner, “Visual problems of the retina during ageing: Compensation mechanisms and colour constancy across the life span,” *Progress in Retinal and Eye Research*, vol. 15, no. 2, pp. 621–645, 1996, ISSN: 13509462. doi: 10.1016/1350-9462(96)00001-8 (cit. on p. 16).
- [54] C. Owsley, “Aging and vision,” *Vision Research*, vol. 51, no. 13, pp. 1610–1622, Jul. 2011. doi: 10.1016/j.visres.2010.10.020 (cit. on p. 16).
- [55] G. J. Andersen, “Aging and vision: changes in function and performance from optics to perception,” *Wiley Interdisciplinary Reviews: Cognitive Science*, vol. 3, no. 3, pp. 403–410, 2012 (cit. on p. 16).

## REFERENCES

- [56] C. A. Curcio, C. L. Millican, K. A. Allen, and R. E. Kalina, “Aging of the human photoreceptor mosaic: Evidence for selective vulnerability of rods in central retina,” *Investigative Ophthalmology and Visual Science*, vol. 34, no. 12, pp. 3278–3296, 1993 (cit. on p. 16).
- [57] J. Marshall, “The ageing retina: physiology or pathology,” *Eye*, vol. 1, no. 2, pp. 282–295, 1987 (cit. on p. 16).
- [58] D. J. Calkins, “Age-related changes in the visual pathways: blame it on the axon,” *Investigative ophthalmology & visual science*, vol. 54, no. 14, ORSF37–ORSF41, 2013 (cit. on p. 16).
- [59] J. S. Werner and V. G. Steele, “Sensitivity of human foveal color mechanisms throughout the life span,” *Journal of the Optical Society of America A*, vol. 5, no. 12, p. 2122, 1988, ISSN: 1084-7529. doi: 10.1364/josaa.5.002122 (cit. on p. 16).
- [60] M. S. Roy, M. J. Podgor, B. Collier, and R. D. Gunkel, “Color vision and age in a normal North American population,” *Graefe’s Archive for Clinical and Experimental Ophthalmology*, vol. 229, pp. 139–144, 1991 (cit. on p. 16).
- [61] A. Guirao, C. Gonzalez, M. Redondo, E. Geraghty, S. Norrby, and P. Artal, “Average optical performance of the human eye as a function of age in a normal population.,” *Investigative Ophthalmology & Visual Science*, vol. 40, no. 1, pp. 203–213, 1999 (cit. on p. 16).
- [62] P. Artal, M. Ferro, I. Miranda, and R. Navarro, “Effects of aging in retinal image quality,” *JOSA A*, vol. 10, no. 7, pp. 1656–1662, 1993 (cit. on p. 16).
- [63] F. W. Campbell and D. G. Green, “Optical and retinal factors affecting visual resolution,” *The Journal of Physiology*, vol. 181, pp. 576–593, 1965. doi: 10.1113/jphysiol.1965.sp007784 (cit. on p. 16).
- [64] J. D. Morrison and C. McGrath, “Assessment of the Optical Contributions To the Age Related Deterioration in Vision,” *Quarterly Journal of Experimental Physiology*, vol. 70, no. 2, pp. 249–269, 1985. doi: 10.1113/expphysiol.1985.sp002907 (cit. on pp. 16, 50, 74).
- [65] R. A. Weale, “Senile changes in visual acuity,” *Transactions of the ophthalmological societies of the United Kingdom*, vol. 95, no. 1, pp. 36–38, 1975 (cit. on p. 16).
- [66] D. Silvestre, A. Arleo, and R. Allard, “Healthy aging impairs photon absorption efficiency of cones,” *Investigative Ophthalmology and Visual Science*, vol. 60, no. 2, pp. 544–551, Feb. 2019. doi: 10.1167/iovs.18-25598 (cit. on pp. 16, 51).

## REFERENCES

- [67] M. E. Sloane, C. Owsley, and S. L. Alvarez, “Aging, senile miosis and spatial contrast sensitivity at low luminance,” *Vision Research*, vol. 28, no. 11, pp. 1235–1246, 1988, ISSN: 0042-6989. doi: 10.1016/0042-6989(88)90039-9 (cit. on pp. 16, 50, 71, 164).
- [68] J. Hoekstra, D. V. der Goot, G. V. den Brink, and F. Bilsen, “The influence of the number of cycles upon the visual contrast threshold for spatial sine wave patterns,” *Vision Research*, vol. 14, no. 6, pp. 365–368, 1974, ISSN: 0042-6989 (cit. on pp. 17, 38).
- [69] E. Howell and R. Hess, “The functional area for summation to threshold for sinusoidal gratings,” *Vision Research*, vol. 18, no. 4, pp. 369–374, 1978, ISSN: 0042-6989 (cit. on pp. 17, 38).
- [70] H. Piper, “Über die Abhängigkeit des Reizwertes leuchtender Objekte von ihrer Flächen-bezw. Winkelgröße [[The effect of area and visual angle on the sensation of self-luminous objects]],” *Zeitschrift für Psychologie und Physiologie der Sinnesorgane*, vol. 32, pp. 98–122, 1903 (cit. on pp. 17, 38).
- [71] V. Manahilov, W. A. Simpson, and D. L. McCulloch, “Spatial summation of peripheral Gabor patches,” *J. Opt. Soc. Am. A*, vol. 18, no. 2, pp. 273–282, Feb. 2001 (cit. on pp. 17, 38, 45).
- [72] K. Mullen, “Colour vision as a post-receptoral specialization of the central visual field,” *Vision Research*, vol. 31, no. 1, pp. 119–130, 1991, ISSN: 0042-6989 (cit. on pp. 17, 38).
- [73] A. Vassilev, M. Zlatkova, V. Manahilov, A. Krumov, and M. Schaumberger, “Spatial summation of blue-on-yellow light increments and decrements in human vision,” *Vision Research*, vol. 40, no. 8, pp. 989–1000, 2000, ISSN: 0042-6989 (cit. on pp. 17, 38).
- [74] A. B. Watson, H. Barlow, and J. Robson, “What does the eye see best?” *Nature*, vol. 302, pp. 419–422, 1983 (cit. on p. 17).
- [75] A. Chaparro, C. Stromeier, E. Huang, R. Kronauer, and R. Eskew, “Colour is what the eye sees best,” *Nature*, vol. 361, pp. 348–350, 1993 (cit. on pp. 17, 44).
- [76] M. Georgeson and G. Sullivan, “Contrast constancy: deblurring in human vision by spatial frequency channels.,” *The Journal of physiology*, vol. 252, no. 3, pp. 627–656, 1975 (cit. on pp. 19, 94, 105).

## REFERENCES

- [77] A. Watanabe, T. Mori, S. Nagata, and K. Hiwatashi, “Spatial sine-wave responses of the human visual system,” *Vision Research*, vol. 8, no. 9, pp. 1245–1263, 1968 (cit. on p. 19).
- [78] C. Blakemore, J. P. Muncey, and R. M. Ridley, “Stimulus specificity in the human visual system,” *Vision research*, vol. 13, no. 10, pp. 1915–1931, 1973 (cit. on p. 19).
- [79] J. Kulikowski, “Effective contrast constancy and linearity of contrast sensation,” *Vision research*, vol. 16, no. 12, pp. 1419–1431, 1976 (cit. on pp. 19, 20, 94, 104, 107, 108, 113).
- [80] R. Hess, “The Ed ridge-Green Lecture Vision at low light levels: role of spatial, temporal and contrast filters,” *Ophthalmic and physiological optics*, vol. 10, no. 4, pp. 351–359, 1990 (cit. on pp. 20, 94).
- [81] E. Peli, J. Yang, R. Goldstein, and A. Reeves, “Effect of luminance on suprathreshold contrast perception,” *Journal of the Optical Society of America A*, vol. 8, no. 8, pp. 1352–1359, 1991 (cit. on pp. 20, 94, 104, 110).
- [82] E. Peli, “Suprathreshold contrast perception across differences in mean luminance: effects of stimulus size, dichoptic presentation, and length of adaptation,” *Journal of the Optical Society of America A*, vol. 12, no. 5, pp. 817–823, 1995 (cit. on p. 20).
- [83] E. Peli, L. Arend, and A. T. Labianca, “Contrast perception across changes in luminance and spatial frequency,” *Journal of the Optical Society of America A*, vol. 13, no. 10, pp. 1953–1959, 1996 (cit. on pp. 20, 106, 107, 110, 113).
- [84] K. Tiippana, J. Rovamo, R. Näsänen, D. Whitaker, and P. Mäkelä, “Contrast matching across spatial frequencies for isoluminant chromatic gratings,” *Vision Research*, vol. 40, no. 16, pp. 2159–2165, 2000 (cit. on p. 20).
- [85] P. B. Delahunt, J. L. Hardy, K. Okajima, and J. S. Werner, “Senescence of spatial chromatic contrast sensitivity. II. Matching under natural viewing conditions,” *Journal of the Optical Society of America A*, vol. 22, no. 1, pp. 60–67, 2005 (cit. on p. 20).
- [86] R. Wanat and R. K. Mantiuk, “Simulating and compensating changes in appearance between day and night vision,” *ACM Transactions on Graphics (TOG)*, vol. 33, no. 4, pp. 1–12, 2014 (cit. on pp. 20, 120, 123).
- [87] M. Rezagholizadeh, T. Akhavan, A. Soudi, H. Kaufmann, and J. J. Clark, “A re-targeting approach for mesopic vision: simulation and compensation,” *Electronic Imaging*, vol. 2016, no. 20, pp. 1–12, 2016 (cit. on pp. 20, 120).

## REFERENCES

- [88] J. Shin, N. Matsuki, H. Yaguchi, and S. Shioiri, “A color appearance model applicable in mesopic vision,” *Optical review*, vol. 11, no. 4, pp. 272–278, 2004 (cit. on p. 20).
- [89] B. E. Schefrin, K. Shinomori, and J. S. Werner, “Contributions of neural pathways to age-related losses in chromatic discrimination,” *Journal of the Optical Society of America A*, vol. 12, no. 6, p. 1233, 1995, ISSN: 1084-7529. doi: 10.1364/josaa.12.001233 (cit. on p. 21).
- [90] S. Wuerger, “Colour constancy across the life span: evidence for compensatory mechanisms,” *PloS one*, vol. 8, no. 5, pp. 1–9, 2013 (cit. on p. 21).
- [91] J. M. Kraft and J. S. Werner, “Aging and the saturation of colors. 1. Colorimetric purity discrimination,” *Journal of the Optical Society of America A*, vol. 16, no. 2, pp. 223–229, 1999, ISSN: 1084-7529. doi: 10.1364/josaa.16.000223 (cit. on p. 21).
- [92] G. V. Paramei, “Color discrimination across four life decades assessed by the Cambridge Colour Test,” *Journal of the Optical Society of America A*, vol. 29, no. 2, A290, 2012, ISSN: 1084-7529. doi: 10.1364/josaa.29.00a290 (cit. on pp. 21, 51).
- [93] K. Knoblauch, F. Vital-Durand, and J. L. Barbur, “Variation of chromatic sensitivity across the life span,” *Vision Research*, vol. 41, no. 1, pp. 23–36, 2001, ISSN: 00426989. doi: 10.1016/S0042-6989(00)00205-4 (cit. on p. 21).
- [94] U. Tulunay-Keesey, J. N. Ver Hoeve, and C. Terkla-McGrane, “Threshold and suprathreshold spatiotemporal response throughout adulthood,” *Journal of Optical Society of America A*, vol. 5, no. 12, pp. 2191–2200, 1988 (cit. on pp. 21, 47, 50).
- [95] D. Gabor, “Theory of communication. Part 1: The analysis of information,” *Journal of the Institution of Electrical Engineers-part III: radio and communication engineering*, vol. 93, no. 26, pp. 429–441, 1946 (cit. on p. 21).
- [96] S. Marêelja, “Mathematical description of the responses of simple cortical cells,” *JOSA*, vol. 70, no. 11, pp. 1297–1300, 1980 (cit. on pp. 21, 22).
- [97] J. J. Kulikowski and P. O. Bishop, “Fourier analysis and spatial representation in the visual cortex,” *Experientia*, vol. 37, no. 2, pp. 160–163, 1981 (cit. on p. 22).
- [98] R. L. De Valois and K. K. De Valois, “Spatial vision,” *Annual review of psychology*, vol. 31, no. 1, pp. 309–341, 1980 (cit. on p. 22).
- [99] A. B. Watson, “Visual detection of spatial contrast patterns: Evaluation of five simple models.,” *Optics Express*, vol. 6, no. 1, pp. 12–33, 2000 (cit. on p. 24).

## REFERENCES

- [100] H. Seetzen, W. Heidrich, W. Stuerzlinger, *et al.*, “High dynamic range display systems,” *ACM Transactions on Graphics*, vol. 23, no. 3, p. 760, Aug. 2004, ISSN: 07300301 (cit. on p. 25).
- [101] M. Kleiner, D. Brainard, and D. Pelli, “What’s new in Psychtoolbox-3?,” 2007 (cit. on pp. 26, 53).
- [102] CIE, “Fundamental chromaticity diagram with psychological axes - part 1,” Central Bureau of the Commission Internationale de l’ Éclairage, Tech. Rep., 2006 (cit. on pp. 26, 27).
- [103] R. S. Berns, “Methods for characterizing CRT displays,” *Displays*, vol. 16, no. 4, pp. 173–182, May 1996, ISSN: 01419382 (cit. on p. 27).
- [104] G. Wagner and R. M. Boynton, “Comparison of Four Methods of Heterochromatic Photometry,” *Journal of the Optical Society of America*, vol. 62, no. 12, pp. 1508–1515, Dec. 1972. doi: 10.1364/JOSA.62.001508 (cit. on p. 28).
- [105] K. S. Gibson and E. P. T. Tyndall, “Visibility of radiant energy,” *Scientific Papers of the Bureau of Standards*, vol. 19, no. 19, pp. 131–191, Jan. 1923 (cit. on p. 28).
- [106] M. Ikeda and H. Shimozono, “Mesopic luminous-efficiency functions,” *J. Opt. Soc. Am.*, vol. 71, no. 3, pp. 280–284, Mar. 1981 (cit. on p. 28).
- [107] D. I. Flitcroft, “The interactions between chromatic aberration, defocus and stimulus chromaticity: Implications for visual physiology and colorimetry,” *Vision Research*, vol. 29, no. 3, pp. 349–360, 1989, ISSN: 00426989 (cit. on pp. 28, 59).
- [108] L. Bilodeau and J. Faubert, “Isoluminance and chromatic motion perception throughout the visual field,” *Vision Research*, vol. 37, no. 15, pp. 2073–2081, 1997, ISSN: 0042-6989 (cit. on p. 28).
- [109] M. P. S. To and D. J. Tolhurst, “V1-based modeling of discrimination between natural scenes within the luminance and isoluminant color planes,” *Journal of Vision*, vol. 19, no. 1, p. 9, 2019, ISSN: 1534-7362 (cit. on p. 28).
- [110] A. Stockman and L. T. Sharpe, “The spectral sensitivities of the middle-and long-wavelength-sensitive cones derived from measurements in observers of known genotype,” *Vision research*, vol. 40, no. 13, pp. 1711–1737, 2000 (cit. on pp. 28, 79).
- [111] B. A. Wandell, *Foundations of vision*. Sinauer Associates Sunderland, MA, 1995 (cit. on p. 28).

## REFERENCES

- [112] D. I. MacLeod and R. M. Boynton, “Chromaticity diagram showing cone excitation by stimuli of equal luminance,” *Journal of the Optical Society of America*, vol. 69, no. 8, pp. 1183–1186, 1979 (cit. on p. 28).
- [113] CIE, *Commission internationale de l'éclairage proceedings, 1931*, 1931 (cit. on p. 28).
- [114] D. H. Brainard, “Cone contrast and opponent modulation color spaces,” *Human color vision*, 1996 (cit. on pp. 29–31).
- [115] P. Capilla, J. Malo, M. J. Luque, and J. M. Artigas, “Colour representation spaces at different physiological levels: a comparative analysis,” *Journal of Optics*, vol. 29, no. 5, pp. 324–338, Oct. 1998 (cit. on p. 30).
- [116] R. Shapley and M. J. Hawken, “Color in the Cortex: single- and double-opponent cells,” *Vision Research*, vol. 51, no. 7, pp. 701–717, 2011, Vision Research 50th Anniversary Issue: Part 1, ISSN: 0042-6989 (cit. on p. 30).
- [117] P. K. Kaiser, *The joy of visual perception: A web book*. York University, 1997 (cit. on p. 31).
- [118] J. D. Mollon and J. Reffin, “A computer-controlled color-vision test that combines the principles of Chibret and of Stilling,” *Journal of Physiology-London*, vol. 414, 1989 (cit. on p. 35).
- [119] A. B. Watson and J. I. Yellott, “A unified formula for light-adapted pupil size,” *Journal of vision*, vol. 12, no. 10, pp. 12–12, 2012 (cit. on pp. 37, 52, 77).
- [120] P. Vangorp, K. Myszkowski, E. W. Graf, and R. K. Mantiuk, “A model of local adaptation,” *ACM Transactions on Graphics*, vol. 34, no. 6, pp. 1–13, Oct. 2015, ISSN: 07300301. doi: 10.1145/2816795.2818086 (cit. on p. 38).
- [121] N. Sekiguchi, D. R. Williams, and D. H. Brainard, “Aberration-free measurements of the visibility of isoluminant gratings,” *Journal of the Optical Society of America A*, vol. 10, no. 10, p. 2105, 1993, ISSN: 1084-7529 (cit. on p. 38).
- [122] A. Rose, “The Sensitivity Performance of the Human Eye on an Absolute Scale\*,” *Journal of the Optical Society of America*, vol. 38, no. 2, pp. 196–208, Feb. 1948 (cit. on p. 42).
- [123] H. De Vries, “The quantum character of light and its bearing upon threshold of vision, differential sensitivity and visual acuity of the eye.,” *Physica*, vol. 10, pp. 553–564, 1943. doi: 10.1016/S0031-8914(43)90575-0 (cit. on p. 42).

## REFERENCES

- [124] M. A. Díez-Ajenjo and P. Capilla, “Spatio-temporal Contrast Sensitivity in the Cardinal Directions of the Colour Space. A Review,” eng, *Journal of Optometry*, vol. 3, no. 1, pp. 2–19, 2010, issn: 1888-4296 (cit. on p. 43).
- [125] G. J. Burton and I. R. Moorhead, “Color and spatial structure in natural scenes,” *Appl. Opt.*, vol. 26, no. 1, pp. 157–170, 1987 (cit. on p. 44).
- [126] O. Luntinen, J. Rovamo, and R. Näsänen, “Modelling the increase of contrast sensitivity with grating area and exposure time,” *Vision Research*, vol. 35, no. 16, pp. 2339–2346, 1995, issn: 0042-6989 (cit. on p. 45).
- [127] T. S. Meese and R. J. Summers, “Area summation in human vision at and above detection threshold,” *Proceedings of the Royal Society B: Biological Sciences*, vol. 274, no. 1627, pp. 2891–2900, 2007 (cit. on p. 45).
- [128] K. Arundale, “An investigation into the variation of human contrast sensitivity with age and ocular pathology,” *British Journal of Ophthalmology*, vol. 62, no. 4, pp. 213–215, 1978, issn: 00071161. doi: 10.1136/bjo.62.4.213 (cit. on pp. 47, 50, 164).
- [129] G. Derefeldt, G. Lennerstrand, and B. Lundh, “Age Variations in Normal Human Contrast Sensitivity,” *Acta Ophthalmologica*, vol. 57, no. 4, pp. 679–690, May 1979, issn: 1755375X. doi: 10.1111/j.1755-3768.1979.tb00517.x (cit. on pp. 47, 50, 164).
- [130] C. McGrath and J. D. Morrison, “the Effects of Age on Spatial Frequency Perception in Human Subjects,” *Quarterly Journal of Experimental Physiology*, vol. 66, no. 3, pp. 253–261, 1981, issn: 1469445X. doi: 10.1113/expphysiol.1981.sp002554 (cit. on pp. 47, 71, 164).
- [131] J. L. Hardy, P. B. Delahunt, K. Okajima, and J. S. Werner, “Senescence of spatial chromatic contrast sensitivity. I. Detection under conditions controlling for optical factors,” *JOSA A*, vol. 22, no. 1, pp. 49–59, 2005 (cit. on pp. 47, 51, 72, 165).
- [132] I. L. Bailey and J. E. Lovie, “New design principles for visual acuity letter charts.,” *American journal of optometry and physiological optics*, vol. 53, no. 11, pp. 740–745, 1976 (cit. on p. 48).
- [133] D. Rosser, D. Laidlaw, and I. Murdoch, “The development of a “reduced logMAR” visual acuity chart for use in routine clinical practice,” *British Journal of Ophthalmology*, vol. 85, no. 4, pp. 432–436, 2001 (cit. on p. 48).
- [134] S. A. Kelly, Y. Pang, and S. Klemencic, “Reliability of the CSV-1000 in adults and children,” *Optometry and Vision Science*, vol. 89, no. 8, pp. 1172–1181, 2012 (cit. on p. 48).

## REFERENCES

- [135] J. Frisby, “The frisby stereotest: an introduction and a review,” *J Chem Inf Model*, no. 53, p. 1689, 2017 (cit. on p. 48).
- [136] I. Shaheen and M. U. Akram, “An integrated framework for clinical grading of cataract,” in *2017 1st International Conference on Next Generation Computing Applications (NextComp)*, IEEE, 2017, pp. 92–97 (cit. on pp. 48, 168).
- [137] R Core Team, *R: A Language and Environment for Statistical Computing*, R Foundation for Statistical Computing, Vienna, Austria, 2021. [Online]. Available: <https://www.R-project.org/> (cit. on pp. 49, 115).
- [138] A. Kuznetsova, P. B. Brockhoff, and R. H. B. Christensen, “lmerTest Package: Tests in Linear Mixed Effects Models,” *Journal of Statistical Software*, vol. 82, no. 13, pp. 1–26, 2017. doi: 10.18637/jss.v082.i13 (cit. on pp. 49, 115).
- [139] M. Kuhn, *caret: Classification and Regression Training*, R package version 6.0-90, 2021. [Online]. Available: <https://CRAN.R-project.org/package=caret> (cit. on pp. 49, 115).
- [140] D. Lüdecke, M. S. Ben-Shachar, I. Patil, P. Waggoner, and D. Makowski, “performance: An R Package for Assessment, Comparison and Testing of Statistical Models,” *Journal of Open Source Software*, vol. 6, no. 60, p. 3139, 2021. doi: 10.21105/joss.03139 (cit. on pp. 49, 115).
- [141] D. Lüdecke, I. Patil, M. S. Ben-Shachar, B. M. Wiernik, P. Waggoner, and D. Makowski, “see: an R package for visualizing statistical models,” *Journal of Open Source Software*, vol. 6, no. 64, p. 3393, 2021 (cit. on pp. 49, 115).
- [142] R. V. Lenth, *emmeans: Estimated Marginal Means, aka Least-Squares Means*, R package version 1.7.0, 2021. [Online]. Available: <https://CRAN.R-project.org/package=emmeans> (cit. on pp. 49, 115).
- [143] H. Wickham, *ggplot2: Elegant Graphics for Data Analysis*. Springer-Verlag New York, 2016, ISBN: 978-3-319-24277-4. [Online]. Available: <https://ggplot2.tidyverse.org> (cit. on pp. 49, 115).
- [144] B. E. Schefrin, S. J. Tregear, L. O. Harvey Jr, and J. S. Werner, “Senescent changes in scotopic contrast sensitivity,” *Vision research*, vol. 39, no. 22, pp. 3728–3736, 1999 (cit. on p. 50).
- [145] J. E. Birren and N. W. Shock, “Age changes in rate and level of visual dark adaptation,” *Journal of Applied Physiology*, vol. 2, no. 7, pp. 407–411, 1950 (cit. on p. 50).

## REFERENCES

- [146] G. R. Jackson and C. Owsley, “Scotopic sensitivity during adulthood,” *Vision research*, vol. 40, no. 18, pp. 2467–2473, 2000 (cit. on p. 50).
- [147] R. D. Gunkel and P. Gouras, “Changes in scotopic visibility thresholds with age,” *Archives of Ophthalmology*, vol. 69, no. 1, pp. 4–9, 1963 (cit. on p. 50).
- [148] G. R. Jackson, C. Owsley, E. P. Cordle, and C. D. Finley, “Aging and scotopic sensitivity,” *Vision research*, vol. 38, no. 22, pp. 3655–3662, 1998 (cit. on p. 50).
- [149] R. A. McFarland, R. G. Domey, A. B. Warren, and D. C. Ward, “Dark adaptation as a function of age: I. A statistical analysis.,” *Journal of Gerontology*, 1960 (cit. on p. 50).
- [150] B. Lundh, G. Lennerstrand, and G. Derefeldt, “Central and peripheral normal contrast sensitivity for static and dynamic sinusoidal gratings,” *Acta Ophthalmologica*, vol. 61, no. 2, pp. 171–182, 1983 (cit. on p. 50).
- [151] D. B. Elliott, “Contrast sensitivity decline with ageing: a neural or optical phenomenon?” *Ophthalmic and Physiological Optics*, vol. 7, no. 4, pp. 415–419, 1987 (cit. on p. 50).
- [152] A. M. Rohaly and C. Owsley, “Modeling the contrast-sensitivity functions of older adults,” *Journal of the Optical Society of America A*, vol. 10, no. 7, pp. 1591–1599, 1993 (cit. on pp. 50, 51, 57).
- [153] J. E. Ross, D. Clarke, and A. J. Bron, “Effect of age on contrast sensitivity function: uniocular and binocular findings,” *British Journal of Ophthalmology*, vol. 69, pp. 51–56, 1985. doi: 10.1136/bjo.69.1.51 (cit. on pp. 50, 164).
- [154] D. W. Kline, F. Schieber, L. C. Abusamra, and A. C. Coyne, “Age, the eye, and the visual channels: contrast sensitivity and response speed,” *Journal of Gerontology*, vol. 38, no. 2, pp. 211–216, 1983 (cit. on p. 50).
- [155] D. Elliott, D. Whitaker, and D. MacVeigh, “Neural contribution to spatiotemporal contrast sensitivity decline in healthy ageing eyes,” *Vision research*, vol. 30, no. 4, pp. 541–547, 1990 (cit. on p. 50).
- [156] B. Crassini, B. Brown, and K. Bowman, “Age-related changes in contrast sensitivity in central and peripheral retina,” *Perception*, vol. 17, no. 3, pp. 315–332, 1988 (cit. on p. 50).

## REFERENCES

- [157] C. Owsley, T. Gardner, R. Sekuler, and H. Lieberman, “Role of the crystalline lens in the spatial vision loss of the elderly.,” *Investigative ophthalmology & visual science*, vol. 26, no. 8, pp. 1165–1170, 1985 (cit. on p. 50).
- [158] J. S. Werner, P. B. Delahunt, and J. L. Hardy, “Chromatic-spatial vision of the aging eye,” *Optical Review*, vol. 11, no. 4, pp. 226–234, Jul. 2004, ISSN: 13406000. doi: 10.1007/s10043-004-0226-9 (cit. on p. 51).
- [159] G. V. Paramei and B. Oakley, “Variation of color discrimination across the life span,” *Journal of the Optical Society of America A*, vol. 31, no. 4, A375, 2014, ISSN: 1084-7529. doi: 10.1364/josaa.31.00a375 (cit. on p. 51).
- [160] M. B. Zlatkova, E. E. Coulter, and R. S. Anderson, “The effect of simulated lens yellowing and opacification on blue-on-yellow acuity and contrast sensitivity,” *Vision Research*, vol. 46, no. 15, pp. 2432–2442, Jul. 2006, ISSN: 00426989. doi: 10.1016/j.visres.2006.01.025 (cit. on p. 51).
- [161] A. Pinckers, “Color Vision and Age,” *Ophthalmologica*, vol. 181, no. 1, pp. 23–30, 1980, ISSN: 1423-0267. doi: 10.1159/000309021 (cit. on p. 51).
- [162] S. Daly, “Visible differences predictor: an algorithm for the assessment of image fidelity,” in *Digital Images and Human Vision*, 1992, A. B. Watson, Ed., vol. 1666, MIT Press, 1993, pp. 179–206, ISBN: 978-0262231718. doi: 10.1117/12.135952 (cit. on p. 51).
- [163] P. G. J. Barten, *Contrast sensitivity of the human eye and its effects on image quality*. SPIE Press, 1999, p. 208, ISBN: 0819434965 (cit. on p. 51).
- [164] A. B. Watson and A. J. Ahumada, “The pyramid of visibility,” *Human Vision and Electronic Imaging 2016, HVEI 2016*, pp. 37–42, 2016. doi: 10.2352/ISSN.2470-1173.2016.16HVEI-102 (cit. on p. 51).
- [165] R. K. Mantiuk, M. Kim, M. Ashraf, *et al.*, “Practical Color Contrast Sensitivity Functions for Luminance Levels up to 10000 cd/m<sup>2</sup>,” *Color and Imaging Conference*, vol. 2020, no. 28, pp. 1–6, Nov. 2020, ISSN: 2166-9635. doi: 10.2352/issn.2169-2629.2020.28.1 (cit. on pp. 51, 84).
- [166] R. K. Mantiuk, M. Ashraf, and A. Chapiro, “StelaCSF: A Unified Model of Contrast Sensitivity as the Function of Spatio-Temporal Frequency, Eccentricity, Luminance and Area,” *ACM Trans. Graph.*, vol. 41, no. 4, Jul. 2022, ISSN: 0730-0301. doi: 10.1145/3528223.3530115 (cit. on pp. 51, 52, 136, 139).

## REFERENCES

- [167] V. Virsu and J. Rovamo, “Visual resolution, contrast sensitivity, and the cortical magnification factor,” *Experimental brain research*, vol. 37, no. 3, pp. 475–494, 1979 (cit. on p. 52).
- [168] S. M. Wuerger, A. B. Watson, and A. J. Ahumada Jr, “Towards a spatio-chromatic standard observer for detection,” in *Human Vision and Electronic Imaging VII*, SPIE, vol. 4662, 2002, pp. 159–172 (cit. on p. 52).
- [169] A. B. Watson and A. J. Ahumada, “A standard model for foveal detection of spatial contrast,” *Journal of vision*, vol. 5, no. 9, pp. 6–6, 2005 (cit. on pp. 52, 82, 83).
- [170] H. De Lange Dzn, “Research into the dynamic nature of the human fovea→ cortex systems with intermittent and modulated light. I. Attenuation characteristics with white and colored light,” *Journal of Optical Society of America*, vol. 48, no. 11, pp. 777–784, 1958 (cit. on p. 52).
- [171] G. J. Van der Horst, “Chromatic flicker,” *Journal of Optical Society of America*, vol. 59, no. 9, pp. 1213–1217, 1969 (cit. on p. 52).
- [172] D. Varner, D. Jameson, and L. M. Hurvich, “Temporal sensitivities related to color theory,” *Journal of Optical Society of America A*, vol. 1, no. 5, pp. 474–481, 1984 (cit. on p. 52).
- [173] W. H. Swanson, T. Ueno, V. C. Smith, and J. Pokorny, “Temporal modulation sensitivity and pulse-detection thresholds for chromatic and luminance perturbations,” *Journal of Optical Society of America A*, vol. 4, no. 10, pp. 1992–2005, 1987 (cit. on p. 52).
- [174] M. R. B. Pérez, “Measuring the Temporal Contrast Sensitivity Function for Isoluminant Chromatic Flicker Stimuli,” M.S. thesis, Eindhoven University of Technology, 2017 (cit. on p. 52).
- [175] X. Kong, M. R. Bueno Pérez, I. M. Vogels, D. Sekulovski, and I. Heynderickx, “Modelling contrast sensitivity for chromatic temporal modulations,” in *Color and Imaging Conference*, Society for Imaging Science and Technology, vol. 2018, 2018, pp. 324–329 (cit. on p. 52).
- [176] S. Hecht and S. Shlaer, “Intermittent stimulation by light: V. The relation between intensity and critical frequency for different parts of the spectrum,” *The Journal of general physiology*, vol. 19, no. 6, pp. 965–977, 1936 (cit. on p. 52).
- [177] E. Hartmann, B. Lachenmayr, and H. Brettel, “The peripheral critical flicker frequency,” *Vision Research*, vol. 19, no. 9, pp. 1019–1023, 1979 (cit. on p. 52).

## REFERENCES

- [178] A. Raninen and J. Rovamo, “Perimetry of critical flicker frequency in human rod and cone vision,” *Vision research*, vol. 26, no. 8, pp. 1249–1255, 1986 (cit. on p. 52).
- [179] R. Mantiuk, K. J. Kim, A. G. Rempel, and W. Heidrich, “HDR-VDP-2: A calibrated visual metric for visibility and quality predictions in all luminance conditions,” *ACM Transactions on Graphics*, vol. 30, no. 4, 40:1–40:14, Jul. 2011, ISSN: 07300301. doi: 10.1145/2010324.1964935 (cit. on pp. 57, 69, 128).
- [180] K. J. Kim, R. Mantiuk, and K. H. Lee, “Measurements of achromatic and chromatic contrast sensitivity functions for an extended range of adaptation luminance,” in *Human Vision and Electronic Imaging XVIII*, B. E. Rogowitz, T. N. Pappas, and H. de Ridder, Eds., International Society for Optics and Photonics, vol. 8651, SPIE, 2013, pp. 319–332 (cit. on pp. 57, 68, 69).
- [181] S. Wuerger, A. B. Watson, and A. J. Ahumada Jr, “Towards a spatio-chromatic standard observer for detection,” in *Human Vision and Electronic Imaging VII*, SPIE, vol. 4662, 2002, pp. 159–172 (cit. on pp. 57, 67, 68).
- [182] A. J. Ahumada Jr and H. A. Peterson, “Luminance-model-based DCT quantization for color image compression,” in *Human vision, visual processing, and digital display III*, International Society for Optics and Photonics, vol. 1666, 1992, pp. 365–374 (cit. on p. 57).
- [183] J. Rovamo, O. Luntinen, and R. Näsänen, “Modelling the dependence of contrast sensitivity on grating area and spatial frequency,” *Vision Research*, vol. 33, no. 18, pp. 2773–2788, 1993, ISSN: 00426989 (cit. on p. 66).
- [184] J. Pokorny, V. C. Smith, and M. Lutze, “Aging of the human lens,” *Applied Optics*, vol. 26, no. 8, pp. 1437–1440, 1987, ISSN: 0003-6935. doi: 10.1364/ao.26.001437 (cit. on pp. 71, 74, 78, 79).
- [185] G. L. Savage, G. Haegerstrom-Portnoy, A. J. Adams, and S. Hewlett, “Age changes in the optical density of human ocular media,” *Clinical vision sciences*, vol. 8, pp. 97–97, 1993 (cit. on p. 71).
- [186] B. Winn, D. Whitaker, D. B. Elliott, and N. J. Phillips, “Factors affecting light-adapted pupil size in normal human subjects,” *Investigative ophthalmology & visual science*, vol. 35, no. 3, pp. 1132–1137, 1994 (cit. on p. 71).
- [187] H. Isono, “Evidence for the Existence of the Craik-O’Brien Effect in Humann Color Vision,” *Electronics and Communications in Japan*, vol. 63-A, no. 4, pp. 30–37, 1980 (cit. on p. 71).

## REFERENCES

- [188] D. H. Kelly, “Spatiotemporal Variation of Chromatic and Achromatic Contrast Thresholds,” *Journal of the Optical Society of America*, vol. 73, no. 6, pp. 742–750, 1983, ISSN: 00303941. doi: 10.1364/JOSA.73.000742 (cit. on p. 71).
- [189] J. Xu, J. Pokorny, and V. C. Smith, “Optical density of the human lens,” *JOSA A*, vol. 14, no. 5, pp. 953–960, 1997 (cit. on p. 74).
- [190] B. Crawford, “The scotopic visibility function,” *Proceedings of the Physical Society. Section B*, vol. 62, no. 5, p. 321, 1949 (cit. on pp. 74, 123).
- [191] R. A. Weale, “Retinal illumination and age,” *Transactions of the illuminating engineering Society*, vol. 26, no. 2, pp. 95–100, 1961 (cit. on p. 74).
- [192] F. S. Said and R. A. Weale, “The variation with age of the spectral transmissivity of the living human crystalline lens,” *Gerontology*, vol. 3, no. 4, pp. 213–231, 1959 (cit. on p. 74).
- [193] K. Nakamura, H. Bissen-Miyajima, S. Oki, and K. Onuma, “Pupil sizes in different Japanese age groups and the implications for intraocular lens choice,” *Journal of Cataract & Refractive Surgery*, vol. 35, no. 1, pp. 134–138, 2009 (cit. on p. 77).
- [194] K. K. De Valois, R. L. De Valois, and E. W. Yund, “Responses of striate cortex cells to grating and checkerboard patterns.,” *The Journal of Physiology*, vol. 291, no. 1, pp. 483–505, 1979 (cit. on p. 82).
- [195] J. Foley, S. Varadharajan, and C. Koh, “Detection of Gabor patterns of different sizes, shapes, phases and eccentricities,” *Vision research*, 2007 (cit. on p. 88).
- [196] D. M. Levi and R. S. Harwerth, “Psychophysical mechanisms in humans with amblyopia.,” *American journal of optometry and physiological optics*, vol. 59, no. 12, pp. 936–951, 1982 (cit. on p. 90).
- [197] J. Verbaken and A. Johnston, “Population norms for edge contrast sensitivity.,” *American Journal of Optometry and Physiological Optics*, vol. 63, no. 9, pp. 724–732, 1986 (cit. on p. 90).
- [198] N. Brady and D. J. Field, “What’s constant in contrast constancy? The effects of scaling on the perceived contrast of bandpass patterns,” *Vision research*, vol. 35, no. 6, pp. 739–756, 1995 (cit. on p. 94).
- [199] M. Mei, S. J. Leat, and J. Hovis, “Supra-threshold contrast matching and the effects of contrast threshold and age,” *Clinical and Experimental Optometry*, vol. 90, no. 4, pp. 272–281, 2007. doi: 10.1111/j.1444-0938.2007.00162.x (cit. on p. 106).

## REFERENCES

- [200] M. E. McCourt, L. M. Leone, and B. Blakeslee, “Brightness induction and suprathreshold vision: Effects of age and visual field,” *Vision Research*, vol. 106, pp. 36–46, Jan. 2015. doi: 10.1016/j.visres.2014.10.028 (cit. on p. 106).
- [201] A. Biondini and M. De Mattiello, “Suprathreshold contrast perception at different luminance levels,” *Vision research*, vol. 25, no. 1, pp. 1–9, 1985 (cit. on p. 114).
- [202] S. S. Stevens, “Neural Events and the Psychophysical Law: Power functions like those that govern subjective magnitude show themselves in neurelectric effects.,” *Science*, vol. 170, no. 3962, pp. 1043–1050, 1970 (cit. on p. 116).
- [203] E. Switkes and M. A. Cognale, “Comparison of color and luminance contrast: apples versus oranges?” *Vision research*, vol. 39, no. 10, pp. 1823–1831, 1999 (cit. on p. 119).
- [204] M. Schultze, “Zur anatomie und physiologie der retina,” *Archiv für mikroskopische Anatomie*, vol. 2, no. 1, pp. 175–286, 1866 (cit. on p. 122).
- [205] J. V. Kries, “Zur Theorie des Tages-und Dämmerungssehens,” in *Handbuch der normalen und pathologischen Physiologie*, Springer, 1929, pp. 679–713 (cit. on p. 122).
- [206] J. E. Purkyne, *Beobachtungen und versuche zur physiologie der sinne*. Reimer, 1825, vol. 2 (cit. on p. 122).
- [207] N. I. Benimoff, S. Schneider, and D. C. Hood, “Interactions between rod and cone channels above threshold: A test of various models,” *Vision Research*, vol. 22, no. 9, pp. 1133–1140, 1982 (cit. on p. 123).
- [208] H. Sun, J. Pokorny, and V. C. Smith, “Brightness induction from rods,” *Journal of Vision*, vol. 1, no. 1, pp. 4–4, 2001 (cit. on p. 123).
- [209] W. Nagel, “Appendix: adaptation, twilight vision and the duality theory,” *Helmholtz’s Treatise on Physiological Optics Translated from the Third German Edition by JPC Southall*, pp. 313–343, 1924 (cit. on p. 123).
- [210] R. W. G. Hunt, “Light and dark adaptation and the perception of color,” *JOSA*, vol. 42, no. 3, pp. 190–199, 1952 (cit. on p. 123).
- [211] V. C. Smith and J. Pokorny, “Spectral sensitivity of the foveal cone photopigments between 400 and 500 nm,” *Vision research*, vol. 15, no. 2, pp. 161–171, 1975 (cit. on pp. 123, 125).

## REFERENCES

- [212] G. Wyszecki and W. S. Stiles, *Color science*. Wiley New York, 1982, vol. 8 (cit. on pp. 123, 125).
- [213] D. Cao, J. Pokorny, V. C. Smith, and A. J. Zele, “Rod contributions to color perception: linear with rod contrast,” *Vision research*, vol. 48, no. 26, pp. 2586–2592, 2008 (cit. on pp. 123, 125, 126, 135, 138).
- [214] J. J. McCann and J. L. Benton, “Interaction of the long-wave cones and the rods to produce color sensations,” *JOSA*, vol. 59, no. 1, pp. 103–107, 1969 (cit. on p. 123).
- [215] W. S. Stiles and J. M. Burch, “NPL colour-matching investigation: final report (1958),” *Optica Acta: International Journal of Optics*, vol. 6, no. 1, pp. 1–26, 1959 (cit. on p. 123).
- [216] CIE, *CIE 170-1/2 Fundamental chromaticity diagram with physiological axes. Parts 1 and 2*. Commission Internationale de L’Éclairage, 2006 (cit. on p. 123).
- [217] CIE, *CIE 15.2 Colorimetry*. Vienna, Austria: Commission Internationale de L’Éclairage, 1986 (cit. on p. 123).
- [218] CIE, *CIE 116 Industrial colour-difference evaluation*. Vienna, Austria: Commission Internationale de L’Éclairage, 1995 (cit. on p. 123).
- [219] M. R. Luo, G. Cui, and B. Rigg, “The development of the CIE 2000 colour-difference formula: CIEDE2000,” *Color Research & Application*, vol. 26, no. 5, pp. 340–350, Oct. 2001, issn: 0361-2317. doi: 10.1002/col.1049 (cit. on p. 123).
- [220] N. Moroney, M. D. Fairchild, R. W. Hunt, C. Li, M. R. Luo, and T. Newman, “The CIECAM02 color appearance model,” in *Color and Imaging Conference*, Society for Imaging Science and Technology, 2002, pp. 23–27 (cit. on p. 123).
- [221] J. Kuang, G. M. Johnson, and M. D. Fairchild, “iCAM06: A refined image appearance model for HDR image rendering,” *Journal of Visual Communication and Image Representation*, vol. 18, no. 5, pp. 406–414, 2007 (cit. on p. 123).
- [222] S. N. Pattanaik, J. A. Ferwerda, M. D. Fairchild, and D. P. Greenberg, “A multiscale model of adaptation and spatial vision for realistic image display,” in *Proceedings of the 25th annual conference on Computer graphics and interactive techniques*, 1998, pp. 287–298 (cit. on p. 123).
- [223] W. B. Thompson, P. Shirley, and J. A. Ferwerda, “A spatial post-processing algorithm for images of night scenes,” *Journal of Graphics Tools*, vol. 7, no. 1, pp. 1–12, 2002 (cit. on p. 123).

## REFERENCES

- [224] R. Mantiuk, S. Daly, and L. Kerofsky, “Display adaptive tone mapping,” in *ACM SIGGRAPH 2008 papers*, ser. SIGGRAPH ’08, Los Angeles, California: Association for Computing Machinery, 2008, pp. 1–10, ISBN: 9781450301121. doi: 10.1145/1399504.1360667 (cit. on p. 123).
- [225] A. Kirk and J. F. O’Brien, “Perceptually based tone mapping for low-light conditions,” Ph.D. dissertation, University of California, Berkeley, 2011 (cit. on pp. 123, 126).
- [226] H. Sun, J. Pokorny, and V. C. Smith, “Rod-cone interactions assessed in inferred magnocellular and parvocellular postreceptoral pathways,” *Journal of Vision*, vol. 1, no. 1, pp. 5–5, 2001 (cit. on p. 124).
- [227] S. Kawamura and S. Tachibanaki, “Rod and cone photoreceptors: molecular basis of the difference in their physiology,” *Comparative Biochemistry and Physiology Part A: Molecular & Integrative Physiology*, vol. 150, no. 4, pp. 369–377, 2008 (cit. on p. 124).
- [228] V. C. Smith and J. Pokorny, “The design and use of a cone chromaticity space: a tutorial,” *Color Research & Application*, vol. 21, no. 5, pp. 375–383, 1996 (cit. on p. 125).
- [229] E. Miyahara, V. C. Smith, and J. Pokorny, “How surrounds affect chromaticity discrimination,” *JOSA A*, vol. 10, no. 4, pp. 545–553, 1993 (cit. on p. 126).
- [230] J. Pokorny and V. C. Smith, “Chromatic discrimination,” in *The visual neurosciences*, L. M. Chalupa and J. S. Werner, Eds., vol. 1, MIT press, 2004, ch. 58 (cit. on p. 126).
- [231] C. Alder, K. Chaing, T. Chong, E. Coates, A. Khalili, and B. Rigg, “Uniform chromaticity scales – new experimental data,” *Journal of the Society of Dyers and Colourists*, vol. 98, no. 1, pp. 14–20, 1982 (cit. on p. 126).
- [232] W. Schultze, “The Usefulness of Colour-Differences Formulae for Fixing Colour Tolerances in Color Metrics Proceedings of the Helmholtz Memorial Symposium,” *Vos, JJ, Friele, LF and Walraven, PL (Association Internationale de la Couleur (AIC): Soesterberg, Holland. p. 254*, 1971 (cit. on p. 126).
- [233] S. S. Guan and M. R. Luo, “Investigation of parametric effects using small colour differences,” *Color Research & Application*, vol. 24, no. 5, pp. 331–343, 1999 (cit. on p. 126).
- [234] D. Alman, “Performance comparison of full and reduced color-difference models,” *unpublished CIE TC*, pp. 1–47, 2000 (cit. on p. 127).

## REFERENCES

- [235] P. A. Garcia, R. Huertas, M. Melgosa, and G. Cui, “Measurement of the relationship between perceived and computed color differences,” *JOSA A*, vol. 24, no. 7, pp. 1823–1829, 2007 (cit. on p. 127).
- [236] M. R. Luo and B. Rigg, “Chromaticity-discrimination ellipses for surface colours,” *Color Research & Application*, vol. 11, no. 1, pp. 25–42, 1986, issn: 03612317. doi: 10.1002/col.5080110107. [Online]. Available: <https://onlinelibrary.wiley.com/doi/10.1002/col.5080110107> (cit. on p. 128).
- [237] Q. Xu, M. R. Luo, and D. Sekulovski, “Investigation of Spatial Chromatic Contrast around 5 Colour Centres,” in *London Imaging Meeting*, Society for Imaging Science and Technology, 2020, pp. 1–4 (cit. on p. 128).
- [238] R. K. Mantiuk, M. Kim, M. Ashraf, *et al.*, “Practical color contrast sensitivity functions for luminance levels up to 10000 cd/m<sup>2</sup>,” in *Color and Imaging Conference*, Society for Imaging Science and Technology, vol. 2020, 2020, pp. 1–6. doi: 10.2352/issn.2169-2629.2020.28.1 (cit. on p. 136).
- [239] M. Kim, M. Ashraf, M. Pérez-ortiz, J. Martinovic, S. Wuerger, and R. K. Mantiuk, “Contrast Sensitivity Functions for HDR Displays,” in *London Imaging Meeting*, 2020. doi: 10.2352/issn.2694-118X.2020.LIM-28 (cit. on p. 136).
- [240] A. Bozorgian, M. Ashraf, and R. Mantiuk, “Spatiotemporal contrast sensitivity functions: Predictions for the critical flicker frequency,” *Electronic Imaging*, vol. 36, pp. 1–8, 2024 (cit. on pp. 136, 139).
- [241] R. K. Mantiuk, P. Hanji, M. Ashraf, Y. Asano, and A. Chapiro, “ColorVideoVDP: A visual difference predictor for image, video and display distortions,” *arXiv preprint arXiv:2401.11485*, 2024 (cit. on p. 136).
- [242] J. V. Mehta, *Impact of vision on falls and fear of falling in older adults*. The University of Liverpool (United Kingdom), 2020 (cit. on p. 138).
- [243] A. E. Allen, F. P. Martial, and R. J. Lucas, “Form vision from melanopsin in humans,” *Nature communications*, vol. 10, no. 1, p. 2274, 2019 (cit. on p. 139).
- [244] R. Sekuler and L. P. Hutman, “Spatial vision and aging. I: Contrast sensitivity,” *Journals of Gerontology*, vol. 35, no. 5, pp. 692–699, 1980. doi: 10.1093/geronj/35.5.692 (cit. on p. 164).
- [245] K. B. Burton, C. Owsley, and M. E. Sloane, “Aging and neural spatial contrast sensitivity: photopic vision,” *Vision Research*, vol. 33, no. 7, pp. 939–946, 1993 (cit. on p. 164).

## REFERENCES

- [246] A. Werner, G. Schwarz, and W. Paulus, “Ageing and chromatic contrast sensitivity,” in *Colour Vision Deficiencies*, B. Drum, Ed., Kluwer Academic Press, 1995, ch. 28, pp. 235–241 (cit. on p. 164).
- [247] M. L. Hennelly, J. L. Barbur, D. F. Edgar, and E. G. Woodward, “The effect of age on the light scattering characteristics of the eye,” *Ophthalmic and Physiological Optics*, vol. 18, no. 2, pp. 197–203, 1998, issn: 0275-5408. doi: 10.1046/j.1475-1313.1998.00333.x (cit. on p. 165).
- [248] H. Gillespie-Gallery, E. Konstantakopoulou, J. A. Harlow, and J. L. Barbur, “Capturing age-related changes in functional contrast sensitivity with decreasing light levels in monocular and binocular vision,” *Investigative Ophthalmology and Visual Science*, vol. 54, no. 9, pp. 6093–6103, Sep. 2013. doi: 10.1167/iovs.13-12119 (cit. on p. 165).
- [249] J. A. Martínez-Roda, M. Vilaseca, J. C. Ondategui, M. Aguirre, and J. Pujol, “Effects of aging on optical quality and visual function,” *Clinical and Experimental Optometry*, vol. 99, no. 6, pp. 518–525, Nov. 2016. doi: 10.1111/cxo.12369 (cit. on p. 165).
- [250] F. F. Yan, F. Hou, Z. L. Lu, X. Hu, and C. B. Huang, “Efficient Characterization and Classification of Contrast Sensitivity Functions in Aging,” *Scientific Reports*, vol. 7, no. 5045, p. 230 022, 2017, issn: 20452322. doi: 10.1038/s41598-017-05294-0 (cit. on p. 165).

## A p p e n d i x A

### TABLE OF AGEING CSF STUDIES

Table A.1: Summary of ageing CSF datasets from literature

Datasets	Demographic	Spatial frequencies	Chromatic directions	Luminance levels	Temporal frequencies	Stimuli nature and size
Arundale [128]	Single group (n=36, 8-67 years); 31 healthy observers with normal vision, 4 with diabetic retinopathy and 1 with early lens opacities and macular degeneration	0.25 - 28 cpd	Achromatic	100 cd/m <sup>2</sup>	50 Hz	Monocular. Sine-wave gratings shown at two distances: 18° × 15° and 6° × 5°
Derefeldt <i>et al.</i> [129]	33 observers; Younger group (6-10 years), middle-aged group (20-40 years), older group (60-70 years)	0.5-40 cpd	Achromatic	120 cd/m <sup>2</sup>	Static (refresh rate not reported)	Monocular and binocular. 4.5° × 5° sine grating
Sekuler and Hutman [244]	Younger group (n=25, mean age=18.5 years), older group (n=10, mean age=73.2 years)	0.5, 1, 2, 4, 8, 16 and 32 cpd	Achromatic	55 cd/m <sup>2</sup>	0.33, 6 Hz	Monocular. Sine wave grating subtending 4.5° × 5.5°
McGrath and Morrison [130]	Single group (n=66, 5-94 years)	2-6 cpd	Achromatic	2 cd/m <sup>2</sup>	Static (refresh rate not reported)	Binocular. Sine-wave gratings shown at two distances: 1.7° and 5.1° diameter
Owsley <i>et al.</i> [32]	91 observers, 19-87 years	0.5, 1, 2, 4, 8, and 16 cpd	Achromatic	103 cd/m <sup>2</sup> °/sec	1.1 and 4.3	Monocular. 4.2° × 5.5° sine grating
Ross <i>et al.</i> [153]	Younger group (n = 17, 20-30 years), older group (n = 53, 50-87 years)	0.4, 0.95, 2.88, 6.73, 12.7, 19.23 cpd	Achromatic	300 cd/m <sup>2</sup>	100 Hz	Monocular and Binocular. 3° × 2° sine grating
Sloane <i>et al.</i> [67]	Younger group (n=12, 19-35 years), older group (n=11, 68-79 years)	0.5, 2, 4, and 8 cpd	Achromatic	0.034, 0.107, 0.338, 1.07, 3.38, 10.7, 33.8, and 107 cd/m <sup>2</sup>	0.5, 7.5 Hz	Monocular. Circular 6° on a 51° × 51° screen
Burton <i>et al.</i> [245]	Younger group (n = 35, 17-29 years, mean age=21), older group (n = 29, 60-80 years, mean age=68)	2, 4, 8, 12, 16, 20, 24, 28, and 32 cpd	Achromatic	7.42 cd/m <sup>2</sup>	Static (refresh rate not reported)	Monocular. Circular 5° interference fringe
Werner <i>et al.</i> [246]	40 observers, 18-67 years (mean age=37.1)	0.3-8.1 cpd	Red-green	26.5 cd/m <sup>2</sup>	1 Hz	Binocular. 9.5° × 9.5° sine gratings

## APPENDIX A. TABLE OF AGEING CSF STUDIES

Hennelly <i>et al.</i> [247]	28 observers, 16-60 years	1.5, 3, 5, 7, 10, 16, and 22 cpd	Achromatic	50 cd/m <sup>2</sup>	8.6 Hz	Binocular. Sine gratings (size not reported)
Hardy <i>et al.</i> [131]	Younger group (n=10, 18-30 years), older group (n=10, 65-77 years)	0.5, 1, 2, and 4 cpd	Red-green (L-M), and lime-violet (S)	15 cd/m <sup>2</sup>	3	Monocular. Annulus ring 15° outer and 7° inner diameter
Gillespie- Gallery <i>et al.</i> [248]	Single group (n = 95, 20-85 years)	7.5, 5 cpd	Achromatic	0.12, 1.6, 3.2, 7.6, and 34 cd/m <sup>2</sup>	120 Hz	Monocular and binocular. Landolt ring; size adjusted for different retinal eccentricities
Martínez- Roda <i>et al.</i> [249]	198 observers, 31-70 years	3, 6, 12, and 18 cpd	Achromatic	Not reported	Static	Binocular. Vector vision chart; viewing distance not reported
Yan <i>et al.</i> [250]	Younger group (n=10, mean age=22.6 years), older group (n=17, mean age=68.4 years)	0.69, 1.2, 2.42, 4.54, 8.52, and 16 cpd	Achromatic	30 cd/m <sup>2</sup>	85 Hz	Binocular. 3° × 3° sine-wave blurred at edges

## DATA VARIABILITY

The variability in the data across different parameters was analysed by calculating the coefficients of variation of the mean ( $CV_{mean}$ ) as follows:

$$CV_{mean} = \frac{\sigma}{\bar{Y}\sqrt{n}}, \quad (\text{B.1})$$

where  $\sigma$  is the standard deviation,  $\bar{Y}$  is the mean, and the  $n$  is the number of data points.

Table B.1:  $CV_{mean}$  of log contrast sensitivity averaged across all spatial frequencies

<b>Luminance (cd/m<sup>2</sup>)</b>	<b>Younger</b>			<b>Older</b>		
	$\mathcal{L} + \mathcal{M}$	$\mathcal{L} - \mathcal{M}$	$\mathcal{S} - (\mathcal{L} + \mathcal{M})$	$\mathcal{L} + \mathcal{M}$	$\mathcal{L} - \mathcal{M}$	$\mathcal{S} - (\mathcal{L} + \mathcal{M})$
0.02	0.0238	0.0231	0.0523	0.0343	0.0169	0.0975
0.2	0.0275	0.0205	0.0295	0.0443	0.0164	0.0326
2	0.0085	0.0114	0.0176	0.018	0.0095	0.0325
20	0.0047	0.0046	0.0080	0.0077	0.0056	0.0125
200	0.0045	0.0037	0.0072	0.007	0.0061	0.0110
2000	0.0075	0.0066	0.0094	0.0088	0.0063	0.0097

Contrast sensitivity measurements at lower luminance levels show higher variations as shown in Table B.1 for both younger and older observer groups for all three chromatic directions. This finding is also consistent with the data from Barbur and Stockman [8] (Figure 3).

Table B.2:  $CV_{mean}$  of log contrast sensitivity averaged across all spatial frequencies and luminance levels

<b>Color directions</b>	<b>Younger</b>	<b>Older</b>	<b>All age groups</b>
$\mathcal{L} + \mathcal{M}$	0.0128	0.0053	0.0090
$\mathcal{L} - \mathcal{M}$	0.0117	0.0101	0.0109
$\mathcal{S} - (\mathcal{L} + \mathcal{M})$	0.0207	0.0326	0.0266

## APPENDIX B. DATA VARIABILITY

Table B.3:  $CV_{mean}$  of matched test contrast averaged across all luminance levels

Color directions	Spatial frequency	Younger			Older		
		Low	Medium	High	Low	Medium	High
$\mathcal{L} + \mathcal{M}$	0.5	0.0942	0.0792	0.0773	0.0916	0.0830	0.0777
	2	0.0822	0.0799	0.0855	0.0857	0.0764	0.0778
	4	0.1112	0.1081	0.0952	0.0951	0.0821	0.0861
$\mathcal{L} - \mathcal{M}$	0.5	0.0843	0.0785	0.0589	0.1013	0.0925	0.0748
	2	0.072	0.0794	0.0783	0.0861	0.0907	0.0710
	4	0.1208	0.0998	0.0827	0.0981	0.0851	0.0674
$\mathcal{S} - (\mathcal{L} + \mathcal{M})$	0.5	0.0771	0.0624	0.0575	0.0958	0.0687	0.0593
	2	0.1153	0.1038	0.0986	0.0865	0.0891	0.0766
	4	0.2307	0.1672	0.1555	0.154	0.1599	0.1111

Table B.4:  $CV_{mean}$  of matched test contrast averaged across all luminance levels and spatial frequencies

Color directions	Younger	Older	All age groups
$\mathcal{L} + \mathcal{M}$	0.0903	0.0839	0.0871
$\mathcal{L} - \mathcal{M}$	0.0838	0.0852	0.0845
$\mathcal{S} - (\mathcal{L} + \mathcal{M})$	0.1187	0.1001	0.1094

## Appendix C

### OPTOMETRY DATA FOR OLDER OBSERVERS

Slit lamp examination was used to characterise cataracts using an integrated framework for grading nuclear, cortical and posterior cataracts [136]. The different types of cataracts are shown in the figure below:

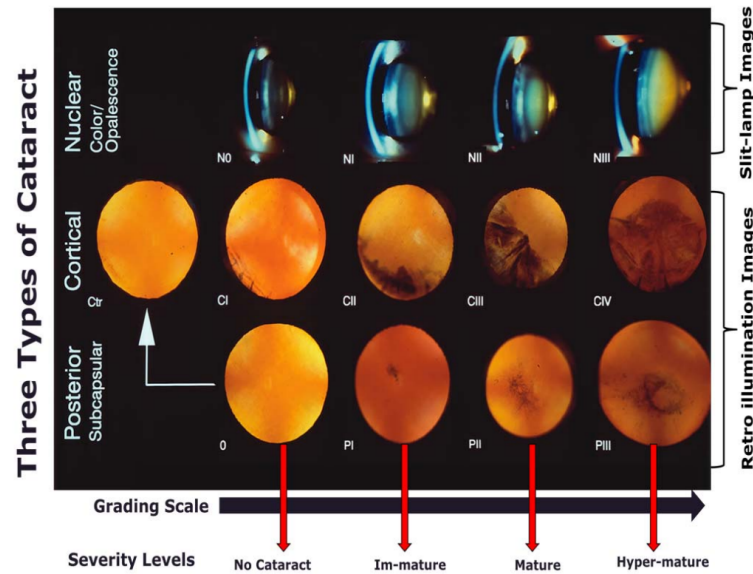


Figure C.1: Cataract grading system. The figure is from Shaheen and Akram [136].

Table C.1: Clinical cataract grading system Shaheen and Akram [136].

Type of cataract	None	Immature	Mature	Hyper-mature
Nuclear	0	1	2	3
Cortical	0/1	2	3	4
Posterior	0	1	2	3

## APPENDIX C. OPTOMETRY DATA FOR OLDER OBSERVERS

Table C.2: Cataract grading for the tested observers. The entries marked with 'NaN' indicate pseudophakia (artificial lens implant). The entries with coloured cells indicate cataracts slightly worse than normal ageing.

Observer ID	Type of cataract					
	Nuclear		Cortical		Posterior	
	Left	Right	Left	Right	Left	Right
1	1	1	0	1	2	0
2	2	2	0	0	0	0
3	2	1	1	2	0	0
4	1	1	0	0	0	0
5	NaN	NaN	NaN	NaN	NaN	NaN
6	NaN	NaN	NaN	NaN	NaN	NaN
7	2	2	0	0	0	0
8	1	1	0	0	0	0
9	1	NaN	0	NaN	0	NaN
10	0.5	0.5	0	0	0	0
11	0.5	0.5	0	0	0	0

Table C.3: Pupil sizes with dark and light adaptation

Observer ID	Pupil diameter (mm)			
	Light		Dark	
	Left	Right	Left	Right
1	3.0	-	4.5	3.7
2	5.3	5.3	6.1	6.7
3	4.3	4.4	5.6	6.1
4	4.3	4.5	6.6	6.8
5	3.0	3.1	7.4	7.5
6	4.5	4.4	6.2	6.9
7	4.2	3.8	4.8	5.2
8	3.0	3.1	5.8	5.6
9	4.2	3.9	5.4	6.4
10	3.1	3.8	6.8	6.5
11	3.4	2.7	5.6	5.4

## APPENDIX C. OPTOMETRY DATA FOR OLDER OBSERVERS

Table C.4: Visual acuity test

Observer ID	Stereo-acuity	Habitual distance vision (logMAR)		Pinhole vision (logMAR)		Near acuity (log-MAR)	visual (log-
		Left	Right	Left	Right		
1	600	0.26	0.44	0.16	0.02	0.50	0.63
2	110	0.12	0.12	0.00	0.12	1.25	1.25
3	110	0.10	0.06	0.06	0.06	0.63	0.63
4	40	0.20	0.20	0.06	0.10	0.50	0.80
5	85	0.20	0.20	0.10	-0.04	1.00	1.00
6	170	0.04	-0.04	0.04	-0.06	0.63	0.50
7	600	1.16	0.00	0.70	0.00	0.16	1.00
8	30	-0.18	-0.20	-0.18	-0.20	1.00	1.00
9	170	0.14	0.00	0.06	0.00	1.00	0.80
10	300	-0.14	-0.02	-0.14	-0.08	1.20	1.00
11	150	0.10	0.20	-0.10	-0.14	0.80	0.40

Table C.5: Contrast sensitivity measured with VectorVision (CSV-1000) chart with and without glare

Observer ID	3 cpd		12 cpd		18 cpd	
	Without glare	With glare	Without glare	With glare	Without glare	With glare
1	1.34	1.49	1.21	1.21	1.25	0.61
2	1.49	1.49	1.38	1.38	1.08	1.08
3	1.49	1.63	1.38	1.38	1.08	0.91
4	1.63	1.78	1.55	1.99	1.25	1.40
5	1.49	1.63	1.38	1.70	1.08	1.40
6	1.49	1.49	1.38	1.38	1.40	1.08
7	1.49	1.63	1.38	1.70	0.91	1.40
8	1.49	1.63	1.99	1.99	1.69	1.84
9	1.34	1.49	1.55	1.55	0.91	1.08
10	1.78	1.78	1.70	1.70	1.69	1.54
11	1.63	1.78	1.99	2.14	1.69	1.69

## Appendix D

### CSF STATISTICAL TESTS

Table D.1: Data transforms and pre-processing

Variable	Unit / Category	Type	Transform / Contrasts coding
Sensitivity	1/Log cone contrast	Continuous	Box car transformed to remove heteroscedasticity
Spatial frequency	Cycles per visual degree ( cpd)	Continuous	Base 2 log
Luminance	Candela per square meter ( cd/m <sup>2</sup> )	Continuous	Base 10 log
Age group	Younger / Older	Categorical	Simple coding (-0.5, 0.5). Intercept = overall mean
Subjects	Anonymous server ID	ob-	Categorical

#### D.1 Achromatic CSF

*Best Model: Sensitivity ~ Age group \* Frequency \* Luminance + (1 | Subjects)*

Table D.2: Estimated model fixed effects. p-values estimated via t-tests using the Satterthwaite approximations to degrees of freedom.

Effect	Estimate	Std. Error	df	t-value	Pr(> t )	
Intercept	1.815	0.036	66.3	50.9	<2.00E-16	***
Frequency	-0.388	0.018	955.8	-21.7	<2.00E-16	***
Luminance	0.289	0.013	963.6	23	<2.00E-16	***
Frequency : Luminance	0.074	0.009	955.3	8.1	0	***
Age group	-0.37	0.071	66.3	-5.2	0	***
Age group : Frequency	-0.094	0.036	955.8	-2.6	0.0087	**
Age group : Luminance	0.095	0.025	963.6	3.8	0.0002	***
Age group : Frequency : Luminance	-0.04	0.018	955.3	-2.2	0.0268	*

Signif. codes: ‘\*\*\*’ 0.001 ‘\*\*’ 0.01 ‘\*’ 0.05

## APPENDIX D. CSF STATISTICAL TESTS

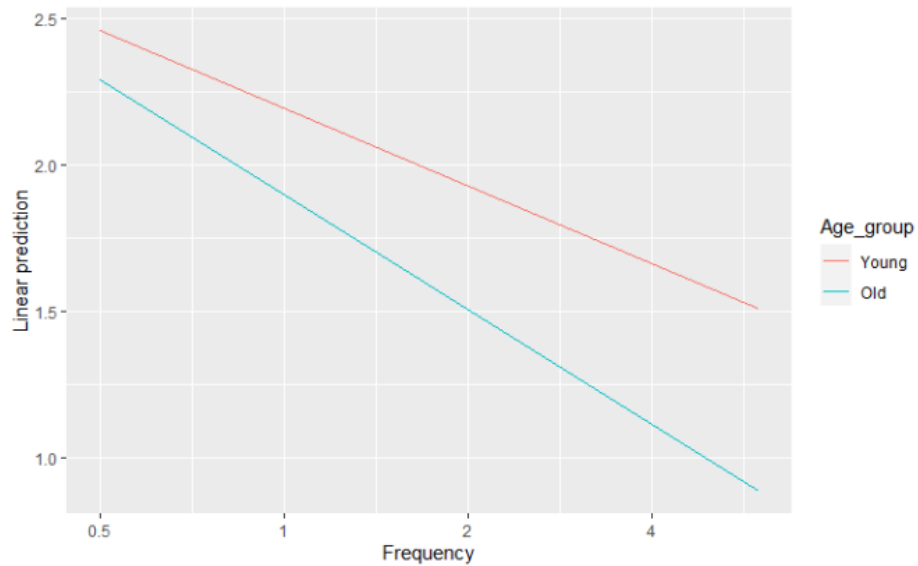


Figure D.1: Decline in contrast sensitivity with increasing spatial frequency. Note the steeper slope of decrement in the older group

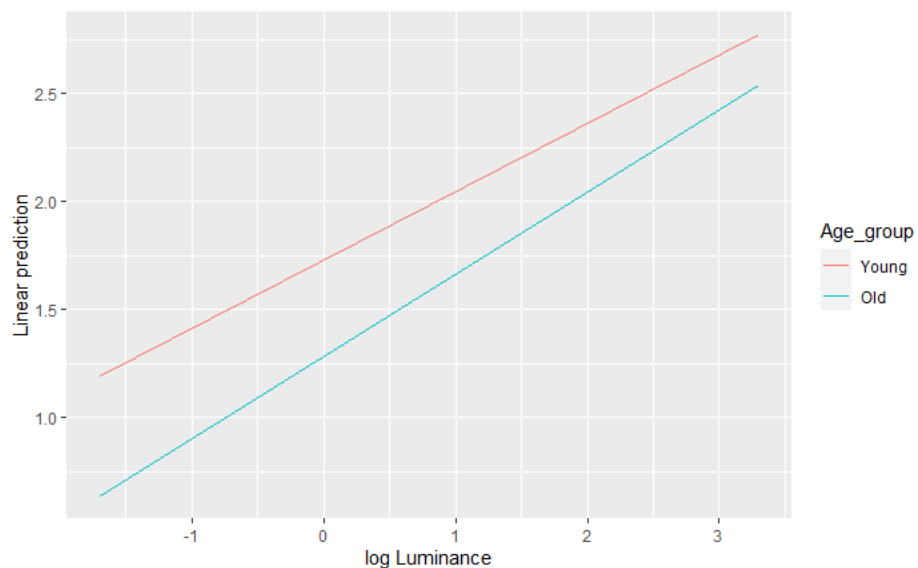


Figure D.2: Increase in contrast sensitivity with increasing luminance level. Note the steeper slope of increment in the older group. At lower luminance, the difference between the two groups is much larger than that at the higher luminance

## APPENDIX D. CSF STATISTICAL TESTS

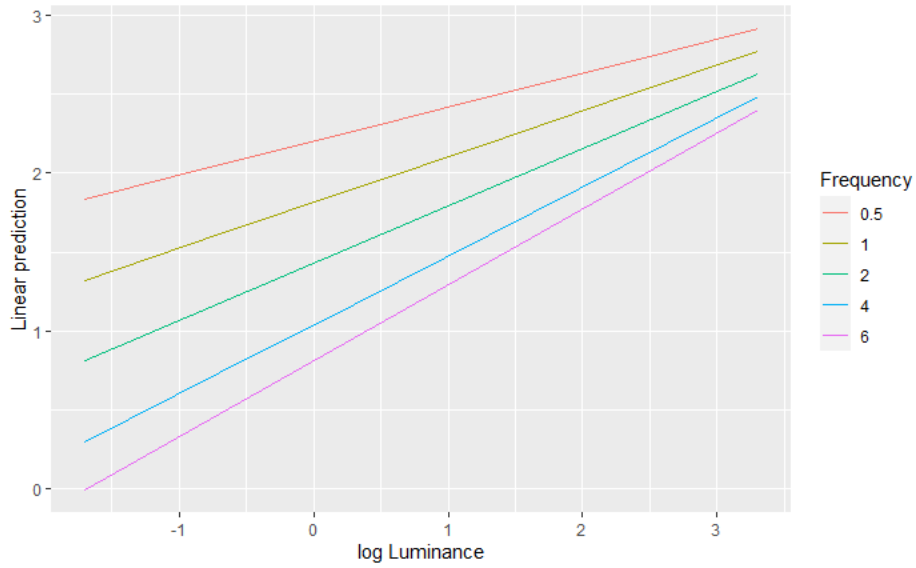


Figure D.3: Increase in contrast sensitivity with increasing luminance level for each frequency channel. The slope of increment increased with spatial frequency

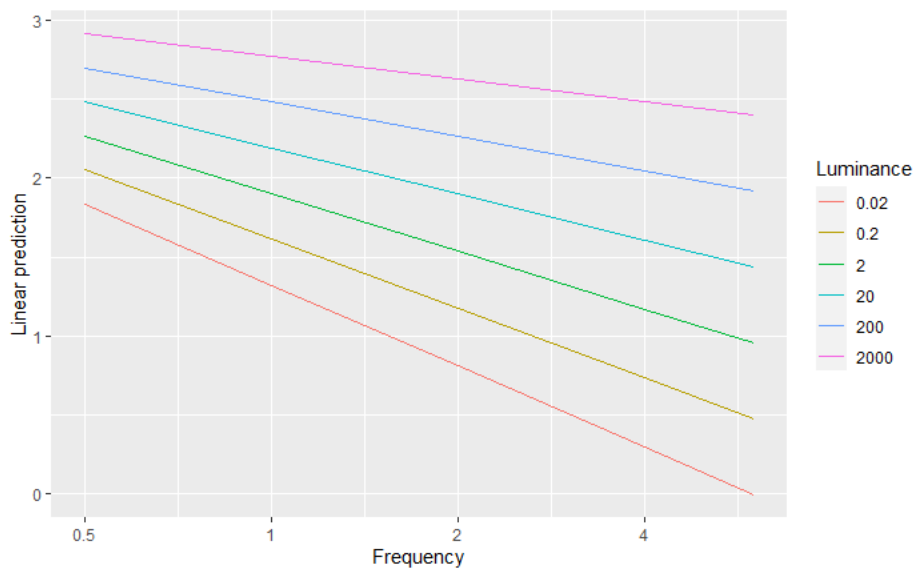


Figure D.4: Decrease in contrast sensitivity with increasing spatial frequency for each luminance level. The slope of increment decreased with increasing luminance level

## APPENDIX D. CSF STATISTICAL TESTS

### D.2 Red-green CSF

*Sensitivity* ~ *Age group* + *Frequency* + *Luminance* + (*I* + *Luminance* | *Subjects*) + *Age group* : *Frequency*

Table D.3: Estimated model fixed effects. p-values estimated via t-tests using the Satterthwaite approximations to degrees of freedom.

Effect	Estimate	Std. Error	df	t-value	Pr(> t )	
Intercept	1.777	0.023	43.2	78.8	<2.00E-16	***
Frequency	-0.413	0.007	901.9	-62.6	<2.00E-16	***
Luminance	0.358	0.007	36	51.5	<2.00E-16	***
Age group	-0.236	0.044	45.2	-5.3	0	***
Age group : Frequency	-0.077	0.013	915.8	-5.9	0	***

Signif. codes: '\*\*\*' 0.001 '\*\*' 0.01 '\*' 0.05

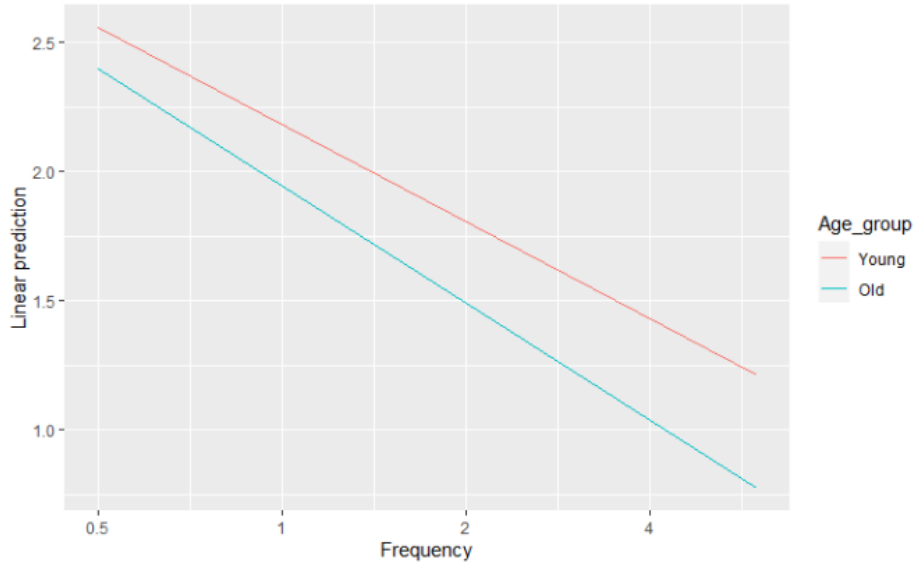


Figure D.5: Decline in contrast sensitivity with increasing spatial frequency. Note the steeper slope of decrement in the older group

## APPENDIX D. CSF STATISTICAL TESTS

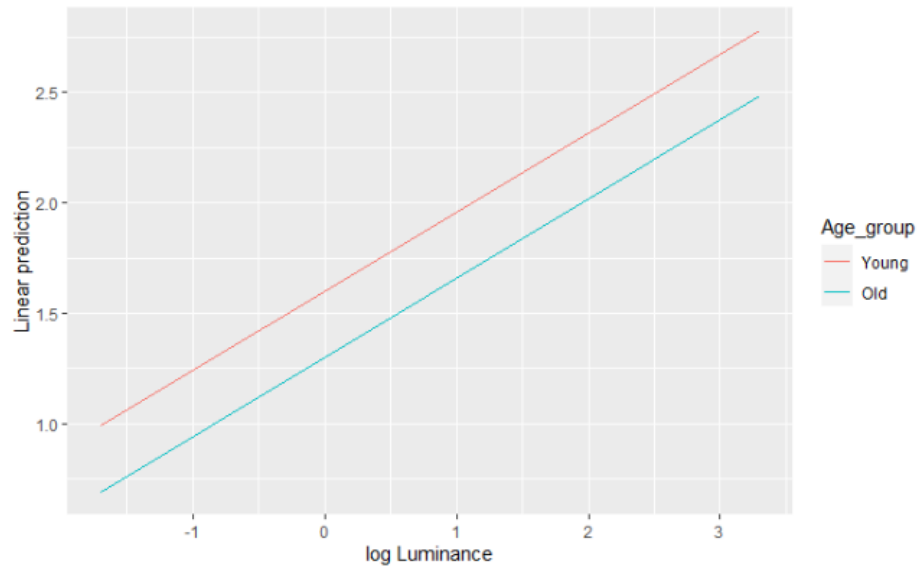


Figure D.6: Increase in contrast sensitivity with increasing luminance level. No effect of luminance between both age groups is observed

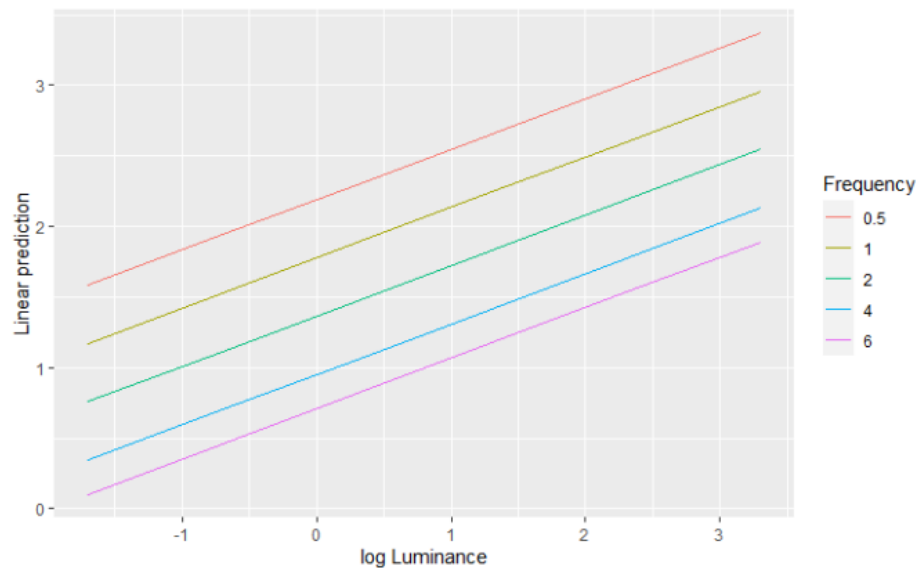


Figure D.7: Increase in contrast sensitivity with increasing luminance level for each frequency channel. The slope of increment remains constant for each frequency

## APPENDIX D. CSF STATISTICAL TESTS

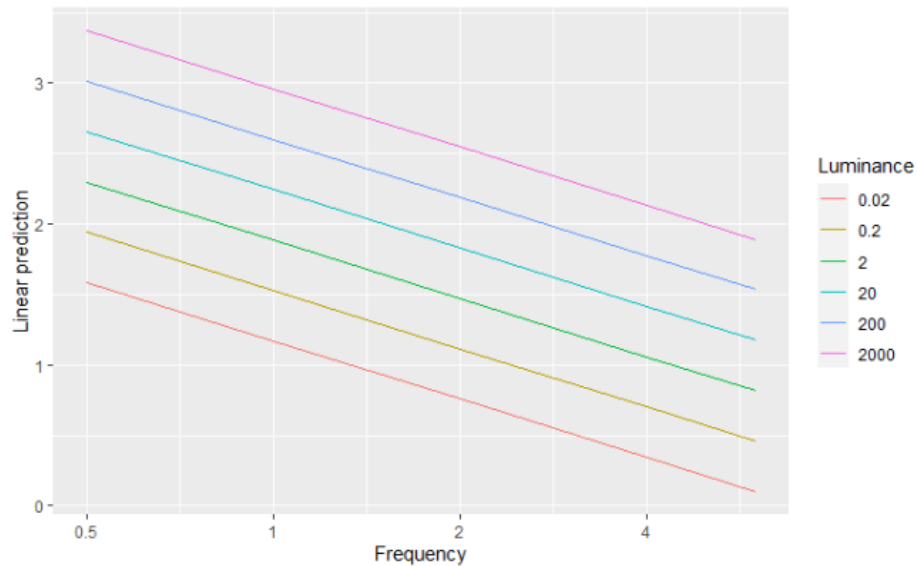


Figure D.8: Decrease in contrast sensitivity with increasing spatial frequency for each luminance level. The slope of increment remains constant for each luminance level

### D.3 Yellow-violet CSF

*Sensitivity ~ Age group \* Frequency \* Luminance + (I + Frequency + Luminance | Subjects)*

Table D.4: Estimated model fixed effects. p-values estimated via t-tests using the Satterthwaite approximations to degrees of freedom

Effect	Estimate	Std. Error	df	t-value	Pr(> t )
Intercept	0.627	0.011	33.1	59.2	<2.00E-16 ***
Frequency	-0.116	0.006	120.4	-18.7	<2.00E-16 ***
Luminance	0.187	0.005	47.5	41.4	<2.00E-16 ***
Frequency : Luminance	-0.024	0.003	769.2	-9	<2.00E-16 ***
Age group	-0.16	0.021	33.1	-7.6	0 ***
Age group : Frequency	0.025	0.012	120.4	2	0.0497 *
Age group : Luminance	0.019	0.009	47.5	2.1	0.0446 *
Age group : Frequency : Luminance	-0.021	0.005	769.2	-3.9	0.0001 ***

Signif. codes: ‘\*\*\*’ 0.001 ‘\*\*’ 0.01 ‘\*’ 0.05

## APPENDIX D. CSF STATISTICAL TESTS

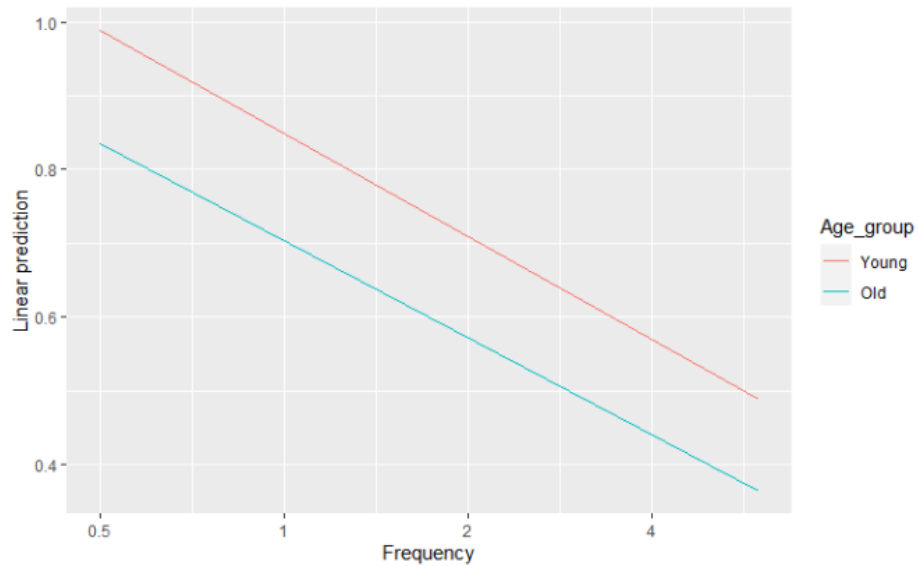


Figure D.9: Decline in contrast sensitivity with increasing spatial frequency. Note the steeper slope of decrement in the older group

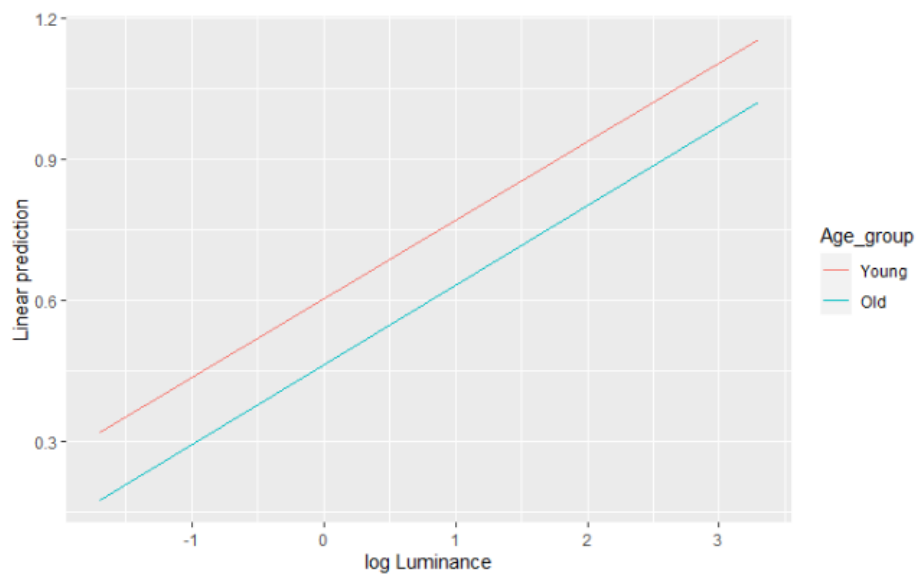


Figure D.10: Increase in contrast sensitivity with increasing luminance level. No effect of luminance between both age groups is observed

## APPENDIX D. CSF STATISTICAL TESTS

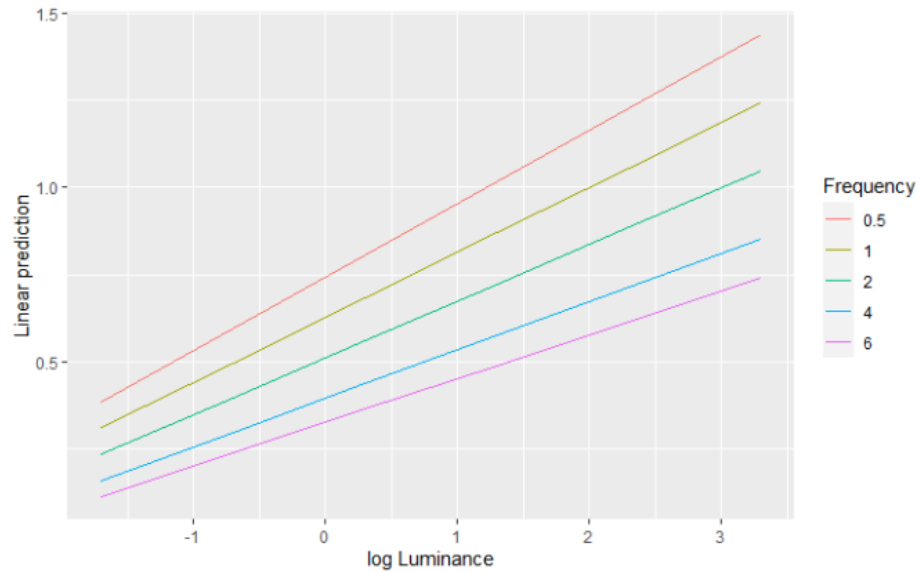


Figure D.11: Increase in contrast sensitivity with increasing luminance level for each frequency channel. The slope of increment decreased with spatial frequency

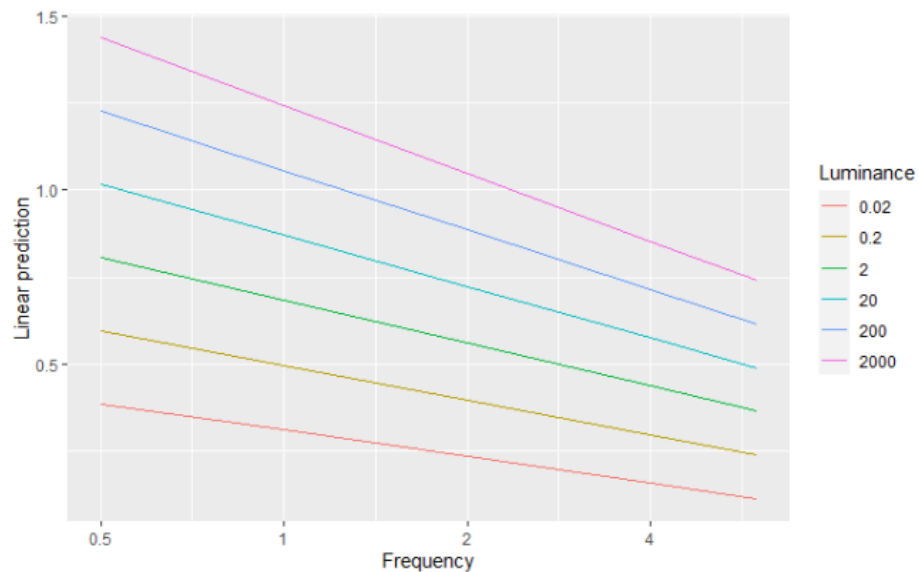


Figure D.12: Decrease in contrast sensitivity with increasing spatial frequency for each luminance level. The slope of increment increased with luminance level

## Appendix E

### CMF STATISTICAL TESTS

Table E.1: Data transforms and pre-processing

Variable	Unit / Category	Type	Transform / Contrasts coding
Test contrast	Cone contrast	Continuous	Box car transformed to remove heteroscedasticity
Contrast level	Low / Medium / High	Categorical	Low vs medium (-0.5, 0.5, 0). Medium vs high (0, -0.5, 0.5)
Spatial frequency	Cycles per visual degree ( cpd)	Continuous	Base 2 log
Luminance	Candela per square meter ( cd/m <sup>2</sup> )	Continuous	Base 10 log
Age group	Younger / Older	Categorical	Simple coding (-0.5, 0.5). Intercept = overall mean
Subjects	Anonymous observer ID	Categorical	

#### E.1 Achromatic contrast matching

*Best Model: Test contrast ~ Frequency + Luminance + Contrast level + (1 + Frequency + Luminance | Subjects) + Frequency : Luminance + Luminance : Contrast level*

## APPENDIX E. CMF STATISTICAL TESTS

Table E.2: Estimated model fixed effects. p-values estimated via t-tests using the Satterthwaite approximations to degrees of freedom

Effect	Estimate	Std. error	df	t-value	Pr(> t )	
Intercept	-1.133	0.043	30.4	-26.3	<2.00E-16	***
Frequency	0.1	0.017	46	5.9	0	***
Luminance	-0.08	0.018	32.2	-4.4	0.0001	***
Contrast level (low vs med)	0.52	0.034	1509	15.2	<2.00E-16	***
Contrast level (med vs high)	0.572	0.035	1509	16.2	<2.00E-16	***
Frequency : Luminance	-0.034	0.005	1529	-6.4	0	***
Luminance : Contrast level (low vs med)	0.153	0.018	1509	8.6	<2.00E-16	***
Luminance : Contrast level (med vs high)	0.154	0.018	1508	8.4	<2.00E-16	***

Signif. codes: ‘\*\*\*’ 0.001 ‘\*\*’ 0.01 ‘\*’ 0.05

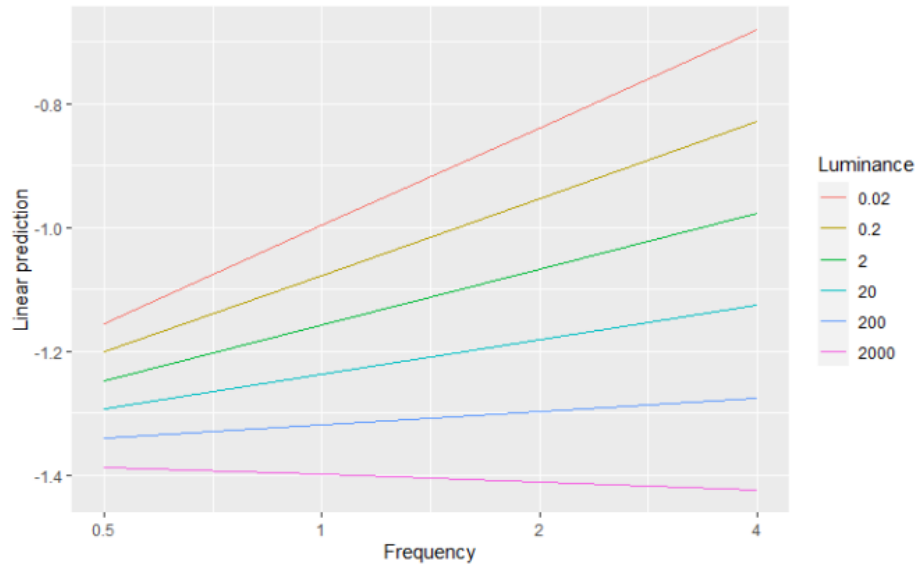


Figure E.1: Increase in predicted test contrast with increasing spatial frequency. The slopes are much smaller for high luminance levels and increase for lower luminances

## APPENDIX E. CMF STATISTICAL TESTS

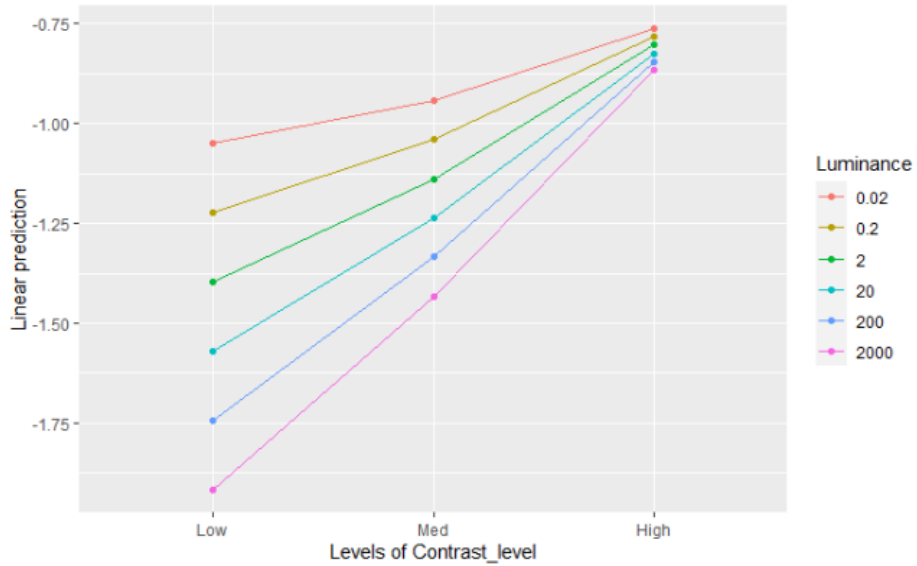


Figure E.2: Increase in test contrast with increasing suprathreshold contrast. Differences between test contrasts for different luminances are much higher for lower suprathreshold levels. The predicted test contrasts converge at higher suprathreshold levels

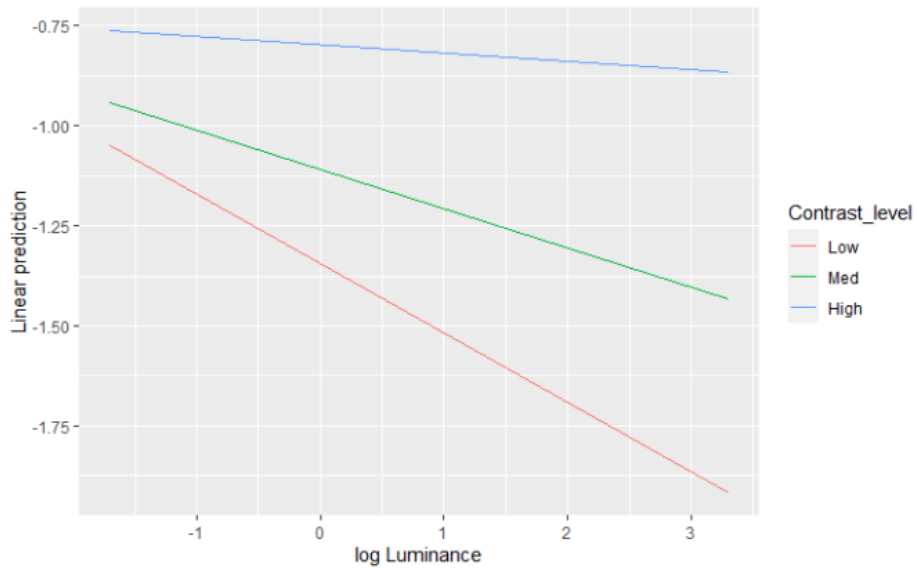


Figure E.3: Decrease in test contrast with increasing luminance level for each suprathreshold level. The negative slopes have larger magnitudes for low suprathreshold level

## APPENDIX E. CMF STATISTICAL TESTS

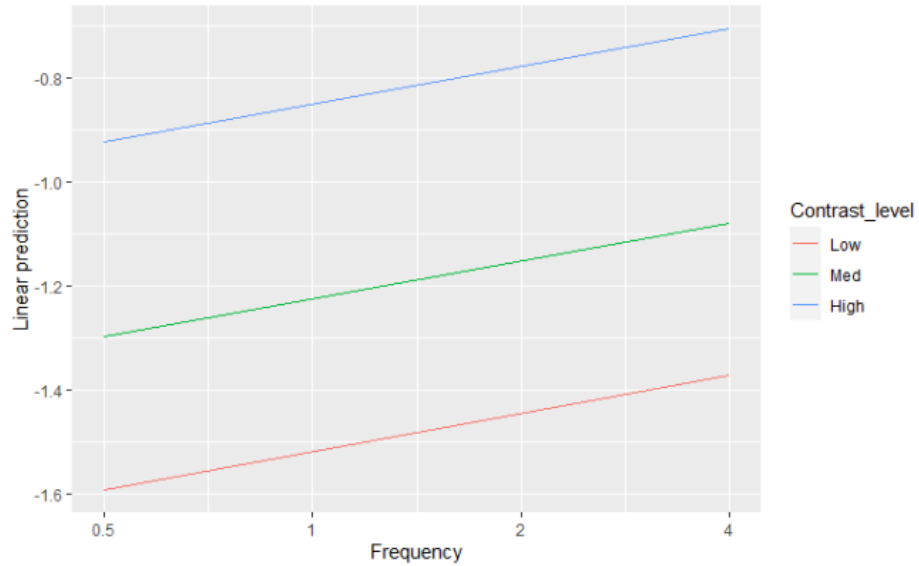


Figure E.4: Increase in contrast sensitivity with increasing spatial frequency for each suprathreshold level. The slope of increment remains constant regardless of suprathreshold level

### E.2 Red-green contrast matching

*Best Model: Test contrast ~ Frequency + Luminance + Contrast level + (1 + Frequency + Luminance | Subjects) + Frequency : Luminance + Frequency : Contrast level + Luminance : Contrast level*

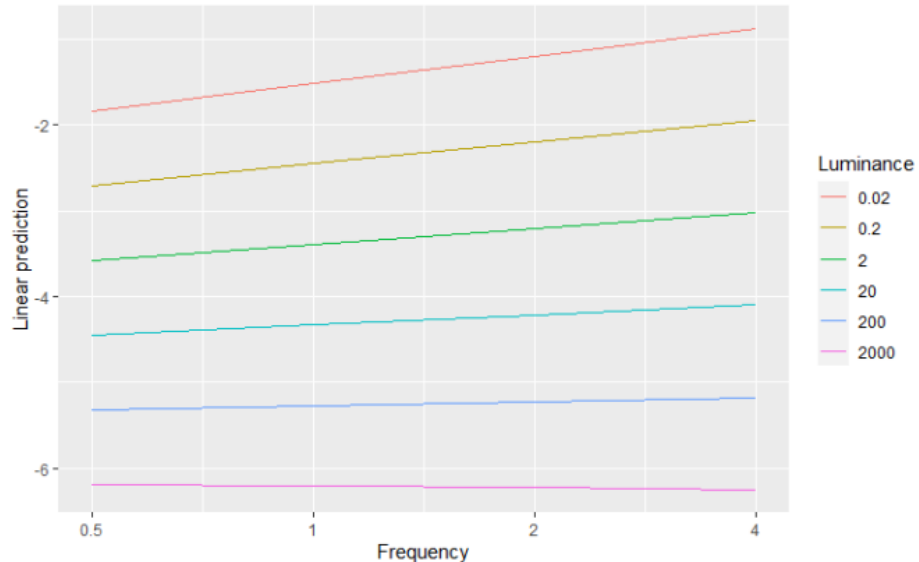


Figure E.5: Increase in predicted test contrast with increasing spatial frequency. The slopes are much smaller for high luminance levels and increase for lower luminances

## APPENDIX E. CMF STATISTICAL TESTS

Table E.3: Estimated model fixed effects. p-values estimated via t-tests using the Satterthwaite approximations to degrees of freedom

Effect	Estimate	Std. error	df	t-value	Pr(> t )	
Intercept	-3.107	0.096	30.7	-32.5	<2.00E-16	***
Frequency	0.203	0.038	41.8	5.4	0	***
Luminance	-0.939	0.04	32.9	-23.6	<2.00E-16	***
Contrast level (low vs med)	1.06	0.077	1515	13.9	<2.00E-16	***
Contrast level (med vs high)	1.065	0.079	1516	13.4	<2.00E-16	***
Frequency : Luminance	-0.068	0.012	1542	-5.8	0	***
Frequency : Contrast level (low vs med)	-0.162	0.049	1514	-3.3	0.0011	**
Frequency : Contrast level (med vs high)	-0.158	0.049	1513	-3.2	0.0015	**
Luminance : Contrast level (low vs med)	0.376	0.039	1514	9.7	<2.00E-16	***
Luminance : Contrast level (med vs high)	0.351	0.04	1514	8.8	<2.00E-16	***

Signif. codes: ‘\*\*\*’ 0.001 ‘\*\*’ 0.01 ‘\*’ 0.05

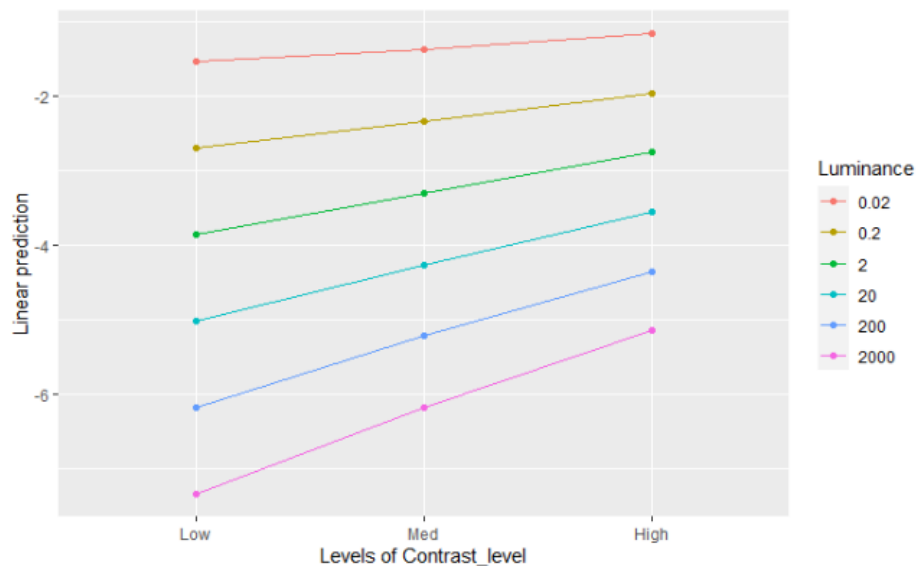


Figure E.6: Increase in test contrast with increasing suprathreshold contrast. Differences between test contrasts for different luminances are higher for lower suprathreshold levels

## APPENDIX E. CMF STATISTICAL TESTS

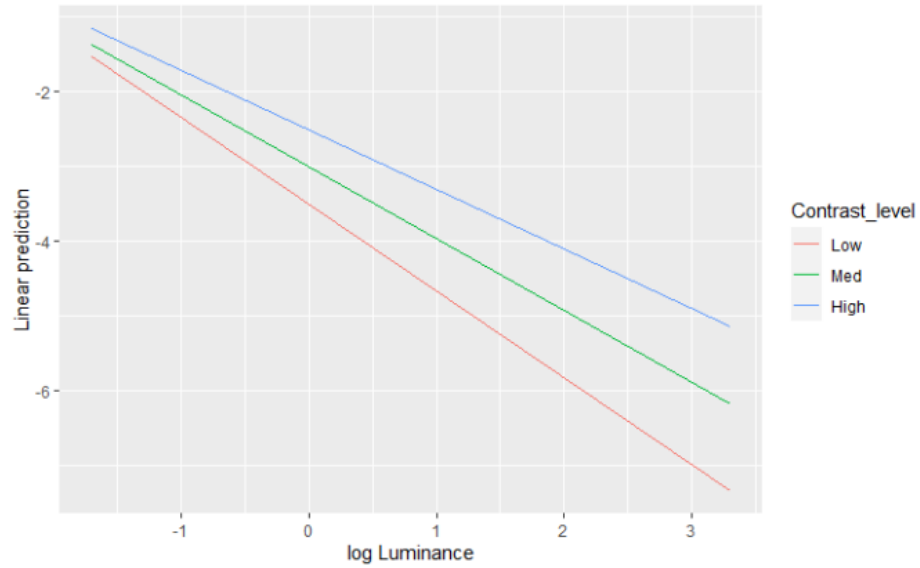


Figure E.7: Decrease in test contrast with increasing luminance level for each suprathreshold level. The negative slopes have a larger magnitude for low suprathreshold level

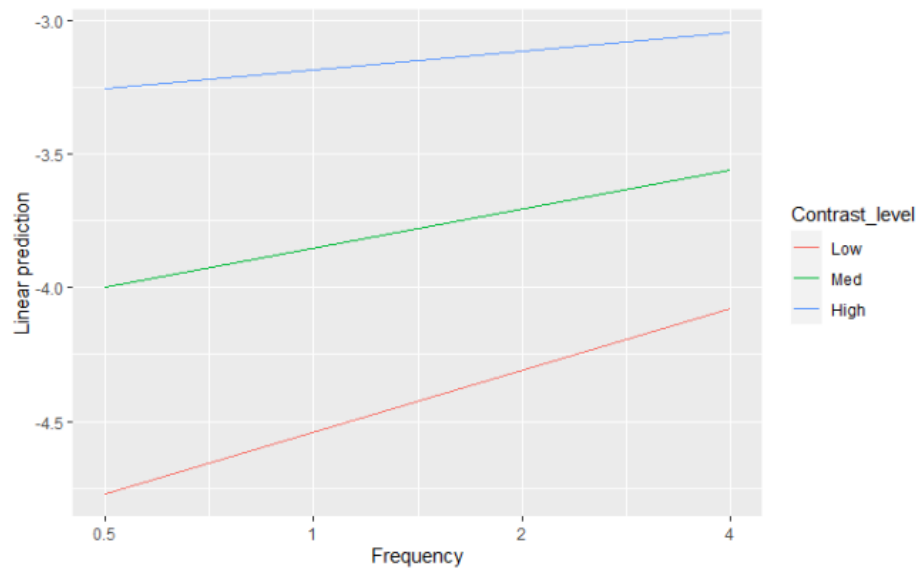


Figure E.8: Increase in contrast sensitivity with increasing spatial frequency for each suprathreshold level. The slopes of increment have larger magnitudes for low suprathreshold level

## APPENDIX E. CMF STATISTICAL TESTS

### E.3 Yellow-violet contrast matching

*Best Model: Test contrast ~ Age group + Frequency + Luminance + Contrast level + (1 + Frequency + Luminance | Subjects) + Age group : Frequency + Age group : Luminance + Frequency : Luminance + Luminance : Contrast level*

Table E.4: Estimated model fixed effects. p-values estimated via t-tests using the Satterthwaite approximations to degrees of freedom

Effect	Estimate	Std. Error	df	t-value	Pr(> t )	
Intercept	-0.6	0.047	30.4	-12.7	0	***
Frequency	-0.101	0.019	44.4	-5.3	0	***
Luminance	-0.231	0.016	33.6	-14.7	0	***
Contrast level (low vs med)	0.406	0.033	1196	12.4	<2.00E-16	***
Contrast level (med vs high)	0.449	0.037	1198	12.2	<2.00E-16	***
Frequency : Luminance	-0.013	0.005	1220	-2.6	0.0088	**
Luminance : Contrast level (low vs med)	0.069	0.016	1194	4.4	0	***
Luminance : Contrast level (med vs high)	0.061	0.017	1196	3.5	0.0004	***
Age group	0.253	0.094	29.9	2.7	0.0116	*
Age group : Frequency	0.083	0.034	29.3	2.4	0.0228	*
Age group : Luminance	-0.067	0.031	31.9	-2.2	0.0385	*

Signif. codes: ‘\*\*\*’ 0.001 ‘\*\*’ 0.01 ‘\*’ 0.05

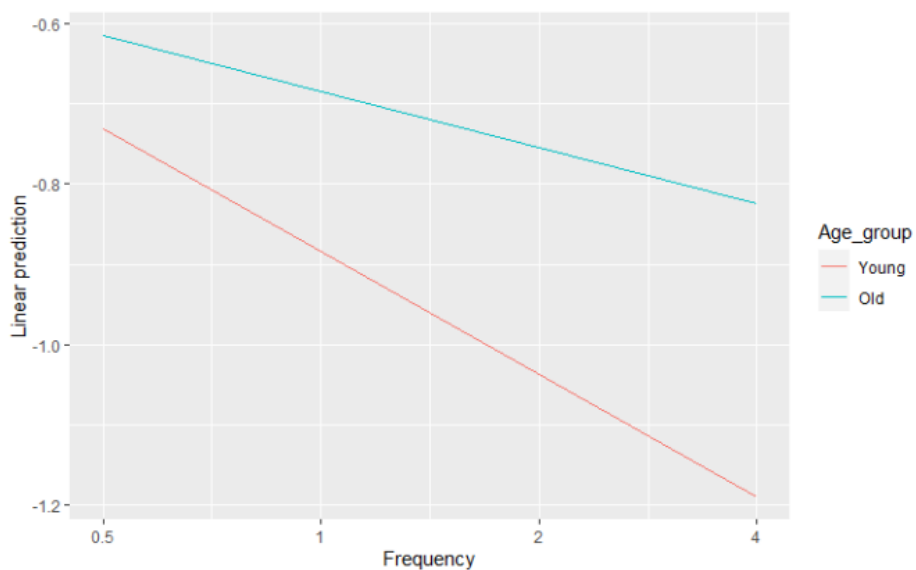


Figure E.9: Decline in test contrast with increasing spatial frequency. Note the steeper slope of decrement in the younger group

## APPENDIX E. CMF STATISTICAL TESTS

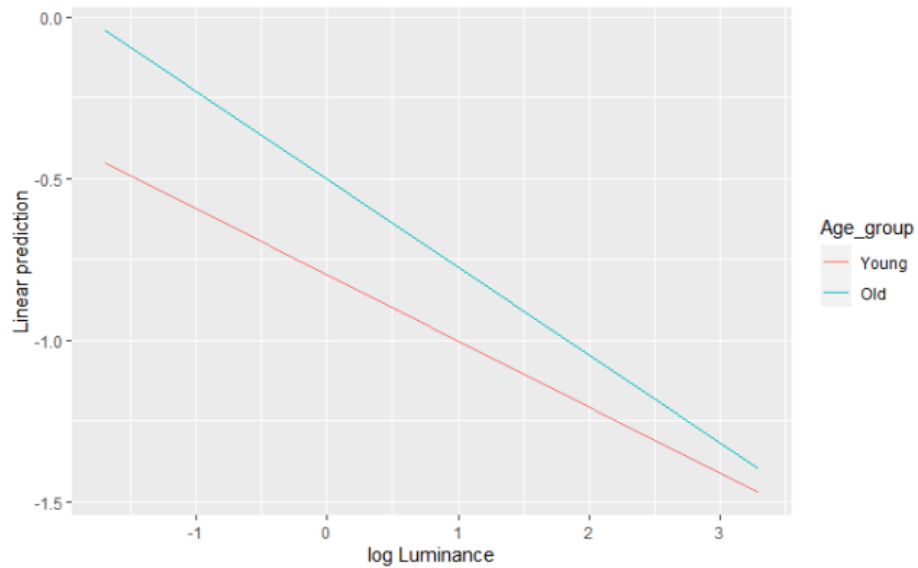


Figure E.10: Decline in test contrast with increasing spatial frequency. Note the steeper slope of decrement in the younger group

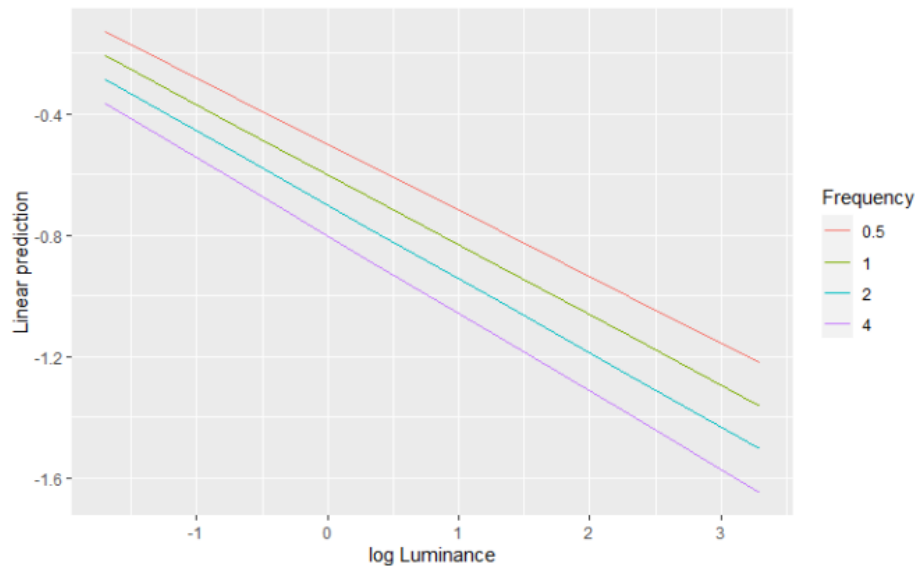


Figure E.11: Decrease in predicted test contrast with increasing luminance. The magnitude of slopes are slightly smaller for high luminance levels and increase for lower frequencies

## APPENDIX E. CMF STATISTICAL TESTS

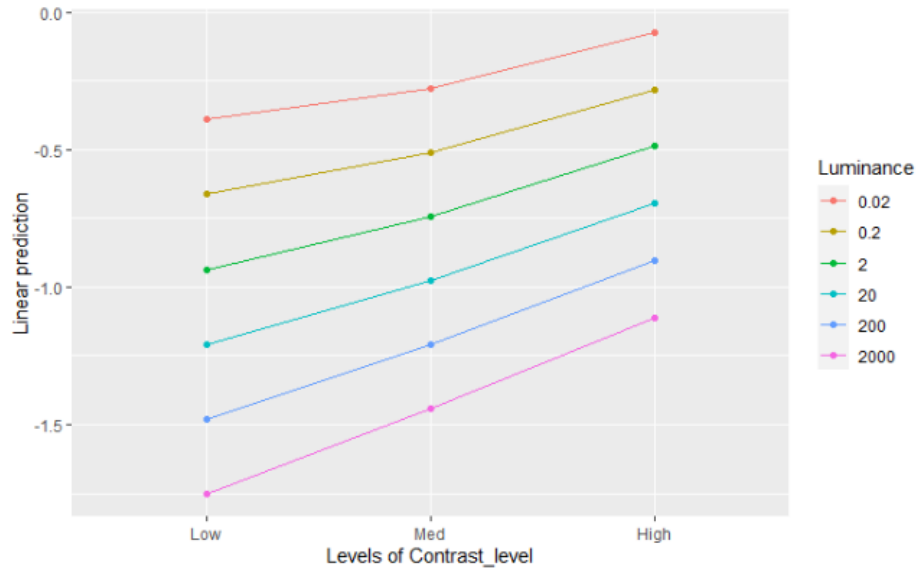


Figure E.12: Increase in test contrast with increasing suprathreshold contrast. Differences between test contrasts for different luminances are slightly higher for lower suprathreshold levels

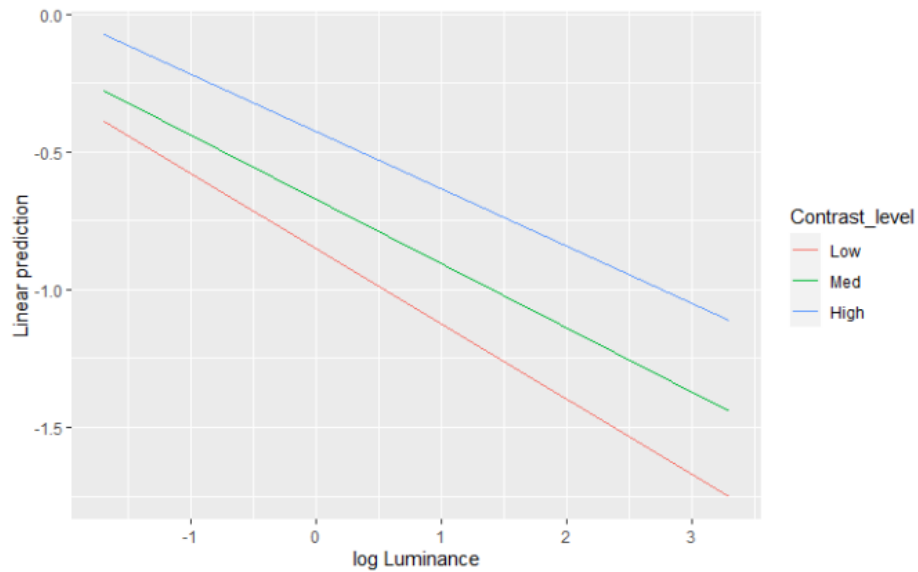


Figure E.13: Decrease in test contrast with increasing luminance level for each suprathreshold level. The negative slopes have a larger magnitude for low suprathreshold level

## APPENDIX E. CMF STATISTICAL TESTS

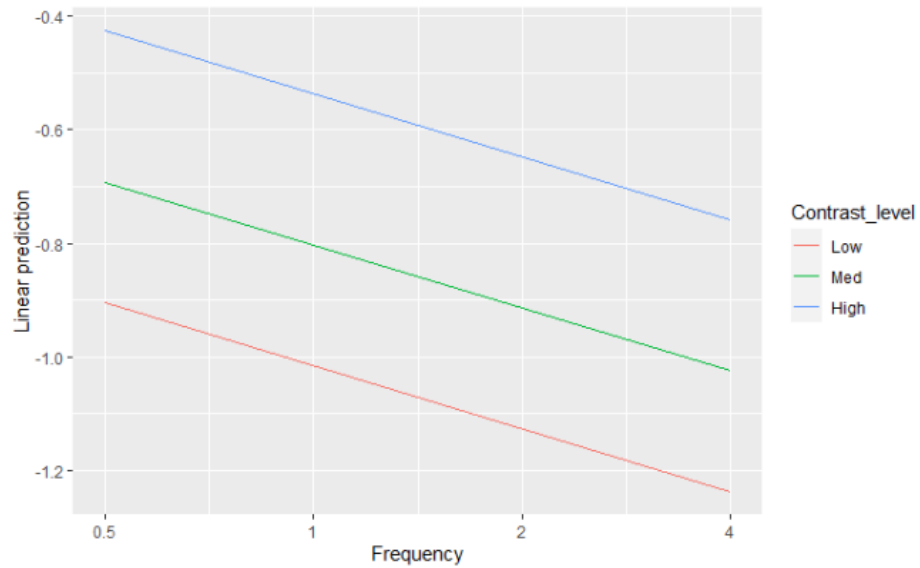


Figure E.14: Decrease in test contrast with increasing spatial frequency for each suprathreshold level. The slope remains constant for each suprathreshold level

## CONTRAST MATCHING MODELLING PARAMETERS

Table F.1: Slopes and intercepts from fitted lines of matching contrast

Colour direction	Spatial Frequency	Reference luminance	Test luminance	Reference threshold	Test threshold	Threshold difference	Slope	Intercept
Achromatic	0.5	200	0.02	0.0432	0.1326	0.0893	1.1944	0.3784
Achromatic	0.5	200	0.2	0.0432	0.0591	0.0159	0.5268	0.1365
Achromatic	0.5	200	2	0.0432	0.0362	-0.0071	0.5185	0.0559
Achromatic	0.5	200	20	0.0432	0.04	-0.0032	0.8014	0.0415
Achromatic	0.5	200	200	0.0432	0.0432	0	0.9462	0.045
Achromatic	0.5	200	2000	0.0432	0.055	0.0117	0.8688	0.087
Achromatic	2	200	0.2	0.0196	0.1095	0.0899	0.6796	0.2365
Achromatic	2	200	2	0.0196	0.0345	0.0148	0.5301	0.0662
Achromatic	2	200	20	0.0196	0.0256	0.0059	0.7459	0.0556
Achromatic	2	200	200	0.0196	0.0196	0	0.9079	0.0388
Achromatic	2	200	2000	0.0196	0.0291	0.0095	0.8515	0.0901
Achromatic	4	200	0.2	0.0292	0.3757	0.3464	0.6869	0.4344
Achromatic	4	200	2	0.0292	0.0883	0.0591	0.6447	0.1417
Achromatic	4	200	20	0.0292	0.0388	0.0096	0.5729	0.1112
Achromatic	4	200	200	0.0292	0.0292	0	0.7701	0.051
Achromatic	4	200	2000	0.0292	0.0413	0.0121	0.7396	0.1038
Red-Green	0.5	200	0.02	0.002	0.0593	0.0573	16.8104	-0.0066
Red-Green	0.5	200	0.2	0.002	0.0213	0.0193	1.6803	0.0583
Red-Green	0.5	200	2	0.002	0.0071	0.0051	1.175	0.0121
Red-Green	0.5	200	20	0.002	0.0035	0.0015	0.9373	0.0107
Red-Green	0.5	200	200	0.002	0.0026	0.0006	0.6807	0.0114
Red-Green	2	200	0.2	0.0052	0.0926	0.0874	2.3139	0.1053
Red-Green	2	200	2	0.0052	0.0284	0.0232	1.2606	0.0251
Red-Green	2	200	20	0.0052	0.011	0.0058	0.8004	0.0154
Red-Green	2	200	200	0.0052	0.0052	0	0.7099	0.0105
Red-Green	2	200	2000	0.0052	0.0062	0.001	0.4994	0.0135
Red-Green	4	200	0.2	0.0153	0.262	0.2466	2.3093	0.2265
Red-Green	4	200	2	0.0153	0.0618	0.0465	1.0991	0.068
Red-Green	4	200	20	0.0153	0.0283	0.013	0.5369	0.0326
Red-Green	4	200	200	0.0153	0.0153	0	0.6705	0.0118
Red-Green	4	200	2000	0.0153	0.0128	-0.0025	0.3333	0.0248
Yellow-Violet	0.5	200	2	0.0168	0.0577	0.0409	0.9102	0.1316
Yellow-Violet	0.5	200	20	0.0168	0.0267	0.0099	0.9234	0.0212
Yellow-Violet	0.5	200	200	0.0168	0.0168	0	0.8085	0.0336
Yellow-Violet	0.5	200	2000	0.0168	0.0196	0.0028	0.3201	0.1412
Yellow-Violet	2	200	2	0.0591	0.172	0.1129	0.4144	0.2148
Yellow-Violet	2	200	20	0.0591	0.1064	0.0473	0.3908	0.1231
Yellow-Violet	2	200	200	0.0591	0.0591	0	0.5101	0.0362
Yellow-Violet	2	200	2000	0.0591	0.0488	-0.0104	0.2484	0.113
Yellow-Violet	4	200	2	0.0893	0.2465	0.1572	0.4216	0.1833
Yellow-Violet	4	200	20	0.0893	0.1568	0.0675	0.4803	0.0094
Yellow-Violet	4	200	200	0.0893	0.0893	0	0.4494	0.0033
Yellow-Violet	4	200	2000	0.0893	0.0887	-0.0006	0.1848	0.113

## CMF MODEL STATISTICAL TESTS

Table G.1: Data transforms and pre-processing

Variable	Unit / Category	Type	Transform / Contrasts coding
Slope	-	Continuous	Box car transformed to remove heteroscedasticity
Intercept	-	Continuous	Box car transformed to remove heteroscedasticity
Spatial frequency	Cycles per visual degree ( cpd)	Continuous	Base 2 log
$\Delta$ Luminance	Candela per sq. meter ( cd/m <sup>2</sup> )	Continuous	Base 10 log
Threshold difference ( $\Delta C^t$ )	Cone contrast	Continuous	-
Threshold ratio ( $r^t$ )	-	Continuous	-
Subjects	Anonymous observer ID	Categorical	-

### G.1 Modelling slopes of contrast matching

#### G.1.1 Achromatic contrast matching

*Best Model:* Slope ~ Frequency +  $\Delta$  Luminance +  $\Delta C^t$  +  $r^t$  + (1 +  $\Delta$  Luminance | Subjects) + Frequency :  $\Delta$  Luminance + Frequency :  $\Delta C^t$  +  $\Delta$  Luminance :  $\Delta C^t$  + Frequency :  $r^t$  +  $\Delta C^t$  :  $r^t$  + Frequency :  $\Delta C^t$  :  $r^t$

Table G.2: Achromatic CMF slope parameter statistical modelling results

Effect	Estimate	Std. Error	df	t value	Pr(> t )	
Intercept	0.9456	0.0666	246.1	14.2	< 2e-16	***
$\Delta$ Luminance	-0.137	0.01859	60.14	-7.369	5.79E-10	***
$r^t$	-0.1021	0.05281	473.5	-1.934	0.05376	.
Frequency : $\Delta$ Luminance	0.04928	0.01268	465.8	3.885	0.000117	***
$\Delta$ Luminance : $\Delta C^t$	2.045	0.4899	479.2	4.174	3.55E-5	***
Frequency : $\Delta C^t$ : $r^t$	-0.14	0.04026	461.8	-3.478	0.000553	***

Signif. codes: ‘\*\*\*’ 0.001 ‘\*\*’ 0.01 ‘\*’ 0.05 ‘.’ 0.1

## APPENDIX G. CMF MODEL STATISTICAL TESTS

### G.1.2 Red-green contrast matching

*Best Model: Slope ~ Frequency \* Δ Luminance \* ΔC<sup>t</sup> \* r<sup>t</sup> + (I + Δ Luminance + Frequency | Subjects)*

Table G.3: Red-green CMF slope parameter statistical modelling results

Effect	Estimate	Std. Error	df	t value	Pr(> t )
Intercept	1.64	0.635	490	2.583	0.01009 *
Frequency	-2.372	0.3831	490.7	-6.193	1.25E-9 ***
Frequency : Δ Luminance	-0.3977	0.1428	490.1	-2.785	0.005565 **
Δ Luminance : ΔC <sup>t</sup>	-64.87	15.81	493.7	-4.103	4.77E-5 ***
Frequency : r <sup>t</sup>	1.992	0.3191	488.7	6.241	9.42E-10 ***
Δ Luminance : r <sup>t</sup>	0.2856	0.157	489.3	1.819	0.06948 .
ΔC <sup>t</sup> : r <sup>t</sup>	33.61	7.756	505.4	4.333	1.78E-5 ***
Frequency : Δ Luminance : r <sup>t</sup>	-0.5633	0.08642	489.1	-6.518	1.78E-10 ***
Frequency : ΔC <sup>t</sup> : r <sup>t</sup>	-19.67	6.265	496.9	-3.139	0.001795 **
Δ Luminance : ΔC <sup>t</sup> : r <sup>t</sup>	-7.256	1.775	500.6	-4.088	5.08E-5 ***
Frequency : Δ Luminance : ΔC <sup>t</sup> : r <sup>t</sup>	5.171	1.519	492.6	3.404	0.000717 ***

Signif. codes: ‘\*\*\*’ 0.001 ‘\*\*’ 0.01 ‘\*’ 0.05 ‘.’ 0.1

### G.1.3 Yellow-violet contrast matching

*Best Model: Slope ~ Frequency + Δ Luminance + ΔC<sup>t</sup> + r<sup>t</sup> + (I + Δ Luminance + Frequency | Subjects) + Frequency : Δ Luminance + Frequency : ΔC<sup>t</sup> + Δ Luminance : ΔC<sup>t</sup> + Frequency : r<sup>t</sup> + Δ Luminance : r<sup>t</sup> + ΔC<sup>t</sup> : r<sup>t</sup> + Frequency : Δ Luminance : ΔC<sup>t</sup> + Frequency : ΔC<sup>t</sup> : r<sup>t</sup>*

Table G.4: Yellow-violet CMF model parameter statistical modelling results

Effect	Estimate	Std. Error	df	t value	Pr(> t )
Intercept	1.926	0.2766	280.1	6.963	2.37E-11 ***
Frequency	-0.1738	0.03891	203.2	-4.467	1.31E-5 ***
Δ Luminance	0.3271	0.0867	222.1	3.773	0.000207 ***
r <sup>t</sup>	-1.25	0.262	256.9	-4.773	3.04E-6 ***
Frequency : Δ Luminance	-0.1279	0.03737	363.6	-3.424	0.000688 ***
Frequency : r <sup>t</sup>	0.08831	0.02429	360.9	3.635	0.000318 ***
Δ Luminance : r <sup>t</sup>	0.3311	0.07647	285.7	4.33	2.06E-5 ***
ΔC <sup>t</sup> : r <sup>t</sup>	-0.6712	0.1609	355.5	-4.171	3.81E-5 ***
Frequency : Δ Luminance : ΔC <sup>t</sup>	-1.654	0.7636	351.6	-2.166	0.031 *
Frequency : ΔC <sup>t</sup> : r <sup>t</sup>	0.3668	0.08101	364.8	4.527	8.1E-6 ***

Signif. codes: ‘\*\*\*’ 0.001 ‘\*\*’ 0.01 ‘\*’ 0.05

## APPENDIX G. CMF MODEL STATISTICAL TESTS

### G.2 Modelling intercept of contrast matching

#### G.2.1 Achromatic contrast matching

*Best Model:* Intercept ~ Frequency +  $\Delta$  Luminance +  $\Delta C^t$  +  $r^t$  + ( $I + \Delta$  Luminance | Subjects) + Frequency :  $\Delta$  Luminance + Frequency :  $\Delta C^t$  +  $\Delta$  Luminance :  $\Delta C^t$  + Frequency :  $r^t$  +  $\Delta$  Luminance :  $r^t$  +  $\Delta C^t$  :  $r^t$  + Frequency :  $\Delta C^t$  :  $r^t$  +  $\Delta$  Luminance :  $\Delta C^t$  :  $r^t$

Table G.5: Achromatic CMF intercept parameter statistical modelling results

Effect	Estimate	Std. Error	df	t value	Pr(> t )
(Intercept)	0.1201	0.07055	476.7	1.703	0.08925 .
$\Delta$ Luminance	-0.03086	0.01793	477.7	-1.722	0.08578 .
$\Delta C^t$	4.693	1.66	470.5	2.827	0.004903 **
Frequency : $\Delta$ Luminance	-0.00925	0.004499	456.2	-2.056	0.04036 *
Frequency : $\Delta C^t$	-1.212	0.5323	466.2	-2.277	0.02325 *
$\Delta$ Luminance : $r^t$	0.03102	0.01767	474.3	1.756	0.07975 .
$\Delta C^t$ : $r^t$	-0.7306	0.2449	481.7	-2.984	0.002993 **
Frequency : $\Delta C^t$ : $r^t$	0.166	0.04662	480.7	3.561	0.000406 ***
$\Delta$ Luminance : $\Delta C^t$ : $r^t$	0.1105	0.04954	480.8	2.231	0.02615 *

Signif. codes: ‘\*\*\*’ 0.001 ‘\*\*’ 0.01 ‘\*’ 0.05 ‘.’ 0.1

#### G.2.2 Red-green contrast matching

*Best Model:* Intercept ~ Frequency \*  $\Delta$  Luminance \*  $\Delta C^t$  \*  $r^t$  + ( $I + \Delta$  Luminance | Subjects)

Table G.6: Red-green CMF intercept parameter statistical modelling results

Effect	Estimate	Std. Error	df	t value	Pr(> t )
Frequency	0.09	0.02	488.6	5.051	6.21E-7 ***
Frequency : $\Delta$ Luminance	0.01	0.01	491.7	1.854	0.0643 .
$\Delta$ Luminance : $\Delta C^t$	3.87	0.76	495.6	5.113	4.54E-7 ***
Frequency : $r^t$	-0.08	0.02	488.9	-5.12	4.4E-7 ***
$\Delta C^t$ : $r^t$	-2.38	0.37	512.8	-6.409	3.32E-10 ***
Frequency : $\Delta$ Luminance : $\Delta C^t$	-1.41	0.56	489.6	-2.543	0.0113 *
Frequency : $\Delta$ Luminance : $r^t$	0.02	0	489.2	5.77	1.41E-8 ***
Frequency : $\Delta C^t$ : $r^t$	1.42	0.3	498.2	4.762	2.51E-6 ***
$\Delta$ Luminance : $\Delta C^t$ : $r^t$	0.47	0.08	504.5	5.542	4.82E-8 ***
Frequency : $\Delta$ Luminance : $\Delta C^t$ : $r^t$	-0.33	0.07	493.1	-4.556	6.57E-6 ***

Signif. codes: ‘\*\*\*’ 0.001 ‘\*\*’ 0.01 ‘\*’ 0.05 ‘.’ 0.1

## APPENDIX G. CMF MODEL STATISTICAL TESTS

### G.2.3 Yellow-violet contrast matching

*Best Model: Intercept ~ Frequency +  $\Delta Luminance + \Delta C^t + r^t + (I + \Delta Luminance + Frequency | Subjects) + Frequency : \Delta Luminance + Frequency : \Delta C^t + \Delta Luminance : \Delta C^t + Frequency : r^t + \Delta C^t : r^t + Frequency : \Delta Luminance : \Delta C^t + Frequency : \Delta C^t : r^t$*

Table G.7: Yellow-violet CMF intercept parameter statistical modelling results

Effect	Estimate	Std. Error	df	t value	Pr(> t )	
Intercept	-0.07443	0.02757	387.8	-2.699	0.00725	**
$\Delta Luminance$	-0.1691	0.02942	327.4	-5.746	2.1E-8	***
$\Delta C^t$	7.185	1.454	306.5	4.941	1.28E-6	***
$r^t$	0.1261	0.02193	354.1	5.749	1.94E-8	***
Frequency : $\Delta C^t$	-2.748	0.6056	357.4	-4.538	7.77E-6	***
$\Delta Luminance : \Delta C^t$	-2.884	0.6644	357.6	-4.34	1.86E-5	***
$\Delta C^t : r^t$	0.1784	0.05812	359.2	3.069	0.00231	**
Frequency : $\Delta Luminance : \Delta C^t$	1.157	0.2774	356.1	4.171	3.81E-5	***
Frequency : $\Delta C^t : r^t$	-0.08034	0.02691	354.4	-2.986	0.00303	**

Signif. codes: ‘\*\*\*’ 0.001 ‘\*\*’ 0.01 ‘\*’ 0.05